

1 **Fires, Asian, and Stratospheric Transport-Las Vegas Ozone Study**  
2 **(FAST-LVOS)**

3 **Report Contract No. CBE 604318-16**

4 **Prepared for the Clark County Department of Air Quality**

5  
6 Zheng Li  
7 Senior AQ modeler

8  
9 Rodney Langston  
10 Principal Planner

11  
12 Clark County Department of Air Quality  
13 Desk Phone: 702 455-1661  
14 Email: [Langston@ClarkCountyNV.gov](mailto:Langston@ClarkCountyNV.gov)

15  
16  
17 **Principal Investigators**

18 Andrew O. Langford  
19 NOAA Earth System Research Laboratory, Chemical Sciences Division

20 Boulder, CO 80305-3337, USA.  
21 Phone: (303) 497-3115  
22 Fax: (303) 497-5273  
23 E-mail: [andrew.o.langford@noaa.gov](mailto:andrew.o.langford@noaa.gov)

24 Christoph J. Senff

25 Cooperative Institute for Research in Environmental Sciences,  
26 University of Colorado, Boulder, CO, 80309, USA.  
27 and

28 NOAA Earth System Research Laboratory, Chemical Sciences Division

29 Phone: (303) 497-6283  
30 Fax: (303) 497-5273  
31 E-mail: [christoph.senff@noaa.gov](mailto:christoph.senff@noaa.gov)

32 December 1, 2019

33

1  
2  
3  
4  
5  
6  
7  
8  
9  
10  
11  
12  
13  
14  
15  
16  
17  
18  
19  
20  
21  
22  
23  
24  
25  
26

**Contributing Researchers**

Raul J. Alvarez<sup>1</sup>, Tim Bonin<sup>1,3</sup>, Alan Brewer<sup>1</sup>, Jerome Brioude<sup>9</sup>, Steven Brown<sup>1</sup>, Dani Caputi<sup>4</sup>, Steven Conley<sup>4</sup>, Patrick Cullis<sup>2,3</sup>, Zach Decker<sup>1,3</sup>, Stéphanie Evan<sup>9</sup>, Zaheer Kamal<sup>4</sup>, Guillaume Kirgis<sup>1,3</sup>, Meiyun Lin<sup>6,7</sup>, Jeff Peischl<sup>1,3</sup>, Irina Petropavlovskikh<sup>2,3</sup>, Tom Ryerson<sup>1</sup>, Scott Sandberg<sup>1</sup>, Chance Sterling<sup>2,3</sup>, Ann Weickmann<sup>1,3</sup>, Li Zhang<sup>6,7,8</sup>

---

<sup>1</sup>NOAA Earth System Research Laboratory, Chemical Sciences Division, Boulder, CO 80305

<sup>2</sup>NOAA Earth System Research Laboratory, Global Monitoring Division, Boulder, CO 80305

<sup>3</sup>Cooperative Institute for Research in Environmental Sciences (CIRES), University of Colorado, Boulder, CO, 80309

<sup>4</sup>Scientific Aviation Inc., Boulder, CO 80301

<sup>6</sup> Atmospheric and Oceanic Sciences, Princeton University, NJ, USA;

<sup>7</sup> NOAA Geophysical Fluid Dynamics Laboratory, Princeton, NJ, USA;

<sup>8</sup> Cooperative Institute for Climate Sciences, Princeton University, Princeton, NJ

<sup>9</sup>Laboratoire de l'Atmosphere et des Cyclones (LACy), UMR 8105, CNRS, Université de La Réunion, Météo-France, Saint-Denis, La Reunion, France,

1 **DISCLAIMER**

2

3 The statements and conclusions in this Report are those of the author from the National  
4 Oceanic and Atmospheric Administration, and not necessarily those of the Clark County  
5 Department of Air Quality. The views, opinions, and findings contained in this report are those  
6 of the author(s) and should not be construed as an official National Oceanic and Atmospheric  
7 Administration or U.S. Government position, policy, or decision.

8 The mention of commercial products, their source, or their use in connection with material  
9 reported herein is not to be construed as actual or implied endorsement of such products.

10 This Report was submitted in fulfillment of Memorandum of Agreement Nos. CBE604318-16  
11 between Clark County, Nevada and NOAA. The NOAA GFDL AM4 model results cited here were  
12 generated under contract CBE605334-19.

13

1 **ACKNOWLEDGEMENTS**

2 The successful execution of the Fires, Asian, and Stratospheric Transport - Las Vegas Ozone  
3 Study (FAST-LVOS) required the efforts of many people. Personnel from the Boulder, Colorado  
4 based Chemical Sciences and Global Monitoring Divisions of the National Oceanic and  
5 Atmospheric Administration Earth System Research Laboratory (NOAA/ESRL/CSD and  
6 NOAA/ESRL/GMD) and from the Cooperative Institute for Research in Environmental Sciences  
7 (CIRES) at the University of Colorado conducted the measurement campaign, along with  
8 personnel from Scientific Aviation, Inc.  
9

10 The TOPAZ lidar measurements were made possible by the hard work of Raul Alvarez,  
11 Guillaume Kirgis, Chris Senff, Andy Langford, Scott Sandberg, Ann Weickmann, and Richard  
12 Marchbanks. Alan Brewer and Scott Sandberg designed and built the  $\mu$ -Doppler lidar which  
13 Scott expertly deployed in the field. Ann Weickmann developed the software that kept the  
14 system running and Tim Bonin created the algorithm to derive mixed layer heights from the  
15 measurements. Jeff Peischl, Zach Decker, Bill Dubé, and Steve Brown mastered the daily drive  
16 to Angel Peak to keep those in-situ measurements going. Skinny Fats misses you! Patrick Cullis  
17 and Chance Sterling flew to Las Vegas on short notice to launch ozonesondes during the IOPs,  
18 and Zaheer Hamal and Dani Caputi spent long hours flying in the Scientific Aviation Mooney and  
19 enduring the lunches at the Big Bear airport.  
20

21 The successful execution of the FAST-VOS project is also due in large part to the unfunded  
22 modeling efforts of Mariuz Pagowski of the NOAA/ESRL Global Systems Division (RAP-Chem) and  
23 Brad Pierce of the Center for Satellite Applications and Research at the Cooperative Institute for  
24 Meteorological Satellite Studies of NOAA and the University of Wisconsin (RAQMS), We are also  
25 grateful to Jerome Brioude and Stéphanie Evan of the Laboratoire de l'Atmosphère et des  
26 Cyclones (LACy), UMR 8105, CNRS, Université de La Réunion, Météo-France, Saint-Denis, La  
27 Reunion, France, for generously providing the FLEXPART calculations used in the subsequent  
28 analyses.  
29

30 We would especially like to thank Zheng Li and Rodney Langston and their colleagues at the  
31 Clark County Department of Air Quality for their hospitality and support in the planning and  
32 execution of the FAST-LVOS. We are particularly grateful to Mickey Turner, Paul Fransioli, and  
33 Andy Gagliardo for key logistical support that made the measurements at the NLVA and Angel  
34 Peak possible.  
35

36 Finally, we would like to acknowledge the additional support from the NOAA Health of the  
37 Atmosphere and Climate Programs and the NASA Tropospheric Ozone Lidar Network (TOLNet,  
38 <http://www-air.larc.nasa.gov/missions/TOLNet/>) that made this project possible.  
39

40

1	<b>CONTENTS</b>	
2	Disclaimer .....	3
3	Acknowledgement .....	4
4	List of Figures .....	7
5	List of Tables .....	15
6	Abstract .....	16
7	Executive Summary .....	17
8	Definitions and Abbreviations.....	19
9	1. Introduction .....	20
10	2. Background.....	22
11		
12	3. The Fires, Asian, and Stratospheric Transport-	
13	Las Vegas Ozone Study ( <i>FAST-LVOS</i> ) .....	24
14		
15	4. <i>FAST-LVOS</i> Measurement Suite.....	25
16	4.1 NOAA ozone and aerosol lidar.....	27
17	4.2 NOAA micro-Doppler lidar.....	28
18	4.3 NOAA mobile sampling laboratory.....	30
19	4.4 NOAA ECC ozonesondes.....	33
20	4.5 Scientific Aviation Mooney aircraft.....	35
21		
22	5. <i>FAST-LVOS</i> Modeling Support.....	37
23		
24	6. Meteorological Context.....	37
25		
26	7. Overview of the <i>FAST-LVOS</i> Measurements.....	41
27	7.1 Clark County measurements.....	41
28	7.2 TOPAZ lidar measurements.....	42
29	7.3 Comparison between lidar and surface measurements.....	45
30		
31	8. Comparison to FLEXPART tracer distributions.....	51
32		
33	9. Weekly summaries of the <i>FAST-LVOS</i> Results.....	56
34	9.1 Week 1: May 17-20.....	56
35	9.2 Week 2: May 21-28 ( <i>IOP1</i> ) .....	60
36	9.3 Week 3: May 28-June 3 ( <i>IOP2</i> ) .....	68
37	9.4 Week 4: June 4-10.....	78
38	9.5 Week 5: June 11-17 ( <i>IOP3</i> ) .....	83

1	9.6 Week 6: June 18-24.....	92
2	9.7 Week 7: June 25-30 (IOP4) .....	99
3		
4	10. Comparison to the NOAA GFDL AM4 model.....	106
5		
6	11. Contrasts between LVOS and FAST-LVOS.....	109
7		
8		
9	References.....	115
10		
11	Appendix A: Model descriptions.....	119
12	Appendix B: Daily summaries.....	122
13	Appendix C: Angel Peak summary plots.....	134
14	Appendix D: GMD ozonesonde plots.....	179
15	Appendix E: Scientific Aviation measurement plots.....	184
16		
17		

1 **LIST OF FIGURES**

2 **Figure 1-1.** Mean contributions (in ppbv) of (a) STT, and (b) Asian pollution, to MDA8 surface O<sub>3</sub>  
3 calculated by the NOAA GFDL AM3 model for May and June 2010. The resolution is 50 km x 50  
4 km. Note the different color scales. Clark County, NV is outlined in black. Adapted from [Lin et  
5 al., 2012a; Lin et al., 2012b].

6  
7 **Figure 2-1.** (a) Map of the southwestern U.S. showing regulatory O<sub>3</sub> monitors reporting to the  
8 U.S. EPA AirNow network (filled black triangles). The blue open circles identify regional monitors  
9 operated by the U.S. National Park Service (USNPS). (b) Expanded view of Clark County with  
10 CCDAQ monitors represented by filled red circles. The large red triangle marks Angel Peak, home  
11 to the 2013 LVOS field campaign.

12  
13 **Figure 2-2.** MDA8 O<sub>3</sub> measured by the Clark County DAQ monitor at Jean in southwestern Clark  
14 County for the years 2012-2016. The horizontal dashed line marks the 70 ppbv NAAQS. May and  
15 June lie between the two vertical dotted lines

16  
17 **Figure 4-1.** The Scientific Aviation Mooney makes a low overpass of the NLVA measurement site.  
18 The NOAA TOPAZ lidar truck and micro-Doppler lidar can be seen in the background behind the  
19 Clark County DAQ radar wind profiler, profiling radiometer, and visibility cameras. The 2B ozone  
20 monitor sampling mast is seen to the left of the red warning light on top of the TOPAZ truck.  
21 Sunrise Mountain can be seen just above the wind profiler (photo by A.O. Langford)

22  
23 **Figure 4-2.** Topographical maps showing the FAST-LVOS measurement domain. The filled red,  
24 green, and black circles locate the regulatory O<sub>3</sub> monitors operated by Clark County, the U.S.  
25 National Park Service, and the State of California, respectively. The white diamonds show the  
26 FAST-LVOS measurement sites at NLVA and AP. The blue trace shows the Scientific Aviation  
27 flight track from June 28, 2017.

28  
29 **Figure 4-3.** The NOAA autonomous micro-Doppler lidar stands on the former RASS pad adjacent  
30 to the TOPAZ lidar truck. (photo by A.O. Langford)

31  
32 **Figure 4-4.** Jeff Peischl of NOAA/ESRL/CSD and CIRES works on the mobile lab instrumentation  
33 at Angel Peak (photo by A.O. Langford).

34  
35 **Figure 4-5.** Aerial view of Angel Peak from the SA Mooney showing the NOAA mobile laboratory.  
36 The TOPAZ mobile lidar was parked in the same spot during LVOS, and the LVOS in-situ  
37 measurements made from the roof of the Clark County building. (photo by D. Caputi).

38  
39 **Figure 4-6.** NOAA mobile laboratory and Scientific Aviation aircraft during standards  
40 comparison at the NLVA. (photo by R. Langston)

41

1 **Figure 4-7.** Patrick Cullis (L) and Chance Sterling (R) of NOAA/ESRL/GMD and CIRES, U. of  
2 Colorado prepare to launch one of the FAST-LVOS ozonesondes from the Estelle Neal municipal  
3 park (photo by R. Langston).

4 **Figure 4-8.** Scientific Aviation 1998 Mooney TLS Bravo M20M (N2132X) on landing approach at  
5 NLVA (photo by A. Langford).

6 **Figure 6-1.** Time series showing the 5-min measurements from the NWS (KVGT) station locate  
7 near the TOPAZ truck at the NLVA. The gray bands mark the four FAST-LVOS IOPs.  
8

9 **Figure 6-2.** Time series of the 1-min meteorological measurements from the mobile laboratory  
10 on Angel Peak (black). The gray bands mark the four FAST-LVOS IOPs.  
11

12 **Figure 6-3.** NCEP NARR Reanalysis 300 hPa 12UT geopotential maps at weekly intervals during  
13 FAST-LVOS.  
14

15 **Figure 7-1.** MDA8 (steps) and 5-min (dots) O<sub>3</sub> mixing ratios measured by the Walter Johnson  
16 (red), Joe Neal (black), and JD Smith (blue) monitors during FAST-LVOS. The horizontal dashed  
17 line shows the 70 ppbv NAAQS.  
18

19 **Figure 7-2.** Time-height curtain plots of the TOPAZ (a) O<sub>3</sub> mixing ratios and (b) particulate  
20 backscatter coefficients. The dotted black line shows the mixed layer heights inferred from the  
21 micro-Doppler lidar measurements and the heavy black boxes enclose the IOP days.  
22

23 **Figure 7-3.** Time series of the TOPAZ O<sub>3</sub> mixing ratios and particulate backscatter coefficients at  
24 (a) 4002.5 and (b) 27.5 m agl. Note that the peak O<sub>3</sub> value of 140 ppbv on June 12 is off scale.  
25 The dashed black lines correspond to the 70 ppbv NAAQS.  
26

27 **Figure 7-4.** (a) Time series of the 27.5 m TOPAZ O<sub>3</sub> measurements and the 1-min in-situ  
28 measurements at the NLVA. The gray bands identify the FAST-LVOS IOPs. The lower panels are  
29 expanded views of the measurements from (b) IOP2 and (c) IOP3. The dashed black lines  
30 correspond to the 70 ppbv NAAQS.  
31

32 **Figure 7-5.** (a) Time series of the 27.5 m TOPAZ O<sub>3</sub> measurements and the 5-min in-situ O<sub>3</sub>  
33 measurements from Joe Neal (C75). The gray bands identify the FAST-LVOS IOPs. The lower  
34 panels are expanded views of the measurements from (b) IOP2 and (c) IOP3. The dashed black  
35 lines correspond to the 70 ppbv NAAQS.  
36

37 **Figure 7-6.** (a) Time series of the 1-min in-situ O<sub>3</sub> measurements from the NLVA (black) and AP  
38 (blue) compared to the 2002.5 m agl (2683.5 km asl) TOPAZ measurements (red). The gray  
39 bands identify the FAST-LVOS IOPs. The lower panels are expanded views of the measurements  
40 from (b) IOP2 and (c) IOP3. The dashed black lines correspond to the 70 ppbv NAAQS.  
41

1 **Figure 7-7.** Time series of the 1-min  $O_3$ ,  $CO$ ,  $CO_2$ , and  $CH_4$  measurements from the mobile  
2 laboratory on Angel Peak (black). The gray bands mark the four FAST-LVOS IOPs. The  $CO$   
3 concentrations on June 22 reached 450 ppbv (arrow).  
4

5 **Figure 7-8.** Time series of the 1-min  $O_3$ ,  $NO_y$ ,  $N_2O$ , and  $H_2O$  measurements from the mobile  
6 laboratory on Angel Peak (black). The gray bands mark the four FAST-LVOS IOPs.  
7

8 **Figure 8-1.** Time-height curtain plots of the (a) STT  $O_3$ , (b) ASCO, and (c) BBCO FLEXPART tracers  
9 above the Las Vegas Valley. All three tracers are plotted with a 0-100 ppb concentration scale  
10

11 **Figure 8-2.** Maps showing the FLEXPART STO3 tracer distribution at 12UT on May 18, May 27,  
12 and June 12 on the (left) 500 hPa and (right) 700 hPa surfaces.  
13

14 **Figure 8-3.** Maps showing the FLEXPART ASCO tracer distributions at 00UT on May 28 and June  
15 10, and 12UT on June 18 on the (left) 500 hPa and (right) 700 hPa surfaces.  
16

17 **Figure 8-4.** Maps showing the FLEXPART BBCO tracer distribution at 00UT on June 21 23, and 28  
18 on the (left) 500 hPa and (right) 700 hPa surfaces.  
19

20 **Figure 9-1.** Time-height curtain plots of the TOPAZ (a) ozone, and (b) backscatter, measured  
21 during Week 1 of FAST-LVOS. The colored horizontal bands at 2.0 and 0.0 km agl in (a) show the  
22 in-situ measurements from the NLVA and AP, respectively. The dark gray trace represents the  
23 local mixed-layer height inferred from the micro-Doppler lidar measurements. Note that the  
24 TOPAZ measurements were truncated by low clouds during the early afternoon of the 18<sup>th</sup>.  
25

26 **Figure 9-2.** Time-height curtain plots of the FLEXPART (a) STO3, (b) ASCO, and (c) BBCO tracer  
27 distributions above the LVV during Week 1 of FAST-LVOS.  
28

29 **Figure 9-3.** Time series of the TOPAZ  $O_3$  mixing ratios at 4.0 km agl (black +) during Week 1  
30 plotted with the 1-min  $O_3$  measurements from the NLVA (black) and AP (green) and the 5-min  
31 measurements from the Walter Johnson (C71, red) and Joe Neal (C75, blue) monitors. The red  
32 and blue steps show the corresponding C71 and C75 MDA8 measurements. The dashed black  
33 line indicates the 70 ppbv NAAQS.  
34

35 **Figure 9-4.** NOAA NESDIS RAQMS model 310 K  $CO$  forecast for May 24 00UT. Forecast initialized  
36 May 21 12UT.  
37

38 **Figure 9-5.** Time-height curtain plots of the TOPAZ (a) ozone, and (b) backscatter, measured  
39 during Week 2 of FAST-LVOS. The ascending Joe Neal ozonesonde profiles from IOP1 are  
40 superimposed. The colored horizontal bands in (a) show the in-situ measurements from the  
41 NLVA and AP. The black line shows the local mixed-layer height from the micro-Doppler lidar.  
42

1 **Figure 9-6.** Profiles of potential temperature (black), O<sub>3</sub> (red), and relative humidity (blue) from  
2 the Joe Neal 1201 PDT ozonesonde on May 24. The dashed black horizontal line marks the top  
3 of the boundary layer.  
4

5 **Figure 9-7.** Time-height curtain plots of the FLEXPART (a) STO<sub>3</sub>, (b) ASCO, and (c) BBCO tracer  
6 distributions above the LVV during Week 2 of FAST-LVOS.  
7

8 **Figure 9-8.** Time series of the TOPAZ O<sub>3</sub> mixing ratios at 4.0 km agl (black +) during Week 2  
9 plotted with the 1-min O<sub>3</sub> measurements from the NLVA (black) and AP (green) and the 5-min  
10 measurements from the Walter Johnson (C71, red) and Joe Neal (C75, blue) monitors. The red  
11 and blue steps show the corresponding C71 and C75 MDA8 measurements. The dashed black  
12 line indicates the 70 ppbv NAAQS.  
13

14 **Figure 9-9.** Flight tracks for the Scientific Aviation TLS Bravo during the first FAST-LVOS IOP (May  
15 23-25). The filled squares, circles, and triangles mark the locations of surface monitors operated  
16 by CCDAQ, CARB, and the USNPS, respectively. The flight tracks are colorized to show the in situ  
17 O<sub>3</sub> and the symbols colorized to show the reported MDA8 O<sub>3</sub>.  
18

19 **Figure 9-10.** Scientific Aviation O<sub>3</sub> profiles above the NLVA, Joe Neal, and Angel Peak during the  
20 first IOP.  
21

22 **Figure 9-11.** Ozone mixing ratios measured along the flights from NLVA to Big Bear, CA and  
23 back during the first IOP.  
24

25 **Figure 9-12.** Time series of the TOPAZ O<sub>3</sub> mixing ratios at 4.0 km agl (black +) during Week 3  
26 plotted with the 1-min O<sub>3</sub> measurements from the NLVA (black) and AP (green) and the 5-min  
27 measurements from the Walter Johnson (C71, red) and Joe Neal (C75, blue) monitors. The red  
28 and blue steps show the corresponding C71 and C75 MDA8 measurements. The dashed black  
29 line indicates the 70 ppbv NAAQS.  
30

31 **Figure 9-13.** Time-height curtain plots of the TOPAZ (a) ozone, and (b) backscatter, measured  
32 during Week 3 of FAST-LVOS. The ascending Joe Neal ozonesonde profiles from IOP2 are  
33 superimposed. The colored horizontal bands in (a) show the in-situ measurements from the  
34 NLVA and AP. The black line shows the local mixed-layer height from the micro-Doppler lidar.  
35

36 **Figure 9-14.** Time-height curtain plots of the FLEXPART (a) STO<sub>3</sub>, (b) ASCO, and (c) BBCO tracer  
37 distributions above the LVV during Week 3 of FAST-LVOS.  
38

39 **Figure 9-15.** Time-height curtain plots of the TOPAZ (a) ozone, and (b) backscatter, measured on  
40 June 2-3. The ascending Joe Neal ozonesonde profiles from IOP2 are superimposed. The colored  
41 horizontal bands in (a) show the in-situ measurements from the NLVA and AP. The black line  
42 shows the local mixed-layer height from the micro-Doppler lidar.  
43

1 **Figure 9-16.** Profiles of potential temperature (black), O<sub>3</sub> (red), and relative humidity (blue) from  
2 the Joe Neal ozonesondes on June 2. The dashed black horizontal line marks the top of the  
3 boundary layer.

4  
5 **Figure 9-17.** Scientific Aviation O<sub>3</sub> profiles above the NLVA, Joe Neal, and Angel Peak during the  
6 second IOP.

7  
8 **Figure 9-18.** Scientific Aviation CH<sub>4</sub> profiles above the NLVA, Joe Neal, and Angel Peak during the  
9 second IOP.

10  
11 **Figure 9-19.** Time series of (a) O<sub>3</sub> and CO, (b) H<sub>2</sub>O and CH<sub>4</sub>, (c) NO<sub>x</sub>, NO<sub>y</sub> and N<sub>2</sub>O, and (d) wind  
12 speed and direction measured by the mobile laboratory on Angel Peak during Week 3 of FAST-  
13 LVOS. The narrow CO and NO<sub>y</sub> spikes near noon on May 31 are probably of local origin.

14  
15 **Figure 9-20.** Scatter plots showing the correlations between in-situ O<sub>3</sub> and (a) CO, (b) N<sub>2</sub>O, (c)  
16 CO<sub>2</sub>, and (d) CH<sub>4</sub> measurements from the mobile lab on Angel Peak. The measurements from the  
17 afternoon and evening (12-23 PDT) of June 2 are colorized by the water vapor measurements.

18  
19 **Figure 9-21.** Time series of the TOPAZ O<sub>3</sub> mixing ratios at 4.0 km agl (black +) during Week 4  
20 plotted with the 1-min O<sub>3</sub> measurements from the NLVA (black) and AP (green) and the 5-min  
21 measurements from the Walter Johnson (C71, red) and Joe Neal (C75, blue) monitors. The red  
22 and blue steps show the corresponding C71 and C75 MDA8 measurements. The dashed black  
23 line indicates the 70 ppbv NAAQS.

24  
25 **Figure 9-22.** Time-height curtain plots of the TOPAZ (a) ozone, and (b) backscatter, measured  
26 during Week 4. The ascending Joe Neal ozonesonde profiles from IOP3 are superimposed. The  
27 colored horizontal bands in (a) show the in-situ measurements from the NLVA and AP. The black  
28 line shows the local mixed-layer height from the micro-Doppler lidar.

29  
30 **Figure 9-23.** Time-height curtain plots of the FLEXPART (a) STO<sub>3</sub>, (b) ASCO, and (c) BBCO tracer  
31 distributions above the LVV during Week 4 of FAST-LVOS.

32  
33 **Figure 9-24.** Time series of (a) O<sub>3</sub> and CO, (b) H<sub>2</sub>O and CH<sub>4</sub>, (c) NO<sub>x</sub>, NO<sub>y</sub> and N<sub>2</sub>O, and (d) wind  
34 speed and direction measured by the mobile laboratory on Angel Peak during Week 4 of FAST-  
35 LVOS.

36  
37 **Figure 9-25.** Scatter plots showing the correlations between in-situ O<sub>3</sub> and CO on Angel Peak.  
38 The measurements from (a) 0000 to 0445 PDT, and (b) 1030-1400 PDT on June 5 are colorized  
39 by the water vapor measurements.

40  
41 **Figure 9-26.** Time series of the TOPAZ O<sub>3</sub> mixing ratios at 4.0 km agl (black +) during Week 5  
42 plotted with the 1-min O<sub>3</sub> measurements from the NLVA (black) and AP (green) and the 5-min  
43 measurements from the Walter Johnson (C71, red) and Joe Neal (C75, blue) monitors. The red

1 and blue steps show the corresponding C71 and C75 MDA8 measurements. The dashed black  
2 line indicates the 70 ppbv NAAQS.

3  
4 **Figure 9-27.** NOAA NESDIS RAQMS model 320 K O<sub>3</sub> forecast for June 12 00UT. Forecast  
5 initialized June 11 1200UT.

6  
7 **Figure 9-28.** RAP-Chem total ozone analyses for 00UT on June 12 at (left to right) 500 hPa, 700  
8 hPa, and the surface. Concentrations are given in ppmv.

9  
10 **Figure 9-29.** Time-height curtain plots of the TOPAZ (a) ozone, and (b) backscatter, measured  
11 during Week 5 of FAST-LVOS. The ascending Joe Neal ozonesonde profiles from IOP3 are  
12 superimposed. The colored horizontal bands in (a) show the in-situ measurements from the  
13 NLVA and AP. The black line shows the local mixed-layer height from the micro-Doppler lidar.  
14 Note that strong winds kept the boundary layer well-mixed throughout the night of June 11-12.

15  
16 **Figure 9-30.** Time-height curtain plots of the FLEXPART (a) STO<sub>3</sub>, (b) ASCO, and (c) BBCO tracer  
17 distributions above the LVV during Week 5 of FAST-LVOS.

18  
19 **Figure 9-31.** Time series of (a) O<sub>3</sub> and CO, (b) H<sub>2</sub>O and CH<sub>4</sub>, (c) NO<sub>x</sub>, NO<sub>y</sub> and N<sub>2</sub>O, and (d) wind  
20 speed and direction measured by the mobile laboratory on Angel Peak during Week 5 of FAST-  
21 LVOS.

22  
23 **Figure 9-32.** Scatter plots showing the correlations between in-situ O<sub>3</sub> and (a) CO, (b) N<sub>2</sub>O, (c)  
24 CO<sub>2</sub>, and (d) CH<sub>4</sub> measurements from the mobile lab on Angel Peak. The measurements from  
25 Week 5 are colorized by the water vapor measurements.

26  
27 **Figure 9-33.** Scientific Aviation O<sub>3</sub> profiles above NLVA, Joe Neal, and Angel Peak on June 13-14.

28  
29 **Figure 9-34.** Scientific Aviation O<sub>3</sub> measurements from the flights on June 13 and 14.

30  
31 **Figure 9-35.** Time series of the TOPAZ O<sub>3</sub> mixing ratios at 4.0 km agl (black +) during Week 6  
32 plotted with the 1-min O<sub>3</sub> measurements from the NLVA (black) and AP (green) and the 5-min  
33 measurements from the Walter Johnson (C71, red) and Joe Neal (C75, blue) monitors. The red  
34 and blue steps show the corresponding C71 and C75 MDA8 measurements. The dashed black  
35 line indicates the 70 ppbv NAAQS.

36  
37 **Figure 9-36.** Time-height curtain plots of the TOPAZ (a) ozone, and (b) backscatter, measured  
38 during Week 6 of FAST-LVOS. The colored horizontal bands in (a) show the in-situ measurements  
39 from the NLVA and AP. The black line shows the local mixed-layer height from the micro-  
40 Doppler lidar.

41  
42 **Figure 9-37.** Time-height curtain plots of the FLEXPART (a) STO<sub>3</sub>, (b) ASCO, and (c) BBCO tracer  
43 distributions above the LVV during Week 6 of FAST-LVOS.

1 **Figure 9-38.** NOAA HRRR-smoke model near surface (top) and vertically integrated (bottom)  
2 smoke forecasts for: (left to right) June 20 15 PDT, June 22 15 PDT, and June 23 11 PDT.

3  
4 **Figure 9-39.** Time series of (a)  $O_3$  and CO, (b)  $H_2O$  and  $CH_4$ , (c)  $NO_2$ ,  $NO_y$  and  $N_2O$ , and (d) wind  
5 speed and direction measured by the mobile laboratory on Angel Peak during Week 6 of FAST-  
6 LVOS. The CO measurements in the Holcomb Fire plume on June 22 reached over 450 ppbv.

7  
8 **Figure 9-40.** Scatter plots showing the correlations between in-situ  $O_3$  and (a) CO, (b)  $N_2O$ , (c)  
9  $CO_2$ , and (d)  $CH_4$  measurements from the mobile lab on Angel Peak. The measurements from  
10 Week 6 are colorized by the water vapor measurements. The CO measurements in the Holcomb  
11 Fire plume are off scale.

12  
13 **Figure 9-41.** Time series of the TOPAZ  $O_3$  mixing ratios at 4.0 km agl (black +) during Week 7  
14 plotted with the 1-min  $O_3$  measurements from the NLVA (black) and AP (green) and the 5-min  
15 measurements from the Walter Johnson (C71, red) and Joe Neal (C75, blue) monitors. The red  
16 and blue steps show the corresponding C71 and C75 MDA8 measurements. The dashed black  
17 line indicates the 70 ppbv NAAQS.

18  
19 **Figure 9-42.** Time-height curtain plots of the TOPAZ (a) ozone, and (b) backscatter, measured  
20 during Week 7 of FAST-LVOS. The ascending Joe Neal ozonesonde profiles from IOP4 are  
21 superimposed. The colored horizontal bands in (a) show the in-situ measurements from the  
22 NLVA and AP. The black line shows the local mixed-layer height from the micro-Doppler lidar.

23  
24 **Figure 9-43.** Time-height curtain plots of the FLEXPART (a)  $STO_3$ , (b) ASCO, and (c) BBCO tracer  
25 distributions above the LVV during Week 7 of FAST-LVOS.

26  
27 **Figure 9-44.** Time-height curtain plots of the TOPAZ (a) ozone, and (b) backscatter, measured on  
28 June 28, 2017. The colored horizontal bands in (a) show the in-situ measurements from the  
29 NLVA and AP, and the nearly vertical colored line shows the profile from the ascending Joe Neal  
30 ozonesonde. The colored tilted lines show the outbound and inbound profiles from the Scientific  
31 Aviation Mooney. The black line represents the local mixed-layer height from the micro-Doppler  
32 lidar.

33  
34 **Figure 9-45.** Profiles of (a) RH, (b)  $O_3$ , and (c)  $CH_4$  above the NLVA/Joe Neal area from the  
35 Scientific Aviation flight on June 28. The black profiles are from the outbound leg near midday  
36 and the red profiles from the inbound leg in the late afternoon. The solid and dashed lines show  
37 the corresponding mixed layer heights.

38  
39 **Figure 9-46.** NOAA HRRR-smoke model vertically integrated smoke forecasts for: (left to right)  
40 June 28, June 29, and June 30 at 18 UT (11 PDT).

41  
42 **Figure 9-47.** Time series of (a)  $O_3$  and CO, (b)  $H_2O$  and  $CH_4$ , (c)  $NO_x$ ,  $NO_y$  and  $N_2O$ , and (d) wind  
43 speed and direction measured by the mobile laboratory on Angel Peak during Week 7 of FAST-  
44 LVOS.

1  
2 **Figure 9-48.** Ozone measurements from Scientific Aviation flights to Big Bear, CA on June 27-30.

3  
4 **Figure 10-1.** Time-height curtain plots of O<sub>3</sub> above NLVA as observed with TOPAZ lidar and  
5 simulated with GFDL-AM4 (≈50 km × 50 km; interpolated from 3-hourly data) and GEOS-Chem  
6 (0.25° × 0.3125°; interpolated from hourly data) during the STT event on (a) June 11–13 and (b)  
7 June 14, 2017 (UTC). The rightmost panel shows AM4 stratospheric O<sub>3</sub> tracer (AM4\_O<sub>3</sub>Strat).  
8 Note that AM4\_O<sub>3</sub>Strat for June 14 is scaled by a factor of 2.5 for clarity. Here and in other  
9 figures, the solid black lines in the O<sub>3</sub> lidar plots represent boundary layer height inferred from  
10 the micro-Doppler lidar measurements.

11  
12 **Figure 10-2.** Same as Figure 10-1, but for (a) the wildfire event on June 22 and (b) the regional  
13 anthropogenic pollution event on June 16, 2017 (UTC). The right panels compare USB O<sub>3</sub> from  
14 the two models.

15  
**Figure 10-3.** Same as Figure 10-1, but for (a) the Asian pollution event on May 24 and (b) the unattributed  
pollution event on June 28, 2017 (UTC).

**Figure 10-4.** Maps of total MDA8 O<sub>3</sub> as observed and simulated with GFDL-AM4 along with the model  
estimated USB level, during the STT event of June 11–14, 2017. (adapted from Zhang et al., 2019).

16 **Figure 11-1.** MDA8 O<sub>3</sub> measured by the Clark County regulatory monitors on two of the three  
17 NAAQS exceedance days that occurred during the 2013 LVOS field campaign: (a) May 25, and  
18 (b) June 21. The white square and triangle show the locations of NLVA and Angel Peak,  
19 respectively.

20  
21 **Figure 11-2.** MDA8 O<sub>3</sub> measured by the Clark County regulatory monitors on days with multiple  
22 exceedances during FAST-LVOS. The white squares and triangles show the locations of the NOAA  
23 measurement sites at NLVA and AP, respectively.

24  
25 **Figure 11-3.** NCEP North American Reanalysis (NARR) 300 hPa geopotential anomalies during  
26 (a) LVOS, and (b) FAST-LVOS field campaigns. Plots provided by the NOAA/ESRL Physical  
27 Sciences Division (PSD).

28  
29 **Figure 11-4.** MDA8 O<sub>3</sub> measured by the Clark County DAQ monitor at Jean for the years (a)  
30 2013 and (b) 2017. The measurements from 2012-2016 shown in Figure 2-2 are plotted in gray.  
31 The horizontal dashed line marks the 70 ppbv NAAQS. May and June lie between the two  
32 vertical dotted lines.

33  
34 **Figure 11-5.** Mean May-June MDA8 O<sub>3</sub> measured at Jean plotted with the Niña 3.4 index  
35 ([https://www.esrl.noaa.gov/psd/gcos\\_wgsp/Timeseries/Nino34/](https://www.esrl.noaa.gov/psd/gcos_wgsp/Timeseries/Nino34/)).

36

1 **LIST OF TABLES**

2 **Table 4-1.** Mobile laboratory payload during FAST-LVOS

3

4 **Table 4-2.** NOAA/ESRL/GMD ozonesonde launch times

5

6 **Table 4-3.** Scientific Aviation research flights during FAST-LVOS

7

8 **Table 7-1.** MDA8 O<sub>3</sub> on high ozone days during FAST-LVOS

9

10 **Table 11-1.** Four highest O<sub>3</sub> days at the Clark County regulatory monitors in 2013

11

12 **Table 11-2.** Four highest O<sub>3</sub> days at the Clark County regulatory monitors in 2017

13

14

1 **Abstract**

2 The Fires, Asian, and Stratospheric Transport-Las Vegas Ozone Study (FAST-LVOS) was  
3 conducted in the late spring and early summer of 2017 to investigate the impact of transported  
4 ozone (O<sub>3</sub>) originating from non-controllable sources on surface concentrations in Clark County,  
5 NV, including the greater Las Vegas area. This 6-week (May 17-June 30) study built on the  
6 findings of the first Las Vegas Ozone Study (LVOS), which brought a more limited measurement  
7 suite to Clark County in May and June of 2013. FAST-LVOS brought an improved version of the  
8 TOPAZ lidar and a micro-Doppler lidar to the North Las Vegas Airport (NLVA), and deployed a  
9 mobile laboratory with in-situ measurements of NO, NO<sub>x</sub>, NO<sub>y</sub>, CO, CO<sub>2</sub>, CH<sub>4</sub>, N<sub>2</sub>O, and O<sub>3</sub> to  
10 Angel Peak in order to investigate the interannual variability of these transport processes, and  
11 more closely examine the influence of wildfires on surface O<sub>3</sub> in Clark County. The quasi-  
12 continuous lidar and in-situ measurements were supplemented by ozonesondes and aircraft  
13 sampling during 4 intensive operating periods (IOPS). In this report, we summarize these  
14 measurements and assess the impact of non-controllable ozone sources (NCOS) on surface O<sub>3</sub>  
15 and NAAQS attainment during the 6-week campaign, and compare the FAST-LVOS results to the  
16 earlier LVOS campaign. The measurements were augmented by a variety of models including  
17 the NOAA/NESDIS RAQMS model, the NOAA/ESRL/GSD RAP-Chem and HRRR-smoke models,  
18 and the FLEXPART particle dispersion model. Our analyses are also compared to the global  
19 model analyses conducted by NOAA GFDL and Princeton University under a separate contract.  
20 In this report, we summarize the FAST-LVOS measurements, and use these measurements  
21 together with model analyses to assess the contributions of transported ozone to surface  
22 concentrations in the Las Vegas Valley and greater Clark County in the late spring and summer  
23 of 2017. We show that this finding is consistent with previous findings on the impact of ENSO  
24 on stratosphere-to-troposphere transport in the western U.S.

25  
26  
27  
28  
29  
30

## 1 **Executive Summary**

2  
3 The Fires, Asian, and Stratospheric Transport-Las Vegas Ozone Study (FAST-LVOS) was  
4 conducted over a 6-week interval (May 17-June 30) in the late spring and early summer of 2017  
5 to investigate the impact of transported ozone (O<sub>3</sub>) on surface concentrations in Clark County,  
6 Nevada. FAST-LVOS built on the findings from the 2013 Las Vegas Ozone Study (LVOS), which  
7 deployed the truck-based TOPAZ (Tunable Optical Profiler for Aerosols and oZone) lidar along  
8 with in-situ O<sub>3</sub> and CO measurements from the NOAA ESRL Chemical Sciences Division to the  
9 Clark County communications facility on Angel Peak, but brought a much larger suite of  
10 instrumentation to Clark County.

11  
12 The primary goals of FAST-LVOS were:

- 13  
14 • Assess the representativeness of the 2013 LVOS measurements and better quantify the  
15 contributions of stratospheric intrusions and Asian pollution to surface ozone in Clark  
16 County.
- 17  
18 • Estimate the importance of these sources relative to wildfires and regional pollution.
- 19  
20 • Investigate the processes by which ozone is transported downward from the free  
21 troposphere to the surface.

22  
23 FAST-LVOS brought a much larger suite of instrumentation to Clark County including the  
24 upgraded TOPAZ lidar which was deployed to the Clark County Department of Air Quality  
25 measurement site at the North Las Vegas Airport (NLVA). A continuously operating vertically-  
26 staring micro-Doppler lidar was also deployed to the NLVA to measure boundary layer heights  
27 and vertical winds and mixing. The TOPAZ lidar acquired data on all 45 days of the field  
28 campaign, operating for a total of 523 hours or an average of nearly 12 hours per day.  
29 NOAA/ESRL/CSD also deployed a mobile laboratory with nearly continuous sampling of NO,  
30 NO<sub>x</sub>, NO<sub>y</sub>, CO, CO<sub>2</sub>, CH<sub>4</sub>, N<sub>2</sub>O, and O<sub>3</sub> to the summit of Angel Peak.

31  
32 The daily lidar and in-situ measurements were supplemented by ozonesondes launched near  
33 the Clark County Joe Neal monitoring site, and airborne sampling from a single engine aircraft  
34 operating out of the NLVA during 4 intensive operating periods (IOPs). Personnel from  
35 NOAA/ESRL/GMD launched a total of 30 ozonesondes over 13 days (1-4 per day) and the  
36 Scientific Aviation Mooney TLS Bravo logged about 90 hours over 15 days during the 4 FAST-  
37 LVOS IOPs. The IOPs were conducted when synoptic conditions appeared conducive to the  
38 formation of stratospheric intrusions above the Western U.S.

39  
40 Planning for the IOPs relied on forecasts from the NCEP Global Forecast System (GFS)) and the  
41 NOAA/ESRL/GSD RAP-Chem and NOAA/NESDIS RAQMS models, and interpretation of the  
42 measurements was aided by the FLEXPART particle dispersion model and the NOAA GFDL AM4  
43 model. The AM4 modelling was directly supported by Clark County under a separate project  
44 (CBE605334-19) and is described in more detail within a separate report.

1  
2 The FAST-LVOS measurements found high levels of O<sub>3</sub> between 4 and 6 km in the free  
3 troposphere above Clark County on nearly all of the 45 measurement days. The measurements  
4 and model analyses show that the O<sub>3</sub> aloft originated primarily from stratospheric intrusions,  
5 transported Asian pollution, and wildfire plumes. Entrainment of free tropospheric O<sub>3</sub> layers  
6 into the mixed layer was directly observed on multiple occasions, confirming the hypothesis  
7 inferred from the LVOS 2013 measurements.

8  
9 The 2015 NAAQS of 70 ppbv was equaled or exceeded by one or more of the Clark County  
10 Department of Air Quality monitors on 10 of the 45 FAST-LVOS measurement: May 23(1), June  
11 3, (1), June 14(2), June 16(3) and 17(3), June 22(4) and 23(3), and June 28(2), 29(1), and 30(3),  
12 where the numbers in parentheses show the number of affected monitors. Our analyses  
13 suggest that transported pollution played a role in at least half of these exceedances. We found  
14 that Asian pollution may have contributed to the exceedance on June 3, and the major  
15 stratospheric intrusion that passed over Clark County on June 11-13 contributed to the total  
16 background O<sub>3</sub> concentrations of 45-50 ppbv that comprised the bulk of the 62-73 ppbv  
17 measured in the Las Vegas Valley on June 14. Our analyses also show that wildfires played a  
18 major role in the exceedances of June 22, 23, and 28, and may also have contributed to the high  
19 ozone on June 29, and 30.

20  
21  
22

1 **Definitions and Abbreviations**

2

3	<b>agl</b>	above ground level
4	<b>asl</b>	above mean sea level
5	<b>AS</b>	Asian
6	<b>BB</b>	biomass burning
7	<b>CC</b>	Clark County
8	<b>CIMSS</b>	Cooperative Institute for Meteorological Satellite Studies
9	<b>CIRES</b>	Cooperative Institute for Research in Environmental Sciences
10	<b>CSD</b>	Chemical Sciences Division
11	<b>DAQ</b>	Department of Air Quality
12	<b>ESRL</b>	Earth System Research Laboratory
13	<b>FAST-LVOS</b>	Fires, Asian, and Stratospheric Transport- Las Vegas Ozone Study
14	<b>GFDL</b>	Geophysical Fluid Dynamics Laboratory
15	<b>GFS</b>	Global Forecasting System
16	<b>GMD</b>	Global Monitoring Division
17	<b>GSD</b>	Global Systems Division
18	<b>HRRR</b>	High-resolution rapid refresh
19	<b>IOP</b>	Intensive operating period
20	<b>LVOS</b>	Las Vegas Ozone Study
21	<b>LVV</b>	Las Vegas Valley
22	<b>MDA8</b>	daily maximum 8-h average
23	<b>NARR</b>	North American Reanalysis
24	<b>NCEP</b>	National Centers for Environmental Prediction
25	<b>NCOS</b>	non-controllable ozone source
26	<b>NESDIS</b>	National Environmental Satellite, Data, and Information Service
27	<b>NOAA</b>	National Oceanic and Atmospheric Administration
28	<b>NPS</b>	National Park Service
29	<b>RAP-Chem</b>	Rapid refresh with chemistry
30	<b>RAQMS</b>	Realtime Air Quality Modeling System
31	<b>NAAQS</b>	National Ambient Air Quality Standard
32	<b>ppbv</b>	parts-per-billion-by-volume
33	<b>SMYC</b>	Spring Mountain Youth Camp
34	<b>SoCAB</b>	South Coast Air Basin
35	<b>ST</b>	stratospheric
36	<b>STT</b>	stratosphere-to-troposphere transport
37	<b>TOPAZ</b>	Tunable Optical Profiler for Aerosols and oZone
38	<b>UT/LS</b>	upper troposphere/lower stratosphere
39	<b>WRCC</b>	Western Regional Climate Center
40		

## 1 1. Introduction

2  
3 High concentrations of ozone (O<sub>3</sub>) are harmful to human health [*U.S. Environmental Protection Agency, 2014*] and impair plant growth and productivity [*Avnery et al., 2011a; b*]. The U.S. Clean Air Act (CAA) accordingly designated ground-level ozone a criteria pollutant and established  
4  
5 primary and secondary National Ambient Air Quality Standards (NAAQS) to protect human  
6  
7 health and welfare, respectively. Compliance with the CAA requires that the design value (DV),  
8  
9 i.e. the 3-yr running average of the 4<sup>th</sup> highest maximum daily 8-h average mixing ratio (MDA8)  
10  
11 O<sub>3</sub> concentration measured annually within an air basin, to be less than or equal to the NAAQS.  
12  
13 The CAA also requires that the NAAQS be reviewed periodically to consider the latest research  
14  
15 on the health effects, and adjusted, if necessary, to ensure an adequate margin of safety for the  
16  
17 public. The primary and secondary NAAQS for ozone were lowered from 75 to 70 parts-per-  
18  
19 billion by volume (ppbv) for the in October 2015 following the most recent such review [*U.S.*  
20  
21 *Environmental Protection Agency, 2015*].

22  
23 Ozone is a secondary pollutant formed by photochemical reactions between nitrogen oxides  
24  
25 (NO<sub>x</sub>) and volatile organic compounds (VOCs) emitted by both natural and anthropogenic  
26  
27 sources. Surface O<sub>3</sub> has declined across much of the U.S. over the last two decades as more  
28  
29 stringent emission controls have led to substantial reductions in anthropogenic NO<sub>x</sub> precursors  
30  
31 [*Gaudel et al., 2018*]. The mean DV for the contiguous U.S. decreased by 17% from 82 to 67  
32  
33 ppbv between 2000 and 2017 (<https://www.epa.gov/air-trends/ozone-trends#ozreg>). The  
34  
35 largest declines occurred in the Southeastern (83 to 62 ppbv or 26% at 145 sites) and South-  
36  
37 Central (87 to 66 ppbv or 24% at 104 sites) U.S., with much smaller changes in the West (82 to  
38  
39 75 ppbv or 8% at 143 sites) and Southwest (77 to 72 ppbv or 7% at 58 sites)<sup>1</sup>. The 4<sup>th</sup> highest  
40  
41 MDA8 O<sub>3</sub> concentrations measured in the West (California and Nevada) and Southwest  
42  
43 (Arizona, New Mexico, Utah and Colorado) during 2017 were higher than those measured in  
44  
45 any other region of the U.S.

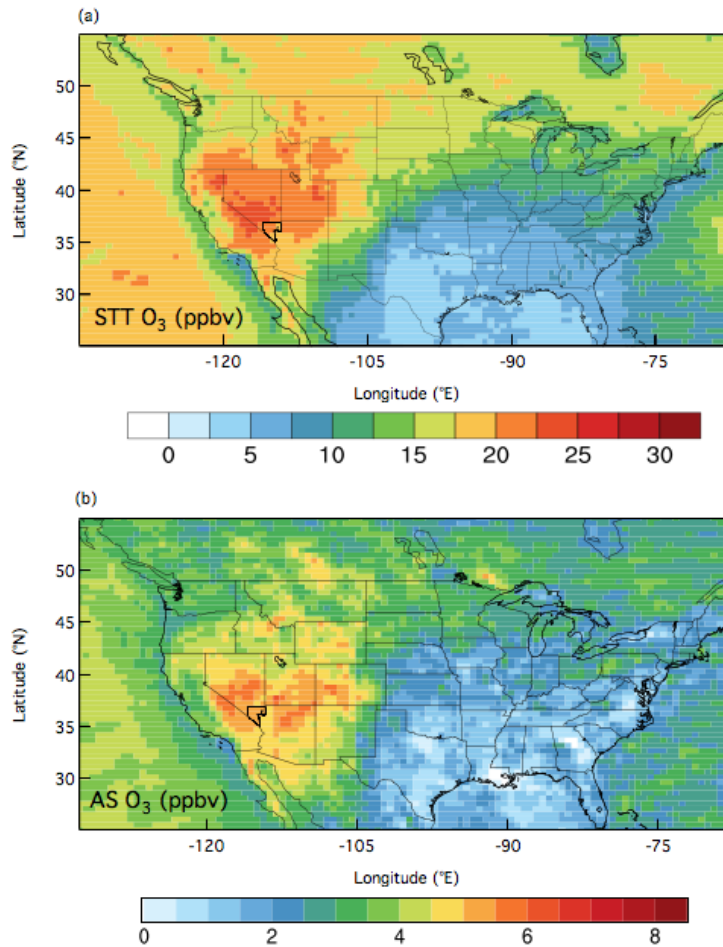
46  
47 The weaker response of ground-level O<sub>3</sub> to declining NO<sub>x</sub> emissions in the western U.S. can be  
48  
49 explained, at least in part, by the presence of much higher background concentrations [*Jaffe et*  
50  
51 *al., 2018*]. Ozone is the only one of the six criteria pollutants (CO, NO<sub>2</sub>, SO<sub>2</sub>, O<sub>3</sub>, Pb, and  
52  
53 particulate matter) with a significant background in the troposphere. This background is  
54  
55 created primarily by downward transport of O<sub>3</sub> from the stratosphere or production of O<sub>3</sub> by  
56  
57 reactions of NO<sub>x</sub> and VOCs from non-anthropogenic sources such as lightning, wildfires, soils,  
58  
59 and vegetation. Since O<sub>3</sub> is relatively long-lived in the free troposphere (≈1 month), the  
60  
61 concentrations measured at any given location may include O<sub>3</sub> formed from natural or  
62  
63 anthropogenic precursors emitted hundreds or thousands of kilometers upwind and even a  
64  
65 small amount of O<sub>3</sub> formed from local or regional precursors that has circumnavigated the  
66  
67 globe.

68  
69 The high western background can be explained by several factors. First, the Southwestern U.S is  
70  
71 a global hotspot for deep tropopause folds [*James et al., 2003; Langford et al., 2012; Skerlak et*

---

<sup>1</sup> The 2000-2017 decline in Las Vegas (78 to 71 ppbv, or about 9%) was similar to the rest of the Southwest

1 *al.*, 2014; Sprenger and Wernli, 2003; Wernli and Bourqui, 2002], intrusions of lower  
2 stratospheric air that penetrate to within 3 km of the ground. These folds are created by jet  
3 streaks in the winds circulating around mid-latitude cyclones and stratosphere-to-troposphere  
4 transport (STT) peaks in late spring when cyclonic activity is still high and the O<sub>3</sub> content of the  
5 lower stratosphere at a maximum. Second, many intrusions entrain wildfire or pollution plumes  
6 transported across the Pacific Ocean from Asia as they descend through the troposphere and  
7 bring this O<sub>3</sub>-enriched air toward the surface with them. Finally, the high average elevation of  
8 the Southwest and Intermountain West increase the likelihood that descending O<sub>3</sub>-rich air will  
9 reach the surface. Global model simulations (**Figure 1-1**) show the largest influxes of  
10 stratospheric O<sub>3</sub> and Asian pollution are in the Intermountain West including Clark County, NV.  
11

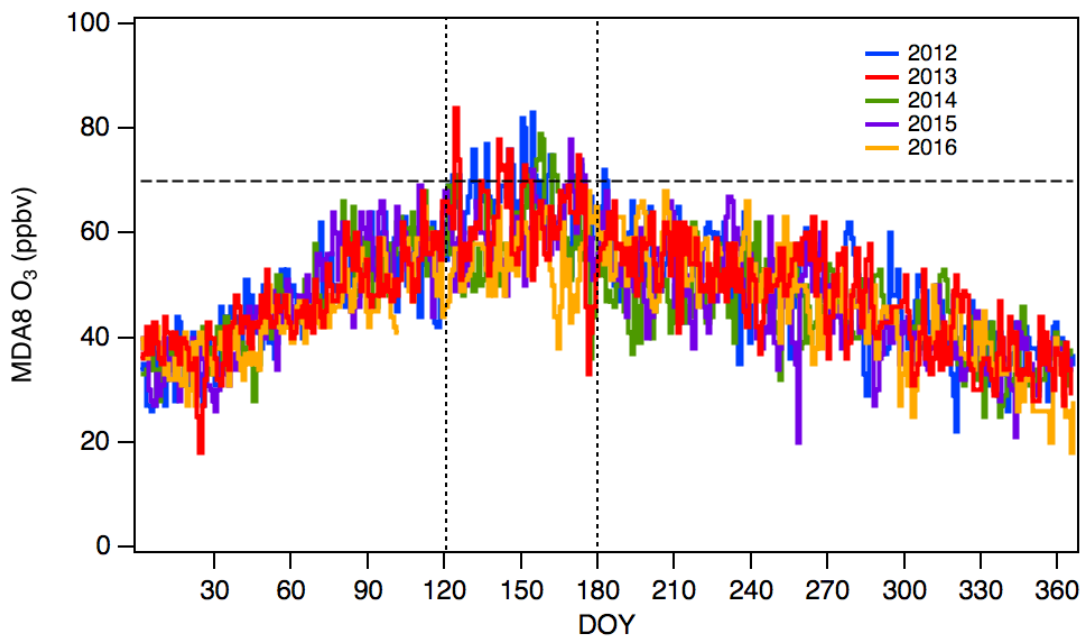


12  
13  
14 **Figure 1-1.** Mean contributions (in ppbv) of (a) STT, and (b) Asian pollution, to MDA8 surface O<sub>3</sub>  
15 calculated by the NOAA GFDL AM3 model for May and June 2010. The resolution is 50 km x 50  
16 km. Note the different color scales. Clark County, NV is outlined in black. Adapted from [Lin et  
17 *al.*, 2012a; Lin et al., 2012b].

18  
19  
20



1 Photochemical production of O<sub>3</sub> depends primarily on sunlight and high temperatures, and  
2 measurements in the LA Basin accordingly show a broad O<sub>3</sub> peak in midsummer. Some of this  
3 O<sub>3</sub> must be transported inland by the prevailing southwesterly winds along the West Coast and  
4 it might be expected that measurements in rural areas of the Desert Southwest would also  
5 show a midsummer peak, particularly since long-range transport of O<sub>3</sub> and other pollutants  
6 from the LA Basin in the lower free troposphere begins with thermally driven orographic lifting  
7 by the mountain ranges surrounding the Basin. Surprisingly, however, five years (2012-2016) of  
8 measurements from the southernmost Clark County monitor at Jean, which lies between Los  
9 Angeles and Las Vegas (cf. **Figure 2-1b**) show that the highest concentrations are typically  
10 measured earlier during May and June (**Figure 2-2**). Similar patterns are found in the  
11 measurements at many of the remote USNPS sites surrounding Clark County (cf. **Figure 2-1**).  
12



13  
14  
15 **Figure 2-2.** MDA8 O<sub>3</sub> measured by the Clark County DAQ monitor at Jean in southwestern Clark  
16 County for the years 2012-2016. The horizontal dashed line marks the 70 ppbv NAAQS. May and  
17 June lie between the two vertical dotted lines.  
18

19 The late spring peak in **Figure 2-2** coincides with the time of year when transport of O<sub>3</sub> from  
20 Asia and the lower stratosphere is greatest. The apparent connection between STT and high  
21 springtime O<sub>3</sub> in Clark County motivated Dr. Zheng Li of the Clark County Department of Air  
22 Quality to propose the Las Vegas Ozone Study (LVOS), which was subsequently conducted in  
23 the late spring and early summer of 2013 [Langford et al., 2015b]. The NOAA/ESRL/CSD  
24 deployed the Tunable Optical Profiler for Aerosol and oZone (TOPAZ) mobile lidar and in-situ  
25 CO and O<sub>3</sub> measurements to the Clark County communications facility on the summit of Angel  
26 Peak (2.7 km asl) about 45 km northwest of Las Vegas in the Spring Mountains [Langford et al.,  
27 2015b].

1 The study lasted for a period of 6 weeks (May 20 to June 28) during which TOPAZ detected  
2 numerous layers of high O<sub>3</sub> between 4 and 6 km asl consistent with intrusions of lower  
3 stratospheric air with or without admixed Asian pollution [Langford et al., 2018], and the direct  
4 descent of one of these intrusions to the summit of Angel Peak coincided with a simultaneous  
5 increase in surface O<sub>3</sub> and decrease in CO and H<sub>2</sub>O. This interpretation was supported by  
6 simulations from the NOAA GFDL AM3 global model and the FLEXPART particle dispersion  
7 model.

8 On three occasions, the appearance of high O<sub>3</sub> layers above Angel Peak during LVOS were  
9 followed by exceedances of the 2008 (75 ppbv) NAAQS in the Las Vegas Valley the next day,  
10 suggesting [Langford et al., 2017] that the elevated layers were entrained and mixed to the  
11 surface in the LVV by the exceptionally deep convective mixed layers that form above the  
12 Mojave Desert [Seidel et al., 2012].

### 13 14 **3. The Fires, Asian, and Stratospheric Transport-Las Vegas Ozone Study (FAST-LVOS)** 15

16 The FAST-LVOS measurement campaign was designed primarily to assess the  
17 representativeness of the 2013 LVOS findings and test the entrainment hypothesis [Langford et  
18 al., 2017]. Another important goal was to better quantify how the contributions of STT and  
19 Asian pollution compare to other sources including local photochemical production, wildfires,  
20 and regional transport from California. A third goal was to examine the interannual variability of  
21 deep STT in the U.S. Southwest, which is influenced by ENSO [Lin et al., 2015] and other large-  
22 scale circulations [Albers et al., 2018].

23  
24 FAST-LVOS brought a greatly expanded suite of measurements to Clark County, including a core  
25 set of lidar and in-situ instruments based at the North Las Vegas Airport (NLVA) and Angel Peak  
26 (AP), respectively, that operated throughout the campaign (May 17 to June 30, 2017). These  
27 core measurements complemented the routine measurements from the Clark County DAQ  
28 monitoring network, and were supplemented by ozonesonde and aircraft sampling during four  
29 2-to-4 day long intensive operating periods (IOPs) called when the synoptic conditions  
30 appeared favorable to the formation of tropopause folds above the western U.S.

31  
32 Daily measurements of ozone and backscatter profiles were made by TOPAZ and a vertically-  
33 staring Doppler lidar, which also measured vertical wind speed and variance. These lidars were  
34 co-located at the NLVA with the Clark County DAQ profiling radiometer and wind profiler.  
35 Nearly continuous in-situ measurements of NO, NO<sub>x</sub>, NO<sub>y</sub>, CO, CO<sub>2</sub>, CH<sub>4</sub>, N<sub>2</sub>O, and O<sub>3</sub> were  
36 made by mobile sampling laboratory that primarily remained on Angel Peak.

37 These measurements from NOAA/ESRL/CSD were augmented by ozonesondes from  
38 NOAA/ESRL/GMD launched ≈7.3 km NW of TOPAZ at the Estelle Neal park adjacent to the  
39 CCDAQ Joe Neal monitoring site, and by aircraft sorties between NLVA and Big Bear, CA by the  
40 Scientific Aviation Mooney single engine research aircraft during the IOPs.

41

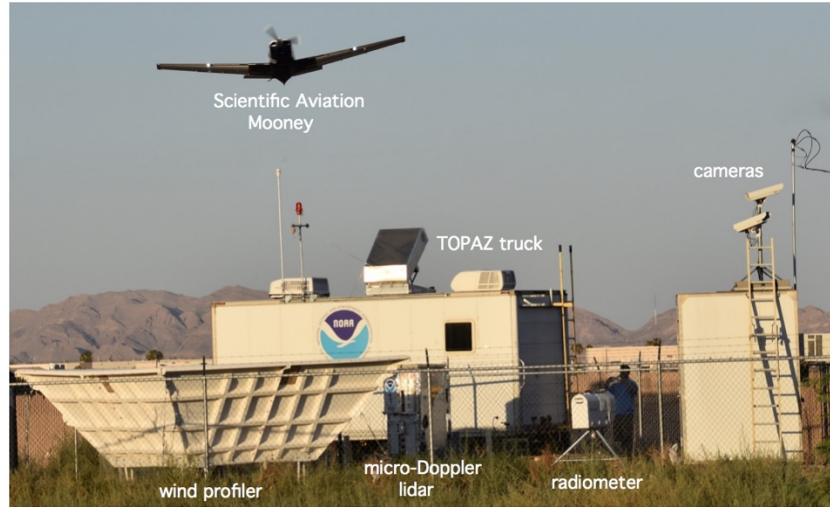
1 The FAST-LVOS study relied on several atmospheric models and tools for forecasting and  
2 planning during the measurement campaign, and for interpretation of the measurements  
3 afterwards. The former group included both operational (e.g. NCEP Global Forecast System  
4 (GFS)) and “quasi-operational” models (e.g. RAP-Chem () and RAQMS ()). The GFS forecasts and  
5 NWS radiosonde profiles were obtained from the Wyoming Weather Web maintained by the  
6 University of Wyoming (<http://weather.uwyo.edu/index.shtml>). The NOAA HRRR-smoke model  
7 () was also used to assess wildfire influences. We also made use of NOAA satellite products  
8 archived by the Cooperative Institute for Research in the Atmosphere (CIRA) at the Colorado  
9 State University (<http://rammb.cira.colostate.edu/ramsd/online/index.asp>) for forecasting  
10 purposes. The post-campaign analysis relied heavily on the FLEXPART particle dispersion model  
11 and the NOAA GFDL AM4 model. The NOAA GFDL AM4 modeling efforts were directly  
12 supported by Clark County (CBE605334-19) and are described in detail in a separate report.  
13

#### 14 **4. FAST-LVOS Measurement Suite**

15

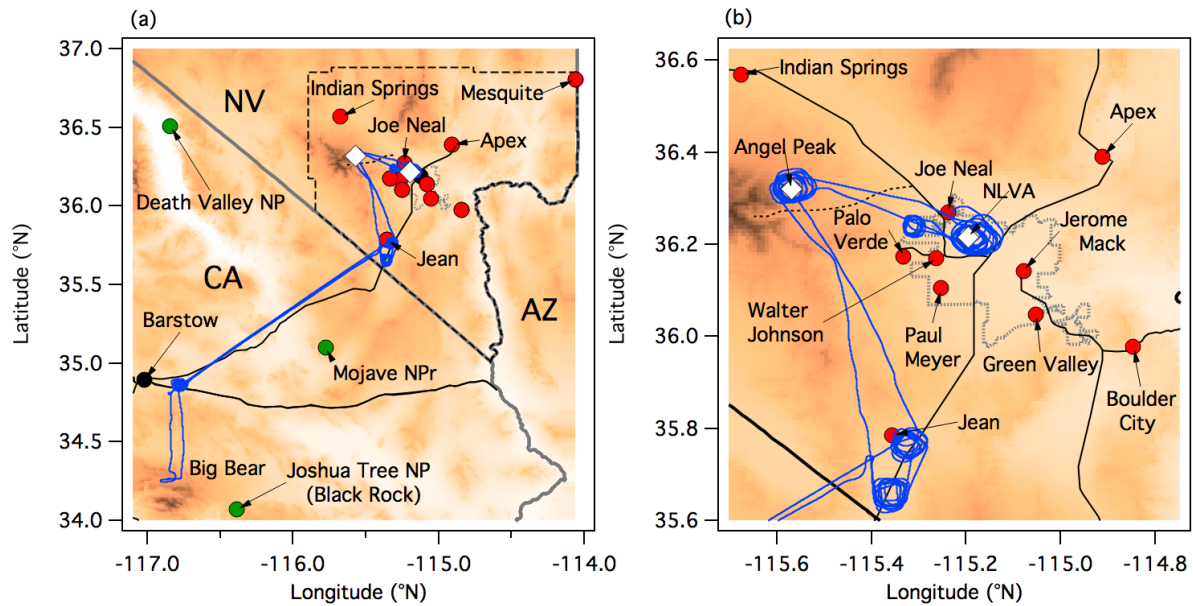
16 The FAST-LVOS field campaign was based primarily at the North Las Vegas Airport (36.2°N, -  
17 115.2°E, 681 m asl), which hosted the NOAA TOPAZ and micro-Doppler lidars (**Figure 4-1**).  
18 These instruments were deployed within the Clark County DAQ enclosure near the radar wind  
19 profiler and profiling radiometer comprising the CCDAQ Integrated Upper-Air Station  
20 ([http://airquality.clarkcountynv.gov/cgi-bin/DAQ/RAOB\\_charts.pl](http://airquality.clarkcountynv.gov/cgi-bin/DAQ/RAOB_charts.pl)). The Scientific Aviation  
21 Mooney TLS Bravo aircraft operated out of the NLVA during the FAST-LVOS IOPs and the  
22 NOAA/ESRL/GMD Ozonesondes were launched adjacent to the nearby (7 km) Joe Neal  
23 monitoring station. The NOAA mobile laboratory spent most of the campaign on the summit of  
24 Angel Peak (Appendix C) where TOPAZ was located during the first LVOS campaign. **Figure 4-2**  
25 shows these sites along with the regulatory O<sub>3</sub> monitors operated by Clark County and other  
26 agencies, and the June 28 flight track of the Mooney.  
27

28 The daily lidar and in-situ measurements at NLVA and Angel Peak were supplemented by  
29 ozonesonde and aircraft measurements during four IOPs (May 23-25, May 31-June 2, June 10-  
30 14, and June 28-30). These intensives were conducted during periods when the synoptic  
31 conditions appeared favorable for the development of tropopause folds above the western U.S.  
32 Planning for the IOPs relied primarily on the NCEP Global Forecast System (GFS) long range  
33 weather forecasts obtained from the University of Wyoming  
34 (<http://weather.uwyo.edu/models/fcst/gfs003.shtml>) and NOAA RAP-Chem  
35 (<https://rapidrefresh.noaa.gov/RAPchem/>) and RAQMS (<http://raqms-ops.ssec.wisc.edu/>)  
36 models which were reviewed daily by the FAST-LVOS Principal Investigator. The ozonesonde  
37 and aircraft teams were typically alerted 48 to 72 hours before the start of the IOP.  
38



1  
2  
3  
4  
5  
6  
7  
8  
9

**Figure 4-1.** The Scientific Aviation Mooney makes a low overpass of the NLVA measurement site. The NOAA TOPAZ lidar truck and micro-Doppler lidar can be seen in the background behind the Clark County DAQ radar wind profiler, profiling radiometer, and visibility cameras. The 2B ozone monitor sampling mast is seen to the left of the red warning light on top of the TOPAZ truck. Sunrise Mountain can be seen just above the wind profiler (photo by A.O. Langford)



10  
11  
12  
13  
14  
15  
16  
17

**Figure 4-2.** Topographical maps showing the FAST-LVOS measurement domain. The filled red, green, and black circles locate the regulatory O<sub>3</sub> monitors operated by Clark County, the U.S. National Park Service, and the State of California, respectively. The white diamonds show the FAST-LVOS measurement sites at NLVA and AP. The blue trace shows the Scientific Aviation flight track from June 28, 2017.

#### 4.1 NOAA TOPAZ ozone and aerosol lidar

The truck-mounted NOAA/ESRL/CSD TOPAZ mobile differential absorption lidar (DIAL) system was located at the North Las Vegas Airport (NLVA) for the duration of the FAST-LVOS campaign. TOPAZ was originally developed for profiling O<sub>3</sub> and particulate backscatter in the boundary layer and lower free troposphere from NOAA Twin Otter aircraft [Alvarez *et al.*, 2011; Langford *et al.*, 2012; Langford *et al.*, 2010; Langford *et al.*, 2011; Senff *et al.*, 2010]. The lidar was reconfigured and installed in a medium-duty 4-wheel drive truck after CalNex, and subsequently deployed in this configuration to several field campaigns including the 2013 Las Vegas Ozone Study (LVOS) [Langford *et al.*, 2015b].

Improvements in the TOPAZ data acquisition system during 2015 greatly extended the operational range of TOPAZ from the 2.5 to 3 km available during LVOS, to 6-8 km during the 2016 CABOTS [Faloona *et al.*, 2019] and 2017 FAST-LVOS campaigns. This improvement allowed the deployment of the lidar at the lower elevation NLVA site without any loss in altitude coverage compared to LVOS.

The TOPAZ lidar uses a low energy ( $\approx 50 \mu\text{J}$ ), high pulse rate (1 kHz) quadrupled Nd:YLF pumped Ce:LiCAF laser that is re-tuned between each pulse to generate light at three different wavelengths ranging from 287 to 294 nm reducing the effective repetition rate to 333 Hz [Alvarez *et al.*, 2011]. The low pulse energies and tunability of TOPAZ allow the system to be operated from airports and other locations where eye safety is a major concern and facilitate optimization of the wavelengths for lower tropospheric measurements. The laser pulses are transmitted and backscatter signals collected by a zenith viewing coaxial transmitter/receiver beneath an opening in the truck roof. A large scanning mirror inserted above the transceiver allows profile measurements at different slant angles. These slant profiles can be combined to create vertical profiles that begin much closer to the ground than conventional vertically staring lidar systems [Proffitt and Langford, 1997]. During FAST-LVOS, the scanning mirror was moved sequentially between elevation angles of 90, 20, 6, and 2° with a 225-s averaging time at 90° and 75-s averaging times at the other 3 angles. The cycle was repeated approximately every 8 minutes and the vertical projections combined to create a composite vertical profile beginning  $27.5 \pm 5$  m above ground level (agl).

In addition to the lidar, the TOPAZ truck is equipped with an *in-situ* O<sub>3</sub> monitor (2B Technologies Model 205) that samples air 5 m above the surface and an Airmar 150WX weather station to measure temperature, pressure, relative humidity, and wind speed and direction.

The O<sub>3</sub> and aerosol profiles were computed using the iterative technique described in [Alvarez *et al.*, 2011]. The O<sub>3</sub> profiles were retrieved using the longest and shortest wavelengths ( $\approx 287$  and 294 nm) with 30 m range gates and a smoothing filter with a varying width that increased from 270 m at the minimum range (800 m) up to 1400 m at the maximum range (8 km). The aerosol backscatter and extinction wavelength dependences, which are needed to correct differential aerosol effects in the O<sub>3</sub> calculation, are assumed to follow a power law. In most cases, a power-law exponent of 0 (no wavelength dependence) was used for the aerosol

1 backscatter with an exponent of -0.5 for aerosol extinction. These values seem to be a good  
2 compromise for a wide range of aerosol types [Völger *et al.*, 1996]. In the second iteration step,  
3 O<sub>3</sub> profiles are computed with an aerosol correction based on the aerosol backscatter and  
4 extinction profiles from the first step. These O<sub>3</sub> profiles are then used to provide a more  
5 accurate O<sub>3</sub> extinction correction of the signal data at 294 nm, which in turn results in more  
6 accurate aerosol profile retrieval. This iteration procedure is repeated until the O<sub>3</sub> profiles  
7 produced in successive iteration steps converge. Convergence is reached when the absolute  
8 difference between successive O<sub>3</sub> profiles is less than  $2.5 \times 10^{15} \text{ m}^{-3}$  (corresponding to about  
9 0.1 ppbv) at all range gates.

10  
11 The DIAL calculations used the temperature dependent O<sub>3</sub> absorption cross-sections from  
12 Malicet *et al.* [Malicet *et al.*, 1995]. The National Centers for Environmental Prediction (NCEP)  
13 North American Regional Reanalysis (NARR) temperature and pressure profiles from the grid  
14 point closest to the TOPAZ lidar location were used to account for the temperature dependence  
15 of the O<sub>3</sub> cross sections and to convert O<sub>3</sub> number densities to mixing ratios. The 3-hourly NARR  
16 temperature and pressure profiles were interpolated to the exact time each individual O<sub>3</sub>  
17 profile was recorded. The total uncertainties in the 8-min ozone retrievals are estimated to  
18 increase from  $\pm 3$  ppbv below 4 km, to  $\pm 10$  ppbv at the top of the profile. Profiles of the  
19 backscatter from aerosols, smoke, and dust were retrieved with 7.5 m resolution at 294 nm.  
20 These unpolarized single wavelength backscatter profiles provide a semiquantitative measure  
21 of the particulate distribution, but do not distinguish between different particle types.

22  
23 An intercomparison at the 2014 Colorado DISCOVER-AQ campaign [Wang *et al.*, 2017] found  
24 that the performance of the original analog data acquisition system developed at NOAA for  
25 aircraft operations in 2004 had deteriorated. This system was accordingly replaced with a new  
26 commercial dual analog/photon counting system prior to CABOTS. This upgrade improved the  
27 stability of the lidar retrievals and greatly expanded the useful altitude range of TOPAZ  
28 compared to earlier studies. The maximum altitude achieved during CABOTS ranged from  
29  $\approx 6$  km during the day to more than 8 km at night depending on the lidar return signal-to-noise  
30 ratios, which varied with laser power, atmospheric extinction, and solar background light.  
31 The improved performance was verified during the California Baseline Ozone Transport Study  
32 (CABOTS) conducted in the summer of 2016 [Langford *et al.*, 2019] and the TOLNet multi-lidar  
33 Southern California Ozone Observation Project (SCOOP) intercomparison at the NASA Jet  
34 Propulsion Laboratory (JPL) Table Mountain Facility (TMF) in the San Gabriel Mountains  
35 immediately after CABOTS [Leblanc *et al.*, 2018].

## 36 37 **4.2 NOAA micro-Doppler lidar**

38  
39 The autonomous micro-Doppler lidar ( $\mu$ DL) used during FAST-LVOS was developed by the  
40 NOAA/ESRL Atmospheric Remote Sensing Group in 2016 and field tested in Visalia, CA during  
41 the CABOTS campaign [Faloona *et al.*, 2019]. This near-infrared eye safe coherent lidar  
42 determines wind speeds from phase shifts in the light backscattered from moving aerosol  
43 particles [Grund *et al.*, 2000]. The  $\mu$ DL was installed adjacent to the CCDAQ radar wind profiler

1 during FAST-LVOS (**Figure 4-3**) and operated in a vertically-staring mode to continuously  
2 measure vertical wind velocities above the NLVA. The variance in the vertical velocities was  
3 then used in conjunction with the aerosol backscatter to infer boundary layer heights and  
4 mixing [*Bonin et al., 2017; Tucker et al., 2009*].  
5  
6  
7



8  
9  
10  
11  
12  
13

**Figure 4-3.** The NOAA autonomous micro-Doppler lidar stands on the former RASS pad adjacent to the TOPAZ lidar truck. (photo by A.O. Langford)

### 4.3 NOAA mobile sampling laboratory

The Chemical Sciences Division also brought a van-based mobile laboratory ([https://esrl.noaa.gov/csd/groups/csd7/measurements/csd\\_mobilelab/](https://esrl.noaa.gov/csd/groups/csd7/measurements/csd_mobilelab/)) for in-situ measurements to FAST-LVOS [Wild *et al.*, 2017] (**Figure 4-4**). The van was outfitted with instrumentation to measure O<sub>3</sub>, CO, CO<sub>2</sub>, CH<sub>4</sub>, NO, NO<sub>2</sub>, NO<sub>y</sub>, N<sub>2</sub>O, H<sub>2</sub>O, and meteorological parameters during FAST-LVOS (**Table 4-1**). All of the measurements can be made while moving with 1-s sampling, but the van can also be connected to external power for stationary operations. The van stayed on Angel Peak (**Figure 4-5**) during most of the study, but also executed a series of Angel Peak-Lee Canyon-Kyle Canyon drives on May 24-25, and relocated to the NLVA for an intercomparison with the SA Mooney on June 15 (**Figure 4-6**).



**Figure 4-4.** Jeff Peischl of NOAA/ESRL/CSD and CIRES works on the mobile lab instrumentation at Angel Peak (photo by A.O. Langford).

The in-situ measurements of O<sub>3</sub>, CO, and H<sub>2</sub>O made at Angel Peak during LVOS provided a simple matrix to help identify air mass origins. Ozone derives from both tropospheric and stratospheric sources, but CO and H<sub>2</sub>O originate at the earth's surface and have greatly decreased concentrations in the stratosphere. Thus, air descending from the upper troposphere/lower stratosphere (UT/LS) leads to enhancements in surface O<sub>3</sub> that are coupled with sharp decreases in CO and H<sub>2</sub>O. Asian pollution plumes transported across the Pacific Ocean in the middle troposphere are nearly as dry, but typically contain elevated levels of CO. Local photochemistry and regional biomass burning plumes typically have both high CO and N<sub>2</sub>O. Marine boundary layer tends to have low O<sub>3</sub> and CO, but high H<sub>2</sub>O. The FAST-LVOS mobile

1 lab measurements provide a more complete matrix to identify different air sources.  
 2 Stratospheric air can be identified by enhancements in O<sub>3</sub> correlated with decreased CO, N<sub>2</sub>O,  
 3 and H<sub>2</sub>O since these species originate at the Earth's surface and have much lower  
 4 concentrations in the stratosphere. The NO, NO<sub>2</sub>, (NO<sub>x</sub>=NO+NO<sub>2</sub>) and NO<sub>y</sub> measurements can  
 5 be used along with CO and CO<sub>2</sub> to identify biomass burning and other combustion sources.  
 6 Methane (CH<sub>4</sub>) provides a marker for oil and gas activities. Summary plots showing the mobile  
 7 laboratory measurements are plotted in Appendix C.

8  
9

10 **Table 4-1. Mobile laboratory payload during FAST-LVOS**

11

Measured Parameter	Method	Time Resolution	Detection Limit
CO <sub>2</sub> and CH <sub>4</sub>	Wavelength scanned cavity ring-down spectroscopy	1 sec	0.2 ppmv for CO <sub>2</sub> 2 ppbv for CH <sub>4</sub>
N <sub>2</sub> O, CO, H <sub>2</sub> O	Integrated cavity output spectroscopy	1 sec.	0.2 ppb for N <sub>2</sub> O 0.2 ppb for CO 100 ppm for H <sub>2</sub> O
NO, NO <sub>2</sub> , NO <sub>y</sub> , O <sub>3</sub>	Cavity ring-down spectroscopy	1 sec	0.1 - 0.001 ppbv
O <sub>3</sub>	2B Technologies, Model 205	10 sec	≈1 ppbv
Position and Met Data	Differential GPS, Airmar Wx and Young 2-D sonic	1 sec	

12  
13  
14  
15

Ozone was measured both by cavity ringdown spectroscopy (CRDS) and by a conventional UV absorption analyzer (2B Model 205).



1  
2  
3  
4  
5  
6  
7  
8

**Figure 4-5.** Aerial view of Angel Peak from the SA Mooney showing the NOAA mobile laboratory. The TOPAZ mobile lidar was parked in the same spot during LVOS, and the LVOS in-situ measurements made from the roof of the Clark County building. (photo by D. Caputi).



9  
10  
11  
12  
13  
14  
15

**Figure 4-6.** NOAA mobile laboratory and Scientific Aviation aircraft during standards comparison at the NLVA. (photo by R. Langston)

1 **4.4 NOAA ECC ozonesondes**

2  
3 NOAA/ESRL GMD launched up to 4 electrochemical cell (ECC) [Johnson et al., 2002].  
4 ozonesondes per day (30 total) on 13 days during the 4 FAST-LVOS IOPs. The balloons were  
5 launched from the Estelle Neal Park (adjacent to the CCDAQ Joe Neal monitoring site) during  
6 the four FAST-LVOS IOPs. These balloon-borne packages combined the ozone sensor with a  
7 GPS-equipped meteorological radiosonde and transmit ozone partial pressures, pressure,  
8 temperature, relative humidity, and winds to a ground station throughout the flight. The  
9 balloons typically ascended to more than 20 km and acquired both tropospheric and  
10 stratospheric O<sub>3</sub> profiles. In some cases, useful data were also obtained during the parachute  
11 descent, although these profiles were often displaced from the launch site by 10-50 km.  
12 Although the ozonesondes lack the temporal resolution of the lidar, they can profile O<sub>3</sub> from  
13 the surface to about 30 km, along with temperature, frost point, relative humidity, and winds.  
14 These measurements provide important information about the atmospheric stability, and the  
15 frost point measurements can help distinguish upper tropospheric from lower stratospheric air.  
16  
17



18  
19  
20  
21 **Figure 4-7.** Patrick Cullis (L) and Chance Sterling (R) of NOAA/ESRL/GMD and CIRES, U. of  
22 Colorado prepare to launch one of the FAST-LVOS ozonesondes from the Estelle Neal municipal  
23 park (photo by R. Langston).

1  
 2 **Table 4-2** lists the ozonesonde launch times. Multiple launches were conducted at 3-hour  
 3 intervals: 0900, 1200, 1500, 1800 PDT. Four ozonesondes were launched on June 11 and 12  
 4 during the major stratospheric intrusion event, and one each during the last three days of the  
 5 study. All of the ozone profiles are shown in Appendix D.  
 6  
 7  
 8  
 9

10 **Table 4-2. NOAA/ESRL/GMD ozonesonde launch times**  
 11

Date	Launch 1 (PDT)	Launch 2 (PDT)	Launch 3 (PDT)	Launch 4 (PDT)
May 23	9:05	12:03		
May 24	9:03	12:01	15:12	
May 25	11:57			
May 31	9:18	12:05		
June 1	9:18	11:56	15:03	
June 2	9:14	12:09	15:01	
June 10	9:08	11:57		
June 11	8:54	11:54	14:53	17:54
June 12	9:02	11:58	14:58	17:56
June 13	8:57	12:02	15:00	
June 28	11:59			
June 29	12:03			
June 30	11:59			

12  
 13  
 14

#### 4.5 Scientific Aviation Mooney aircraft

Scientific Aviation, Inc. (<http://www.scientificaviation.com>) conducted research flights during the FAST-LVOS intensives using a single-engine Mooney TLS Bravo aircraft (**Figure 4.8**). The aircraft carried a pilot and technician, along with a 2B Technologies Model 205 O<sub>3</sub> monitor, an Aerodyne Research Cavity Attenuated Phase Shift (CAPS) NO<sub>2</sub> monitor, and a Picarro 2301f Wavelength-scanned Cavity Ring-Down Spectrometer (WS-CRDS) to measure CO<sub>2</sub>, CH<sub>4</sub>, C<sub>2</sub>H<sub>6</sub>, and H<sub>2</sub>O [Trousdel et al., 2016]. The 2B O<sub>3</sub> data were sampled every 2 s, which corresponds to a mean distance of 150 m at the typical level leg flight speed of 75 m s<sup>-1</sup>. The airborne 2B O<sub>3</sub> measurements were compared to TOPAZ lidar profiles during the California Baseline Ozone Transport Study (CABOTS) in the summer of 2016 [Langford et al., 2019].



**Figure 4-8.** Scientific Aviation 1998 Mooney TLS Bravo M20M (N2132X) on landing approach at NLVA (photo by A. Langford).

The typical research flight (cf. **Figure 4-2**) included a spiral climb to  $\approx 6$  km after takeoff from the NLVA followed by transit to Angel Peak and a spiral descent from there into the western valley. The aircraft then flew to Jean and conducted another spiral profile near the CCDAQ monitor. The aircraft then transited to the airport at Big Bear Lake, CA at various altitudes, where it landed and re-fueled. The aircraft conducted a spiral near Barstow after taking off from Big Bear and reversed the outbound flight plan on the return leg to NLVA. **Table 4-3** lists the 90 hours of Scientific Aviation research flights made during FAST-LVOS. All of the aircraft measurements are shown in Appendix E.

1  
2  
3  
4  
5  
6

**Table 4-3. Scientific Aviation research flights during FAST-LVOS**

Date	Takeoff (PDT)	Landing (PDT)	Duration (hours)
May 23	11:53	16:16	4:23
May 24	10:05	16:12	6:07
May 25	9:49	15:19	5:30
			0:00
May 31	10:15	16:19	6:04
June 1	12:13	18:27	6:14
June 2	12:30	18:47	6:17
			0:00
June 10	11:54	18:06	6:12
June 11	11:51	13:13	1:22
June 12	12:08	19:26	7:18
June 13	12:15	18:44	6:29
June 14	12:17	19:00	6:43
			0:00
June 27	12:10	18:43	6:33
June 28	12:11	18:50	6:39
June 29	12:21	19:24	7:03
June 30	12:22	19:12	6:50

7  
8  
9  
10

## 5. FAST-LVOS Modeling Support

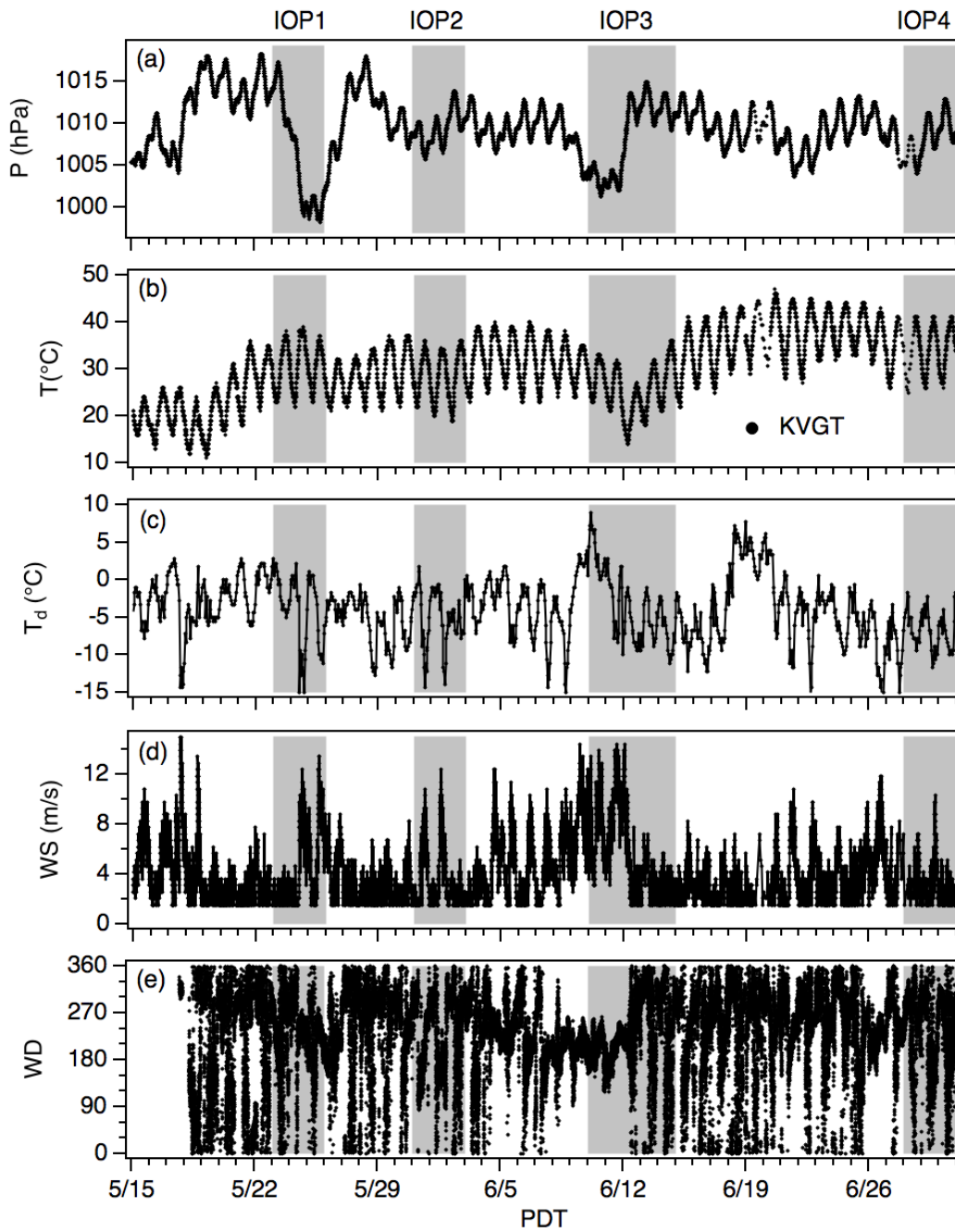
The FAST-LVOS project relied on several atmospheric models for planning purposes during the measurement phase of the campaign. Synoptic weather forecasts, radiosonde profiles, and upper air analyses from the operational NOAA NCEP Global Forecast System (GFS) were obtained from the Wyoming Weather Web maintained by the University of Wyoming (<http://weather.uwyo.edu/index.shtml>). These sources were used in conjunction with O<sub>3</sub> and CO forecasts from the NOAA/ESRL/GSD RAP-Chem (<https://rapidrefresh.noaa.gov/RAPchem/>) provided by Mariusz Pagowski, and the NOAA NESDIS RAQMS (<http://raqms-ops.ssec.wisc.edu/>) model developed by R. Bradley Pierce to plan the daily operations and IOPs. This information was assimilated by the Principal Investigator who recalled the ozonesonde and aircraft teams to Las Vegas when synoptic conditions favorable for STT were developing.

Several other models aided the interpretation of the measurements. Meiyun Lin and Alex Zhang of NOAA GFDL and Princeton University used two global models (GFDL-AM4 and GEOS-Chem) to investigate the various sources for the high O<sub>3</sub> observed above Clark County during FAST-LVOS. These efforts were directly supported by Clark County under a separate contract (CBE-605334-19) and are described in more detail in a separate report. Jerome Brioude and Stephanie Evan of the Université de La Réunion provided FLEXPART particle dispersion model simulations of stratospheric ozone, Asian pollution, and biomass burning influences during the campaign. Wildfire influences were also assessed using an early version of the NOAA/ESRL/GSD Rapid Refresh-Smoke (HRRR-Smoke) air quality modeling system (<https://rapidrefresh.noaa.gov/hrrr/HRRRsmoke/>) developed by Ravan Ahmadov, which simulated the emissions and transport of smoke from wildfires detected by the VIIRS/JPSS satellite fire product in high spatial resolution (3km) over the CONUS domain. Appendix A describes these models in more detail.

## 6. Meteorological Context

Summer-like conditions arrive early in the Desert Southwest and the warmer temperatures lead to the development of regional-scale southwest-northeast plains-mountain circulations and locally-driven valley and slope flows in the Las Vegas Valley [Stewart *et al.*, 2002]. These diurnal wind patterns lead to southeasterly to southerly flow during the morning transition, but the winds shift to the southwest by mid-afternoon as the mixed layer grows in depth, and plains-mountain winds driven by the thermal contrast between the land and Gulf of California develop. This regional-scale flow converges with southeasterly up-valley flow in the LVV, and these winds typically persist until well into the night when downslope flows from the east and southwest converge in Las Vegas. This diurnal pattern can be seen in the wind measurements at both the NLVA and AP plotted in the lower panels of **Figures 6-1** and **6-2**, respectively.

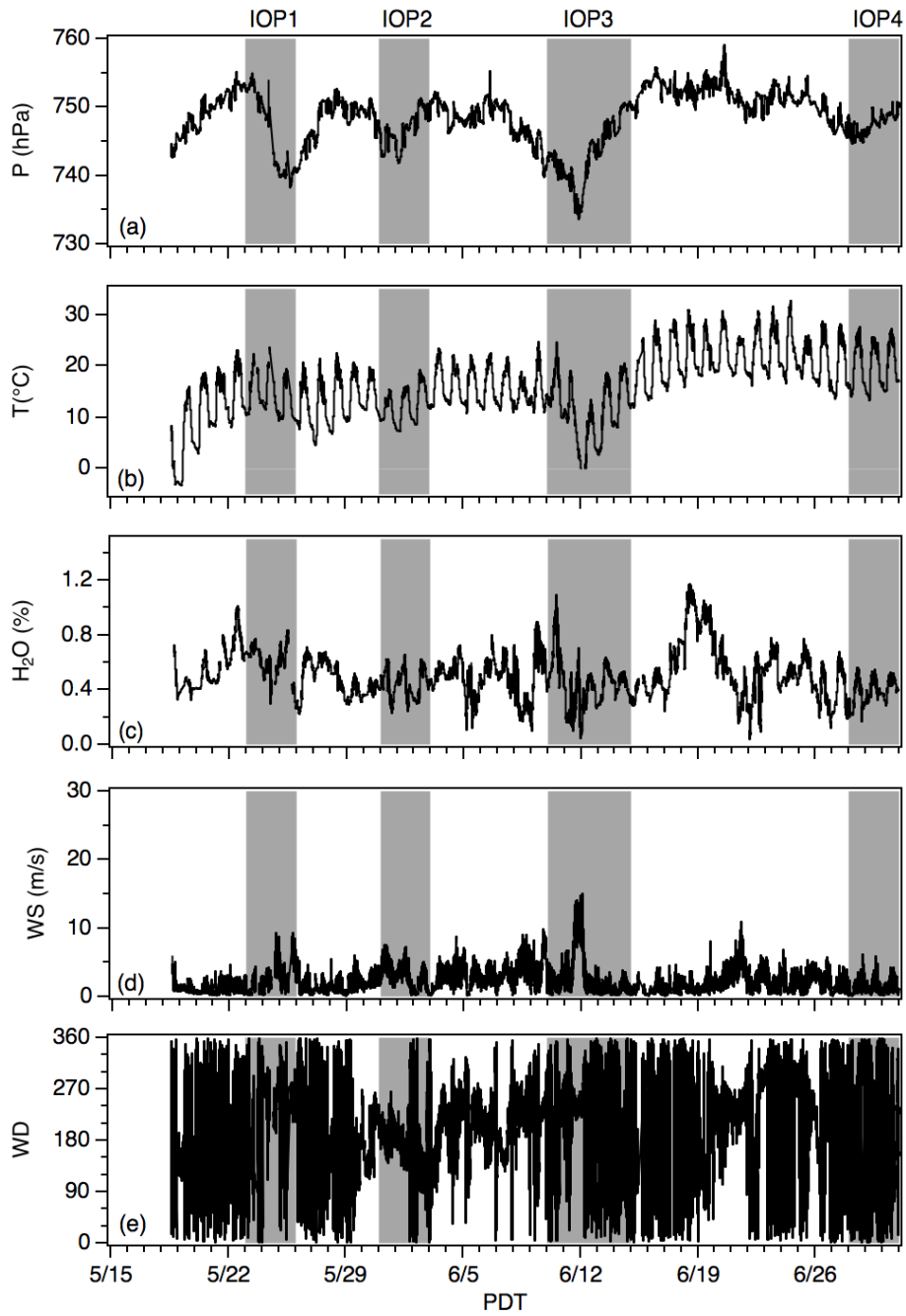
1  
2



3  
4  
5  
6  
7  
8  
9  
10

**Figure 6-1.** Time series showing the 5-min measurements from the NWS (KVG T) station locate near the TOPAZ truck at the NLVA. The gray bands mark the four FAST-LVOS IOPs.

1  
2



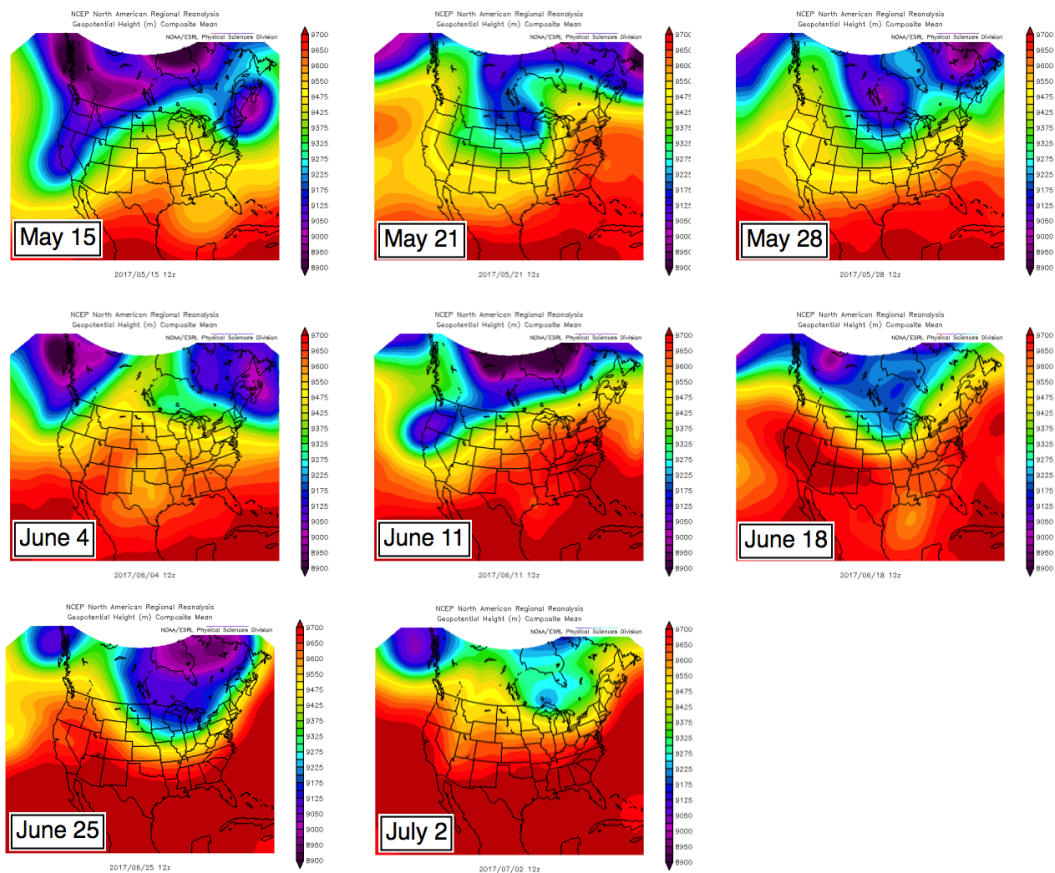
3  
4  
5  
6  
7

**Figure 6-2.** Time series of the 1-min meteorological measurements from the mobile laboratory on Angel Peak (black). The gray bands mark the four FAST-LVOS IOPs.

1 This diurnal pattern is periodically interrupted by the passage of deep midlatitude cyclones that  
2 gradually become shallower and less frequent as the jet stream migrates northward into  
3 Canada in June. This gradual shift is seen in **Figure 6-3**, which shows 300 hPa geopotential plots  
4 from the NCEP NARR Reanalysis at weekly intervals from May 15 to July 2, 2017. The changes in  
5 pressure, temperature, and wind speed and direction during the passage of the upper level  
6 troughs and their associated surface cold fronts can be seen in the NLVA and AP  
7 measurements. There was no measurable precipitation at the NLVA during the entire 6-week  
8 campaign.

9  
10 The temperatures in the LVV climbed dramatically after the passage of the last deep low on  
11 June 12, as strong ridging brought an incursion of moist subtropical air into southern Nevada.  
12 The maximum high temperature of 117°F (47.2°C) on June 20 tied the all-time Las Vegas record  
13 high. These high temperatures were briefly moderated by the passage of the shallow trough  
14 seen above northern California on June 11, and returned to near climatological values during  
15 the passage of the final low-pressure system in the last days of the campaign.

16  
17



18  
19  
20 **Figure 6-3.** NCEP NARR Reanalysis 300 hPa 12UT geopotential maps at weekly intervals during  
21 FAST-LVOS.

1 **7. Overview of the FAST-LVOS Measurements**

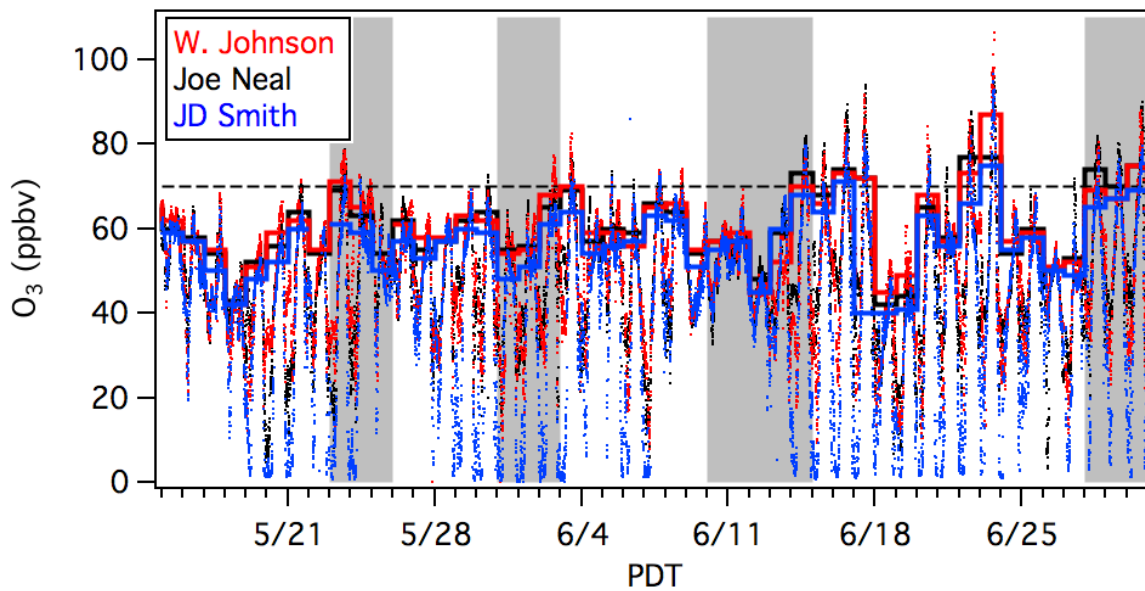
2

3 **7.1 Clark County measurements**

4

5 The Clark County Department of Air Quality maintains a network of continuous air monitoring  
6 sites (CAMS) in the Las Vegas Valley and surrounding areas. This network included 11 active  
7 ozone monitors (cf. **Figure 2-1**) during the FAST-LVOS campaign, including two (JD Smith and  
8 Apex) that have subsequently been deactivated. The measurements from these regulatory  
9 monitors provide context for the following discussions of the FAST-LVOS measurements. **Figure**  
10 **7-1** plots time series of the 5-min and MDA8 O<sub>3</sub> measurements from the Walter Johnson, Joe  
11 Neal, and JD Smith monitors. These monitors were all located about 7 km from the NLVA, which  
12 lies near the center of an equilateral triangle formed by these three sites. The Walter Johnson  
13 and Joe Neal monitors recorded the largest number of ozone exceedances during FAST-LVOS  
14 and **Figure 7-1** shows that most of those high ozone days occurred during or immediately after  
15 one of the FAST-LVOS IOPs.

16



17

18

19 **Figure 7-1.** MDA8 (steps) and 5-min (dots) O<sub>3</sub> mixing ratios measured by the Walter Johnson  
20 (red), Joe Neal (black), and JD Smith (blue) monitors during FAST-LVOS. The horizontal dashed  
21 line shows the 70 ppbv NAAQS.

22

23 **Table 7-1** lists all of the instances when one or more of the regulatory monitors equaled or  
24 exceeded the 2015 NAAQS during FAST-LVOS. This occurred on 10 of the 45 measurement days,  
25 with 3 or more monitors at or above the NAAQS on 6 of those 10 days. These days (June 16, 17,  
26 22, 23, 28, and 30) all occurred during the last two weeks of the field campaign.

27

28

1 **Table 7-1. MDA8 O<sub>3</sub> on high ozone days during FAST-LVOS**

2

	CAMS	May 23	June 3	June 14	June 16	June 17	June 22	June 23	June 28	June 29	June 30
Mesquite	23	49	52	54	54	50	61	51	62	59	60
Paul Meyer	43	65	66	67	67	64	64	71	61	63	68
Walter Johnson	71	71	70	70	73	72	73	87**	69	67	75
Palo Verde	73	68	66	68	75	67	73	76	69	65	72
Joe Neal	75	69	69	73	74	72	77	77	74	70	75
Green Valley	298	57	64	65	68	72	63	65	65	68	69
Jerome Mack	540	53	60	62	65	66	60	65	59	61	63
Boulder City	601	51	58	63	66	64	66	62	69	65	66
Jean	1016	51	54	57	63	63	62	60	65	63	69
JD Smith*	2002	61	64	68	71	70	66	75	65	67	69
Apex*	22	55	62	65	68	68	70	64	71	66	65
NLVA#	N/A	72	70	74	76	73	76	83	74	71	76
AP#	N/A	64	60	71	74	61	63	53	68	71	74

3  
4 \* now inactive

5 \*\* MDA8 based on 6-hour average because of maintenance

6 # NOAA/ESRL/CSD measurements

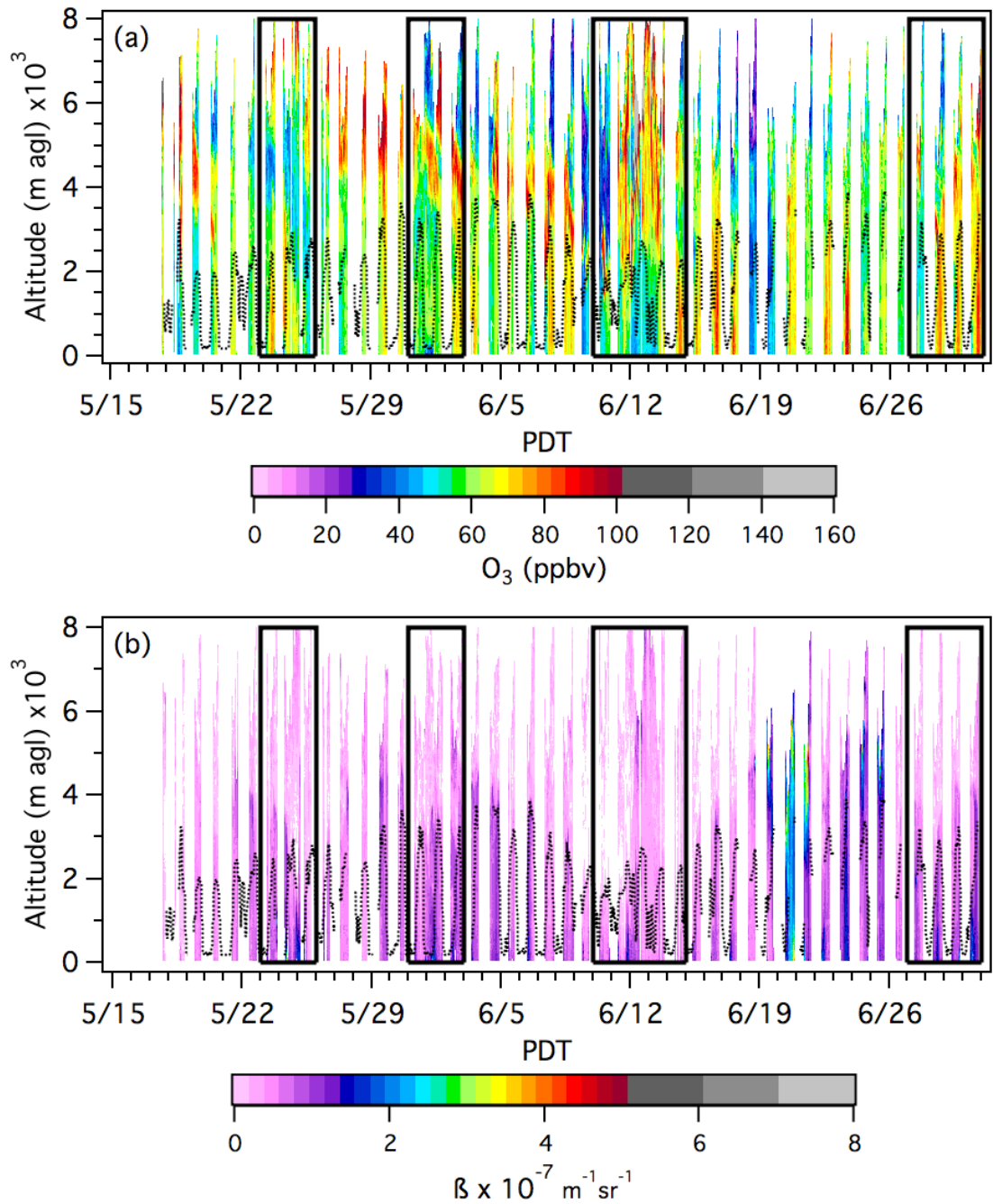
7  
8 **7.2 TOPAZ lidar measurements**

9  
10 The TOPAZ lidar acquired ozone and backscatter data on all 45 days (May 17-June 30) of the  
11 FAST-LVOS campaign, operating a total of 523 hours for an average of nearly 12 hours per day.  
12 The O<sub>3</sub> and backscatter ( $\beta$ ) measurements are summarized as a series of time-height curtain  
13 plots in **Figure 7-2**. The dotted black lines show the mixed layer heights inferred from the co-  
14 located micro-Doppler lidar and the heavy black boxes show the IOP days when aircraft and/or  
15 ozonesonde measurements were also made.

16  
17 The upper panel of **Figure 7-2** shows high O<sub>3</sub> aloft during much of FAST-LVOS including the  
18 slowly descending band of high O<sub>3</sub> at the end of May and beginning of June, and the deep  
19 tropopause fold with mixing ratios exceeding 270 ppbv at 6 km asl (5.3 km agl) on June 11-13.  
20 This elevated O<sub>3</sub> sometimes reached the top of the mixed layer, which was usually more than 3  
21 km deep during June. These general observations are consistent with the measurements from  
22 the first LVOS campaign.

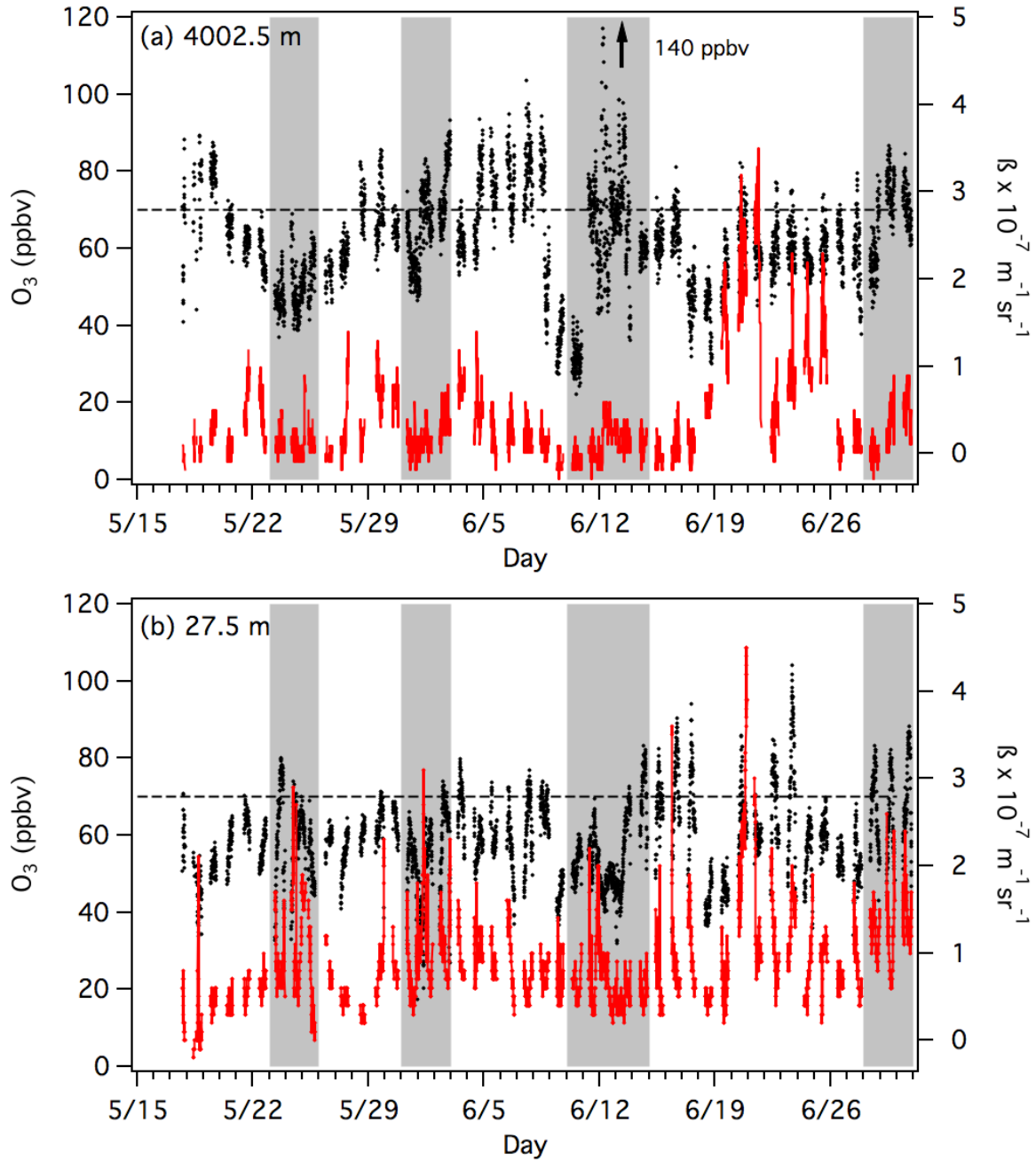
23  
24 **Figure 7-3** plots time series of the O<sub>3</sub> mixing ratios and backscatter coefficients measured above  
25 the top of the mixed layer at 4002.5 m agl, and just above the surface at 27.5 m agl. The O<sub>3</sub>  
26 mixing ratios at both altitudes often exceeded 70 ppbv, but higher O<sub>3</sub> was measured aloft more

- 1 frequently during the first two weeks of June, and near the surface during the last two weeks.
- 2 The highest backscatter was measured between June 19 and 21 at both altitudes.
- 3



- 4
- 5
- 6 **Figure 7-2.** Time-height curtain plots of the TOPAZ (a)  $O_3$  mixing ratios and (b) particulate
- 7 backscatter coefficients. The dotted black line shows the mixed layer heights inferred from the
- 8 micro-Doppler lidar measurements and the heavy black boxes enclose the IOP days.
- 9

1  
2



3  
4  
5  
6  
7  
8  
9

**Figure 7-3.** Time series of the TOPAZ O<sub>3</sub> mixing ratios and particulate backscatter coefficients at (a) 4002.5 and (b) 27.5 m agl. Note that the peak O<sub>3</sub> value of 140 ppbv on June 12 is off scale. The dashed black lines correspond to the 70 ppbv NAAQS.

1 **7.3 Comparison between lidar and surface measurements**  
2

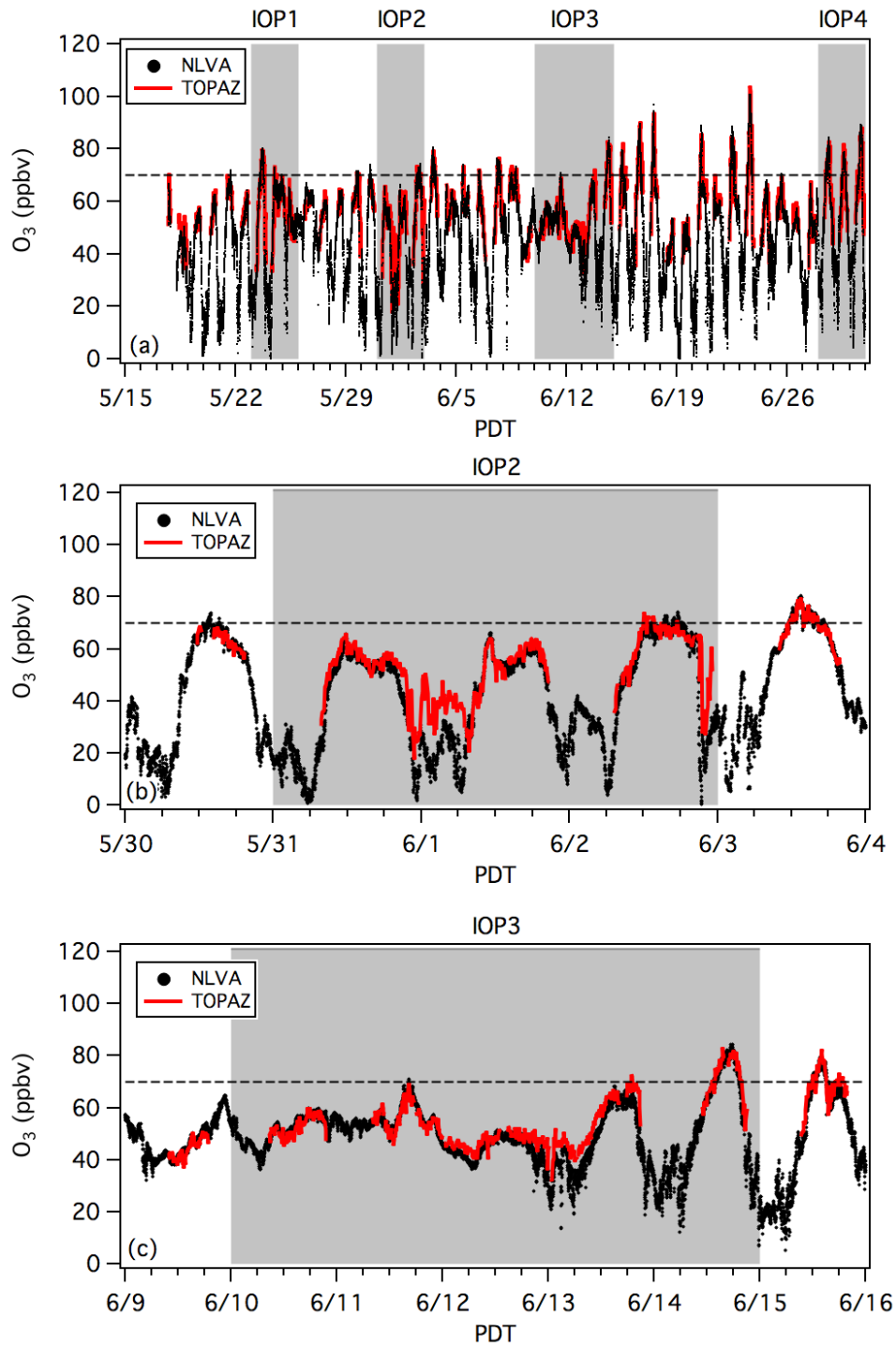
3 The variations in surface O<sub>3</sub> at the NLVA are more easily seen in **Figure 7-4**, which compares the  
4 lowest elevation (27.5 m agl) TOPAZ O<sub>3</sub> retrievals with the in-situ measurements made at the  
5 TOPAZ truck (5 m agl). The time series are in excellent agreement during the day when the  
6 boundary layer was well-mixed, but usually diverged at night (e.g. June 1-2) when a shallow  
7 nocturnal boundary layer formed and surface O<sub>3</sub> was destroyed by deposition and NO<sub>x</sub> titration.  
8 The latter was particularly significant at the NLVA sampling site which was located next to a  
9 staging area for heavy construction vehicles that were often left idling during the early morning  
10 hours. These local NO<sub>x</sub> sources did not affect the TOPAZ mixing ratios, which were measured  
11 about 800 m downrange of the TOPAZ truck. Note that the in-situ and lidar measurements did  
12 not diverge during the night of June 11-12 when high winds associated with the cold front and  
13 descending tropopause fold kept the lower troposphere well mixed.  
14

15 **Figure 7-5** is similar to **Figure 7-4**, but compares the 27.5 m agl TOPAZ measurements with the  
16 5-min O<sub>3</sub> mixing ratios measured by the Joe Neal monitor located 7.3 km to the NNW. The  
17 agreement between these measurements is also excellent with much less divergence at night,  
18 confirming that the TOPAZ measurements were representative of the North Las Vegas area.  
19

20 **Figure 7-6** compares the in-situ surface measurements from the NLVA with those from the  
21 CRDS instrument in the NOAA ESRL mobile laboratory on Angel Peak (2.68 km asl). The absence  
22 of a strong diurnal variation in the AP measurements shows that mobile laboratory instruments  
23 usually sampled free tropospheric air during the night. Surface O<sub>3</sub> was usually lower on AP in  
24 the afternoon, but the AP and NLVA time series often converged (e.g. May 31-June 1) when the  
25 mixed layer was sufficiently deep. The daytime O<sub>3</sub> concentrations on AP exceeded those at the  
26 NLVA on only a few days (June 5 and June 9-11). **Figure 7-6** also compares the AP  
27 measurements with the TOPAZ measurements made at the same altitude (2002.5 m agl or 2.68  
28 km asl). These measurements were usually in good agreement despite the 36 km separation,  
29 but TOPAZ measured higher concentrations when ozone was descending from the upper  
30 troposphere (e.g. June 10-12).  
31

32 **Figures 7-7** and **7-8** compare the AP O<sub>3</sub> measurements to the other in-situ measurements from  
33 the mobile laboratory. As noted above and shown below, the correlations between these  
34 species and O<sub>3</sub> can help elucidate the origins of the sampled airmasses. Particularly striking are  
35 the high H<sub>2</sub>O and low O<sub>3</sub>, CO, and CH<sub>4</sub> concentrations during the subtropical incursion on June  
36 18-19 and the off scale (450 ppbv) CO peak on June 21-22 coinciding with the enhancements in  
37 TOPAZ backscatter.  
38  
39  
40  
41  
42  
43  
44

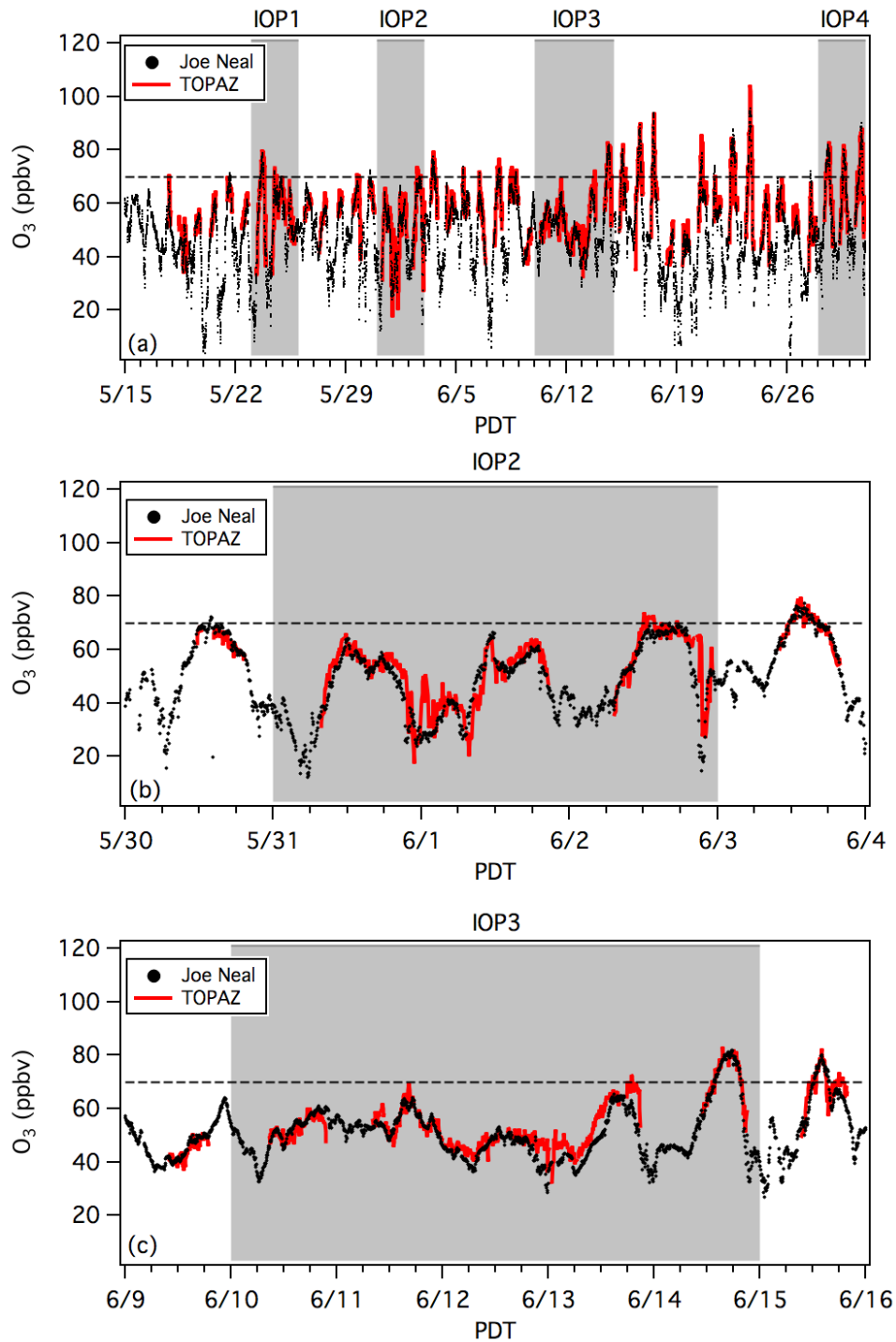
1  
2



3  
4  
5  
6  
7  
8

**Figure 7-4.** (a) Time series of the 27.5 m TOPAZ O<sub>3</sub> measurements and the 1-min in-situ measurements at the NLVA. The gray bands identify the FAST-LVOS IOPs. The lower panels are expanded views of the measurements from (b) IOP2 and (c) IOP3. The dashed black lines correspond to the 70 ppbv NAAQS.

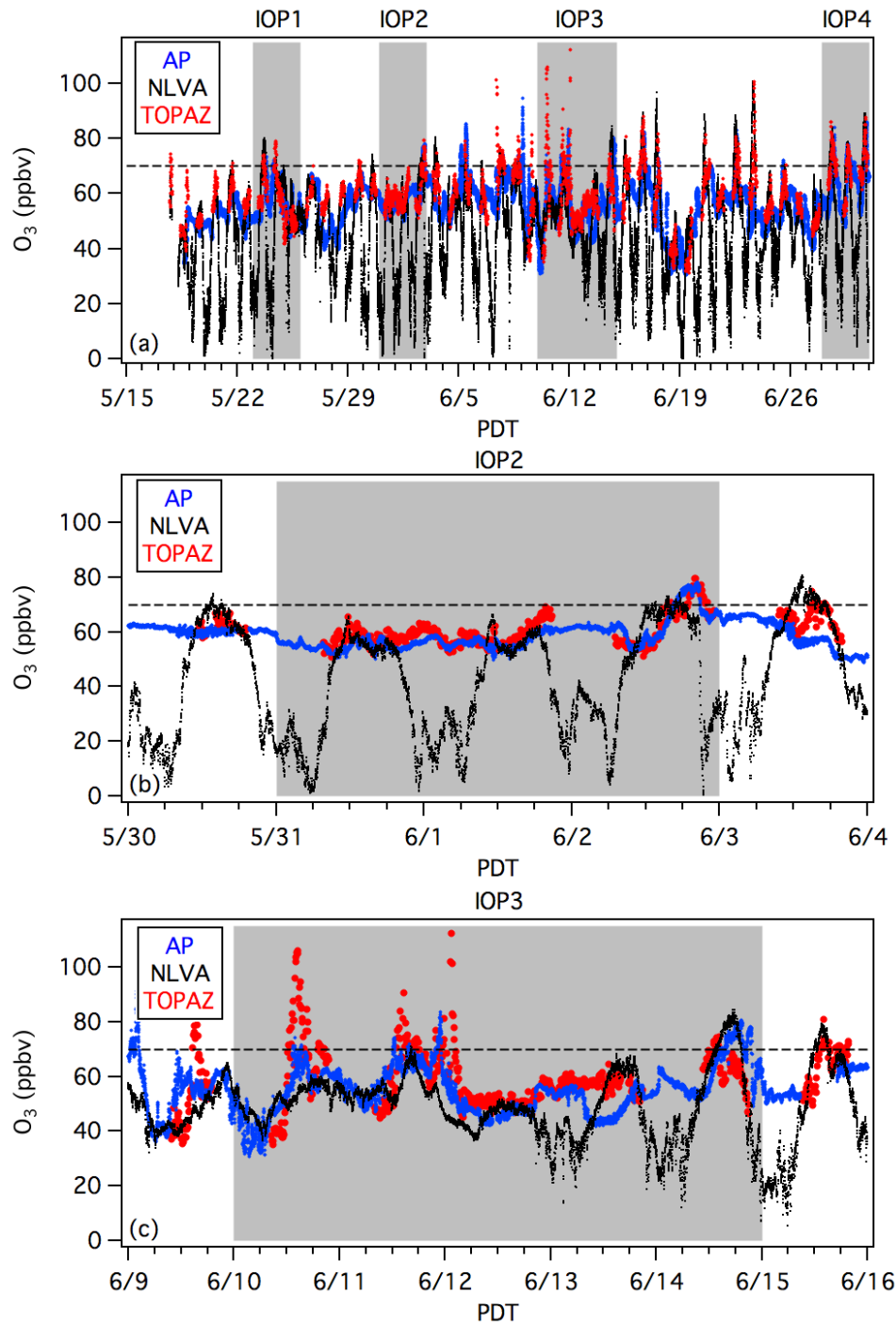
1  
2



3  
4

5 **Figure 7-5.** (a) Time series of the 27.5 m TOPAZ O<sub>3</sub> measurements and the 5-min in-situ O<sub>3</sub>  
6 measurements from Joe Neal (C75). The gray bands identify the FAST-LVOS IOPs. The lower  
7 panels are expanded views of the measurements from (b) IOP2 and (c) IOP3. The dashed black  
8 lines correspond to the 70 ppbv NAAQS.

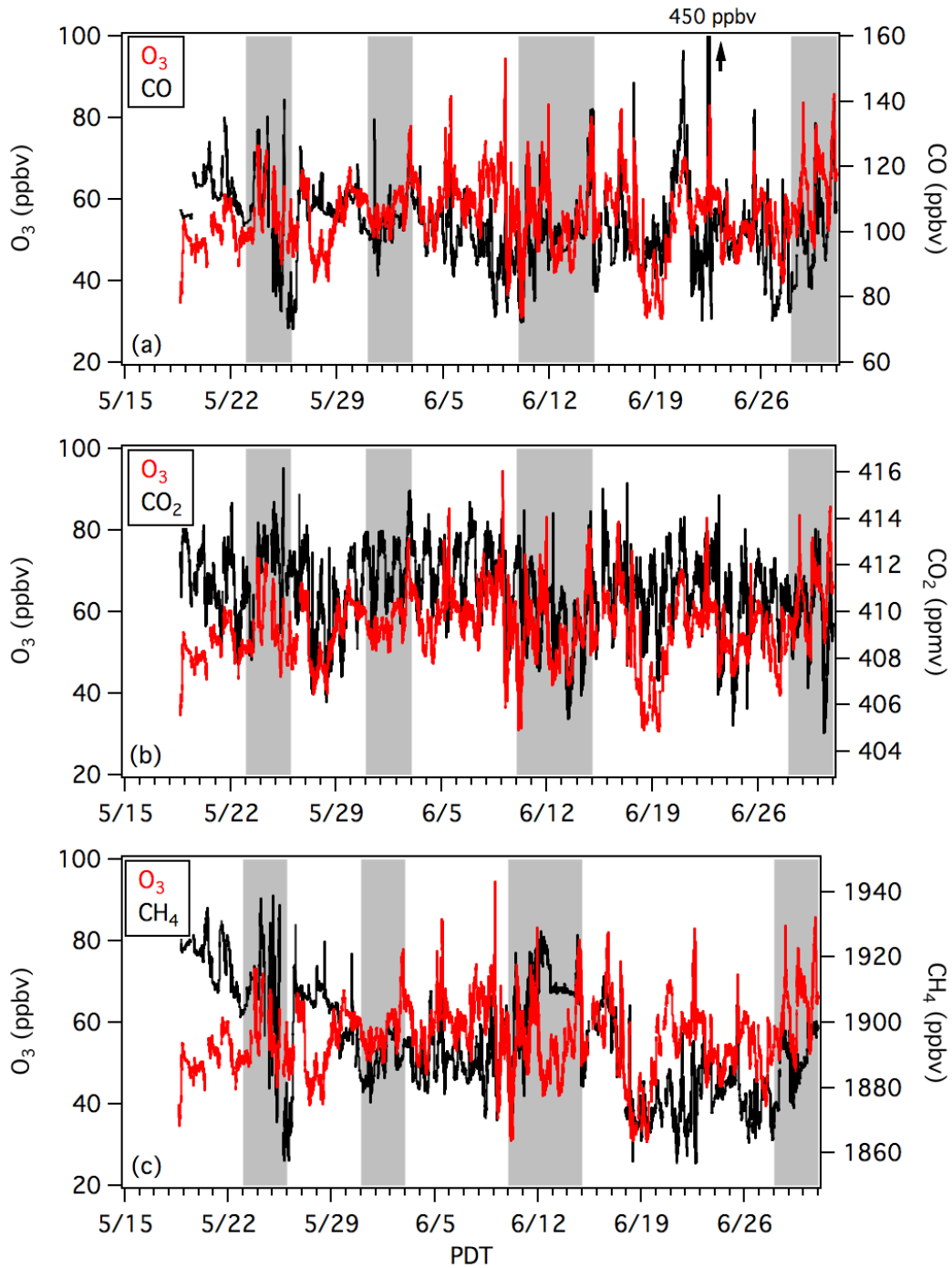
1  
2



3  
4

5 **Figure 7-6.** (a) Time series of the 1-min in-situ  $O_3$  measurements from the NLVA (black) and AP  
6 (blue) compared to the 2002.5 m agl (2683.5 km asl) TOPAZ measurements (red). The gray  
7 bands identify the FAST-LVOS IOPs. The lower panels are expanded views of the measurements  
8 from (b) IOP2 and (c) IOP3. The dashed black lines correspond to the 70 ppbv NAAQS.

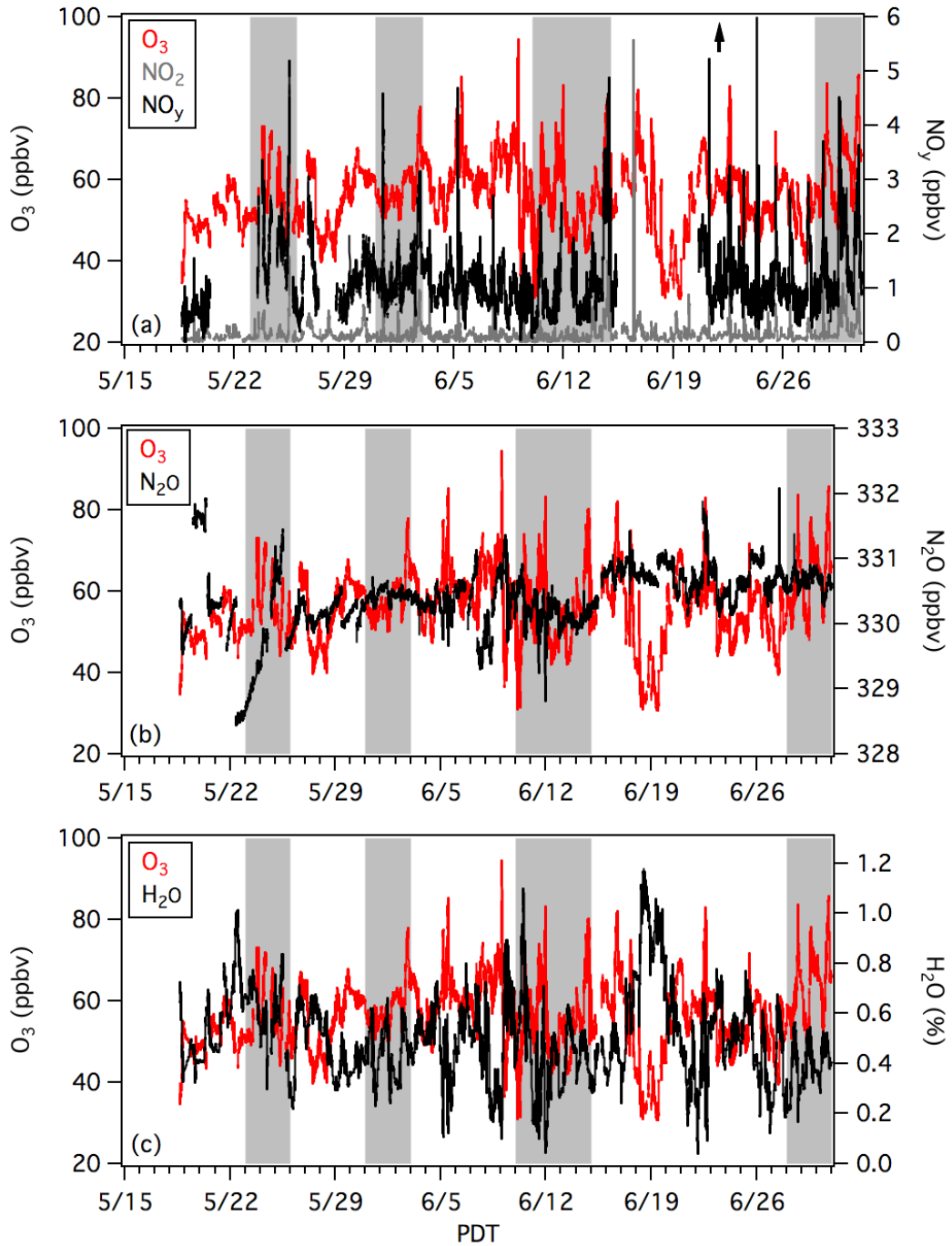
1  
2



3  
4  
5  
6  
7  
8  
9

**Figure 7-7.** Time series of the 1-min O<sub>3</sub>, CO, CO<sub>2</sub>, and CH<sub>4</sub> measurements from the mobile laboratory on Angel Peak (black). The gray bands mark the four FAST-LVOS IOPs. The CO concentrations on June 22 reached 450 ppbv (arrow).

1  
2



3  
4 **Figure 7-8.** Time series of the 1-min O<sub>3</sub>, NO<sub>y</sub>, N<sub>2</sub>O, and H<sub>2</sub>O measurements from the mobile  
5 laboratory on Angel Peak (black). The gray bands mark the four FAST-LVOS IOPs.  
6

## 8. Comparison to FLEXPART tracer distributions

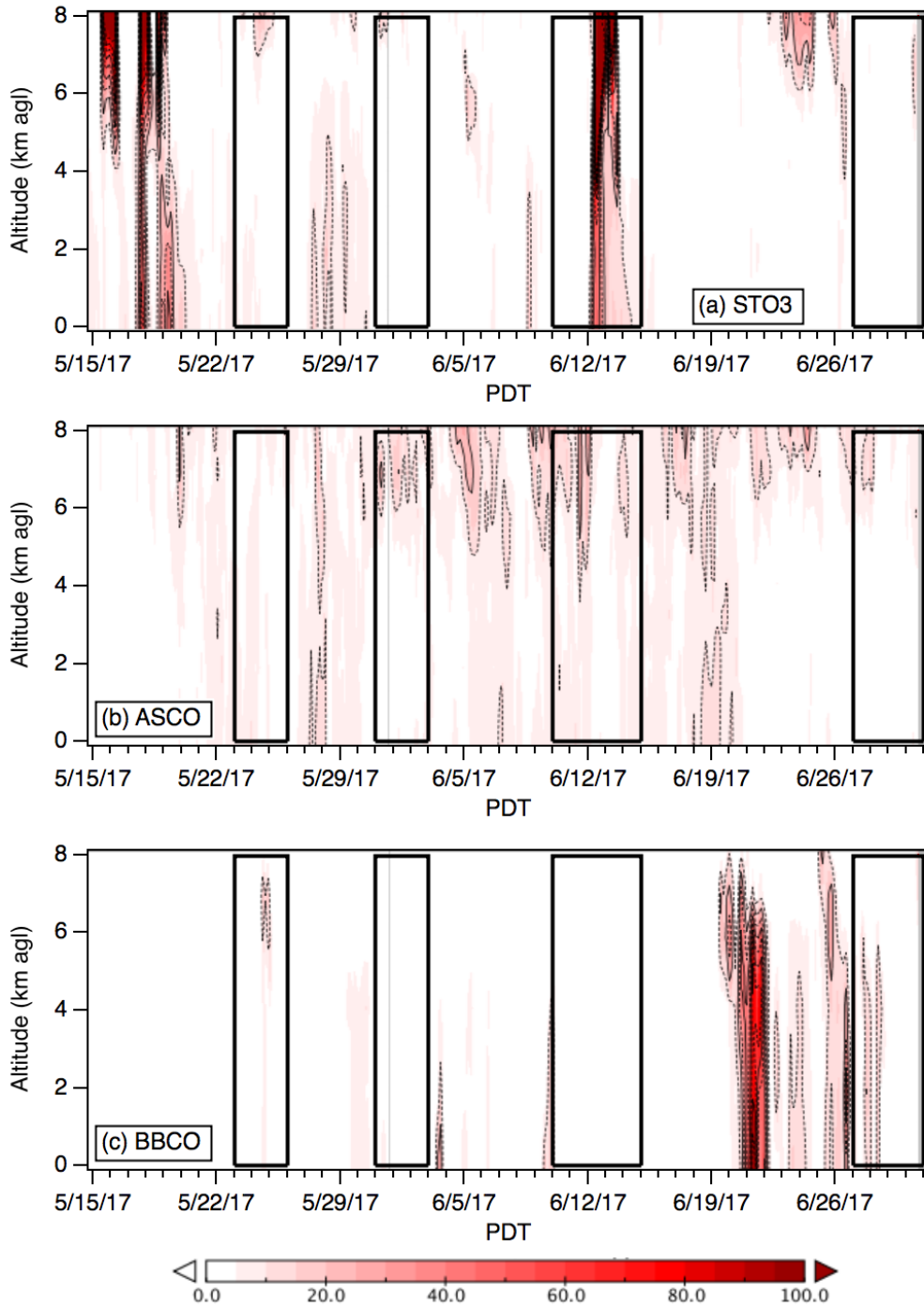
**Figure 8-1** shows time-height curtain plots of the FLEXPART tracer distributions (**Appendix A**) over the  $0.5^\circ \times 0.5^\circ$  grid cell centered at  $36.25^\circ\text{N}$ ,  $-119.25^\circ\text{E}$ . This grid cell encompasses most of the Las Vegas Valley, with Angel Peak lying just beyond the western edge. These plots are analogous to the lidar ozone and backscatter curtains shown in **Figure 7-2**, and qualitatively reproduce many of the features seen in these plots. All three of the tracers are plotted using a 0-100 ppb concentration scale. The ASCO and BBCO tracers can be compared directly, but neither can be quantitatively compared with the STO3 tracer because of the wide range of  $\text{O}_3/\text{CO}$  ratios observed in biomass burning and pollution plumes. An approximate range is on the order of 0.2 to 0.5 {Langford, 2012 #5717}, suggesting that the ASCO and BBCO tracer concentrations can be considered very conservative upper limits for ASO3 and BBO3.

The STO3 tracer plot in **Figure 8-1a** shows significant amounts of stratospheric  $\text{O}_3$  penetrating all the way to the surface during two major (May 16-21 and June 11-15) and one minor (May 28-31) intrusion events. The tracer surface concentrations peaked at nearly 60 ppbv at 0200 UT on May 18 and 50 ppbv at 1400 UT on June 12. Note that the first intrusion event was well underway when TOPAZ first started measuring at 0037 UT on June 18 (1737 PDT on June 17).

The ASCO curtain plot in **Figure 8-1b** shows a more continuous influx of Asian pollution in the middle and upper troposphere, with the largest surface contributions ( $>10$  ppbv of CO) on May 28, June 7, and June 18. The biomass burning tracer in **Figure 8-1c** shows little enhancement prior to June 20, but BBCO tracer surface enhancements of up to 100 ppbv occurred during the last 10 days of the study. Note that the BBCO tracer plot appears qualitatively similar to the TOPAZ backscatter curtain (**Figure 7-2**).

**Figure 8-2** shows the STO3 tracer distributions for 12UT on May 18, May 27, and June 12 on the 500 and 700 hPa surfaces (roughly 5.6 and 3.1 km asl). The tracer distributions in the May 18 and June 12 plots have the classic appearance of recent tropopause folds curling cyclonically around the low-pressure centers. The older intrusion on May 27 has started to dissipate and is less well-defined. The ASCO tracer distributions in **Figure 8-3** are generally more diffuse, but sometimes appear to be intertwined with descending stratospheric air as on May 27-28. The BBCO distributions in **Figure 8-4** suggest that large backscatter enhancement on June 20 was caused by diffuse smoke from widespread agricultural burning.

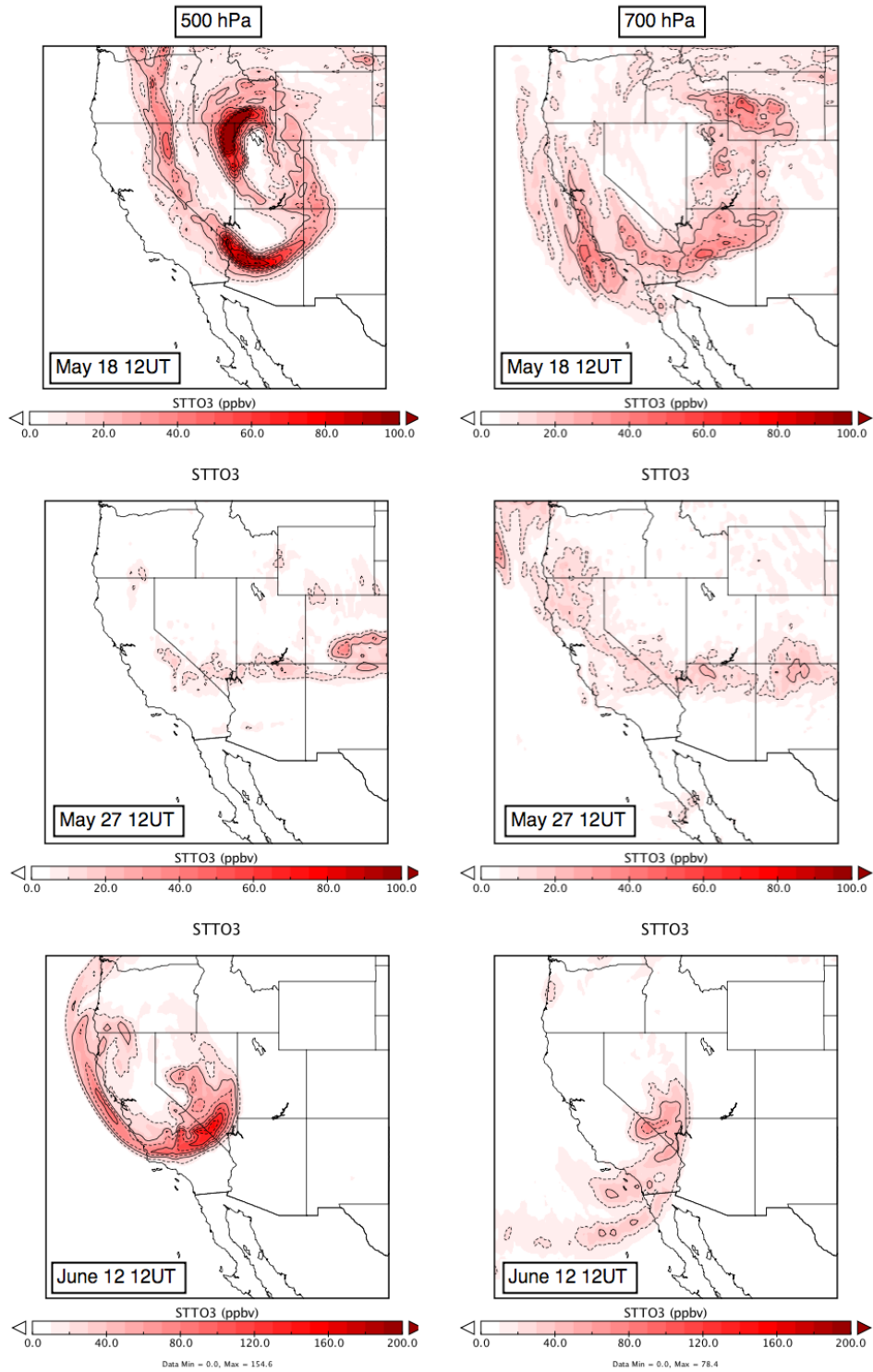
1  
2



3  
4  
5  
6  
7  
8

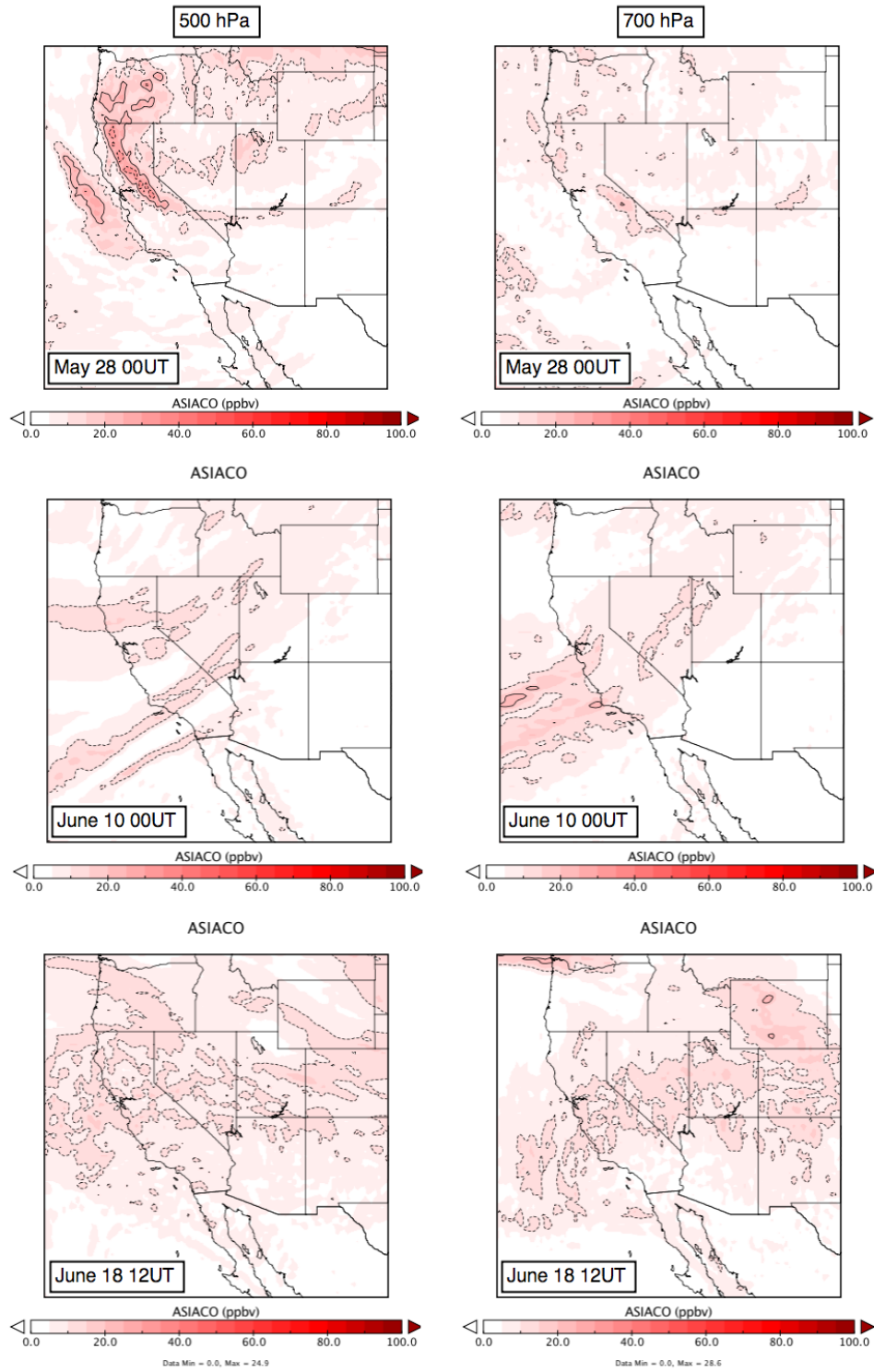
**Figure 8-1.** Time-height curtain plots of the (a) STT O3, (b) ASCO, and (c) BBCO FLEXPART tracers above the Las Vegas Valley. All three tracers are plotted with a 0-100 ppb concentration scale.

1



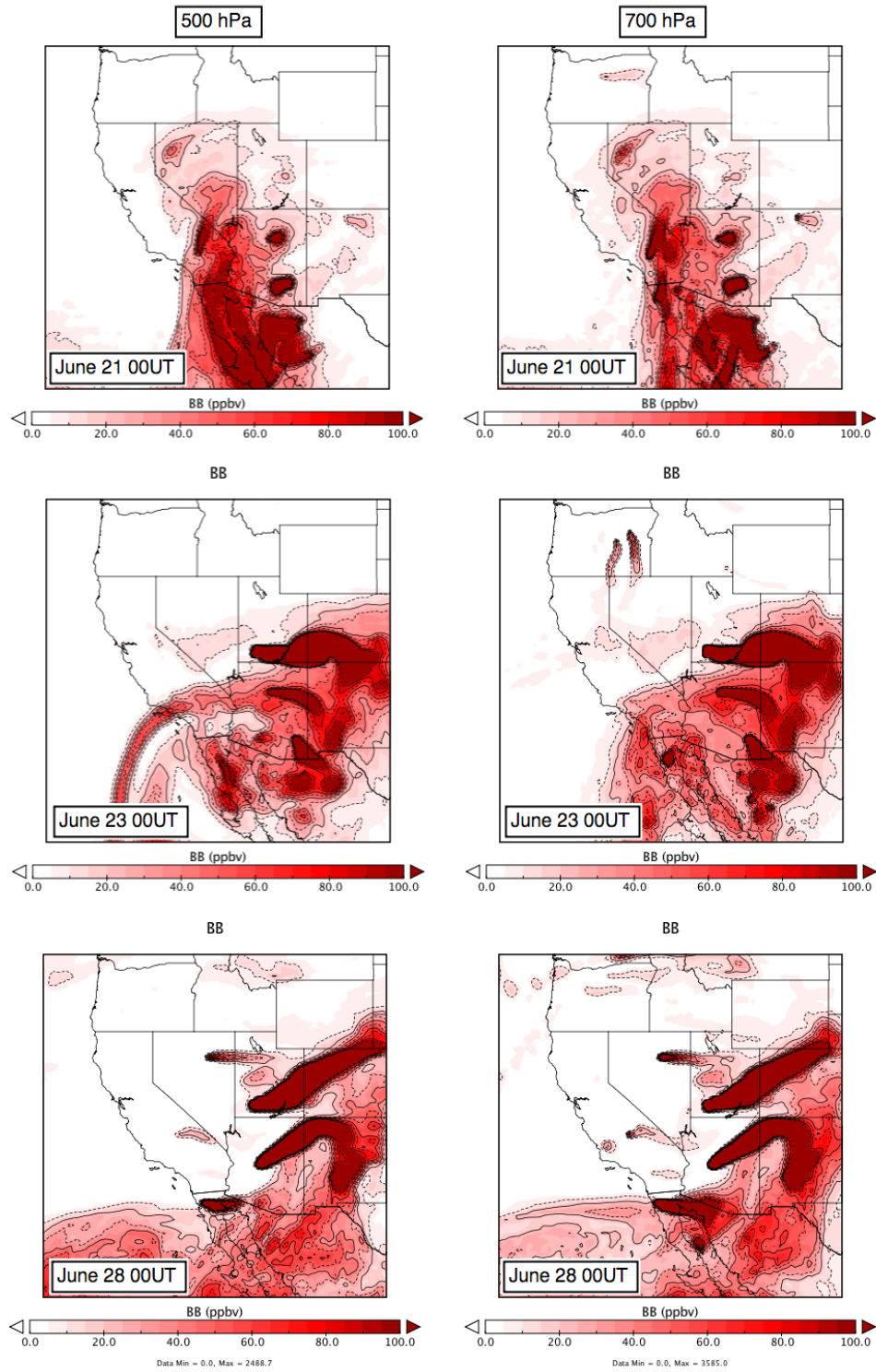
2  
3  
4  
5

**Figure 8-2.** Maps showing the FLEXPART STO3 tracer distribution at 12UT on May 18, May 27, and June 12 on the (left) 500 hPa and (right) 700 hPa surfaces.



1  
2  
3  
4  
5

**Figure 8-3.** Maps showing the FLEXPART ASIACO tracer distributions at 00UT on May 28 and June 10, and 12UT on June 18 on the (left) 500 hPa and (right) 700 hPa surfaces.



1  
2  
3  
4  
5  
6

**Figure 8-4.** Maps showing the FLEXPART BBCO tracer distribution at 00UT on June 21 23, and 28 on the (left) 500 hPa and (right) 700 hPa surfaces.

## 9. Weekly summaries of the FAST-LVOS Results

The TOPAZ summary plots in **Figure 7.2** hide a wealth of detail in the lidar and in-situ measurements. In the following sections, we take a closer look at the TOPAZ and in-situ measurements in week long segments. We compare the enlarged TOPAZ curtain plots with the corresponding FLEXPART tracer distributions, and with selected plots from the other FAST-LVOS measurements to assess the potential contributions of transport to the high ozone days in Clark County. The remaining FAST-LVOS measurements are summarized in the Appendices.

### 9.1 Week 1: May 17-20

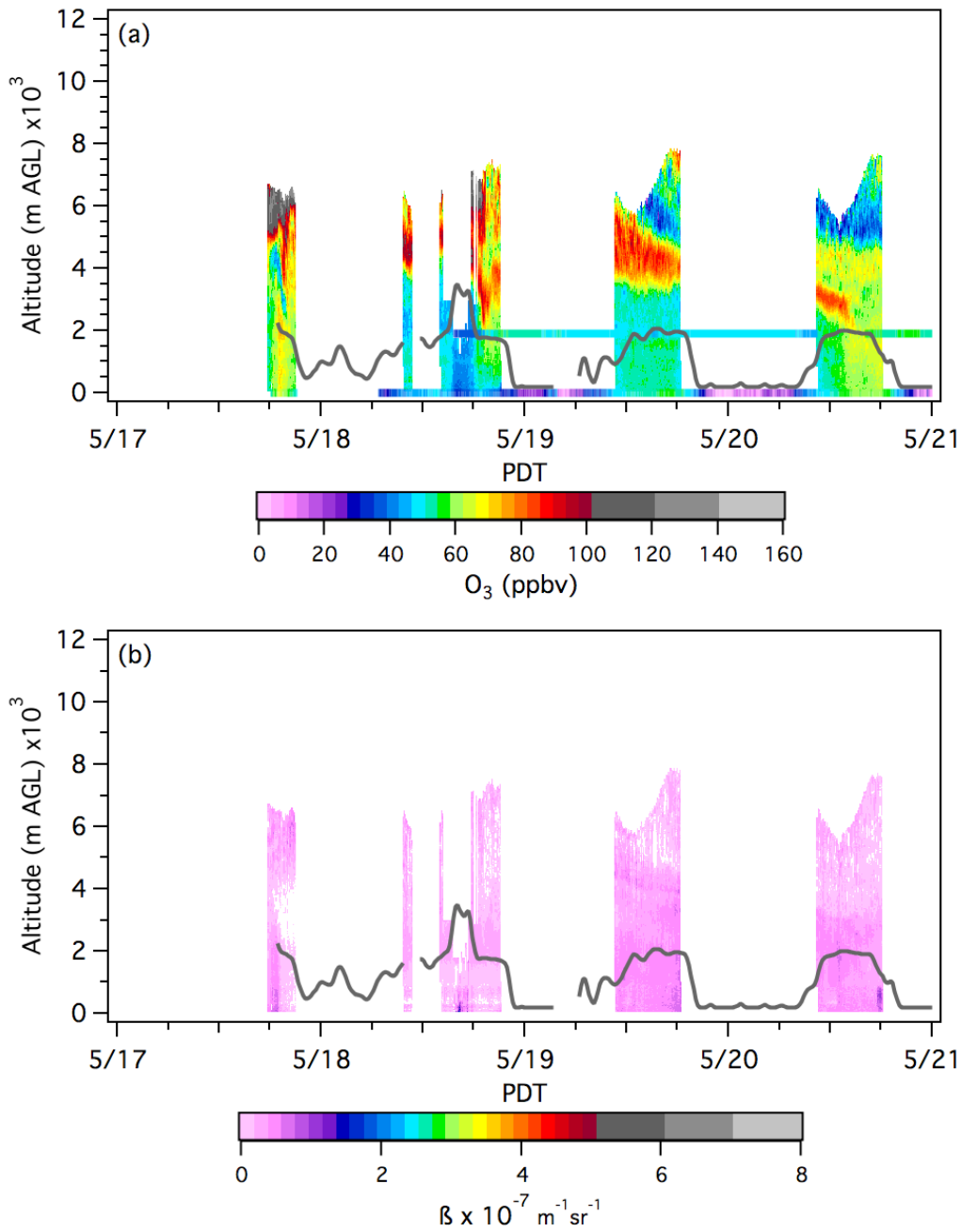
Temperatures in the Las Vegas Valley were well below normal at the start of the FAST-LVOS measurement campaign as a spring storm generated by the first upper level trough shown in **Figure 6-3** passed through Nevada. This trough also spawned the stratospheric intrusion shown in **Figure 8-2**. The TOPAZ truck drove through late season snow in Utah and arrived at the North Las Vegas Airport around 1300 PDT on Wednesday May 17. The first TOPAZ and in-situ measurements at the NLVA were made later that afternoon. The intrusion appears as a layer with more than 100 ppbv of O<sub>3</sub> between 5 and 6 km agl on May 17 in **Figure 9-1**, an expanded version of the curtain plots in **Figure 7-2**. TOPAZ also measured elevated O<sub>3</sub> (with low backscatter) above the top of the mixed layer on the following three days.

**Figure 9-2** shows a similar view of the FLEXPART tracer distributions from **Figure 8-1**. The top panel shows a strong influx of stratospheric O<sub>3</sub> into the free troposphere between May 17 and 21 with up to 35 ppbv reaching the surface on the evening of May 17, and 30 ppbv reaching the surface on the late morning of May 19. The TOPAZ measurements appear to show some descent to the top of the boundary layer on May 17, but the surface concentrations remained relatively low. The ASCO tracer plot shows up to 20 ppbv of ASCO above 6 km on May 20, in qualitative agreement with the elevated O<sub>3</sub> layers seen in the TOPAZ measurements, and some of this elevated O<sub>3</sub> appears to have been entrained into the mixed layer on May 20. The FLEXPART BBCO flux was negligible, in agreement with the low backscatter.

The mobile laboratory began measurements on Angel Peak on May 18, but some of instruments were not fully operational until the following week. The 1-min in-situ O<sub>3</sub> measurements from the NLVA and AP are plotted along with the 5-min measurements from the Walter Johnson and Joe Neal monitors in **Figure 9-3**. The TOPAZ O<sub>3</sub> mixing ratios at 4.0 km agl are also plotted; these were generally larger than the surface values.

The Walter Johnson and Joe Neal measurements show two narrow peaks with up to 68 ppbv around 1705 PDT on May 17 that appear to be correlated with the ozone at 4 km. The TOPAZ curtain plot shows that this spike coincided with the apparent descent and entrainment of O<sub>3</sub> from a layer with more than 100 ppbv that was initially detected by between 5 and 6 km agl. The measurements from May 20 also show possible entrainment and more uniform mixing in the boundary layer, but the MDA8 O<sub>3</sub> concentrations at both Walter Johnson and Joe Neal remained well below the NAAQS on both days.

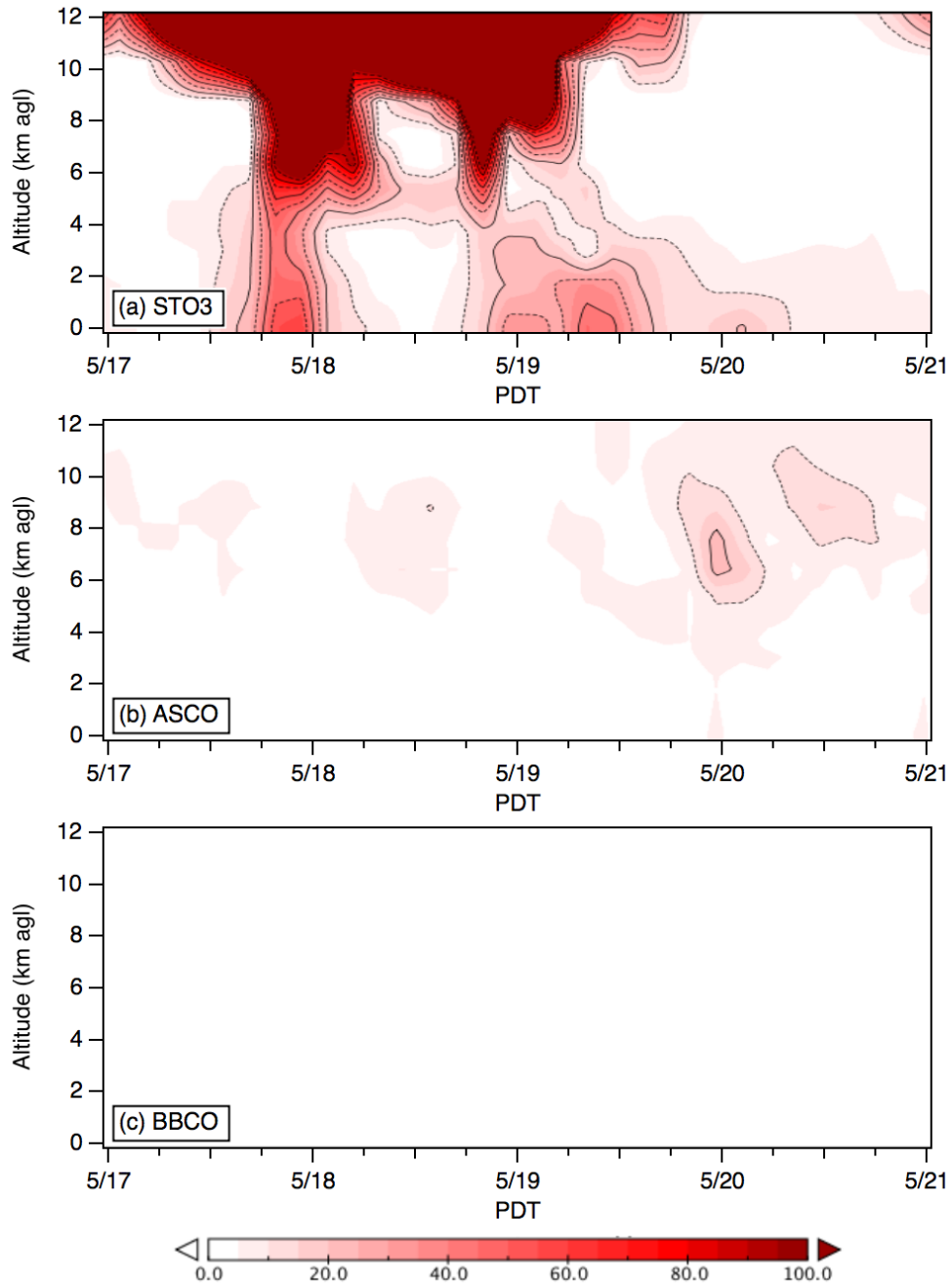
1  
2



3  
4  
5  
6  
7  
8  
9  
10

**Figure 9-1.** Time-height curtain plots of the TOPAZ (a) ozone, and (b) backscatter, measured during Week 1 of FAST-LVOS. The colored horizontal bands at 2.0 and 0.0 km agl in (a) show the in-situ measurements from the NLVA and AP, respectively. The dark gray trace represents the local mixed-layer height inferred from the micro-Doppler lidar measurements. Note that the TOPAZ measurements were truncated by low clouds during the early afternoon of the 18<sup>th</sup>.

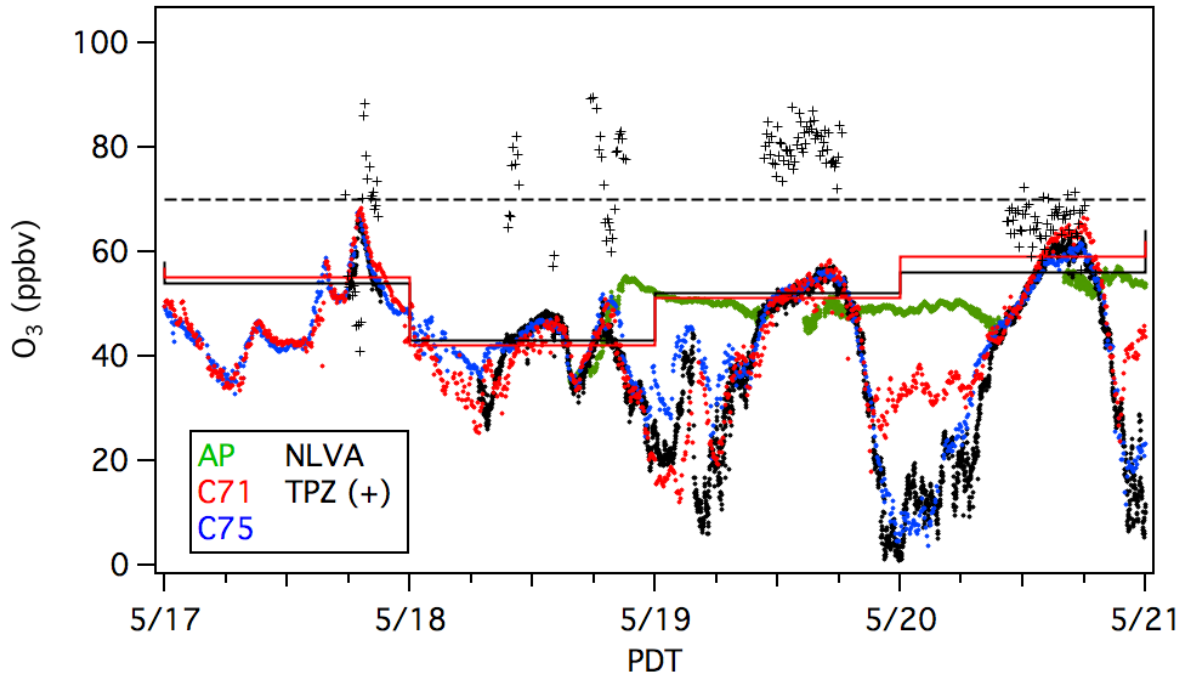
1  
2



3  
4  
5  
6  
7

**Figure 9-2.** Time-height curtain plots of the FLEXPART (a) STO3, (b) ASCO, and (c) BBCO tracer distributions above the LVV during Week 1 of FAST-LVOS.

1  
2  
3  
4  
5  
6



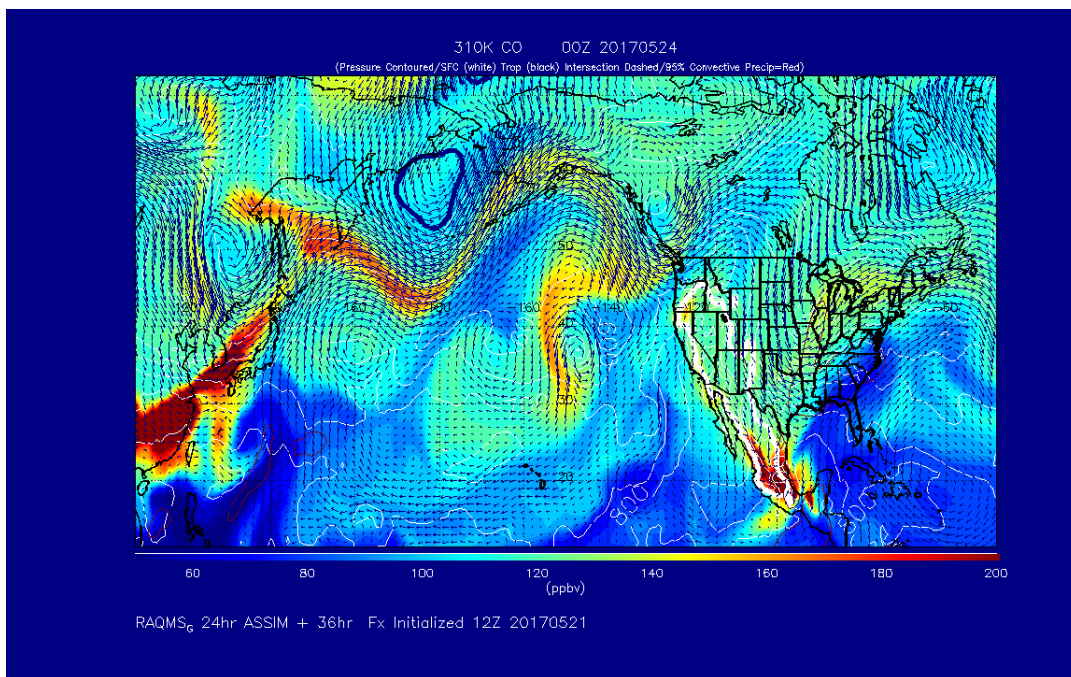
7  
8  
9  
10  
11  
12  
13  
14  
15  
16  
17  
18  
19  
20

**Figure 9-3.** Time series of the TOPAZ O<sub>3</sub> mixing ratios at 4.0 km agl (black +) during Week 1 plotted with the 1-min O<sub>3</sub> measurements from the NLVA (black) and AP (green) and the 5-min measurements from the Walter Johnson (C71, red) and Joe Neal (C75, blue) monitors. The red and blue steps show the corresponding C71 and C75 MDA8 measurements. The dashed black line indicates the 70 ppbv NAAQS.

1 **9.2 Week 2: May 21-28 (IOP1)**

2  
3 The second week of operations saw a return to normal and above average temperatures with  
4 daily highs at the KVGT station reaching 37.8 and 38.9°C (100 and 102°F) on May 23 and 24,  
5 respectively. The average temperatures on both days were about 5°C (9°F) above normal. The  
6 NESDIS RAQMS model forecast showed a large band of CO from Asia approaching the western  
7 U.S. and the first FAST-LVOS IOP was scheduled for May 23-25. Two ozonesondes were  
8 launched on May 23, three on May 24, and one on May 25, and the Mooney also conducted  
9 research flights to Big Bear, CA and back on all three days.

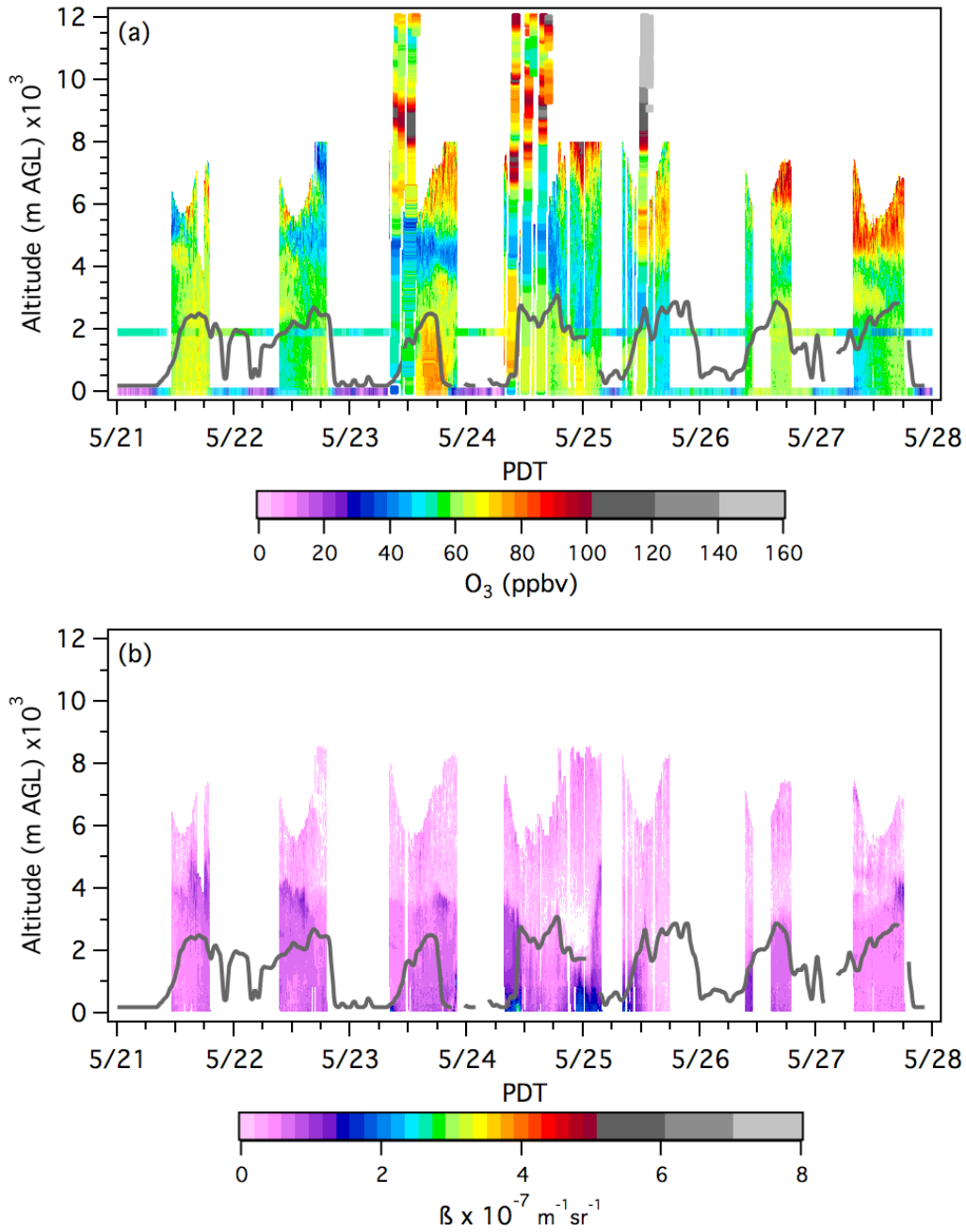
10  
11  
12



13  
14  
15  
16  
17  
18  
19  
20  
21  
22  
23  
24  
25  
26

**Figure 9-4.** NOAA NESDIS RAQMS model 310 K CO forecast for May 24 00UT. Forecast initialized May 21 12UT.

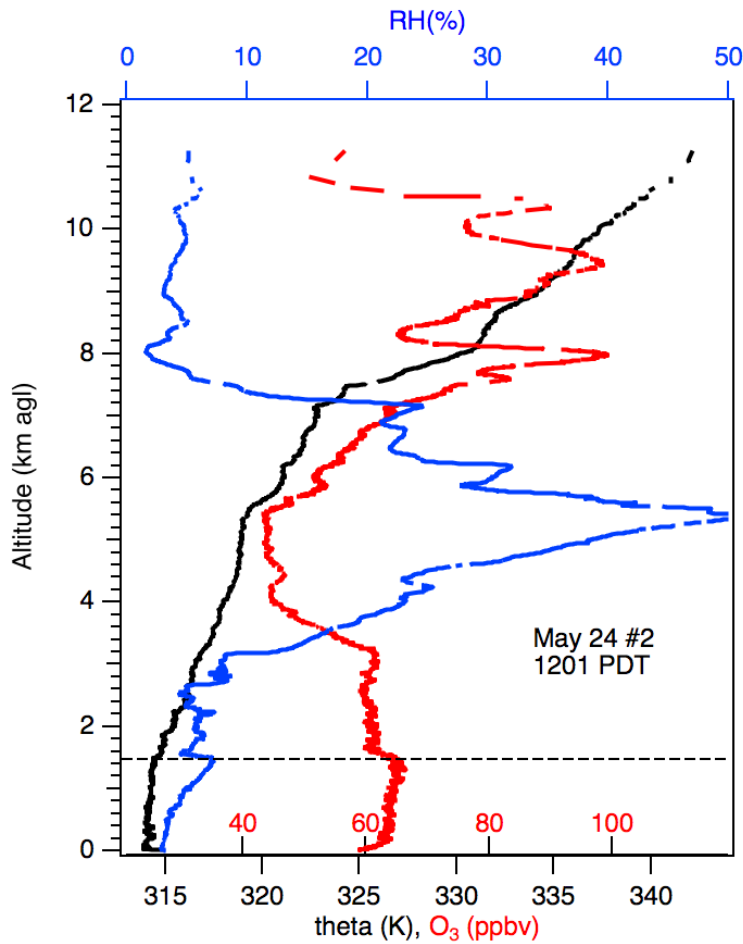
The lidar/ozonesonde curtain plots in **Figure 9-5** show that both TOPAZ and the ozonesondes detected high O<sub>3</sub> above 6 km agl most of the week, but they also detected an intervening layer of relatively moist Pacific background air (cf. **Figure 9-6**) with lower O<sub>3</sub> concentrations that mixed down to the surface on May 25.



1  
2  
3  
4  
5  
6  
7  
8  
9  
10

**Figure 9-5.** Time-height curtain plots of the TOPAZ (a) ozone, and (b) backscatter, measured during Week 2 of FAST-LVOS. The ascending Joe Neal ozonesonde profiles from IOP1 are superimposed. The colored horizontal bands in (a) show the in-situ measurements from the NLVA and AP. The black line shows the local mixed-layer height from the micro-Doppler lidar.

1  
2  
3



4  
5

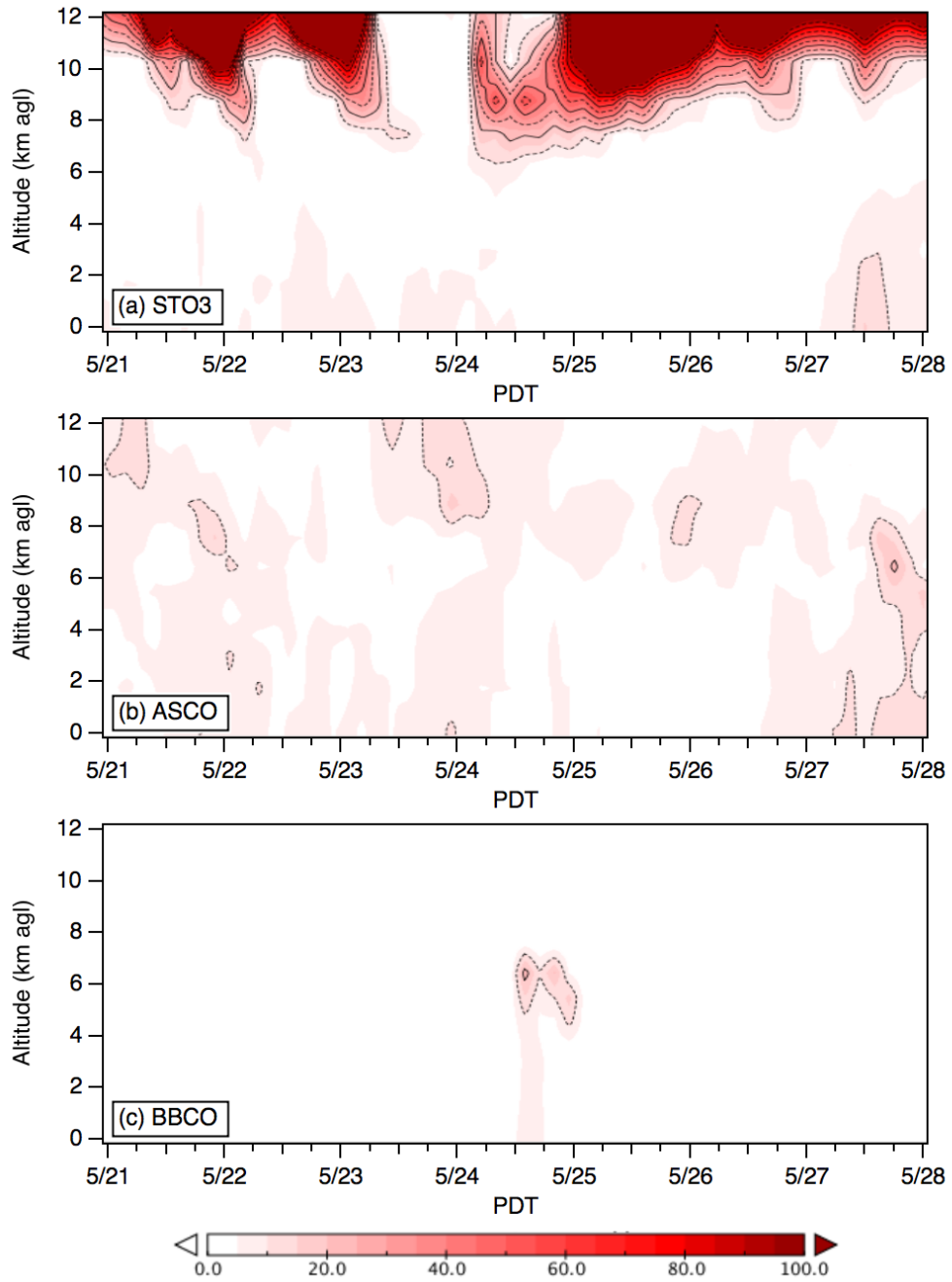
6 **Figure 9-6.** Profiles of potential temperature (black), O<sub>3</sub> (red), and relative humidity (blue) from  
7 the Joe Neal 1201 PDT ozonesonde on May 24. The dashed black horizontal line marks the top  
8 of the boundary layer.

9  
10

11 The FLEXPART STO3 tracer distributions in **Figure 9-7** show stratospheric air in the upper  
12 troposphere throughout the week, and the ASCO tracer shows modest influxes of Asian  
13 pollution throughout the troposphere. The BBCO tracer also shows a small wildfire plume  
14 between the surface and 6 km on the evening of May 24, which is qualitatively consistent with  
15 the backscatter measurements. However, none of these tracers show any significant surface  
16 impacts and cannot explain the high surface O<sub>3</sub> measured on May 23.

17  
18  
19  
20

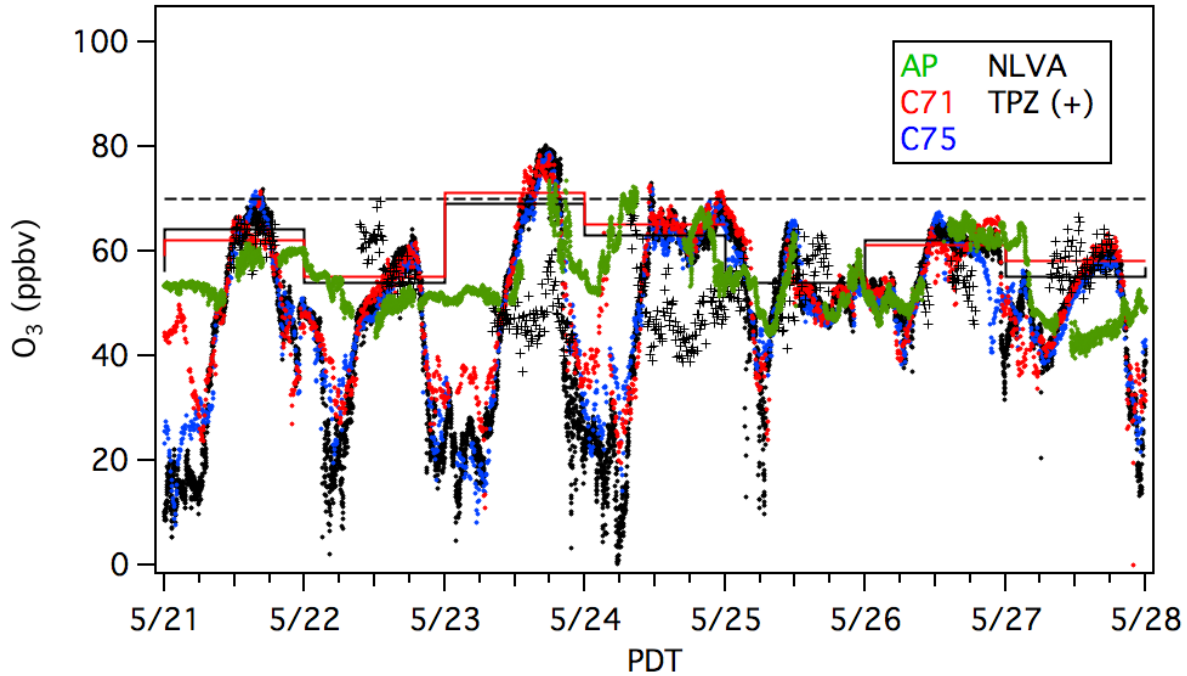
1  
2



3  
4  
5  
6  
7  
8  
9

**Figure 9-7.** Time-height curtain plots of the FLEXPART (a) STO3, (b) ASCO, and (c) BBCO tracer distributions above the LVV during Week 2 of FAST-LVOS.

1 The TOPAZ curtain plot also shows high O<sub>3</sub> in the boundary layer on May 23 and the Walter  
 2 Johnson monitor recorded the first NAAQS exceedance of *FAST-LVOS* (71 ppbv) on that day  
 3 with the nearby Palo Verde (68 ppbv) and Joe Neal (69 ppbv) monitors following close behind.  
 4 The Paul Meyer and JD Smith monitors also measured MDA8 O<sub>3</sub> in excess of 60 ppbv, but the  
 5 outlying monitors (e.g. Jean, Indian Springs, and Mesquite) only reported about 50 ppbv. Ozone  
 6 was more uniformly distributed on May 24 when all of the Clark County monitors recorded  
 7 MDA8 O<sub>3</sub> mixing ratios between 63 and 66 ppbv.  
 8

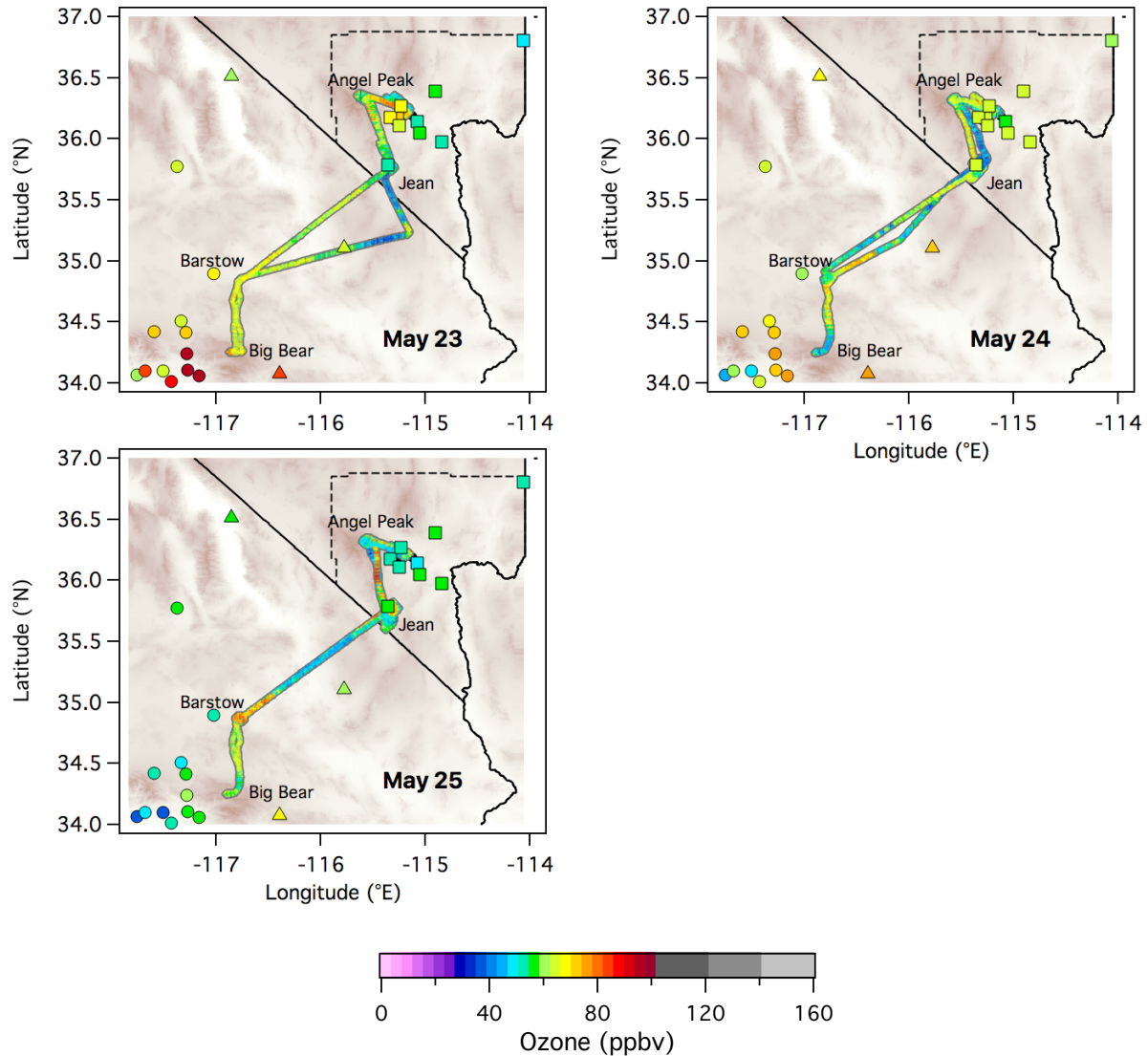


9  
 10 **Figure 9-8.** Time series of the TOPAZ O<sub>3</sub> mixing ratios at 4.0 km agl (black +) during Week 2  
 11 plotted with the 1-min O<sub>3</sub> measurements from the NLVA (black) and AP (green) and the 5-min  
 12 measurements from the Walter Johnson (C71, red) and Joe Neal (C75, blue) monitors. The red  
 13 and blue steps show the corresponding C71 and C75 MDA8 measurements. The dashed black  
 14 line indicates the 70 ppbv NAAQS.

15  
 16 The O<sub>3</sub> mixing ratios at 4.0 km were similar to or less than the surface concentrations (**Figure 9-**  
 17 **8**). The mixing ratios at AP were similar to those in the LVV, but the Angel Peak record has gaps  
 18 during the afternoons of May 23 and 24 when the mobile laboratory descended into the  
 19 western LVV.

20  
 21 More insight into the high O<sub>3</sub> on May 23 is provided by the Scientific Aviation measurements  
 22 which are summarized in **Figures 9-9** through **9-11**. The aircraft distributions above the LVV in  
 23 **Figure 9-10** appear very similar to the TOPAZ and ozonesonde profiles, with the highest O<sub>3</sub>  
 24 measured below 2 km during the landing approach on the afternoon of May 23. The latitudinal  
 25 transect from May 23 plotted in **Figure 9-11** shows that this high O<sub>3</sub> was confined to the

1 boundary layer above the LVV and therefore of local origin. The aircraft flight on May 24 shows  
2 the more regional distribution also seen in the surface measurements.  
3  
4  
5  
6

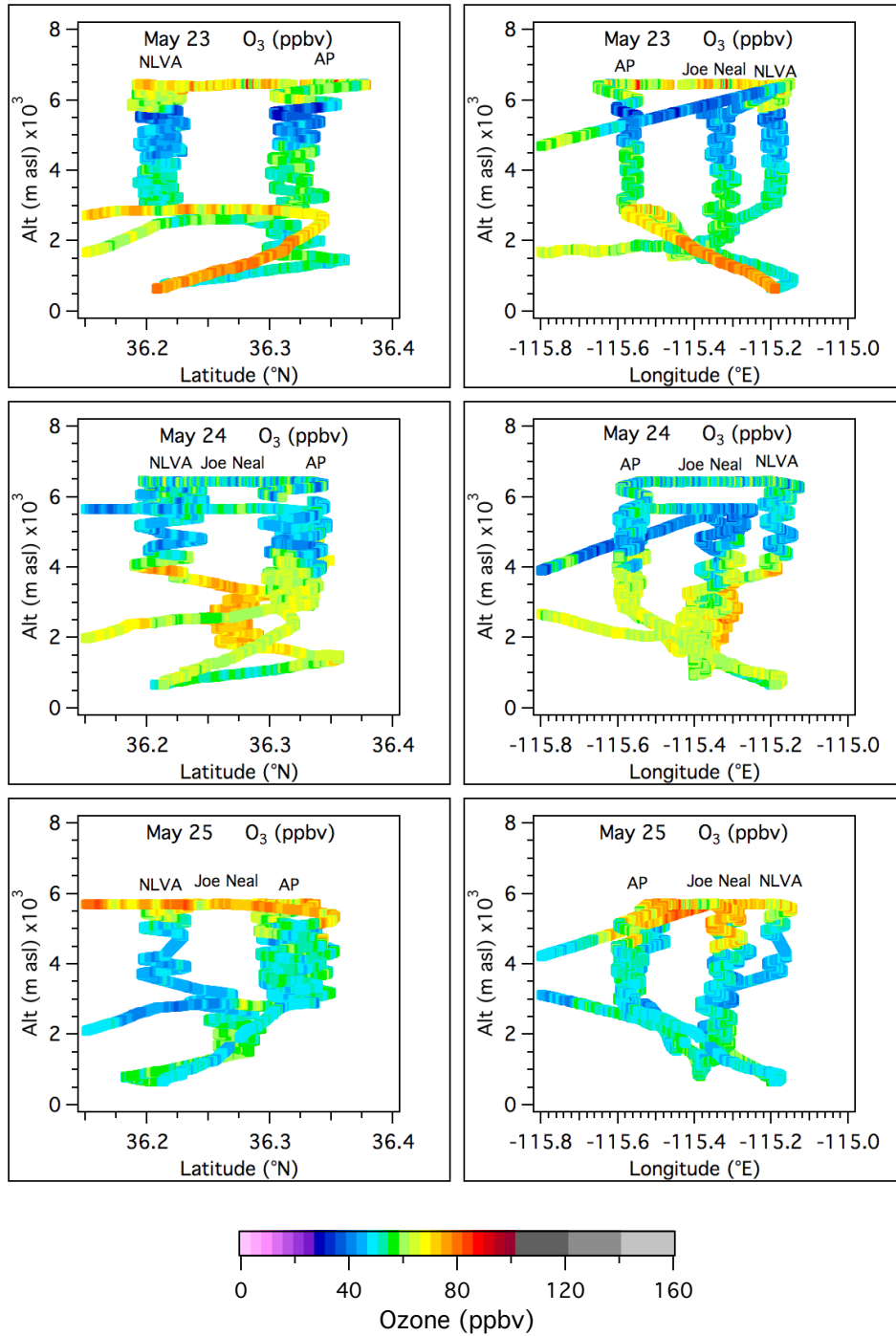


7  
8

9  
10

11 **Figure 9-9.** Flight tracks for the Scientific Aviation TLS Bravo during the first FAST-LVOS IOP (May  
12 23-25). The filled squares, circles, and triangles mark the locations of surface monitors operated  
13 by CCDAQ, CARB, and the USNPS, respectively. The flight tracks are colored to show the in situ  
14  $O_3$  and the symbols colored to show the reported MDA8  $O_3$ .  
15  
16  
17  
18

1  
2

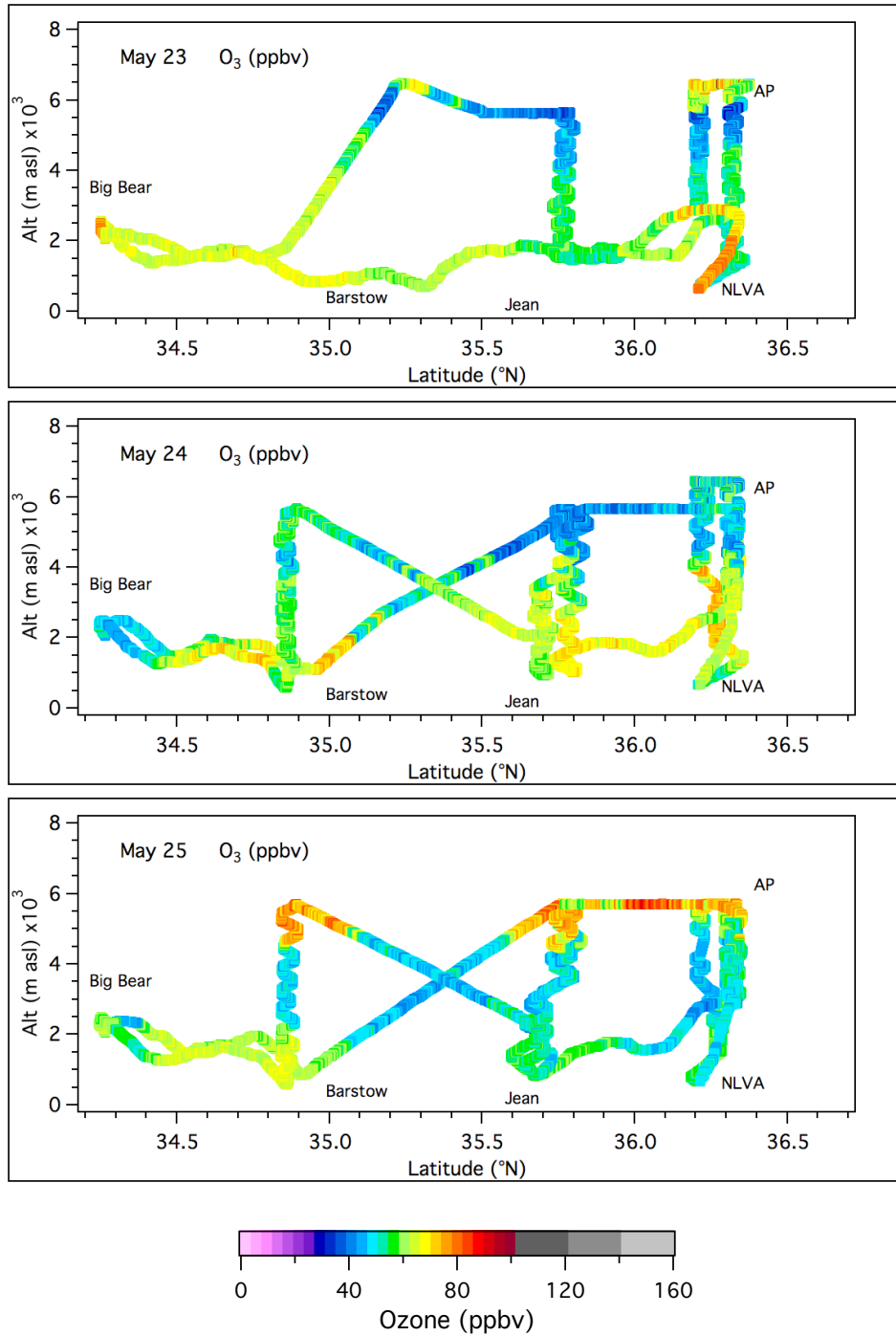


3  
4

5  
6

7 **Figure 9-10.** Scientific Aviation O<sub>3</sub> profiles above the NLVA, Joe Neal, and Angel Peak during the  
8 first IOP.

1  
2



3  
4

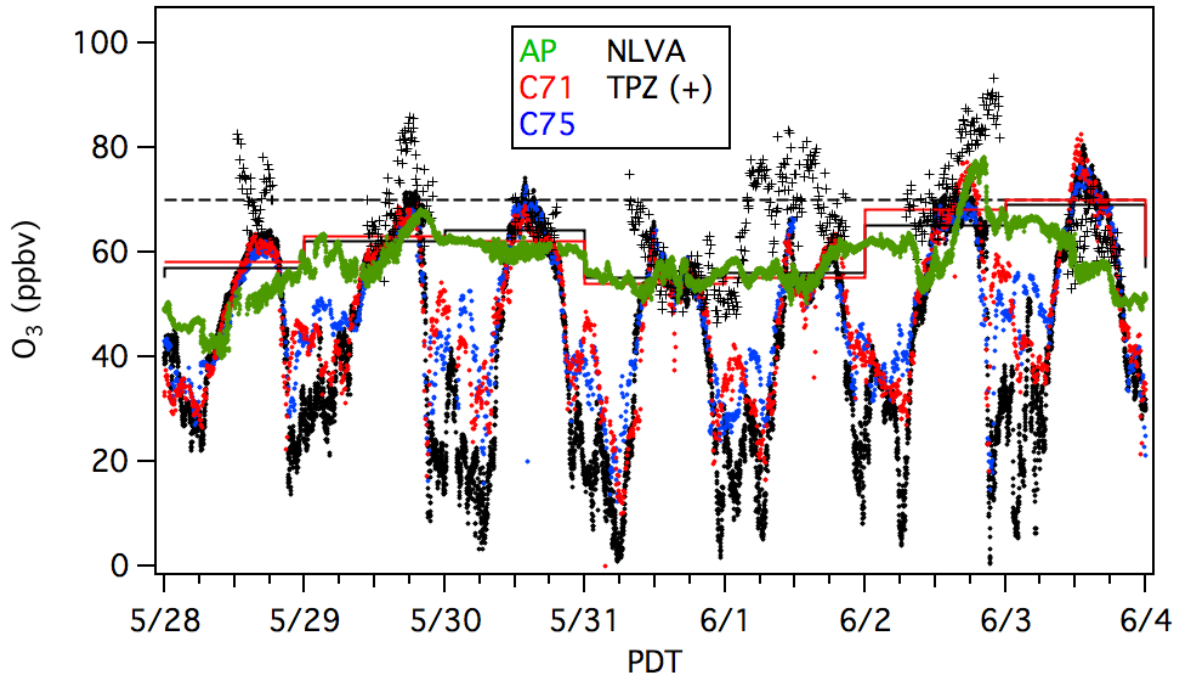
5  
6  
7  
8  
9  
10  
11

**Figure 9-11.** Ozone mixing ratios measured along the flights from NLVA to Big Bear, CA and back during the first IOP.

1 **9.3 Week 3: May 28-June 3 (IOP2)**

2  
3 The third week of FAST-LVOS featured slightly above average temperatures. The highs at the  
4 KVGT tower ranged between 34.4 and 38.9°C (94 and 102°F). The synoptic forecasts for the end  
5 of May showed the approach of another upper level low and the possibility of a tropopause  
6 fold. The second IOP began on May 31 with ozonesondes launched at 0900 and 1200 PDT.  
7 Three more ozonesondes were launched on both June 1 and 2 at around 0900, 1200, and 1500  
8 PDT. Scientific Aviation conducted research flights on all three days.  
9

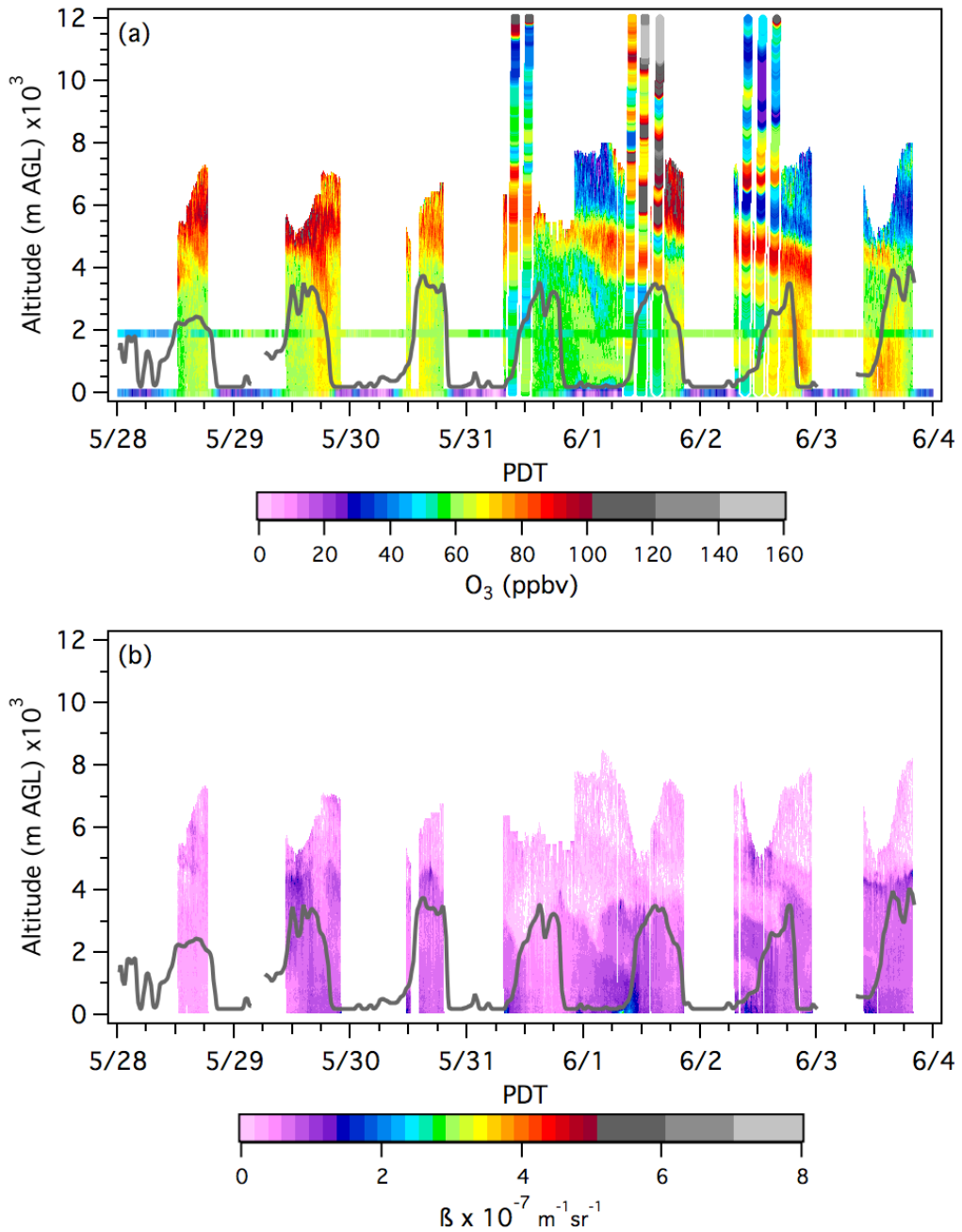
10 The surface measurements plotted in **Figure 9-12** show elevated O<sub>3</sub>, but no exceedances at the  
11 LVV surface monitors. The Walter Johnson and Joe Neal monitors recorded MDA8 O<sub>3</sub>  
12 concentrations of 68 and 65 ppbv on June 2, and 70 and 69 ppbv on June 3. TOPAZ measured  
13 higher O<sub>3</sub> at 4 km on those days as well as on May 28-29, suggesting that there may have been  
14 some transport to the surface.  
15



16  
17 **Figure 9-12.** Time series of the TOPAZ O<sub>3</sub> mixing ratios at 4.0 km agl (black +) during Week 3  
18 plotted with the 1-min O<sub>3</sub> measurements from the NLVA (black) and AP (green) and the 5-min  
19 measurements from the Walter Johnson (C71, red) and Joe Neal (C75, blue) monitors. The red  
20 and blue steps show the corresponding C71 and C75 MDA8 measurements. The dashed black  
21 line indicates the 70 ppbv NAAQS.  
22

23 The high O<sub>3</sub> aloft is more easily seen in the curtain plot of **Figure 9-13**. The lower panel **also**  
24 shows higher backscatter than was observed in the previous weeks that is sometimes  
25 correlated with and sometimes anticorrelated with O<sub>3</sub>. The curtain plots appear to show  
26 entrainment of O<sub>3</sub> from above on the afternoons of May 29 and June 2.

1  
2  
3



4  
5  
6  
7  
8  
9  
10

**Figure 9-13.** Time-height curtain plots of the TOPAZ (a) ozone, and (b) backscatter, measured during Week 3 of FAST-LVOS. The ascending Joe Neal ozonesonde profiles from IOP2 are superimposed. The colored horizontal bands in (a) show the in-situ measurements from the NLVA and AP. The black line shows the local mixed-layer height from the micro-Doppler lidar.

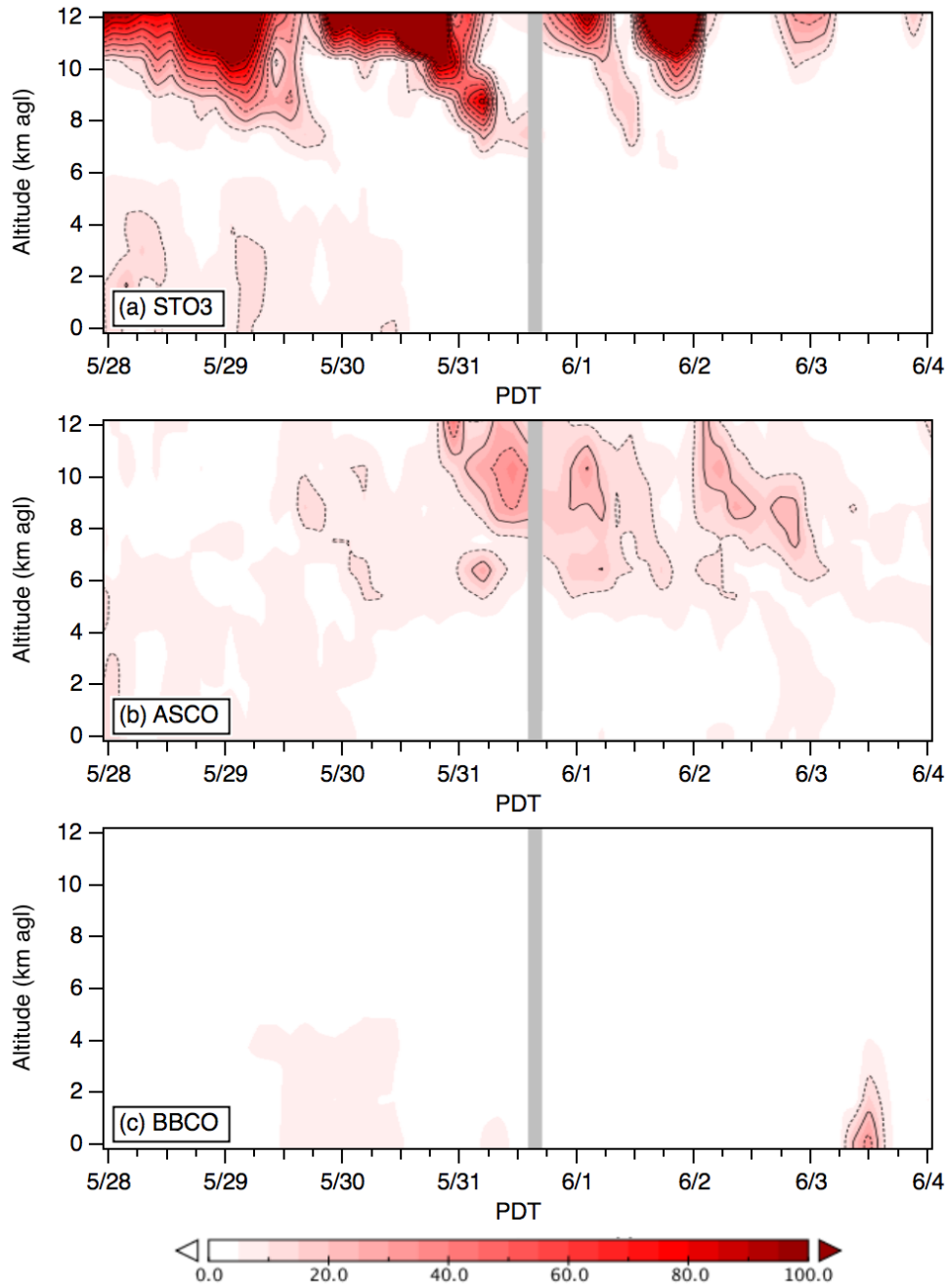
1 The FLEXPART curtain plots in **Figure 9-14** show multiple tongues of STO3 tracer descending  
2 into the upper troposphere that were followed several days later by filaments of the ASCO  
3 tracer (cf. **Figures 8-2** and **8-3**). Smaller concentrations of both tracers reached the surface on  
4 May 28-30, and some ASCO tracer appears near the surface on June 2. The bottom panel also  
5 shows small enhancements in the BBCO tracer near the surface on May 30 and June 3.

6  
7 **Figure 9-15** displays enlarged curtain plots for the TOPAZ measurements from June 2 and 3,  
8 which show the complex relationship between  $O_3$  and  $\beta$  on these days more clearly. The NLVA  
9 and AP in-situ measurements and June 2 ozonesonde profiles are superimposed as before. The  
10 low-lying residual layer with about 70 ppbv of  $O_3$  seen just above the top of the boundary layer  
11 on the morning of June 2 has relatively low aerosol loading, as does the thin layer with about 80  
12 ppbv of  $O_3$  that slopes downward from 4 km to the top of the afternoon mixed layer. The  
13 intervening layer with less than 60 ppbv of  $O_3$  has higher aerosol, however, and the ozonesonde  
14 profiles in **Figure 9-16** show that this layer also has high relative humidity. The highly laminar  
15 band with about 100 ppbv of  $O_3$  that slopes downward from about 5 to 4 km also has high  
16 aerosol, but low relative humidity. The relatively high aerosol loading suggests that these layers  
17 were caused by Asian pollution or Siberian wildfires and not stratospheric intrusions or North  
18 American biomass burning plumes. This interpretation is supported by the FLEXPART tracer  
19 distributions in **Figure 9-14** (the FLEXPART biomass burning tracer only includes North American  
20 sources). The low relative humidity seen in the ozonesonde profiles suggests that the pollution  
21 was transported across the Pacific in the upper in the upper troposphere. The regular  
22 undulations seen in the ozone and relative humidity profiles and parallel sloping bands in the  
23 ozone and backscatter curtain plots on June 2 are probably caused by horizontally propagating  
24 gravity waves [Langford *et al.*, 1996] that may have contributed to the downward transport of  
25 the Asian pollution.

26  
27 The Scientific Aviation flights above the LVV and Angel Peak during IOP2 provide additional  
28 evidence that the elevated ozone was primarily transported Asian pollution. **Figures 9-17** and **9-**  
29 **18** show that  $CH_4$  was also elevated in the 5 km layer with high  $O_3$ ,  $\beta$ , and low RH.

30  
31 The Angel Peak in-situ measurements plotted in **Figure 9-19** and **9-20** show that  $O_3$  and CO  
32 were positively correlated during most of the week. The highest  $O_3$  was measured on the  
33 evening of June 2 after a period of southeasterly upslope flow, and was accompanied by  
34 increases in CO,  $NO_2$ , and  $NO_y$ . The peak in the time series coincides with the rapid descent of  
35 the  $O_3$  from the transport layer as the mixed layer subsided (**Figure 9-15**). The curtain plot  
36 suggests that this high  $O_3$  remained in the residual layer above the LVV and was entrained the  
37 following morning to contribute to the high surface  $O_3$  on June 3.

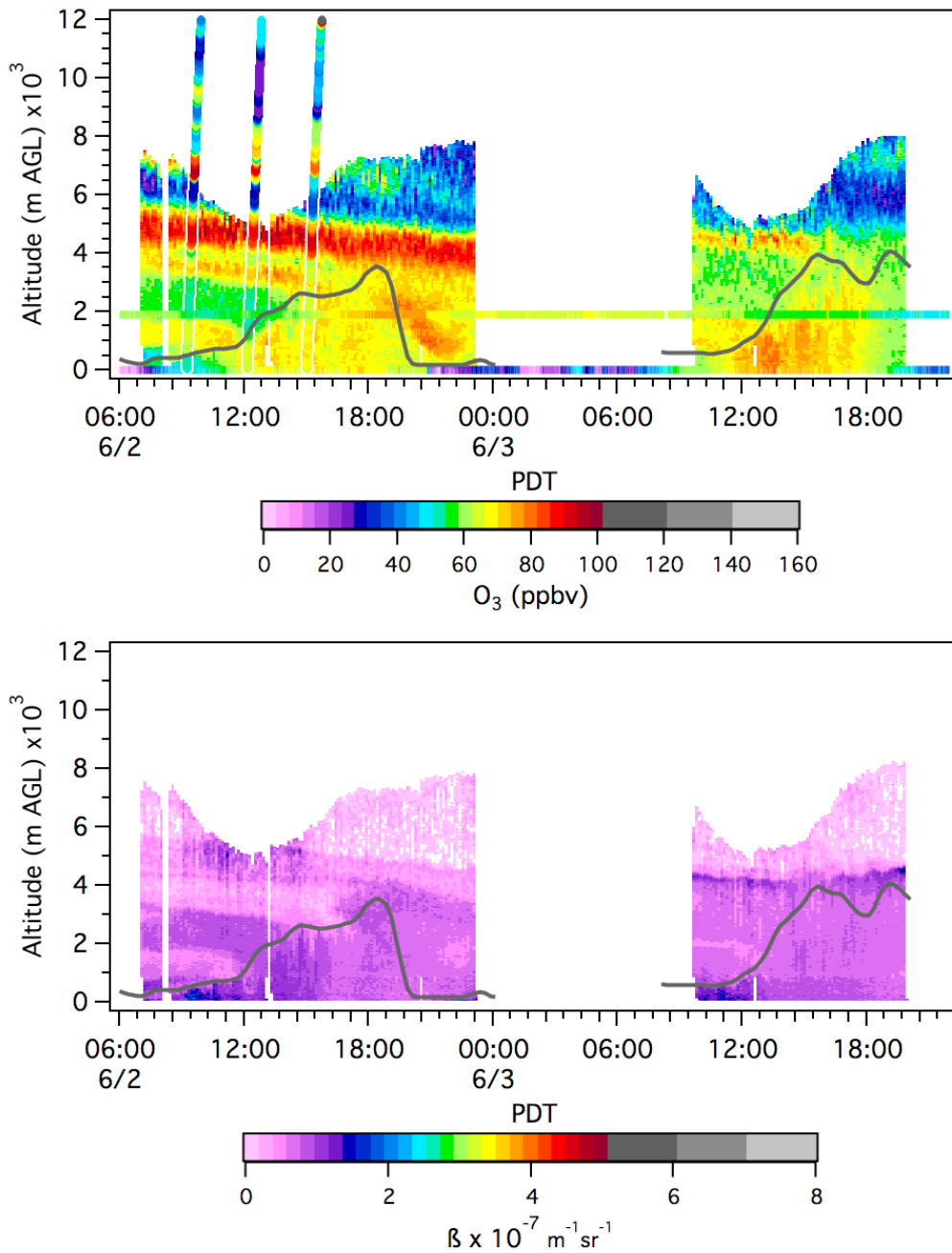
1  
2



3  
4  
5  
6  
7  
8  
9  
10

**Figure 9-14.** Time-height curtain plots of the FLEXPART (a) STO3, (b) ASCO, and (c) BBCO tracer distributions above the LVV during Week 3 of FAST-LVOS.

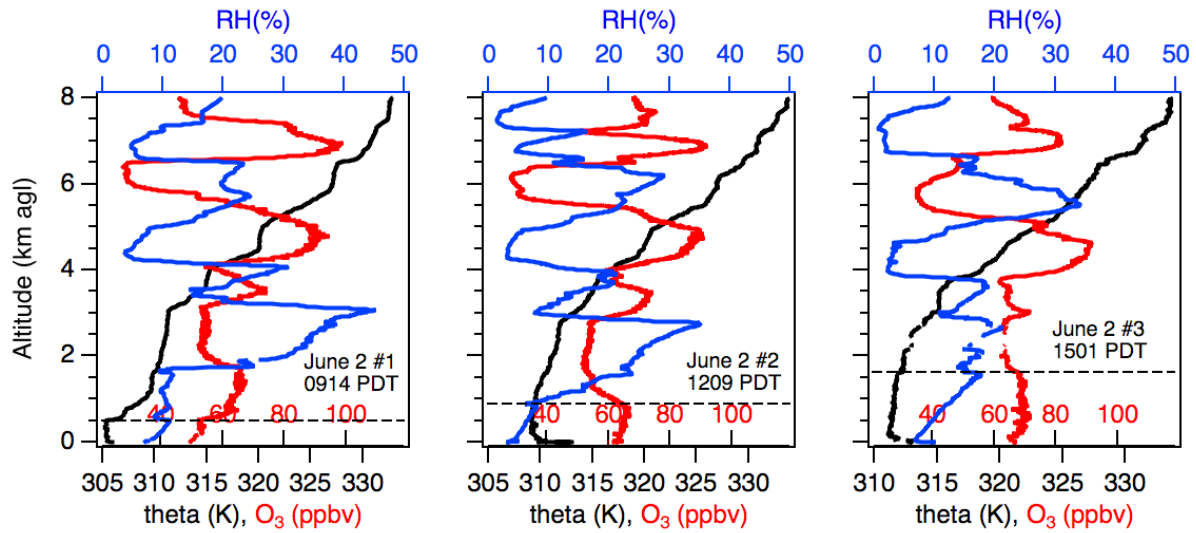
1  
2



3  
4  
5  
6  
7  
8  
9

**Figure 9-15.** Time-height curtain plots of the TOPAZ (a) ozone, and (b) backscatter, measured on June 2-3. The ascending Joe Neal ozonesonde profiles from IOP2 are superimposed. The colored horizontal bands in (a) show the in-situ measurements from the NLVA and AP. The black line shows the local mixed-layer height from the micro-Doppler lidar.

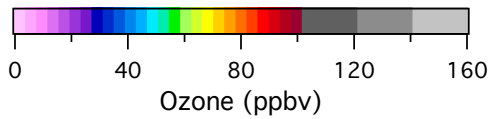
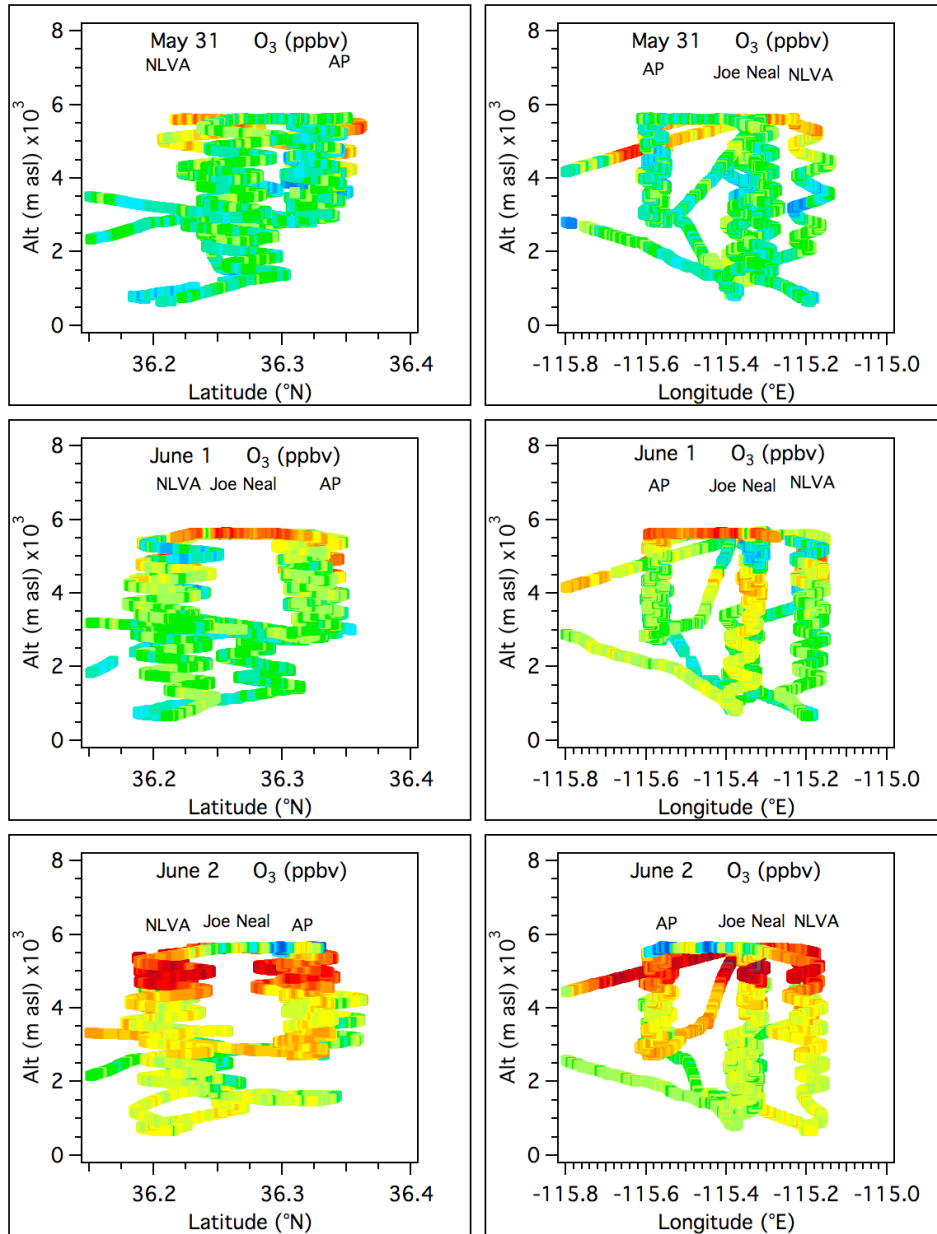
1  
2  
3  
4  
5  
6



7  
8  
9  
10  
11  
12  
13  
14  
15  
16

**Figure 9-16.** Profiles of potential temperature (black), O<sub>3</sub> (red), and relative humidity (blue) from the Joe Neal ozonesondes on June 2. The dashed black horizontal line marks the top of the boundary layer.

1  
2



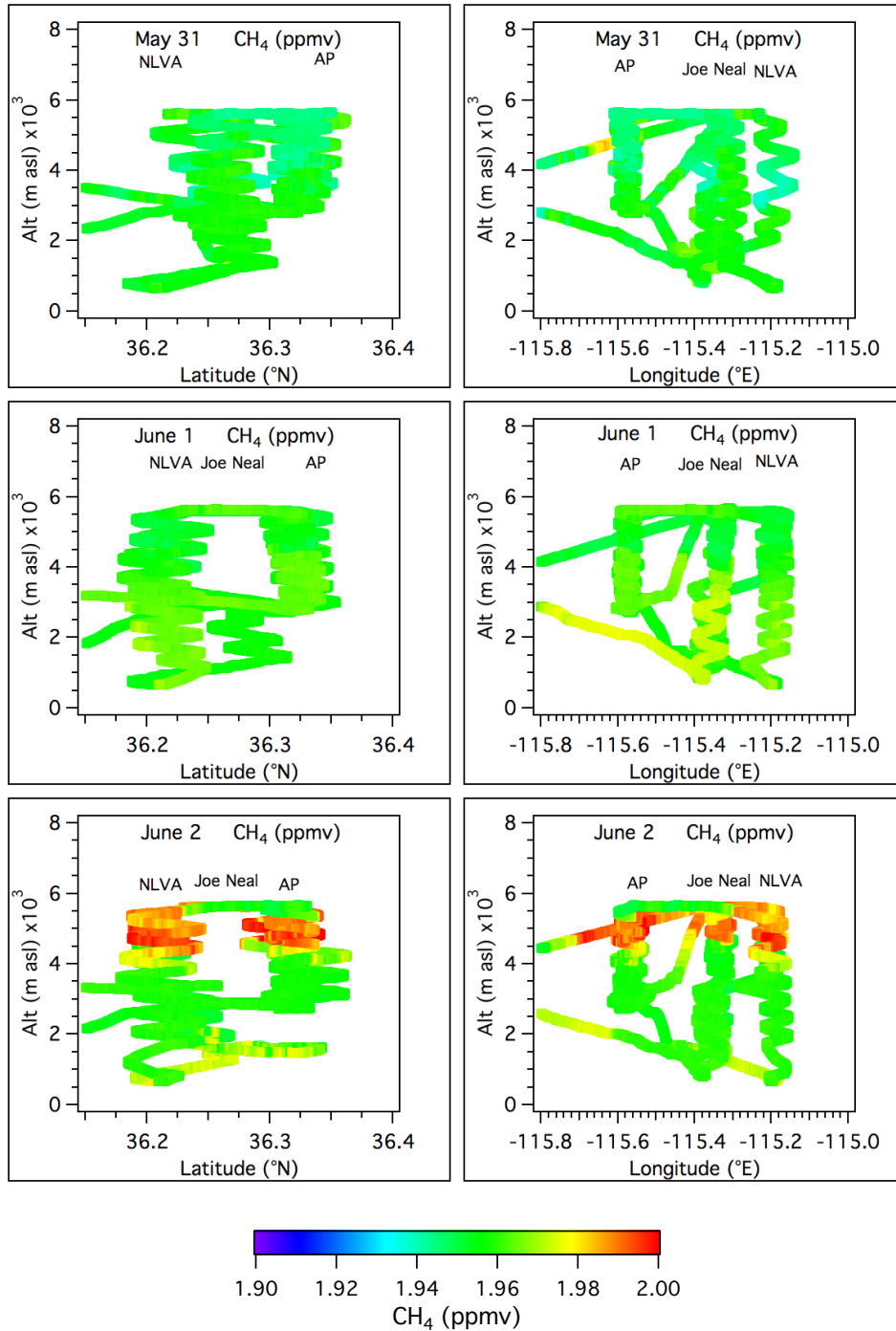
3  
4  
5

6  
7

8 **Figure 9-17.** Scientific Aviation O<sub>3</sub> profiles above the NLVA, Joe Neal, and Angel Peak during the  
9 second IOP.

10  
11

1  
2



3  
4

5  
6

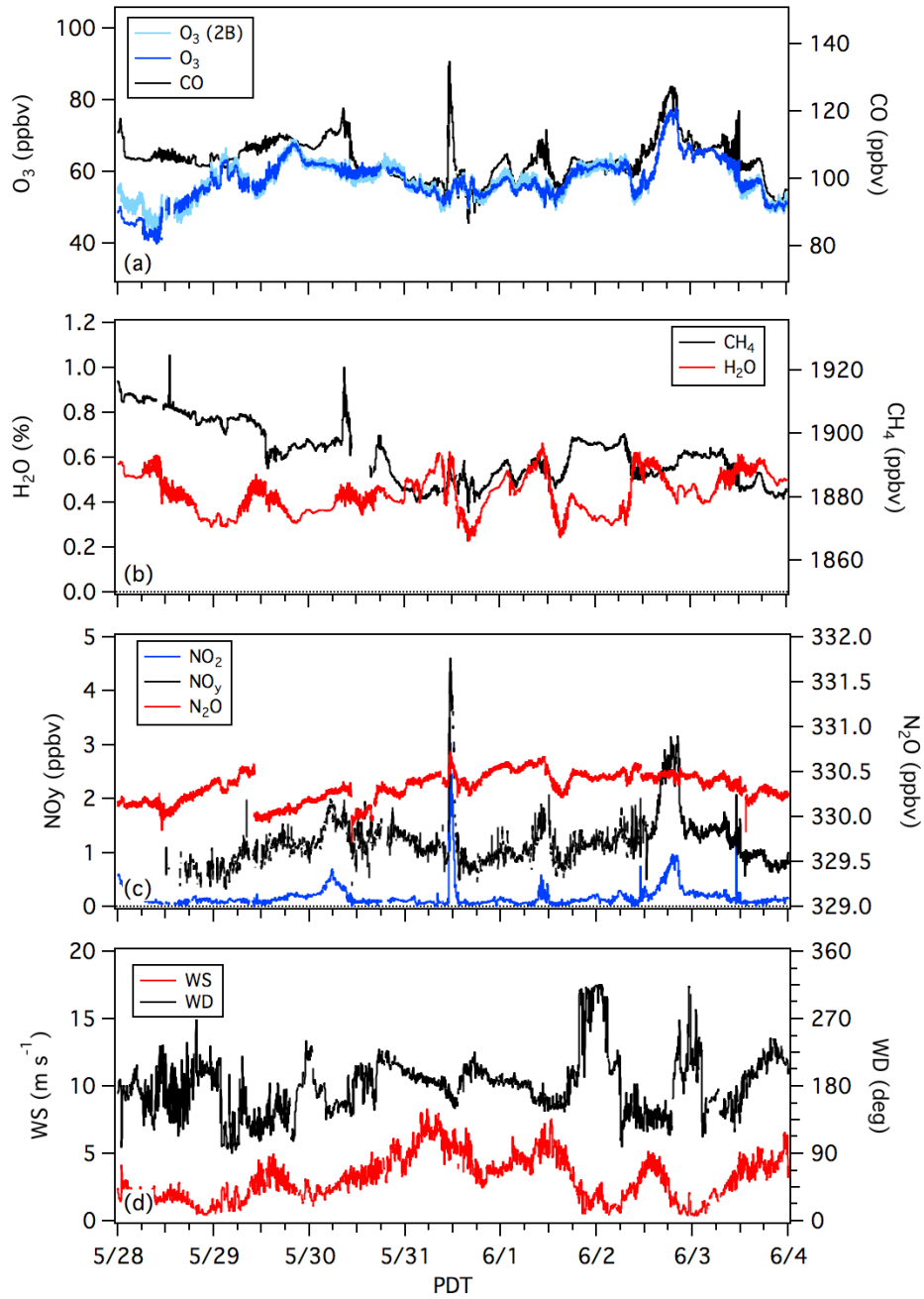
7 **Figure 9-18.** Scientific Aviation CH<sub>4</sub> profiles above the NLVA, Joe Neal, and Angel Peak during the  
8 second IOP.

9

10

11

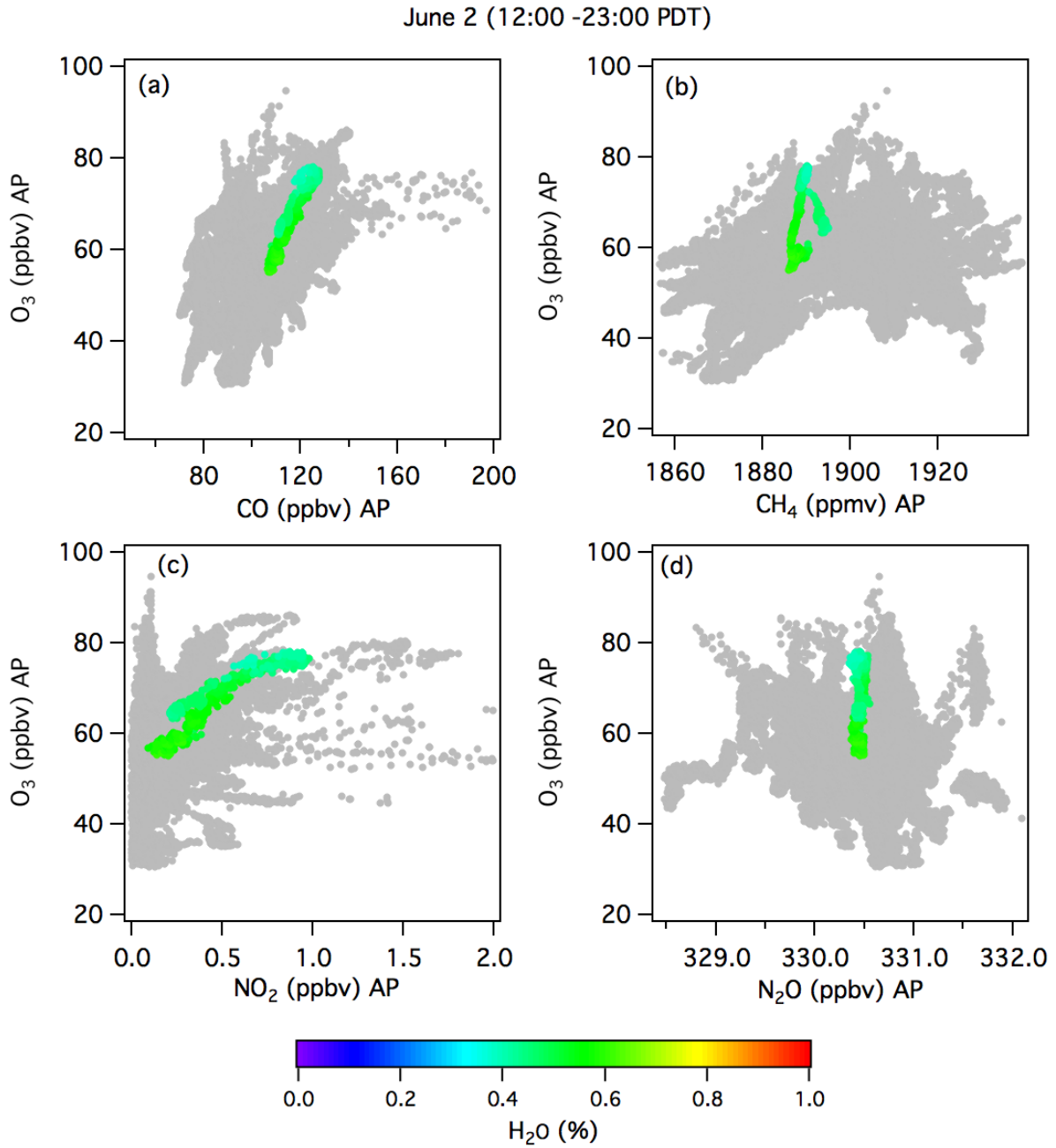
1  
2



3  
4  
5  
6  
7  
8  
9  
10

**Figure 9-19.** Time series of (a) O<sub>3</sub> and CO, (b) H<sub>2</sub>O and CH<sub>4</sub>, (c) NO<sub>x</sub>, NO<sub>y</sub> and N<sub>2</sub>O, and (d) wind speed and direction measured by the mobile laboratory on Angel Peak during Week 3 of FAST-LVOS. The narrow CO and NO<sub>y</sub> spikes near noon on May 31 are probably of local origin.

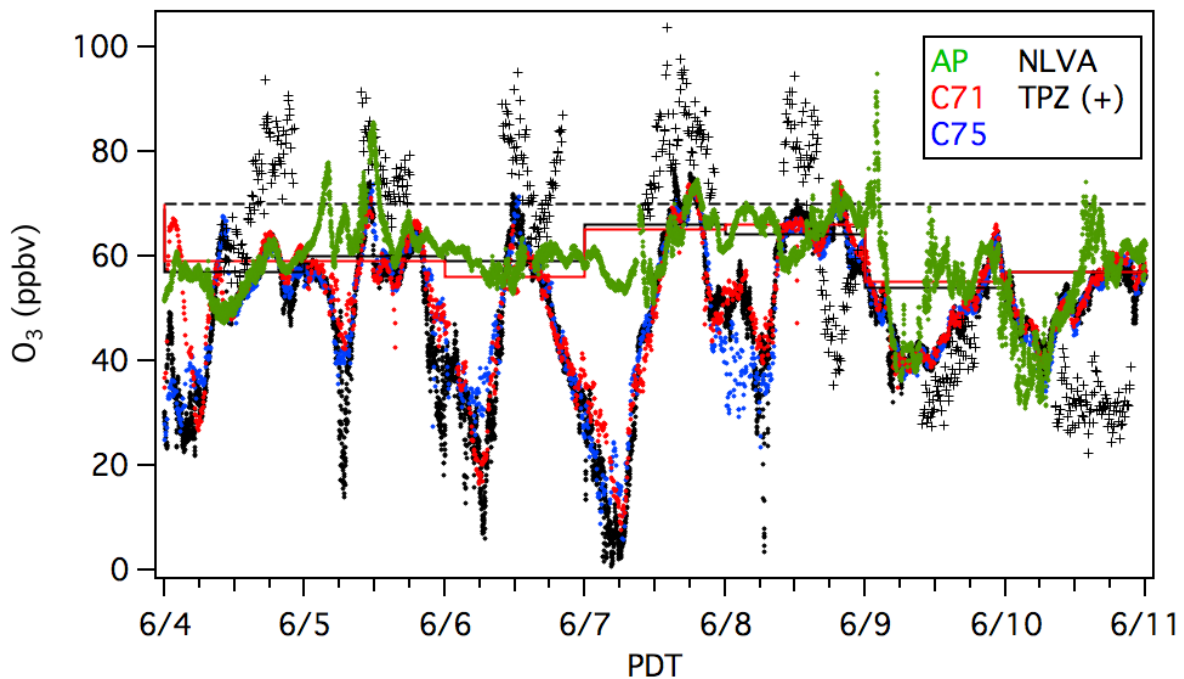
1  
2  
3  
4



5  
6 **Figure 9-20.** Scatter plots showing the correlations between in-situ O<sub>3</sub> and (a) CO, (b) N<sub>2</sub>O, (c)  
7 CO<sub>2</sub>, and (d) CH<sub>4</sub> measurements from the mobile lab on Angel Peak. The measurements from the  
8 afternoon and evening (12-23 PDT) of June 2 are colored by the water vapor measurements.  
9

1 **9.4 Week 4: June 4-10**

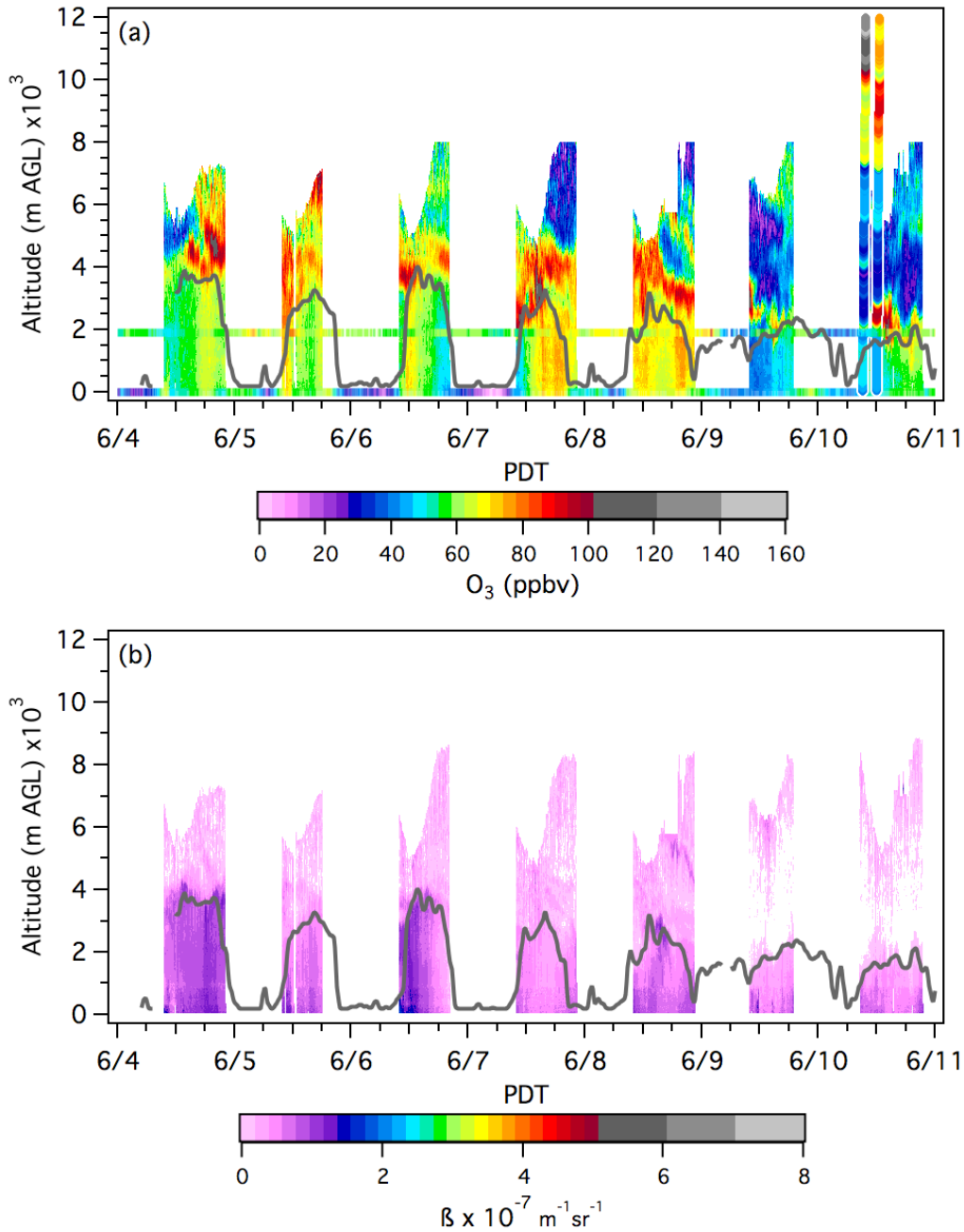
2  
3 The second week of June started out very hot with the daily highs exceeding 37.8°C (100°F)  
4 from the 4<sup>th</sup> to the 8<sup>th</sup>. The high dropped to 35°C (95°F) on June 9 with the arrival of the cold  
5 front preceding the large tropopause fold event of the following week (cf. **Figure 8-2**). June 10  
6 marked the first day of IOP3. There were no exceedances of the 2015 NAAQS during Week 4,  
7 but **Figure 9-21** shows that the MDA8 O<sub>3</sub> at the Walter Johnson and Joe Neal monitors  
8 increased from about 55 ppbv on June 4, to 65 ppbv on June 7 and 8. The concentrations fell to  
9 much lower values with the arrival of the cold front. The ozone curtain plot in **Figure 9-22**  
10 shows high O<sub>3</sub> around 4 km between June 4 and June 8, and appears to show some of this O<sub>3</sub>  
11 being entrained into the mixed layer on each day.  
12



13  
14  
15 **Figure 9-21.** Time series of the TOPAZ O<sub>3</sub> mixing ratios at 4.0 km agl (black +) during Week 4  
16 plotted with the 1-min O<sub>3</sub> measurements from the NLVA (black) and AP (green) and the 5-min  
17 measurements from the Walter Johnson (C71, red) and Joe Neal (C75, blue) monitors. The red  
18 and blue steps show the corresponding C71 and C75 MDA8 measurements. The dashed black  
19 line indicates the 70 ppbv NAAQS.

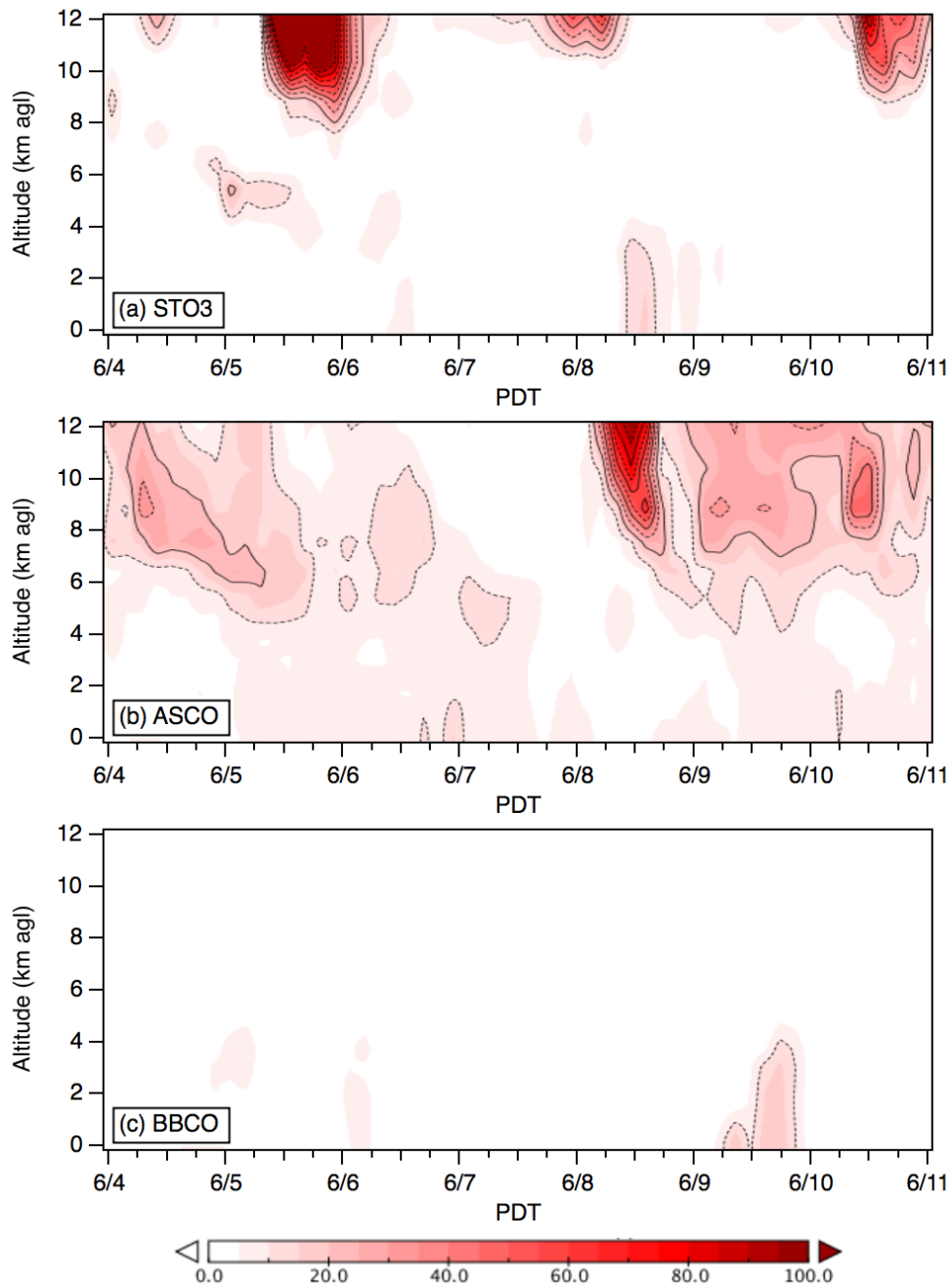
20  
21 The FLEXPART curtains in **Figure 9-23** (and map in **Figure 8-3**) show some stratospheric O<sub>3</sub> and  
22 large amounts of Asian pollution above Las Vegas during Week 4. Unfortunately, there were no  
23 ozonesondes or aircraft sorties during the first part of the week to help establish the source of  
24 the high O<sub>3</sub>.  
25  
26

1



2  
3  
4  
5  
6  
7  
8  
9  
10

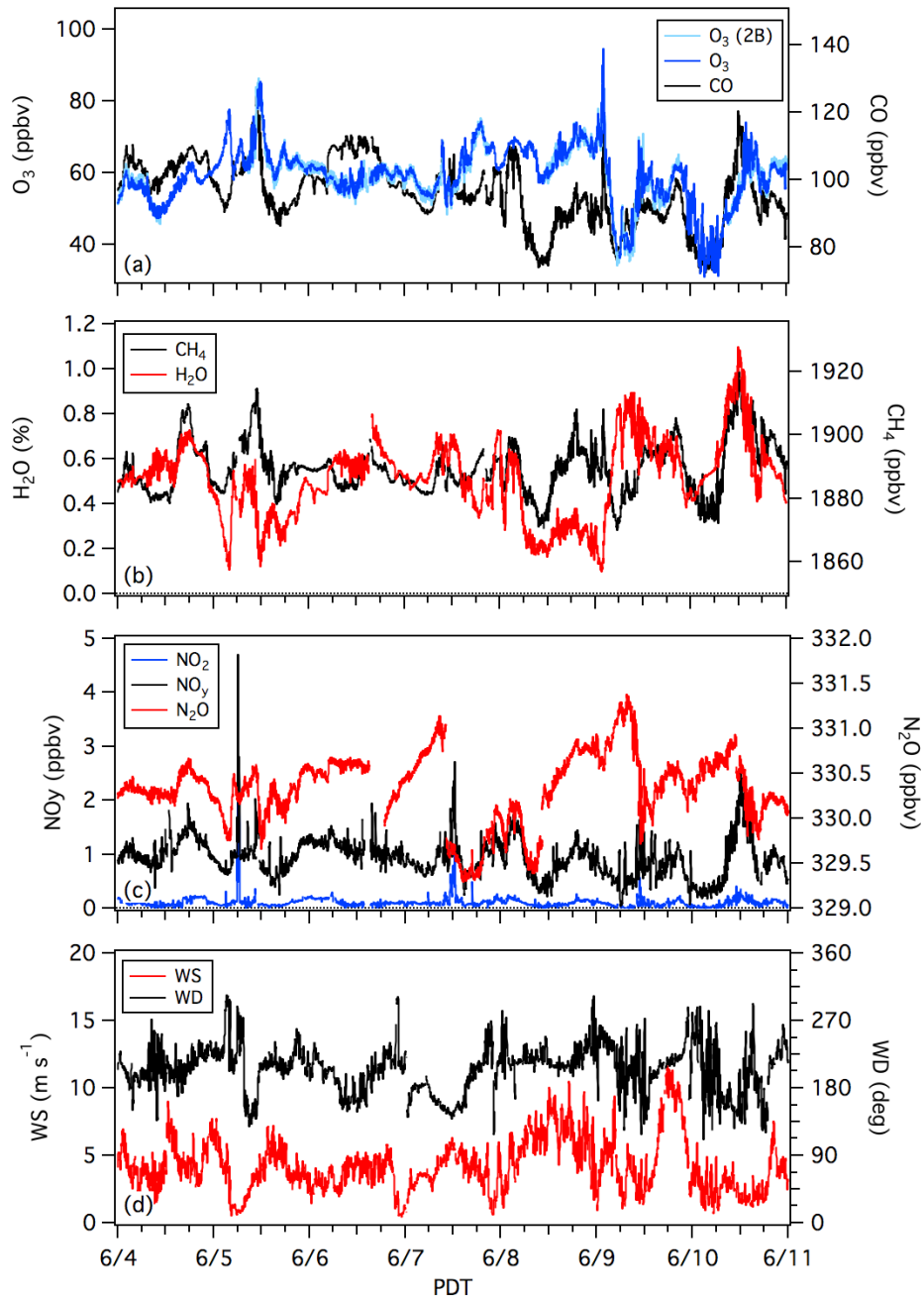
**Figure 9-22.** Time-height curtain plots of the TOPAZ (a) ozone, and (b) backscatter, measured during Week 4. The ascending Joe Neal ozonesonde profiles from IOP3 are superimposed. The colored horizontal bands in (a) show the in-situ measurements from the NLVA and AP. The black line shows the local mixed-layer height from the micro-Doppler lidar.



1  
2  
3  
4  
5  
6

**Figure 9-23.** Time-height curtain plots of the FLEXPART (a) STO3, (b) ASCO, and (c) BBCO tracer distributions above the LVV during Week 4 of FAST-LVOS.

1 **Figures 9-21 and 9-22** show that some of the O<sub>3</sub> aloft reached the summit of Angel Peak on the  
 2 morning of June 5, and the time series in **Figure 9-24** show that the first peak to 77 ppbv at  
 3 about 0400 PDT was accompanied by decreases in CO and CH<sub>4</sub>, but the second peak of 85 ppbv  
 4 around local noon was accompanied first by increased, and then decreased CO and CH<sub>4</sub>.  
 5



6  
 7  
 8 **Figure 9-24.** Time series of (a) O<sub>3</sub> and CO, (b) H<sub>2</sub>O and CH<sub>4</sub>, (c) NO<sub>x</sub>, NO<sub>y</sub> and N<sub>2</sub>O, and (d) wind  
 9 speed and direction measured by the mobile laboratory on Angel Peak during Week 4 of FAST-  
 10 LVOS.

1 These correlations (**Figure 9-25**) show that the descending air was composed of intermingled  
2 stratospheric air and Asian pollution. **Figure 9-24a** also shows a narrow  $O_3$  spike around 0200  
3 PDT on June 9 that was accompanied by increased CO and  $CH_4$  consistent with Asian pollution.  
4  
5

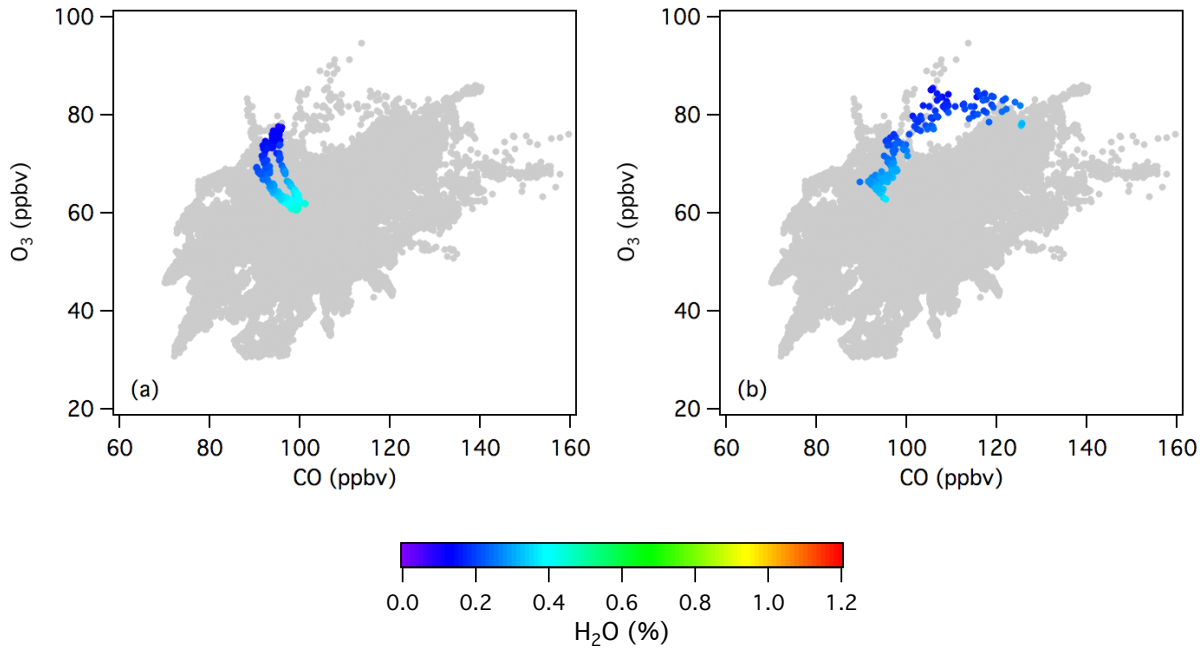
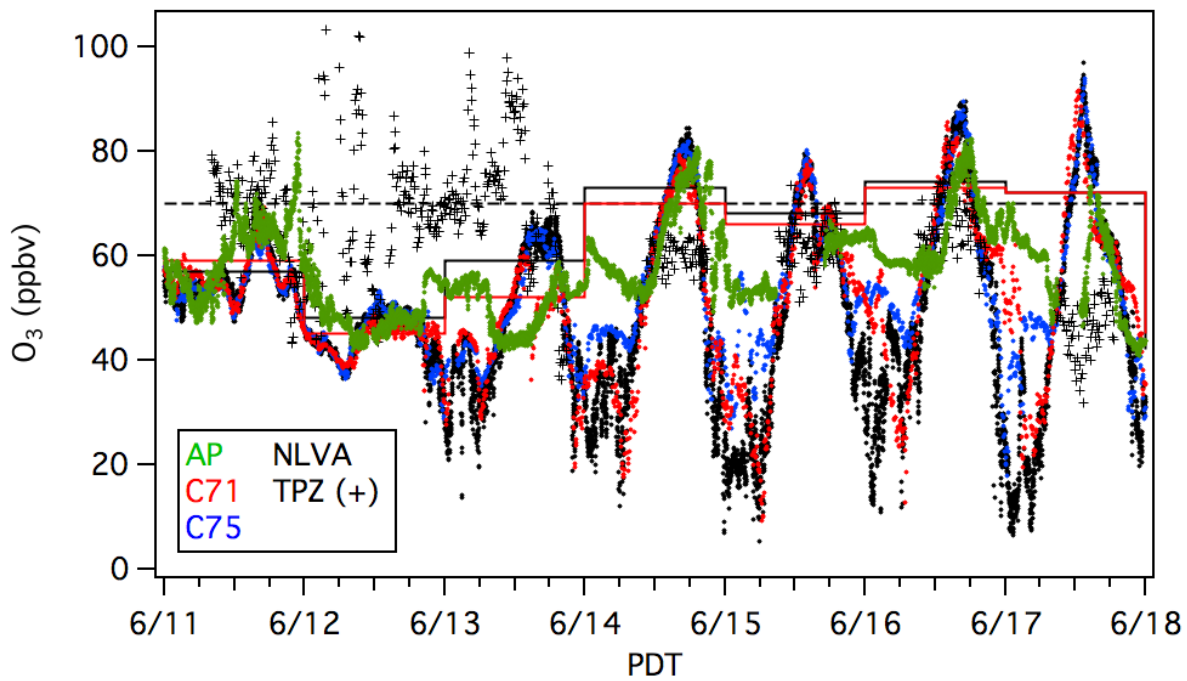


**Figure 9-25.** Scatter plots showing the correlations between in-situ  $O_3$  and CO on Angel Peak. The measurements from (a) 0000 to 0445 PDT, and (b) 1030-1400 PDT on June 5 are colorized by the water vapor measurements.

1 **9.5 Week 5: June 11-17 (IOP3)**

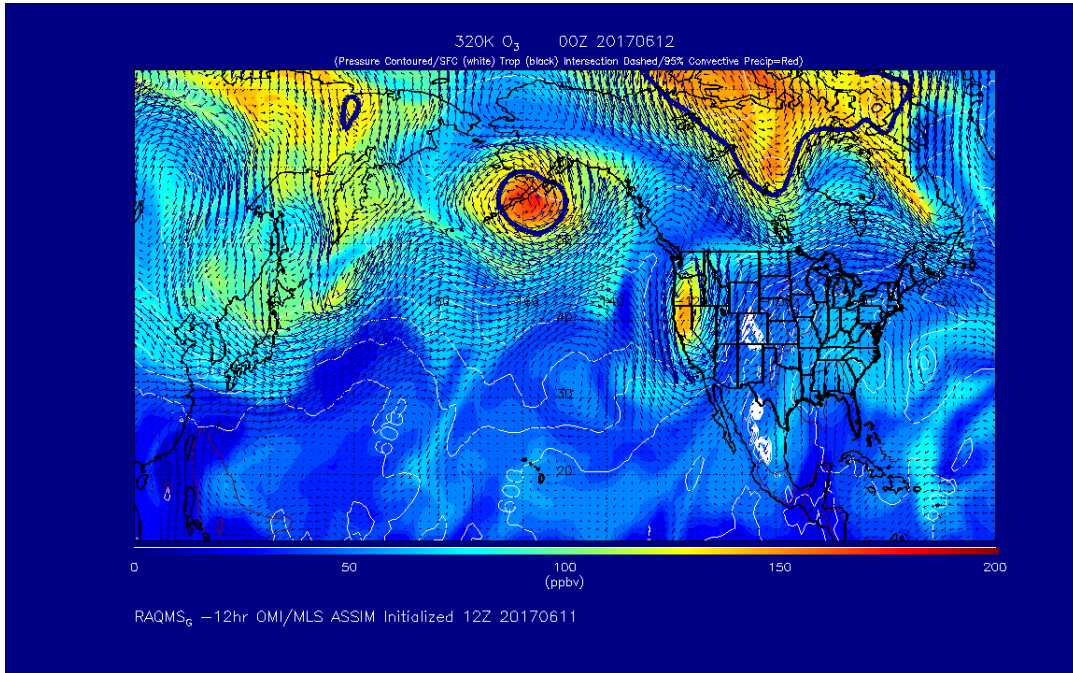
2  
3 The arrival of the cold front ahead of the deep upper-level trough (cf. **Figure 6-3**) brought  
4 welcome relief from the hot weather of the previous week. The temperatures dropped below  
5 freezing at Angel Peak on the morning of on June 12 (cf. **Figure 6-2**) and the daily high  
6 temperature reached only 26.7 at the KVG T station with a low of 20.6°C (80 and 69°F,  
7 respectively). Sustained southerly winds of up to 15 m s<sup>-1</sup> kept the nocturnal boundary layer  
8 from forming so that the concentrations did not fall during the night of June 11-12, and **Figure**  
9 **9-26** shows that surface ozone fell below 50 ppbv at both the NLVA and AP on June 12 as free  
10 tropospheric air descended ahead of the tropopause fold. Ozone remained high at 4 km  
11 through the evening of June 13, but then decreased as the trough receded eastward and was  
12 followed by a strong ridge and a return to hot conditions. The peak MDA8 concentrations in the  
13 LVV increased to values between 68 and 75 ppbv over the next 4 days as the temperatures  
14 climbed to a high of 42.8°C (109°F).  
15  
16



17  
18  
19 **Figure 9-26.** Time series of the TOPAZ O<sub>3</sub> mixing ratios at 4.0 km agl (black +) during Week 5  
20 plotted with the 1-min O<sub>3</sub> measurements from the NLVA (black) and AP (green) and the 5-min  
21 measurements from the Walter Johnson (C71, red) and Joe Neal (C75, blue) monitors. The red  
22 and blue steps show the corresponding C71 and C75 MDA8 measurements. The dashed black  
23 line indicates the 70 ppbv NAAQS.  
24  
25

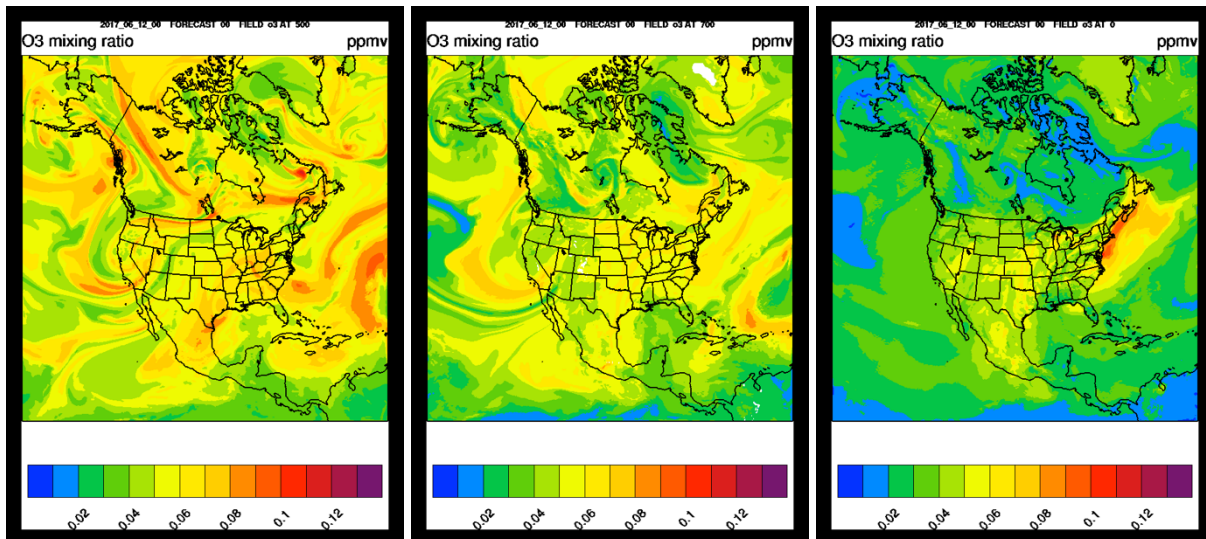
1 The tropopause fold appeared in both the RAQS and RAP-Chem forecasts (**Figures 9-27 and 9-**  
2 **28**) and the third IOP was scheduled for June 10-14.

3  
4



5  
6  
7  
8  
9  
10

**Figure 9-27.** NOAA NESDIS RAQMS model 320 K O<sub>3</sub> forecast for June 12 00UT. Forecast initialized June 11 12UT.



11  
12  
13  
14  
15

**Figure 9-28.** RAP-Chem total ozone analyses for 00UT on June 12 at (left to right) 500 hPa, 700 hPa, and the surface. Concentrations are given in ppmv.

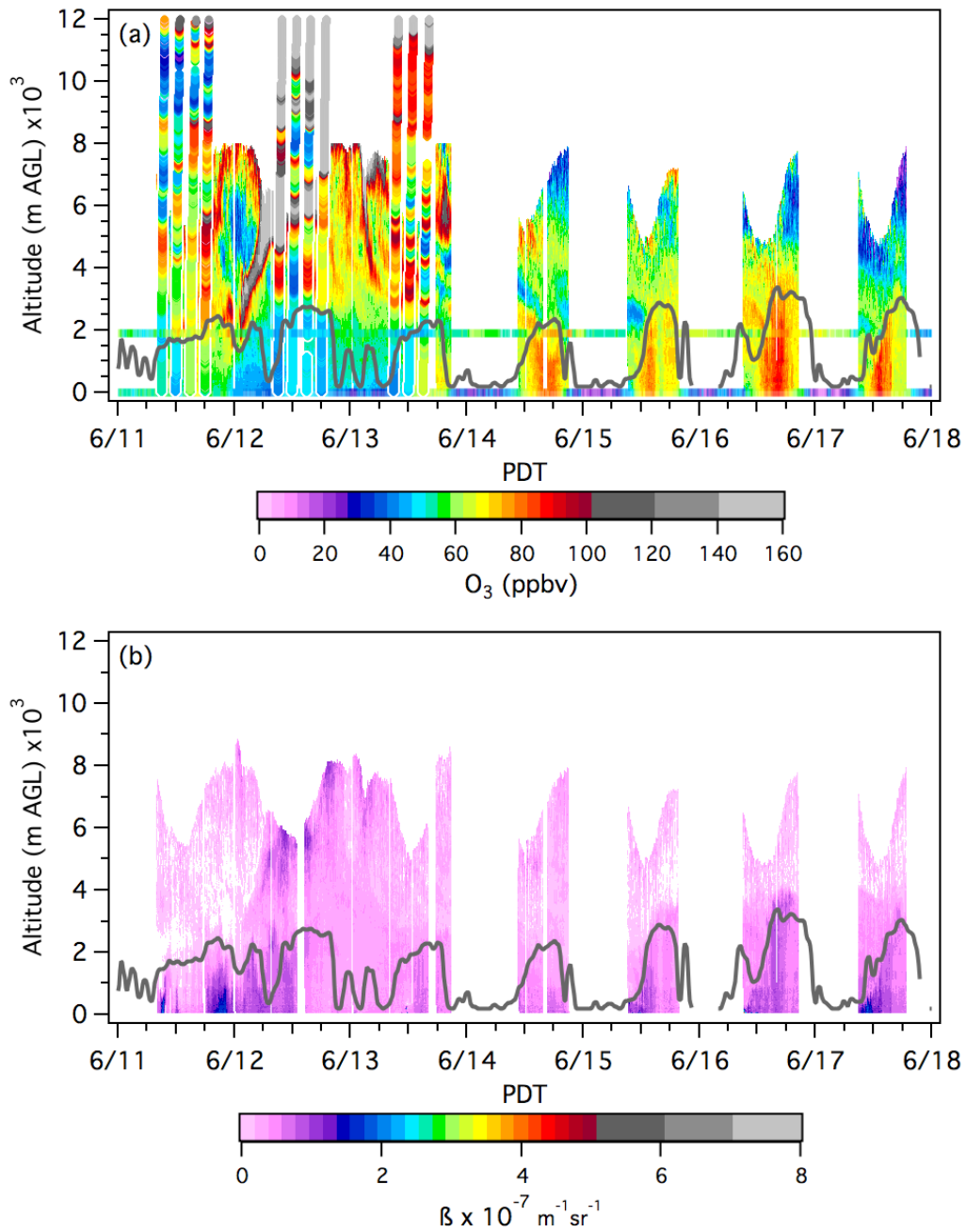
1 The TOPAZ measurements and June 11-13 ozonesondes in **Figure 9-29** show a great deal of fine  
2 structure in the ozone measurements from the continuous 60-hour lidar run lasting from the  
3 morning of June 11 through the evening of June 13. Both the lidar and one of the Joe Neal  
4 ozonesondes measured O<sub>3</sub> mixing ratios in excess of 200 ppbv around 6 km agl at 0900 PDT on  
5 June 12. The TOPAZ O<sub>3</sub> curtains also appear to show entrainment from aloft on June 14 and 16.  
6

7 The FLEXPART STO3 curtain in **Figure 9-30** shows the descent of more than 30 ppbv of  
8 stratospheric ozone to the surface on the morning of June 12 (cf. **Figure 8-2**) with smaller fluxes  
9 through the night of the 13<sup>th</sup>. **Figure 9-30** also shows significant enhancements in the ASCO  
10 tracer throughout the week.  
11

12 The Angel Peak measurements in **Figures 9-31** and **9-32** show a short-lived spike in O<sub>3</sub> to more  
13 than 80 ppbv around midnight on June 11-12, with corresponding dips in CO, CH<sub>4</sub>, N<sub>2</sub>O, and  
14 H<sub>2</sub>O. This appearance of this stratospheric filament coincided with the lowest descent of the  
15 gray high O<sub>3</sub> tongue in the **Figure 9-29** curtain plot. Except for this brief occurrence, the surface  
16 O<sub>3</sub> at and in the valley remained low during the passage of the tropopause fold. This seemingly  
17 paradoxical occurrence reflects the fact that the deep descent of tropopause fold can cause a  
18 local *decrease* in surface O<sub>3</sub> if the previously polluted boundary layer is fumigated by  
19 descending free tropospheric air before it is replaced by a mixture of upper tropospheric and  
20 lower stratospheric air with 45-50 ppbv of O<sub>3</sub> [*Langford et al., 2012*]. The stratospheric air does  
21 not simply add more ozone to that which is already present. The convective entrainment of  
22 quasi-horizontal filaments originating from tropopause folds that form farther upstream is  
23 much more likely to cause an O<sub>3</sub> exceedance since the entrained O<sub>3</sub> *does* add to the local  
24 pollution. The tropopause fold may have significantly contributed to the widespread  
25 exceedances reported in Arizona on June 13-14, but probably had a relatively small impact on  
26 Clark County.  
27

28 The Angel Peak measurements from June 14, and to a lesser extent those from the following 3  
29 days, show large afternoon increases in O<sub>3</sub>, CO, CH<sub>4</sub>, and NO<sub>y</sub> that appear to be caused by  
30 upslope flow from the LVV. Scientific Aviation conducted an additional flight on June 14, and  
31 the airborne O<sub>3</sub> measurements from the flights on June 13 and 14 are compared in **Figures 9-33**  
32 and **9-34**. The measurements from June 13 show highly structured filaments of O<sub>3</sub> trailing  
33 behind the receding fold between 4 and 6 km that are consistent with the lidar and ozonesonde  
34 measurements. These filaments appear not only above the LVV, but also above the Mojave  
35 Desert between the LVV and Big Bear. The measurements from June 14 appear quite different,  
36 however, with high O<sub>3</sub> in the mixed layer above both the NLVA and Barstow, but much lower  
37 concentrations above Jean and the Mojave Desert that lies between them. These observations,  
38 together with those from Angel Peak, imply that 20-25 ppbv of the surface O<sub>3</sub> in the LVV on  
39 June 14 was formed by local photochemistry. High O<sub>3</sub> spread across much of the Southwest on  
40 June 16 and 17 as stagnation developed, and the MDA8 concentrations measured by the Joe  
41 Neal monitor on those days (74 and 72 ppbv) were only ≈10-15 ppbv higher than those  
42 measured at Jean (63 and 63 ppbv) and the Grand Canyon National Park (59 and 60 ppbv).  
43

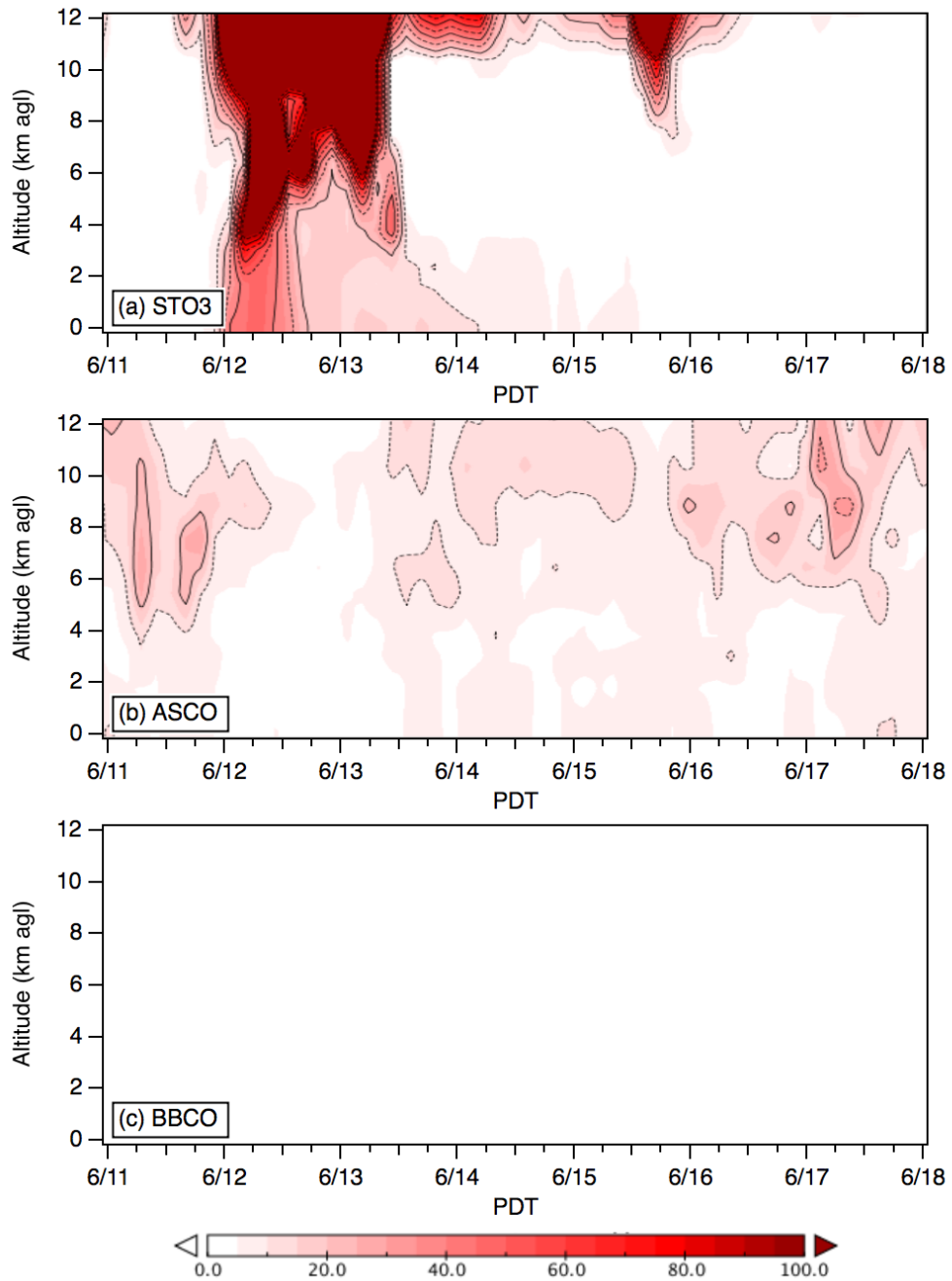
1  
2



3  
4  
5  
6  
7  
8  
9  
10

**Figure 9-29.** Time-height curtain plots of the TOPAZ (a) ozone, and (b) backscatter, measured during Week 5 of FAST-LVOS. The ascending Joe Neal ozonesonde profiles from IOP3 are superimposed. The colored horizontal bands in (a) show the in-situ measurements from the NLVA and AP. The black line shows the local mixed-layer height from the micro-Doppler lidar. Note that strong winds kept the boundary layer well-mixed throughout the night of June 11-12.

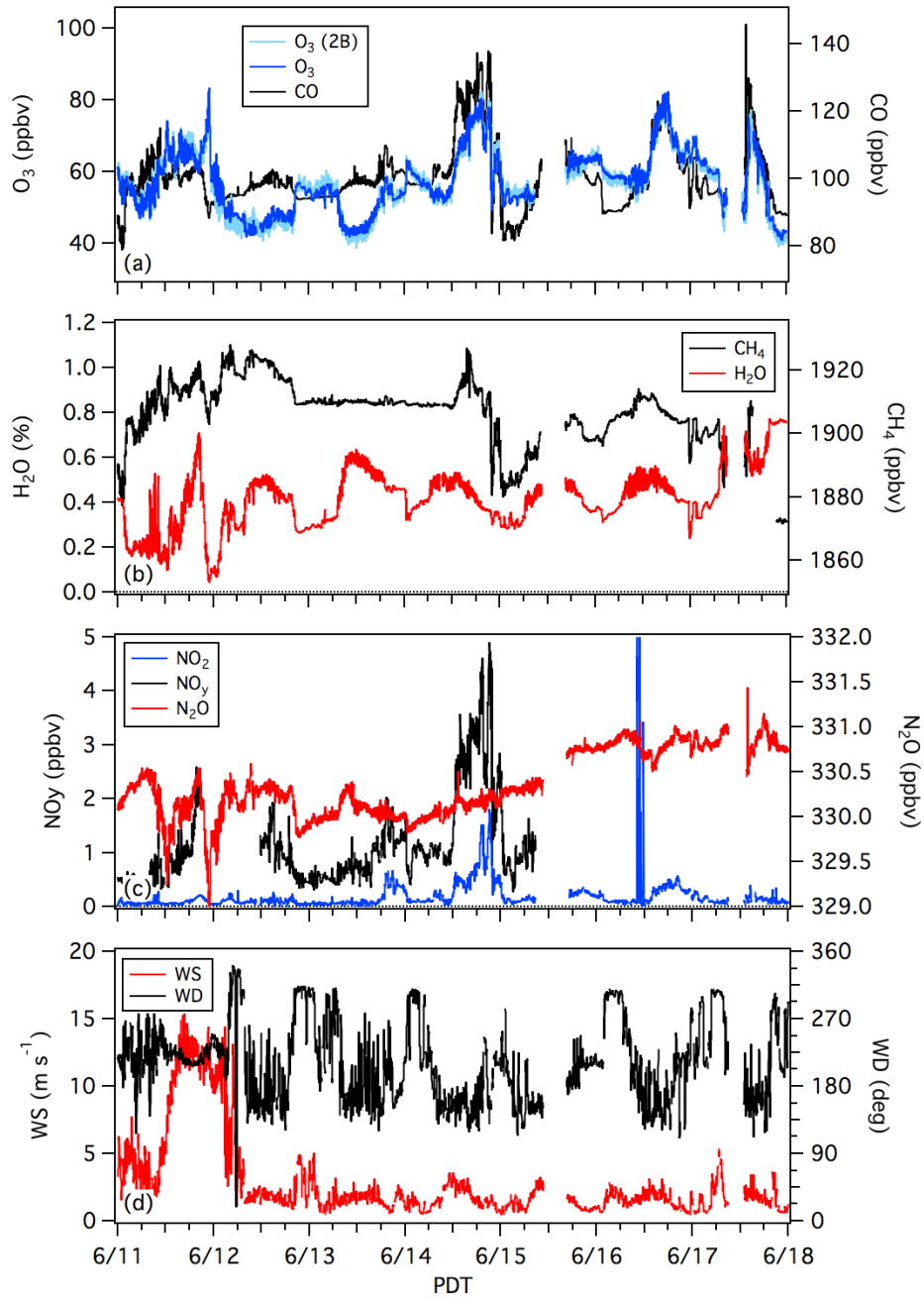
1  
2  
3



4  
5  
6  
7  
8  
9  
10

**Figure 9-30.** Time-height curtain plots of the FLEXPART (a) STO3, (b) ASCO, and (c) BBCO tracer distributions above the LVV during Week 5 of FAST-LVOS.

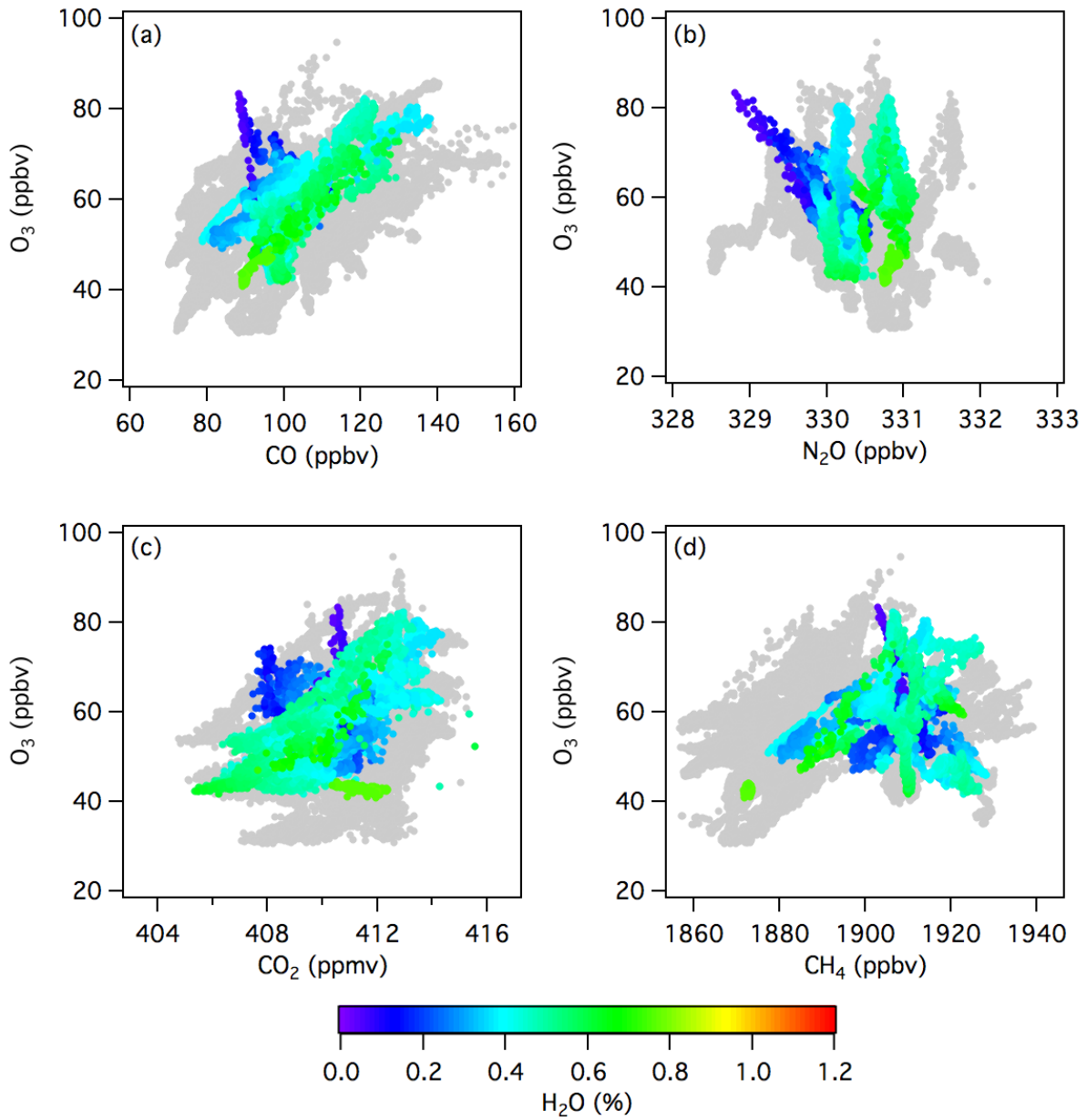
1  
2



3  
4  
5  
6  
7  
8  
9  
10

**Figure 9-31.** Time series of (a) O<sub>3</sub> and CO, (b) H<sub>2</sub>O and CH<sub>4</sub>, (c) NO<sub>x</sub>, NO<sub>y</sub> and N<sub>2</sub>O, and (d) wind speed and direction measured by the mobile laboratory on Angel Peak during Week 5 of FAST-LVOS.

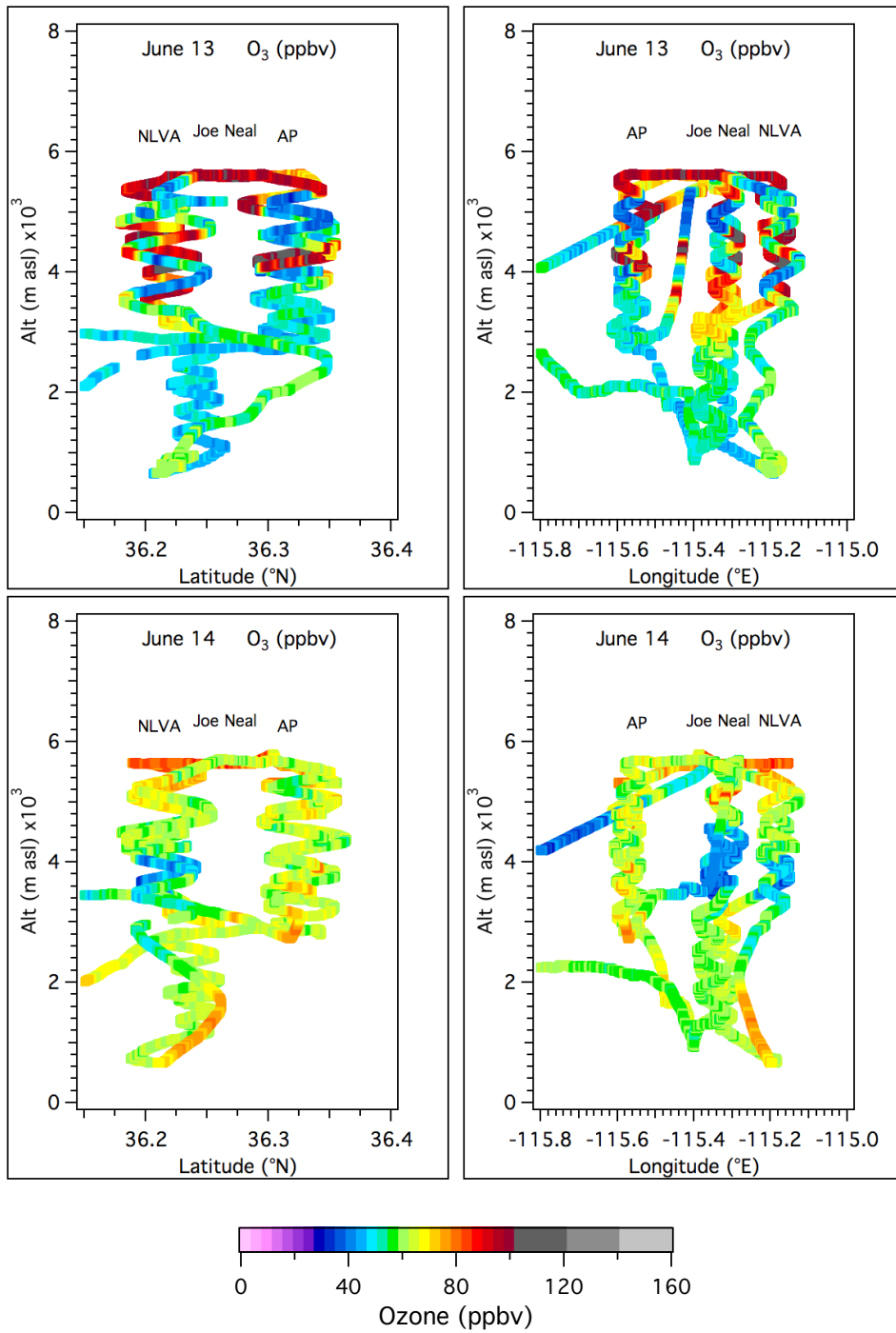
1  
2



3  
4  
5  
6  
7  
8  
9  
10  
11  
12

**Figure 9-32.** Scatter plots showing the correlations between in-situ  $O_3$  and (a) CO, (b)  $N_2O$ , (c)  $CO_2$ , and (d)  $CH_4$  measurements from the mobile lab on Angel Peak. The measurements from Week 5 are colorized by the water vapor measurements.

1  
2  
3



4  
5

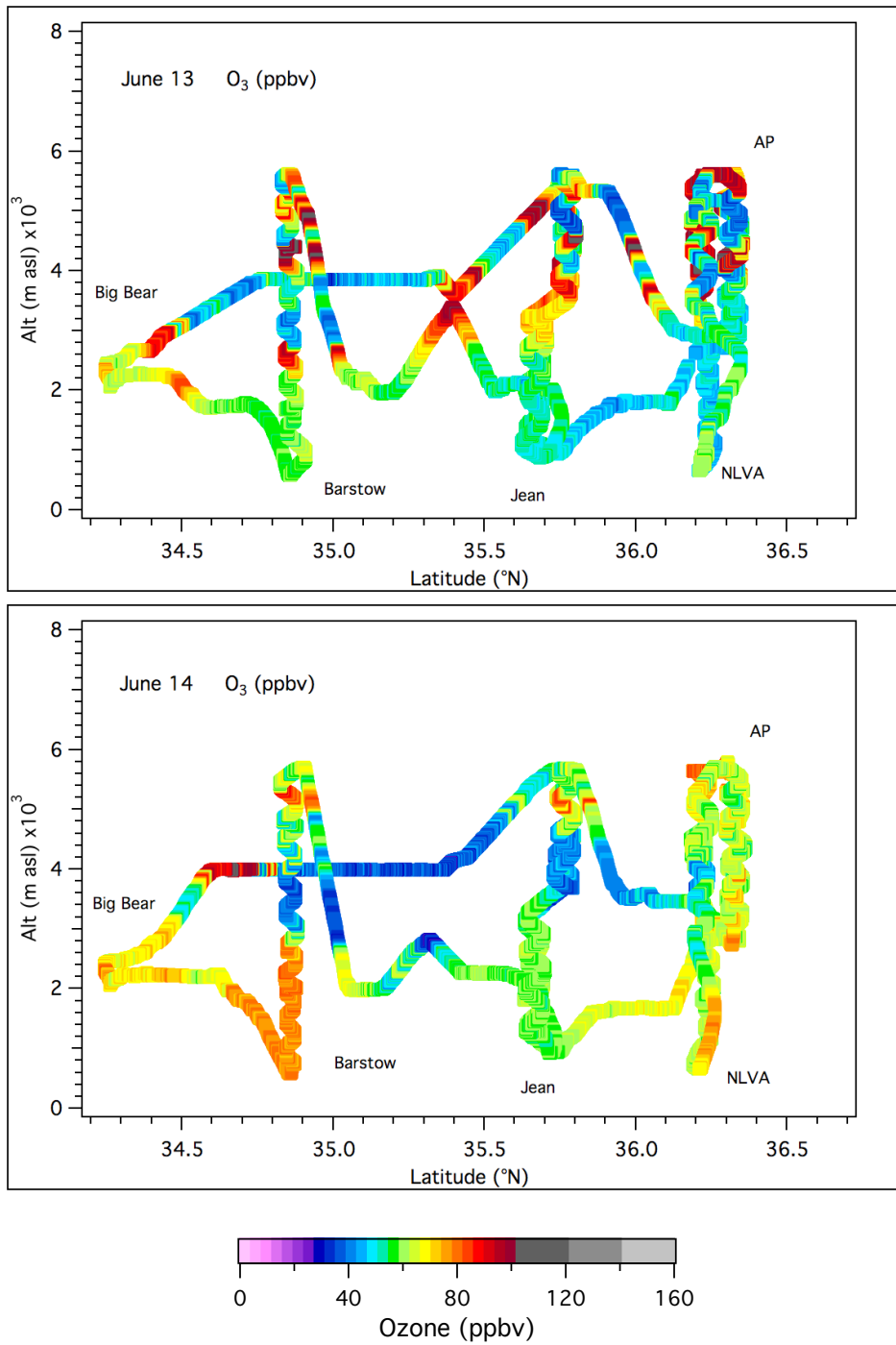
6  
7

8  
9

10  
11

**Figure 9-33.** Scientific Aviation O<sub>3</sub> profiles above the NLVA, Joe Neal, and Angel Peak on June 13 and 14.

1  
2  
3



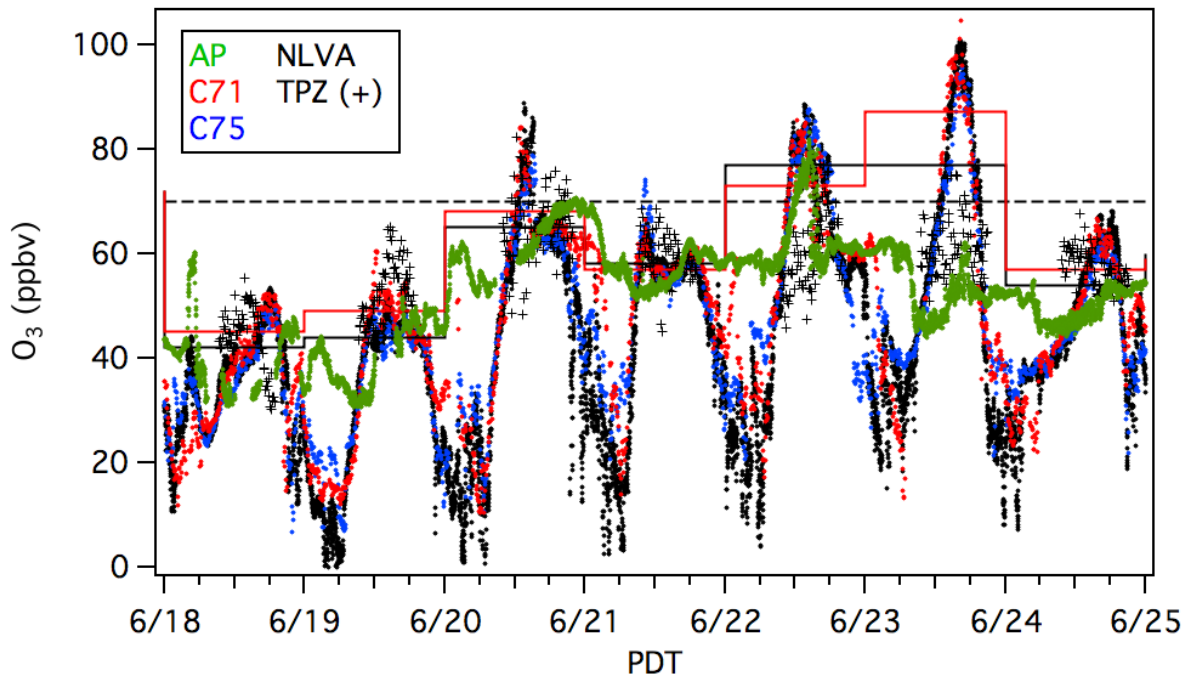
4  
5

6  
7  
8  
9  
10  
11

**Figure 9-34.** Scientific Aviation O<sub>3</sub> measurements from the flights on June 13 and 14.

1 **9.6 Week 6: June 18-24**

2  
3 The week of June 18-24 was extremely hot with daily maximum temperatures ranging from  
4 43.3 to 46.7°C (110 to 116°F) at the nearby NWS KVG T station. The official KVEF station at  
5 McCarran International Airport reached 117°F on June 20, tying the all-time Las Vegas record  
6 set on July 24, 1942 (this record was also tied on June 30, 2013, the final day of the LVOS field  
7 campaign). The week began with the lowest measured surface O<sub>3</sub> concentrations of the entire  
8 campaign and ended with the highest. The low concentrations at the beginning of the week  
9 followed the advection of clean marine air into the Desert Southwest from the Eastern Pacific,  
10 and the MDA8 O<sub>3</sub> did not exceed 49 ppbv at any of the monitoring sites in the LVV on June 18.  
11 Multiple O<sub>3</sub> exceedances occurred on both June 22 (4 monitors) and 23 (5 monitors), however.  
12 The highest concentrations were measured on June 23 when the MDA8 O<sub>3</sub> at the Joe Neal  
13 monitor reached 77 ppbv. The Walter Johnson monitor officially reported 87 ppbv for June 23,  
14 but this value was based on a 6-h average and would have been closer to 77 ppbv had the  
15 monitor not been offline for much of the morning. **Figure 9-35** shows that the O<sub>3</sub> mixing ratios  
16 at 4 km were less than or equal to the surface concentrations all week.  
17



18  
19  
20 **Figure 9-35.** Time series of the TOPAZ O<sub>3</sub> mixing ratios at 4.0 km agl (black +) during Week 6  
21 plotted with the 1-min O<sub>3</sub> measurements from the NLVA (black) and AP (green) and the 5-min  
22 measurements from the Walter Johnson (C71, red) and Joe Neal (C75, blue) monitors. The red  
23 and blue steps show the corresponding C71 and C75 MDA8 measurements. The dashed black  
24 line indicates the 70 ppbv NAAQS.  
25  
26

1 The FLEXPART BBCO tracer plots in **Figures 8-1 and 8-4** show a large increase in fire activity  
2 across the Southwestern U.S. and Mexico during the last two weeks of the study, and the  
3 TOPAZ backscatter curtain plot in **Figure 9-36** shows high backscatter appearing around 4 km  
4 on the evening of June 18 and filling the lower troposphere on June 20. The backscatter  
5 remained high at 4 km on June 21, and was also elevated near the surface on June 23 and at 4  
6 km on June 24. The O<sub>3</sub> curtain shows low O<sub>3</sub> extending all the way from the surface to at least 8  
7 km on June 18 and remaining low near the surface on June 19. Ozone increased along with  
8 backscatter on June 20, and was very high in the mixed layer on June 22 and 23 when the  
9 NAAQS exceedances occurred.

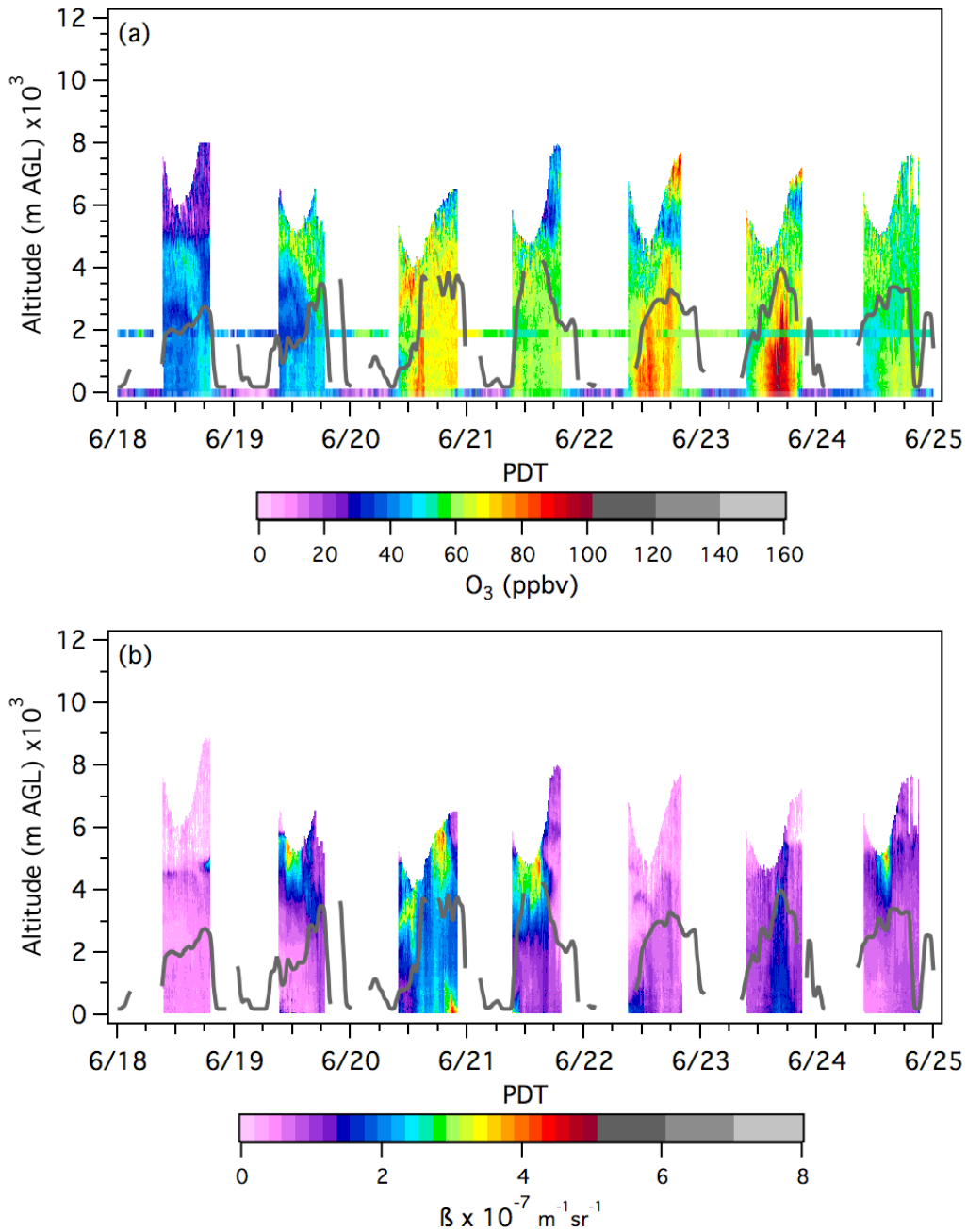
10  
11 The FLEXPART STO3 tracer curtain in **Figure 9-37** shows tongues of stratospheric O<sub>3</sub> and Asian  
12 CO descending into the upper troposphere over the course of the week. The ASCO tracer also  
13 shows some transported pollution filling the tropospheric column on June 18-19 when the low  
14 O<sub>3</sub> was observed. The BBCO tracer appears quite similar to the backscatter distribution in  
15 **Figure 9-36** with the highest values on the night of June 20-21 and a lesser peak on June 23. The  
16 BBCO maps in **Figure 8-4** suggest that the tracer appearing above the LVV on June 20 was  
17 advected anticyclonically from agricultural fires in Mexico. This conclusion is also supported by  
18 the HRRR-smoke model; **Figure 9-38** shows near surface and vertically integrated smoke  
19 distribution forecasts for the afternoons (22 UT or 15 PDT) of June 20 and 22. The Mexican  
20 smoke was much reduced on June 22, and HRRR-smoke indicates that the tenuous smoke  
21 reaching the LVV on that day arrived in a narrow plume from the small (1503 acres) Holcomb  
22 Fire near Big Bear. HRRR-smoke also shows the plume from the much larger and closer Brian  
23 Head Fire (68407 acres) that started on June 17 in southwestern Utah is streaming eastward  
24 and away from Clark County on June 20 and 22, but shows some of the Brian Head smoke  
25 reaching the LVV on the morning of June 23 when the highest O<sub>3</sub> was measured.

26  
27 The in-situ measurements from Angel Peak (**Figure 9-39 and 9-40**) show broad CO, NO<sub>y</sub>, and O<sub>3</sub>  
28 peaks on June 20 when the TOPAZ backscatter was highest. The O<sub>3</sub> mixing ratios in the aged  
29 Mexican smoke plume reached about 70 ppbv. The measurements also show a series of narrow  
30 peaks with up to 450 ppbv of CO between 1000 and 1600 PDT on June 22. Matching peaks are  
31 also seen in the CH<sub>4</sub>, H<sub>2</sub>O, and N<sub>2</sub>O measurements, and in both the NO<sub>2</sub> and NO<sub>y</sub>  
32 measurements. The presence of NO<sub>2</sub> shows that the plume is fresh, and the O<sub>3</sub> peak of about  
33 80 ppbv shows an enhancement of about 20 ppbv compared to the background. This  
34 enhancement is also seen in the 5-min measurements at Walter Johnson and Joe Neal, which  
35 peaked at more than 85 ppbv, with the MDA8 O<sub>3</sub> concentrations reaching 73 and 77 ppbv,  
36 respectively.

37  
38 The HRRR-smoke forecast for June 23 in **Figures 9-38** indicates that most of the smoke from the  
39 Brian Head Fire smoke was transported into the LVV near the surface in the early morning, and  
40 **Figures 9-35 and 39** show only a small increase in CO and O<sub>3</sub> at Angel Peak created by upslope  
41 transport from the LVV. Nevertheless, it seems likely that the Brian Head plume contributed to  
42 the very high surface O<sub>3</sub> (5-min peak of 104 ppbv at Walter Johnson) on June 23.

43  
44

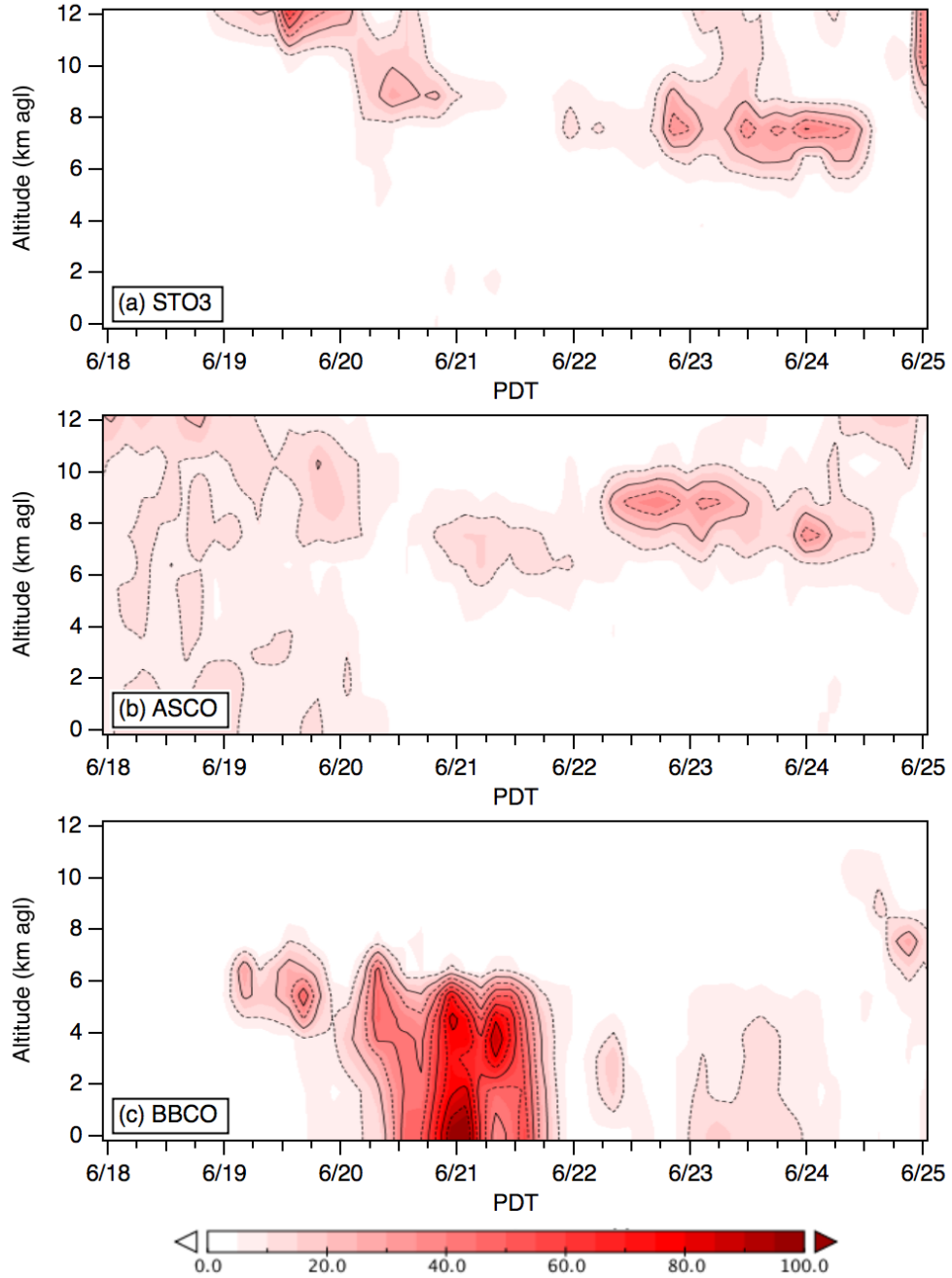
1  
2  
3



4  
5  
6  
7  
8  
9  
10

**Figure 9-36.** Time-height curtain plots of the TOPAZ (a) ozone, and (b) backscatter, measured during Week 6 of FAST-LVOS. The colored horizontal bands in (a) show the in-situ measurements from the NLVA and AP. The black line shows the local mixed-layer height from the micro-Doppler lidar.

1  
2  
3  
4

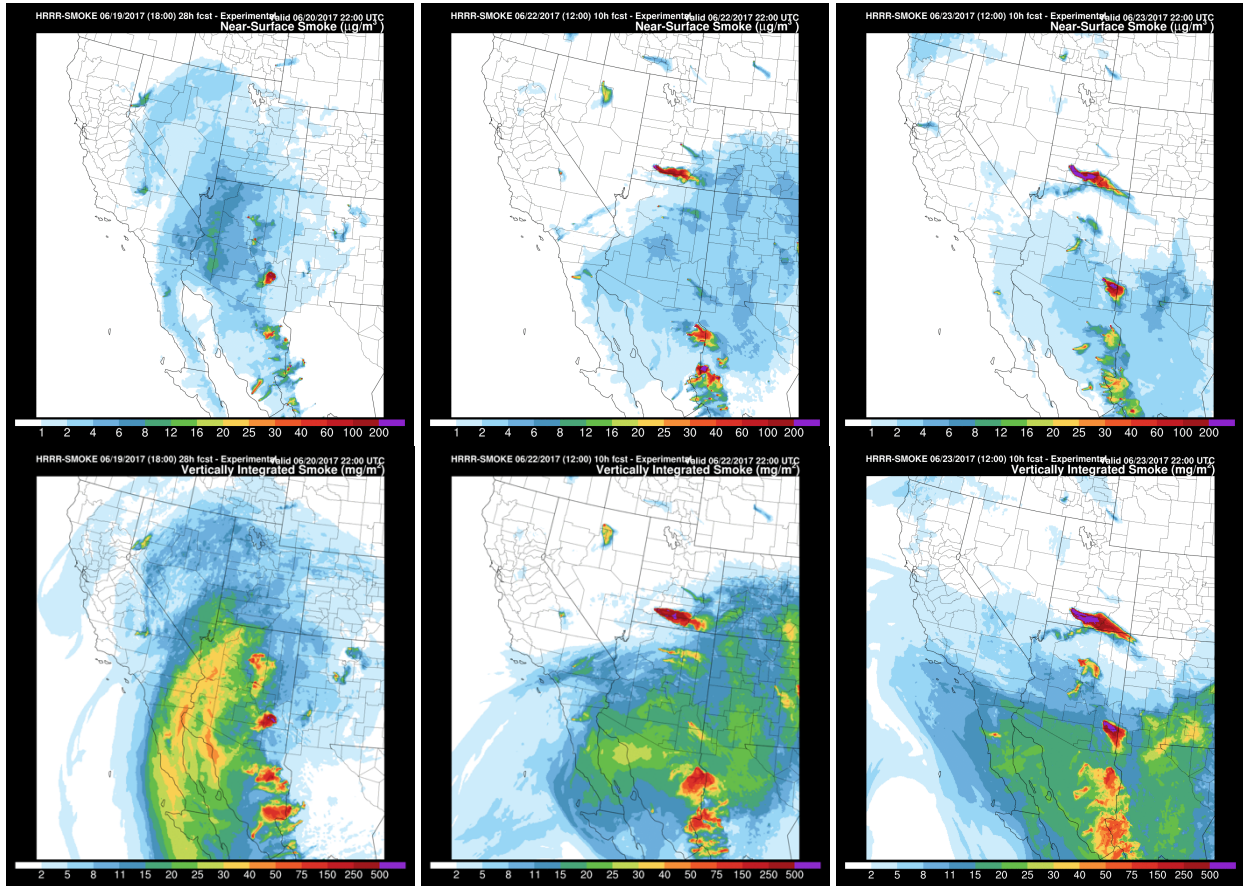


5  
6  
7  
8  
9  
10

**Figure 9-37.** Time-height curtain plots of the FLEXPART (a) STO3, (b) ASCO, and (c) BBCO tracer distributions above the LVV during Week 6 of FAST-LVOS.

1  
2  
3  
4  
5  
6  
7  
8

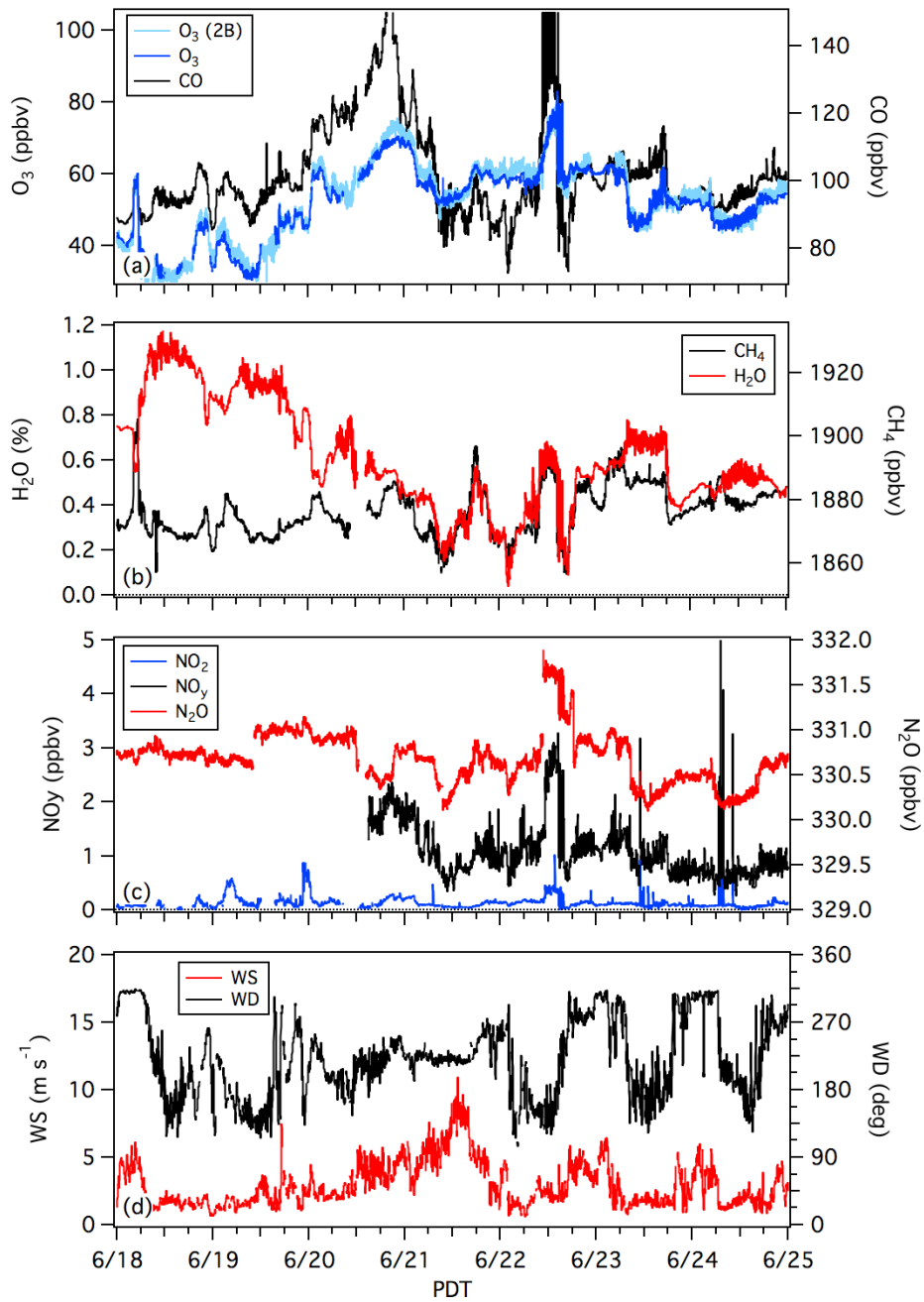
9



10  
11  
12  
13  
14  
15  
16  
17  
18  
19  
20  
21  
22  
23

**Figure 9-38.** NOAA HRRR-smoke model near surface (top) and vertically integrated (bottom) smoke forecasts for: (left to right) June 20 15 PDT, June 22 15 PDT, and June 23 11 PDT.

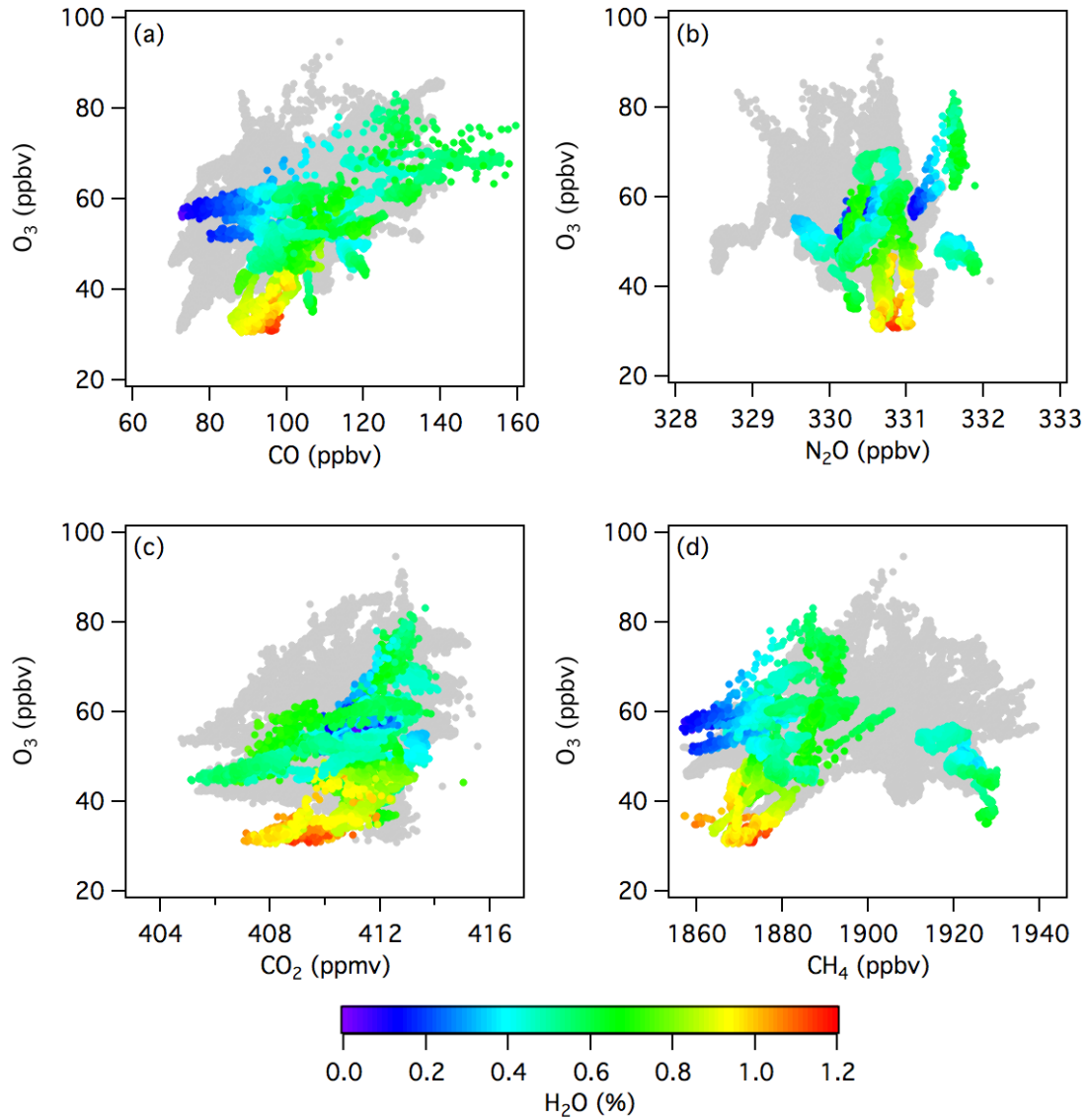
1  
2  
3



4  
5  
6  
7  
8  
9  
10

**Figure 9-39.** Time series of (a) O<sub>3</sub> and CO, (b) H<sub>2</sub>O and CH<sub>4</sub>, (c) NO<sub>2</sub>, NO<sub>y</sub> and N<sub>2</sub>O, and (d) wind speed and direction measured by the mobile laboratory on Angel Peak during Week 6 of FAST-LVOS. The CO measurements in the Holcomb Fire plume on June 22 reached over 450 ppbv.

1  
2  
3  
4  
5  
6



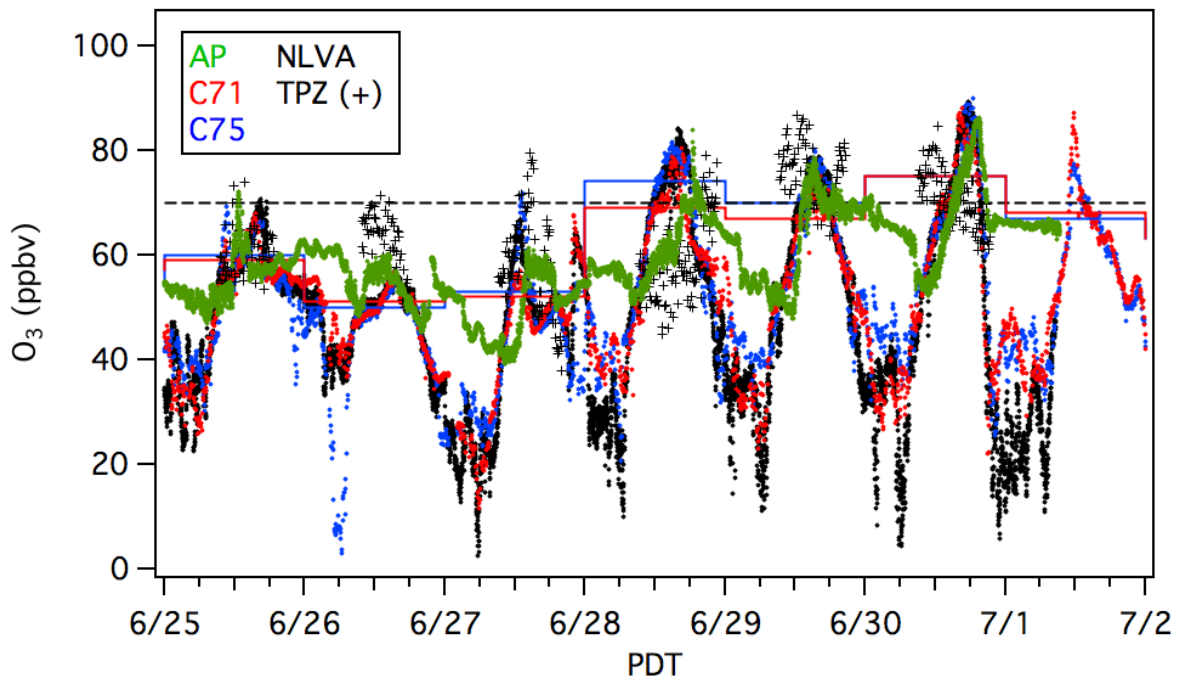
7  
8  
9  
10  
11  
12  
13  
14  
15

**Figure 9-40.** Scatter plots showing the correlations between in-situ O<sub>3</sub> and (a) CO, (b) N<sub>2</sub>O, (c) CO<sub>2</sub>, and (d) CH<sub>4</sub> measurements from the mobile lab on Angel Peak. The measurements from Week 6 are colorized by the water vapor measurements. The CO measurements in the Holcomb Fire plume are off scale.

1 **9.7 Week 7: June 25-30 (IOP4)**

2  
3 The last week of FAST-LVOS was also very hot with the daily high temperatures at KVGT ranging  
4 between 44.4 (112°F) on June 25 and 41.1°C (106°F) on June 30. The GFS model showed  
5 another developing trough and the final three ozonesondes were launched at local noon on  
6 June 28, 29, and 30. The final Scientific Aviation flight hours were expended in flights on June  
7 27, 28, 29, and 30. The campaign ended with O<sub>3</sub> exceedances at Walter Johnson and/or Joe  
8 Neal on June 28 and 30, but the **Figure 9-41** shows that the O<sub>3</sub> measured by TOPAZ at 4 km was  
9 similar to the surface O<sub>3</sub> in the LVV and at AP.

10

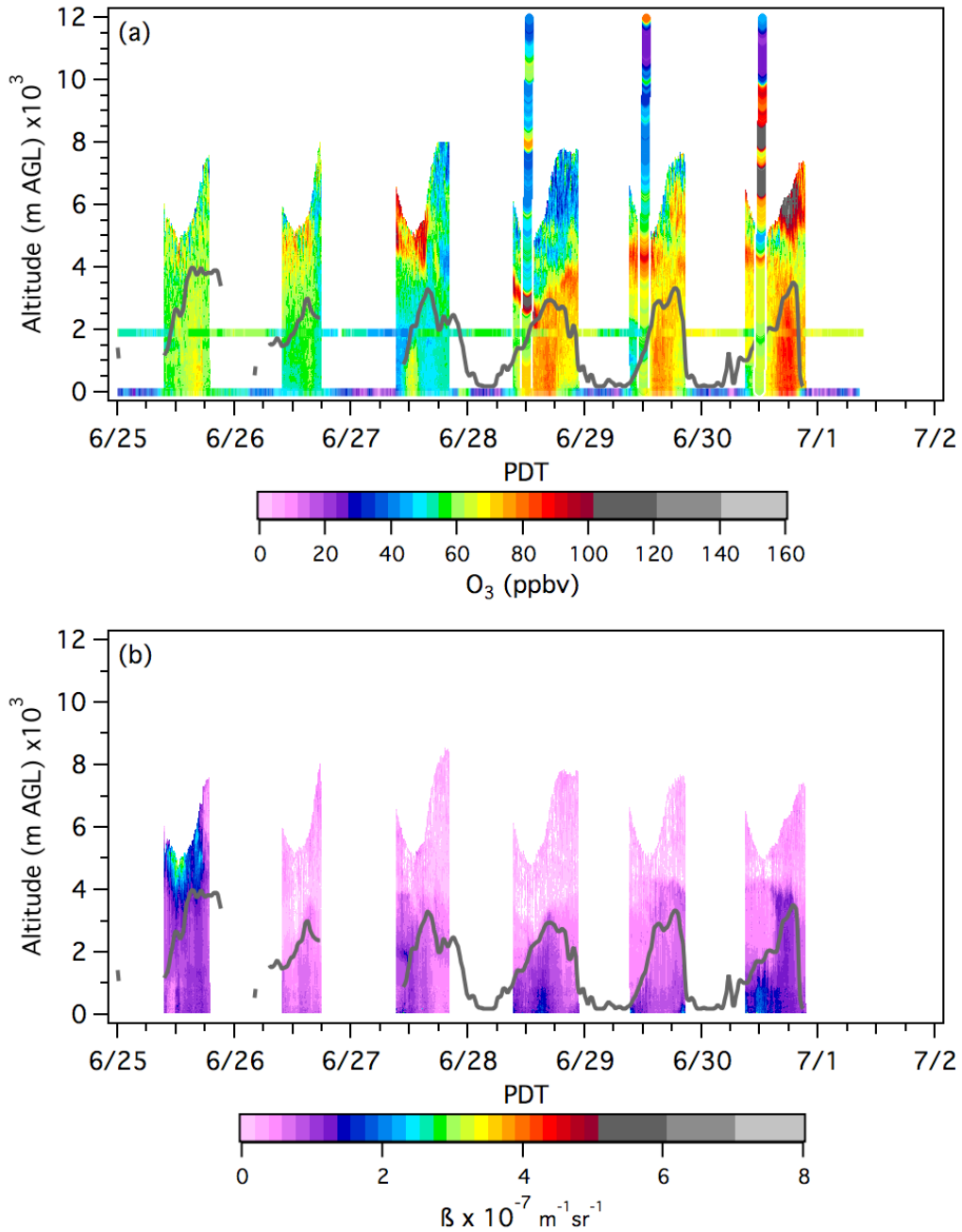


11  
12 **Figure 9-41.** Time series of the TOPAZ O<sub>3</sub> mixing ratios at 4.0 km agl (black +) during Week 7  
13 plotted with the 1-min O<sub>3</sub> measurements from the NLVA (black) and AP (green) and the 5-min  
14 measurements from the Walter Johnson (C71, red) and Joe Neal (C75, blue) monitors. The red  
15 and blue steps show the corresponding C71 and C75 MDA8 measurements. The dashed black  
16 line indicates the 70 ppbv NAAQS.

17  
18 The ozone curtain plot in **Figure 9-42** shows high O<sub>3</sub> above 4 km on July 27,29, and 30, with very  
19 high concentrations around 6 km on June 30. The backscatter curtain plot shows smoke above  
20 4 km on June 25, and possibly in the boundary layer on June 28 and 30. The FLEXPART STO3  
21 curtain in **Figure 9-43** show a weak stratospheric intrusion descending into the lower  
22 troposphere on June 25. It also shows a small enhancement around 6 km in the early morning  
23 of June 30, but the simulations ended in the morning and did not capture the apparent  
24 stratospheric intrusion. The ASCO tracer shows Asian pollution in the upper troposphere on all  
25 6 days, and the BBCO tracer shows wildfire influence in the lower troposphere on June 25-28.

26

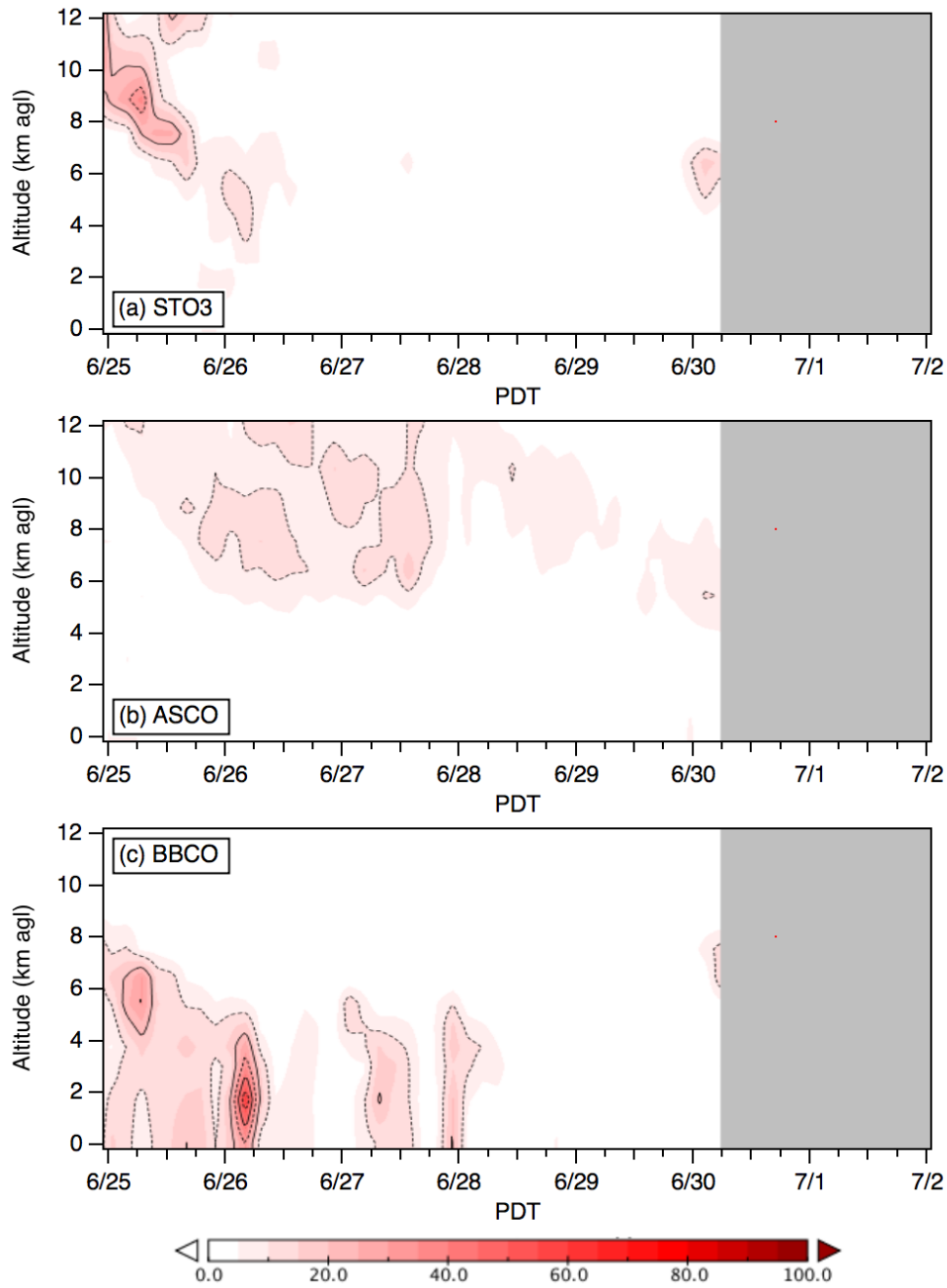
1



2  
3  
4  
5  
6  
7  
8  
9  
10

**Figure 9-42.** Time-height curtain plots of the TOPAZ (a) ozone, and (b) backscatter, measured during Week 7 of FAST-LVOS. The ascending Joe Neal ozonesonde profiles from IOP4 are superimposed. The colored horizontal bands in (a) show the in-situ measurements from the NLVA and AP. The black line shows the local mixed-layer height from the micro-Doppler lidar.

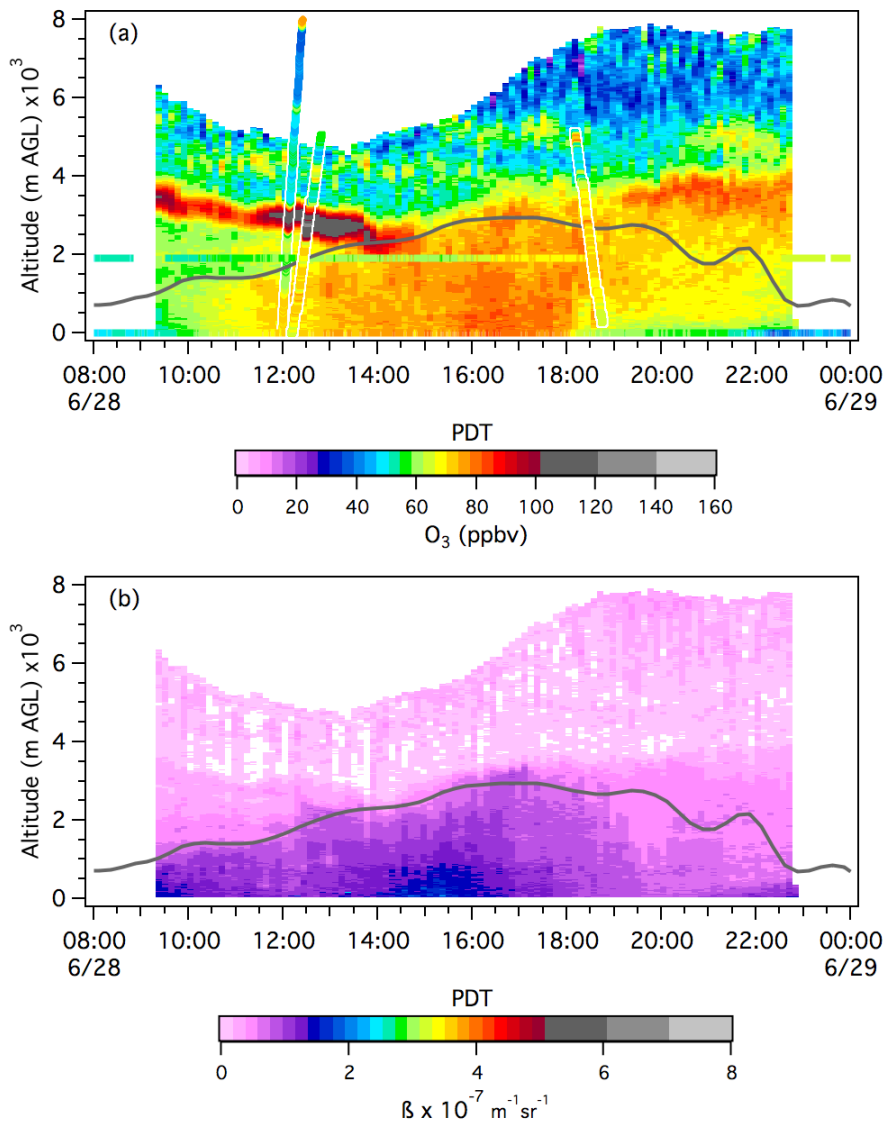
1



2  
3  
4  
5  
6

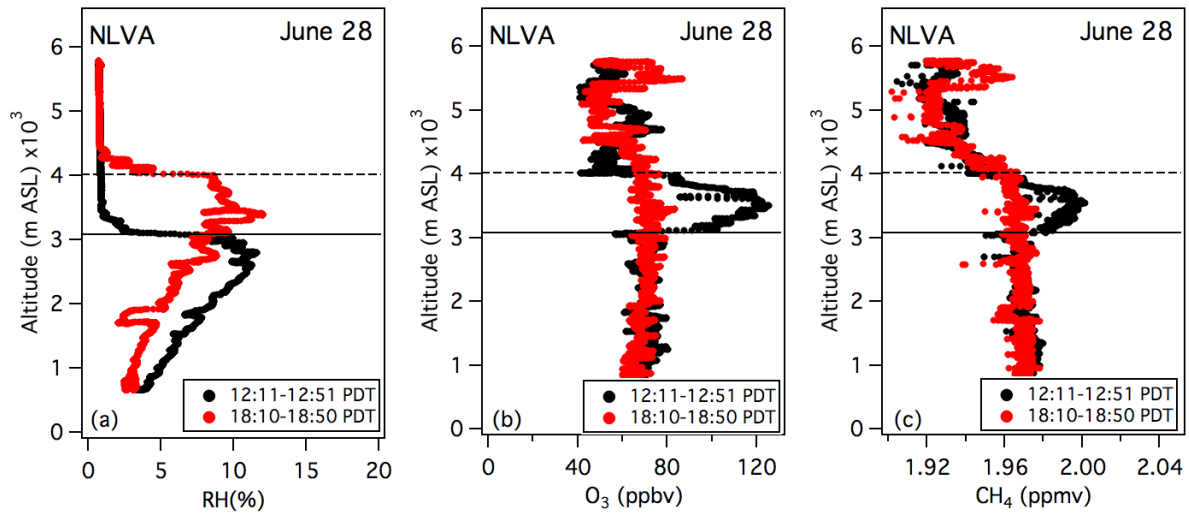
**Figure 9-43.** Time-height curtain plots of the FLEXPART (a) STO3, (b) ASCO, and (c) BBCO tracer distributions above the LVV during Week 7 of FAST-LVOS.

1 The measurements from June 28 give the clearest example of an elevated  $O_3$  plume being  
 2 entrained by the mixed layer. The expanded curtain plots in **Figure 9-44** show a thin plume with  
 3 more than 100 ppbv being entrained by the growing mixed layer around 1400 PDT. The  
 4 superimposed profiles show that the plume was also sampled above the LVV by the Joe Neal  
 5 ozonesonde and the Scientific Aviation Mooney. The Mooney profiles (**Figure 9-45**) show that  
 6 the layer also had high  $CH_4$  showing that it didn't originate in the stratosphere.  
 7



8  
 9  
 10 **Figure 9-44.** Time-height curtain plots of the TOPAZ (a) ozone, and (b) backscatter, measured on  
 11 June 28, 2017. The colored horizontal bands in (a) show the in-situ measurements from the  
 12 NLVA and AP, and the nearly vertical colored line shows the profile from the ascending Joe Neal  
 13 ozonesonde. The colored tilted lines show the outbound and inbound profiles from the Scientific  
 14 Aviation Mooney. The black line represents the local mixed-layer height from the micro-Doppler  
 15 lidar.

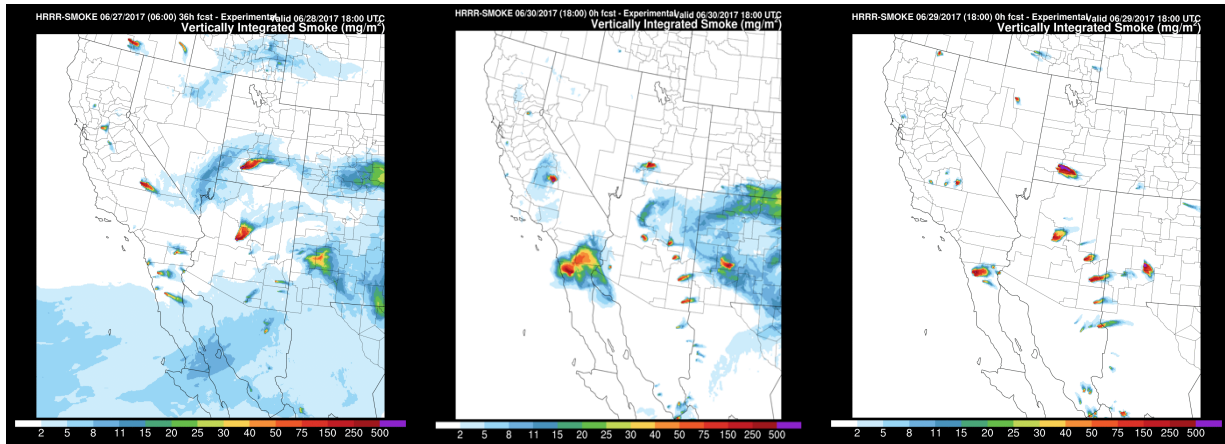
1  
2



3  
4  
5  
6  
7  
8  
9  
10  
11  
12  
13  
14

**Figure 9-45.** Profiles of (a) RH, (b) O<sub>3</sub>, and (c) CH<sub>4</sub> above the NLVA/Joe Neal area from the Scientific Aviation flight on June 28. The black profiles are from the outbound leg near midday and the red profiles from the inbound leg in the late afternoon. The solid and dashed lines show the corresponding mixed layer heights.

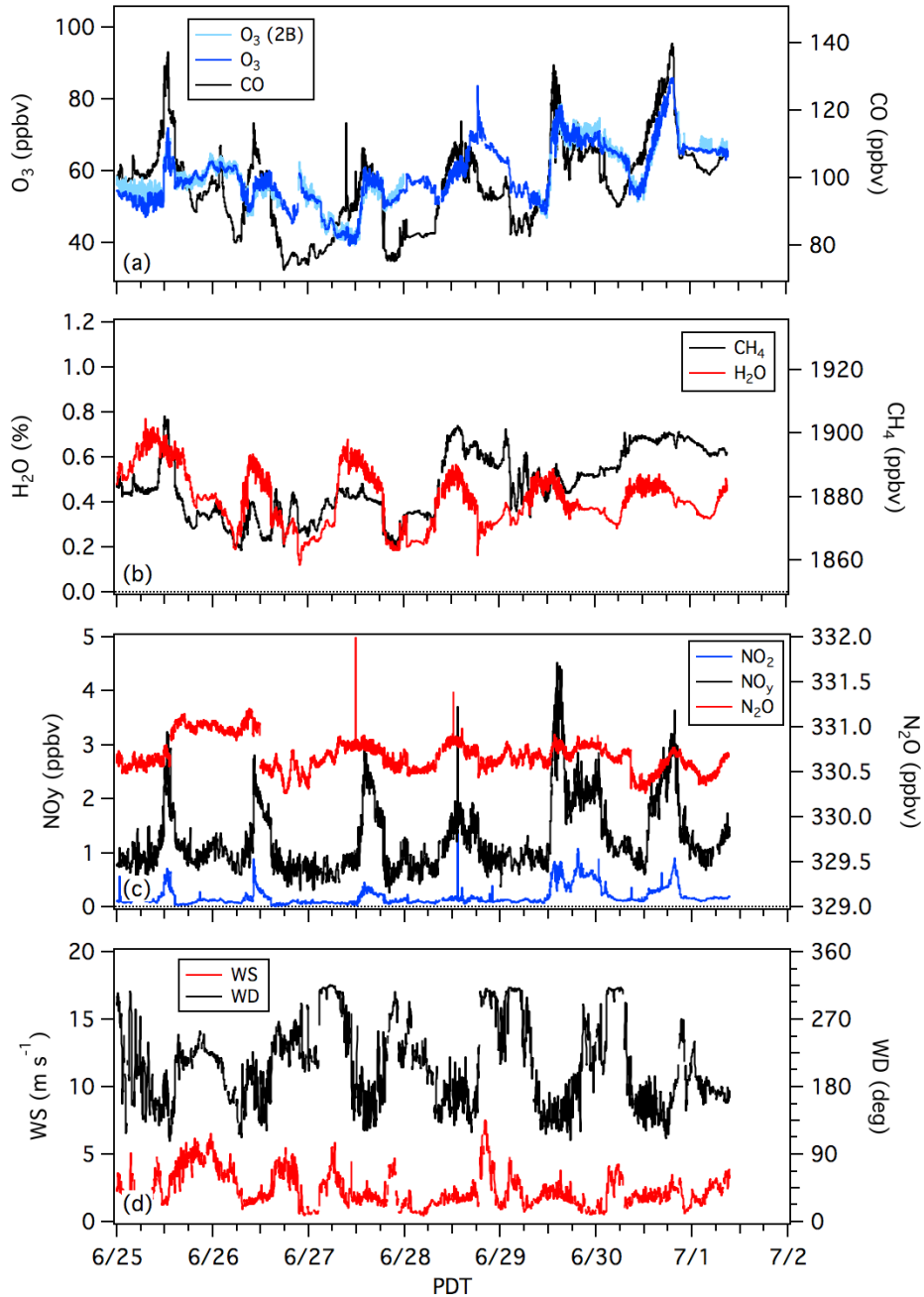
The HRRR-smoke model (**Figure 9-46**) suggests that entrained plume originated from the 16,031-acre Schaeffer Fire in Sequoia National Forest that was started by lightning on June 24.



15  
16  
17  
18  
19  
20

**Figure 9-46.** NOAA HRRR-smoke model vertically integrated smoke forecasts for: (left to right) June 28, June 29, and June 30 at 18 UT (11 PDT).

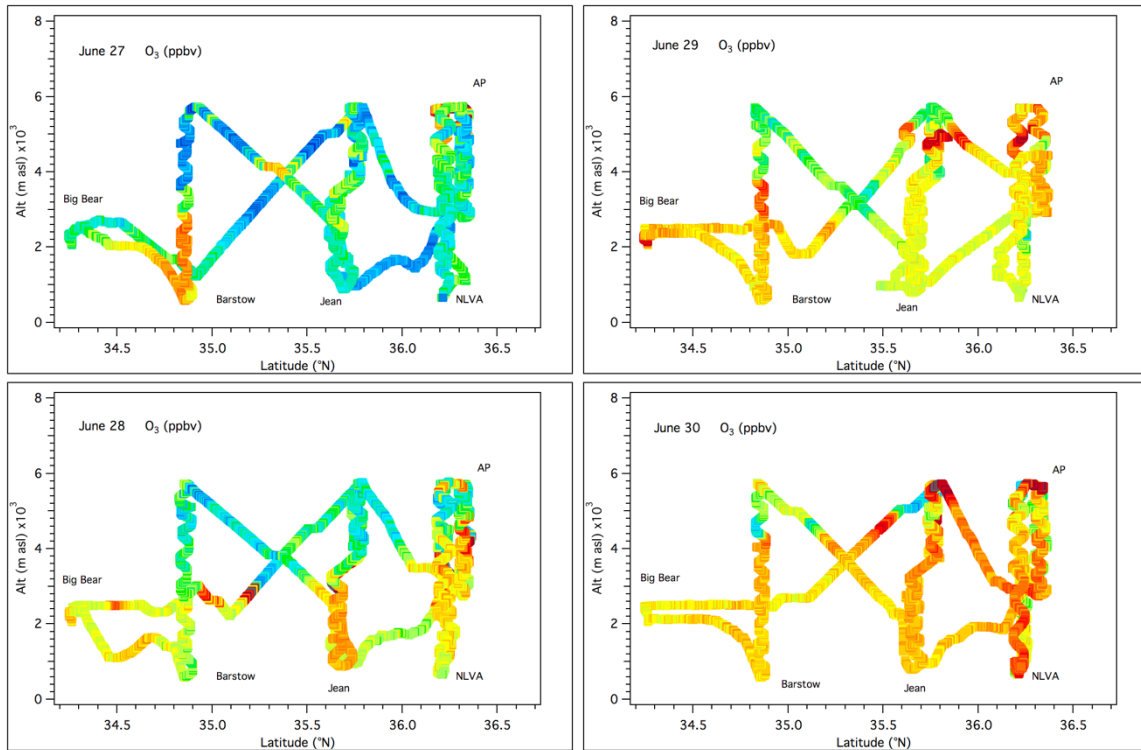
1 **Figure 9-44** suggests that the smoke plume did not directly impact Angel Peak, and the  
2 afternoon peaks in O<sub>3</sub>, CO, NO<sub>y</sub>, and H<sub>2</sub>O in the in-situ measurements from the mobile  
3 laboratory plotted in **Figure 9-47** show that the summit was strongly impacted by upslope  
4 transport from the LVV on June 28-30.  
5



6  
7  
8  
9  
10  
11

**Figure 9-47.** Time series of (a) O<sub>3</sub> and CO, (b) H<sub>2</sub>O and CH<sub>4</sub>, (c) NO<sub>x</sub>, NO<sub>y</sub> and N<sub>2</sub>O, and (d) wind speed and direction measured by the mobile laboratory on Angel Peak during Week 7 of FAST-LVOS.

1 The Scientific Aviation flights from IOP4 show the gradual buildup of O<sub>3</sub> across the Mojave  
2 Desert during the last 4 days of June. The MDA8 O<sub>3</sub> concentrations on June 30 were highest in  
3 the western LVV with 75 ppbv at both Walter Johnson and Joe Neal, but the MDA8 also reached  
4 69 ppbv at Jean and 66 ppbv at Grand Canyon National Park.  
5  
6



7  
8  
9 **Figure 9-48.** Ozone measurements from the Scientific Aviation flights to Big Bear, CA on June 27-  
10 30.  
11  
12  
13

## 10. Comparison with the NOAA GFDL AM4 model

The preceding analyses can be compared to the global model results of Li Zhang and Meiyun Lin of NOAA GFDL and Princeton University that were conducted under a separate contract (CBE-605334-19) with Clark County. NOAA GFDL used the AM4 and GEOS-Chem global models to examine ozone in the southwestern U.S. during the FAST-LVOS study period. The following discussion is based primarily on a summary of the AM4 results recently submitted for publication by Zhang et al. [Zhang et al., 2019]. Details of the model calculations are given in that publication and in the final report for Contract No. CBE605334-19.

The GFDL analyses focused on the deep stratospheric intrusion event of June 11–14 (Section 9-5), the wildfire event of June 22 (Section 9-6), the regional pollution episode of June 16 (Section 9-5), the Asian transport event of May 24 (Section 9-2), and the “mysterious” event of June 28 (Section 9-7), which we attribute to the Schaeffer Fire. Figures 10-1 to 10-3, which are adapted from Zhang et al. [Zhang et al., 2019], show curtain plots comparing the AM4 and GEOS-Chem model results to the TOPAZ measurements.

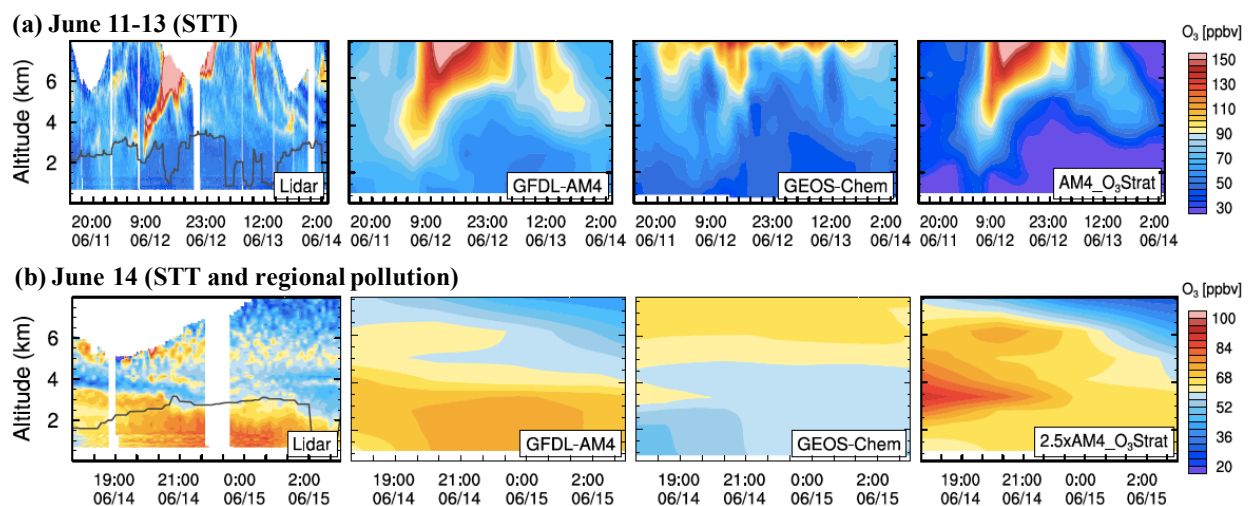
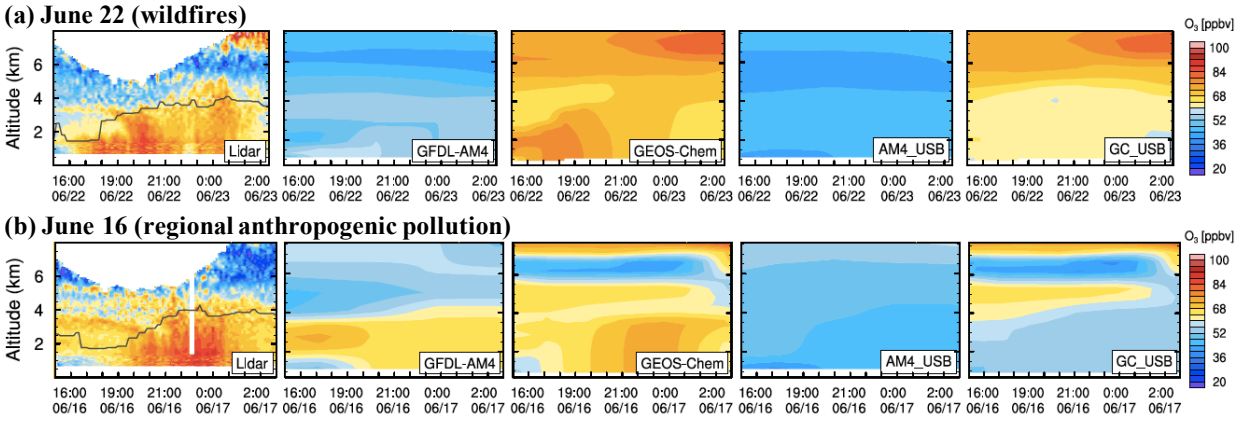
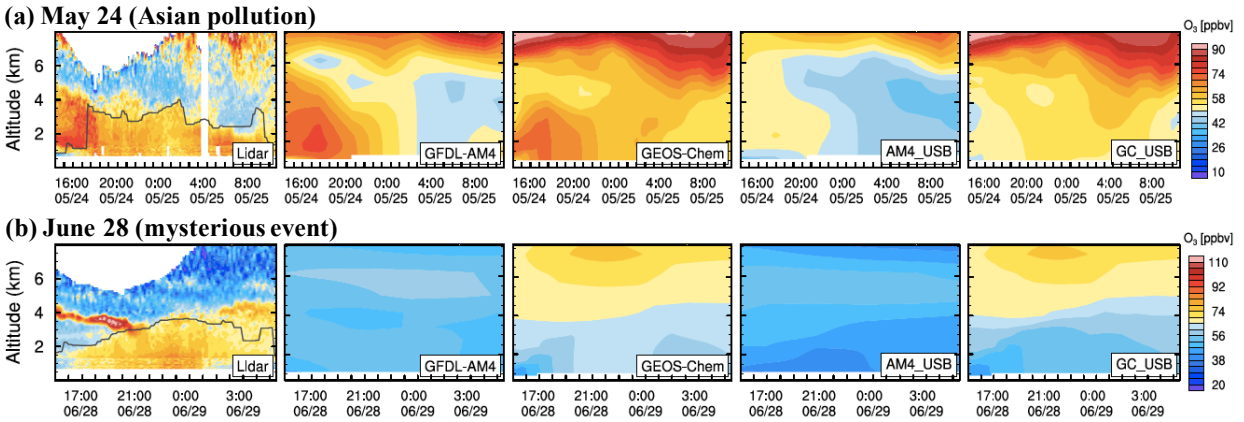


**Figure 10-1.** Time-height curtain plots of  $O_3$  above NLVA as observed with TOPAZ lidar and simulated with GFDL-AM4 ( $\approx 50 \text{ km} \times 50 \text{ km}$ ; interpolated from 3-hourly data) and GEOS-Chem ( $0.25^\circ \times 0.3125^\circ$ ; interpolated from hourly data) during the STT event on (a) June 11–13 and (b) June 14, 2017 (UTC). The rightmost panel shows AM4 stratospheric  $O_3$  tracer (AM4\_  $O_3$ Strat). Note that AM4\_  $O_3$ Strat for June 14 is scaled by a factor of 2.5 for clarity. Here and in other figures, the solid black lines in the  $O_3$  lidar plots represent boundary layer height inferred from the micro-Doppler lidar measurements.



1  
2  
3  
4  
5  
6

**Figure 10-2.** Same as Figure 10-1, but for (a) the wildfire event on June 22 and (b) the regional anthropogenic pollution event on June 16, 2017 (UTC). The right panels compare USB O<sub>3</sub> from the two models.



7  
8

**Figure 10-3.** Same as Figure 10-1, but for (a) the Asian pollution event on May 24 and (b) the unattributed pollution event on June 28, 2017 (UTC).

9

10 **Figures 10-1 through 10-3** show that AM4 does a good job of capturing the stratospheric  
 11 intrusion (June 11-13), regional pollution (June 14 and 16), and Asian pollution (May 24)  
 12 events, but is unable to resolve the two wildfire events (June 22 and 28) due to the relatively large grid  
 13 size of the global model. The GEOS-Chem model fails to reproduce the stratospheric intrusion,  
 14 but does a better job with the regional and Asian pollution events. The higher resolution GEOS-  
 15 Chem model also captures the first wildfire event, but misses the June 28 fire plume.

16

17

1 The global model simulations should, in principle, be better able to resolve the contributions of  
2 intermingled sources as when stratospheric intrusions mix with local or regional pollution.  
3 **Figure 10-4** separates the U.S. Background (USB), which includes the stratospheric contribution,  
4 from the AM4 total model MDA8 O<sub>3</sub>. The modeled surface USB in Clark County peaks at about  
5 60 ppbv on June 11 and decreases to about 50 ppbv on June 12. These results are in good  
6 agreement with the Clark County surface measurements from June 11 and 12 plotted in **Figure**  
7 9-26. The USB continues to decrease to 45-50 ppbv on June 14 as the intrusion tracks south and  
8 east. This suggests that the local and regional contribution to the total MDA8 of ≈70 ppbv on  
9 June 14 is about 20-25 ppbv.

10  
11

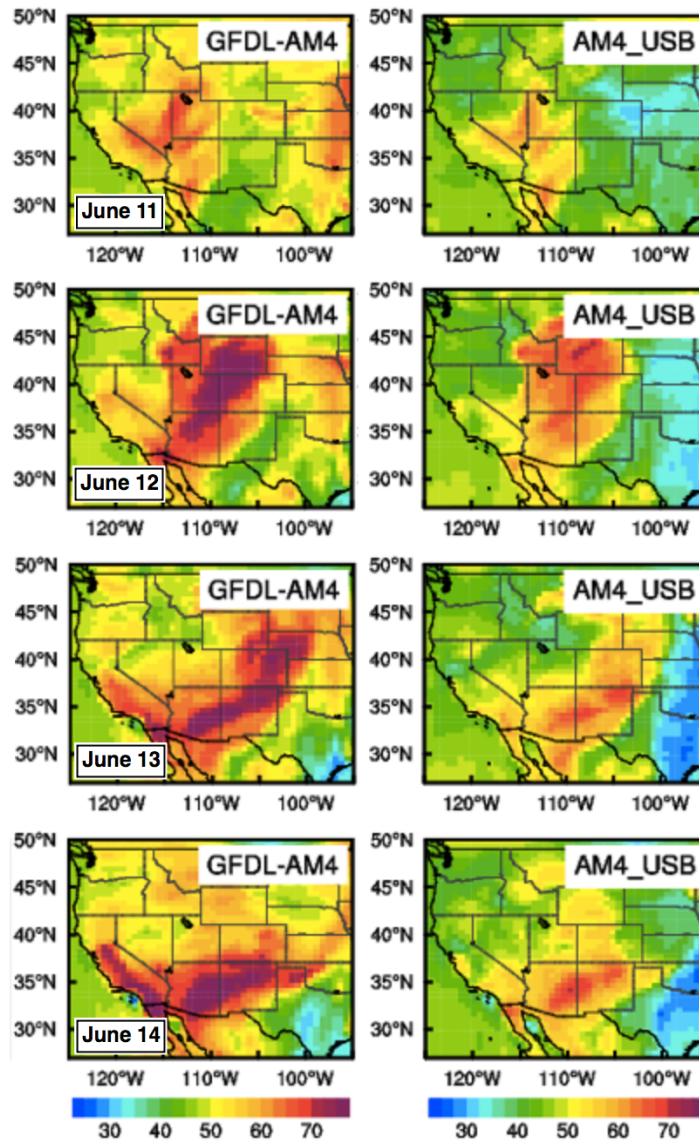


**Figure 10-4.** Maps of total MDA8 O<sub>3</sub> as observed and simulated with GFDL-AM4 along with the model estimated USB level, during the STT event of June 11–14, 2017. (adapted from Zhang et al., 2019).

1 **11. Contrasts between LVOS and FAST-LVOS**

2  
3 The FAST-LVOS measurements directly confirm the hypothesis that entrainment of high O<sub>3</sub>  
4 layers aloft by the deep mixed layers of the Mojave Desert can and does influence surface O<sub>3</sub>  
5 concentrations in the LVV. In contrast to 2013, however, this entrainment did not directly lead  
6 to exceedances of the O<sub>3</sub> NAAQS in Clark County during FAST-LVOS. In the following section, we  
7 examine the differences between the 2013 and 2017 measurements and consider possible  
8 explanations and implications.  
9

10 **Table 11-1** lists the 4 highest MDA8 O<sub>3</sub> values measured by each of the active Clark County  
11 regulatory monitors during 2013 ([http://airquality.clarkcountynv.gov/cgi-bin/8hr\\_4highest.pl](http://airquality.clarkcountynv.gov/cgi-bin/8hr_4highest.pl)).  
12 The MDA8 values are highlighted to reflect the revised Air Quality Index (AQI) with values  
13 exceeding the 2015 NAAQS shown in red or orange. The 2008 NAAQS (75 ppbv) then in effect  
14 was exceeded by one or more of the Clark County regulatory O<sub>3</sub> monitors on 6 days in 2013  
15 with 18 reported exceedances. The 2015 NAAQS was exceeded 82 times on 25 days  
16 ([http://airquality.clarkcountynv.gov/cgi-bin/8hr\\_exceed.pl](http://airquality.clarkcountynv.gov/cgi-bin/8hr_exceed.pl)).  
17  
18

19 **Table 11-1. Four highest O<sub>3</sub> days at the Clark County regulatory monitors in 2013**

Area	Monitoring Site	POC	Highest			Second Highest			Third Highest			Fourth Highest		
			Date	Time	Value	Date	Time	Value	Date	Time	Value	Date	Time	Value
<b>Clark County</b>														
	<a href="#">Apex</a>	1	06/21/2013	1000	78	04/30/2013	0800	74	05/05/2013	0600	73	05/04/2013	1400	73
	<a href="#">Mesquite</a>	1	05/22/2013	1100	68	05/16/2013	1100	68	06/21/2013	1100	67	06/18/2013	1100	67
	<a href="#">Paul Meyer</a>	1	07/03/2013	1100	87	05/04/2013	1400	80	05/25/2013	1000	76	06/21/2013	1000	75
	<a href="#">Walter Johnson</a>	1	07/03/2013	1100	87	05/04/2013	1400	80	05/25/2013	1200	75	07/19/2013	0900	74
	<a href="#">Palo Verde</a>	1	07/03/2013	1000	83	05/04/2013	1400	82	05/25/2013	1200	76	07/19/2013	1000	74
	<a href="#">Joe Neal</a>	1	07/03/2013	1100	81	06/21/2013	1000	77	05/04/2013	1400	77	07/20/2013	1000	76
	<a href="#">Winterwood</a>	2	05/04/2013	1600	76	06/21/2013	1000	75	05/25/2013	0900	73	05/21/2013	1500	71
	<a href="#">Jerome Mack</a>	1	05/04/2013	1400	74	05/25/2013	1100	73	06/21/2013	1000	72	05/21/2013	1400	69
	<a href="#">Boulder City</a>	1	06/21/2013	1100	74	05/22/2013	1400	72	05/21/2013	1600	72	06/22/2013	1000	71
	<a href="#">Jean</a>	1	05/04/2013	1300	84	05/21/2013	1400	78	05/25/2013	1100	76	06/21/2013	1100	75
POC (Parameter Occurrence Code): a code used to correctly separate data from multiple instruments at one site.														

20  
21  
22  
23 Three of the six 75 ppbv exceedance days occurred during the LVOS field campaign: May 21,  
24 May 25, and June 21. The LVOS measurements and modeling convincingly showed that all of  
25 these exceedances were caused, at least in part, by non-controllable ozone sources (NCOS)  
26 [Jaffe et al., 2018] including stratospheric intrusions and Asian pollution. There is strong  
27 evidence that the other 3 exceedance days in 2013 were also influenced by NCOS, with the  
28 highest O<sub>3</sub> concentrations (July 3) linked to the nearby 28,000-acre Carpenter 1 Fire on Mt.  
29 Charleston and the next highest (May 4) with the stratospheric intrusion and wind driven  
30 24,251-acre Springs Fire in Ventura County, CA [Langford et al., 2015a]. The high O<sub>3</sub>  
31 concentrations measured on the one remaining exceedance day (July 19) were likely influenced

1 by the 27,531-acre Mountain Fire in Riverside County, CA. These regional and synoptic-scale  
 2 events affected hundreds of km<sup>2</sup> and raised the O<sub>3</sub> concentrations across most of Clark County.

3  
 4 **Table 11-2** shows the corresponding 4 highest O<sub>3</sub> days for 2017. The total number of NAAQS  
 5 exceedances was much smaller in 2017 with 10 reported exceedances of the 2008 NAAQS and  
 6 43 exceedances of the 2015 NAAQS ([http://airquality.clarkcountynv.gov/cgi-](http://airquality.clarkcountynv.gov/cgi-bin/8hr_exceed.pl)  
 7 [bin/8hr\\_exceed.pl](http://airquality.clarkcountynv.gov/cgi-bin/8hr_exceed.pl)). The corresponding number of days with exceedances of the 2008 and 2015  
 8 NAAQS were 6 and 18, respectively. The highest MDA8 of 87 ppbv recorded in both 2013 and  
 9 2017 was measured by the Walter Johnson monitor<sup>2</sup>.

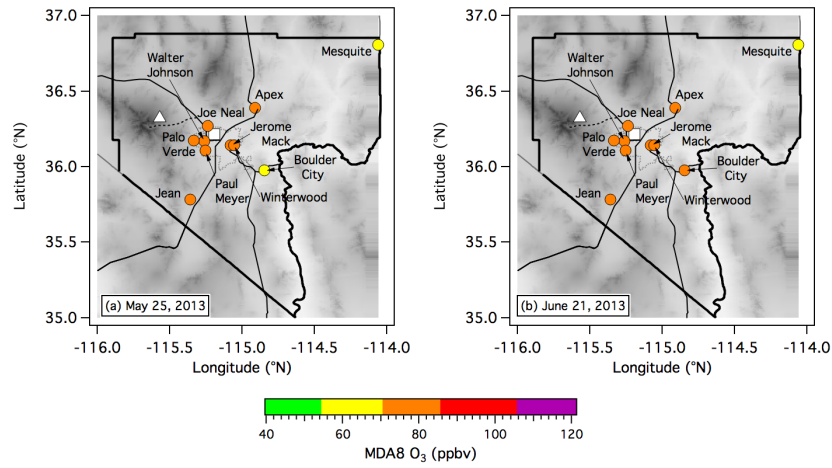
10  
 11  
 12 **Table 11-2. Four highest O<sub>3</sub> days at the Clark County regulatory monitors in 2017**

Area	Monitoring Site	POC	Highest			Second Highest			Third Highest			Fourth Highest		
			Date	Time	Value	Date	Time	Value	Date	Time	Value	Date	Time	Value
<b>Clark County</b>														
	Apex	1	07/11/2017	1000	73	06/28/2017	1000	71	06/22/2017	1000	70	07/04/2017	0900	69
	Mesquite	1	05/14/2017	1100	63	05/12/2017	1400	63	04/23/2017	1100	63	07/02/2017	1000	62
	Paul Meyer	1	08/31/2017	0900	76	07/12/2017	0900	71	06/23/2017	1000	71	07/15/2017	0900	70
	Walter Johnson	1	06/23/2017	1000	87	07/07/2017	0900	79	07/04/2017	0900	76	06/30/2017	1100	75
	Palo Verde	1	07/07/2017	0900	76	06/23/2017	1000	76	06/16/2017	0900	75	07/12/2017	0900	74
	Joe Neal	1	07/04/2017	0900	80	06/23/2017	1100	77	06/22/2017	0900	77	07/15/2017	1000	76
	Green Valley	1	07/11/2017	0900	73	06/17/2017	0900	72	08/31/2017	1000	71	07/08/2017	0900	70
	Jerome Mack	1	08/31/2017	1000	70	07/04/2017	0900	67	06/17/2017	0900	66	07/11/2017	1100	65
	Boulder City	1	06/28/2017	1200	69	05/13/2017	1000	68	07/11/2017	0900	67	04/23/2017	1200	67
	Jean	1	06/30/2017	1000	69	04/11/2017	1200	69	07/03/2017	1100	67	10/04/2017	1100	66
	Indian Springs	1	07/03/2017	0900	69	07/04/2017	0900	66	07/01/2017	0900	66	05/11/2017	1000	66
POC (Parameter Occurrence Code): a code used to correctly separate data from multiple instruments at one site.														

13  
 14  
 15  
 16 **Tables 11-1** and **11-2** appear qualitatively different with fewer monitors exceeding the 2015  
 17 NAAQS in 2017 than in 2013. Furthermore, in contrast to 2013 when nearly all of the monitors  
 18 exceeded the NAAQS on the highest O<sub>3</sub> days (**Figure 11-1**) no more than 4 monitors exceeded  
 19 the NAAQS on the 2017 highest O<sub>3</sub> days in 2017 (**Figure 11-2**). Note that while several  
 20 monitoring stations were not operational during both 2013 and 2017, the core monitors were  
 21 the same in both years. The more limited spatial extent of the high surface O<sub>3</sub> in 2017  
 22 compared to 2013 suggests that stratospheric intrusions did not contribute as much to the  
 23 2017 exceedances. The O<sub>3</sub> scale in both figures reflects the EPA AQI colors, with yellow colors  
 24 corresponding to “Moderate” concentrations and orange colors “Unhealthy for Sensitive  
 25 Groups”.

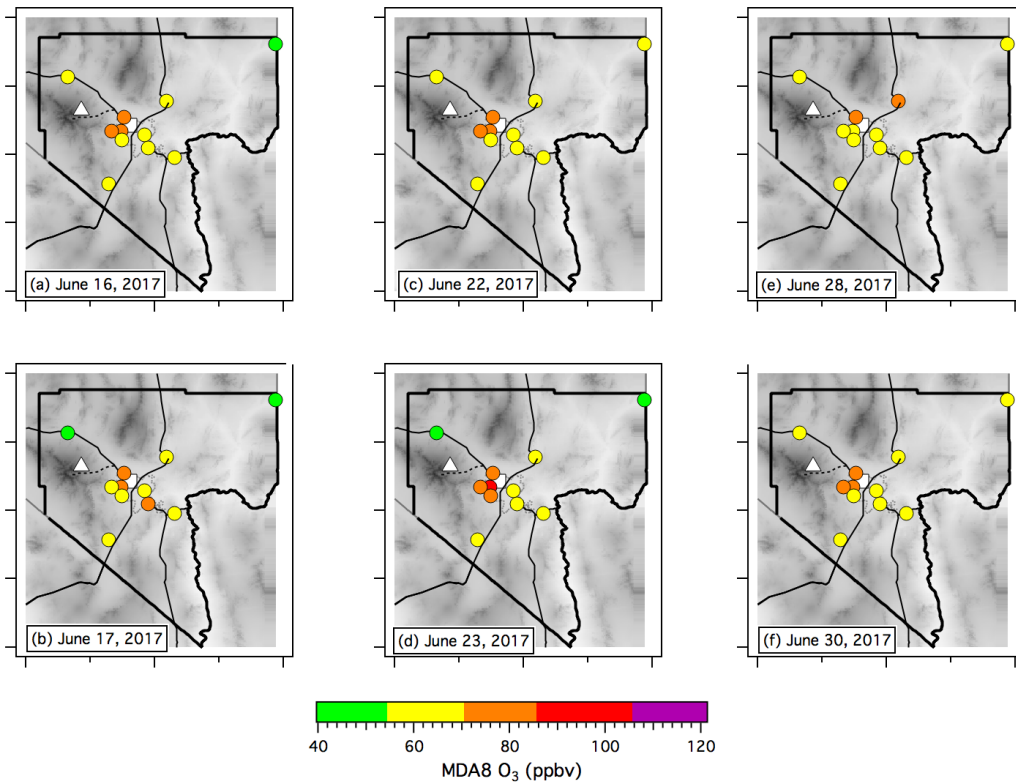
26  
 27  
<sup>2</sup> The MDA8 of 87 ppbv recorded at Walter Johnson on June 23, 2017 is only a 6-h average since  
 the monitor was offline for calibration in the morning. Comparisons with the nearby Joe Neal  
 and Palo Verde monitors suggest that the full 8-h MDA8 would have been closer to 77 ppbv.

1  
2



3  
4  
5  
6  
7  
8  
9

**Figure 11-1.** MDA8 O<sub>3</sub> measured by the Clark County regulatory monitors on two of the three NAAQS exceedance days that occurred during the 2013 LVOS field campaign: (a) May 25, and (b) June 21. The white square and triangle show the locations of NLVA and Angel Peak, respectively.



10  
11  
12  
13

**Figure 11-2.** MDA8 O<sub>3</sub> measured by the Clark County regulatory monitors on days with multiple exceedances during FAST-LVOS. The white squares and triangles show the locations of the NOAA measurement sites at NLVA and AP, respectively.

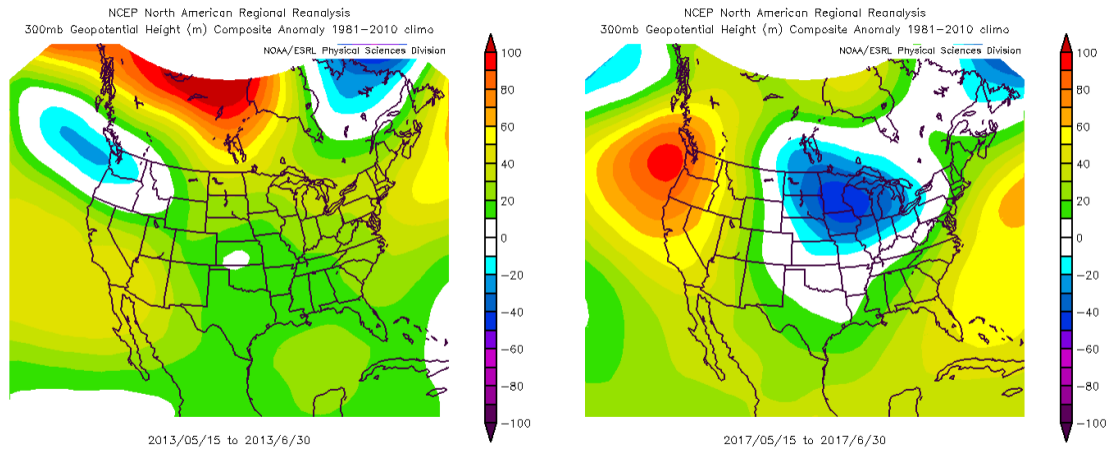
1  
2  
3 The contributions of STT to tropospheric O<sub>3</sub> in the western U.S. have been linked to climatic  
4 oscillations including ENSO [Lin et al., 2015] and the Northern Annular Mode (NAM) [Albers et  
5 al., 2018]. ENSO modulates STT by changing the mean positions of the subtropical [Langford et  
6 al., 1998] and polar front jets [Lin et al., 2015]. Under El Niño conditions, the PFJ migrates  
7 northward over Canada and the subtropical jet moves eastward toward the coast of southern  
8 California. This leads to increased STT of O<sub>3</sub> into the middle and upper troposphere by the STJ  
9 [Langford, 1999], but less STT of O<sub>3</sub> into the lower troposphere. Under La Niña conditions, the  
10 STJ shifts westward and the PFJ meanders southward over the western U.S. where it creates  
11 more deep tropopause folds.

12  
13 The equatorial Pacific remained in an ENSO-neutral state during the winter (November 2012-to  
14 January 2013) preceding the LVOS campaign, but the precipitation patterns in the western U.S.  
15 (<https://www.ncdc.noaa.gov/sotc/synoptic/201301>) more closely resembled La Niña  
16 conditions. The late spring of 2013 was accordingly characterized by a very active jet stream  
17 that brought frequent upper-level troughs through the Pacific Northwest and across the  
18 contiguous U.S. during both May and June (<https://www.ncdc.noaa.gov/sotc/synoptic/201306>).  
19 These upper-level lows spawned several large tropopause folds and were sufficiently deep and  
20 frequent to create a low-pressure anomaly on the 300 hPa geopotential surface compared to  
21 the 30-year (1981-2010) climatology (**Figure 11-3a**).

22  
23 The equatorial Pacific was characterized by La Niña conditions in November of 2016, but  
24 became ENSO-neutral by January 2017 (<https://www.ncdc.noaa.gov/sotc/synoptic/201701>).  
25 The precipitation patterns above the western U.S. exhibited none of the La Niña of 2013, and  
26 the upper-level troughs that moved through the western U.S. during FAST-LVOS did not dip as  
27 far south or penetrate as deeply into the troposphere as those that occurred during LVOS.  
28 **Figure 11-3b** shows a persistent high-pressure ridge parked over the U.S. West Coast that  
29 pushed the jet stream northward into Canada during FAST-LVOS, bringing warmer and drier-  
30 than-normal weather and an active wildfire season to the Southwestern U.S.  
31 (<https://www.ncdc.noaa.gov/sotc/synoptic/201705>). This greatly diminished the influence of  
32 stratospheric intrusions and Asian pollution on surface O<sub>3</sub> in Clark County compared to 2013.

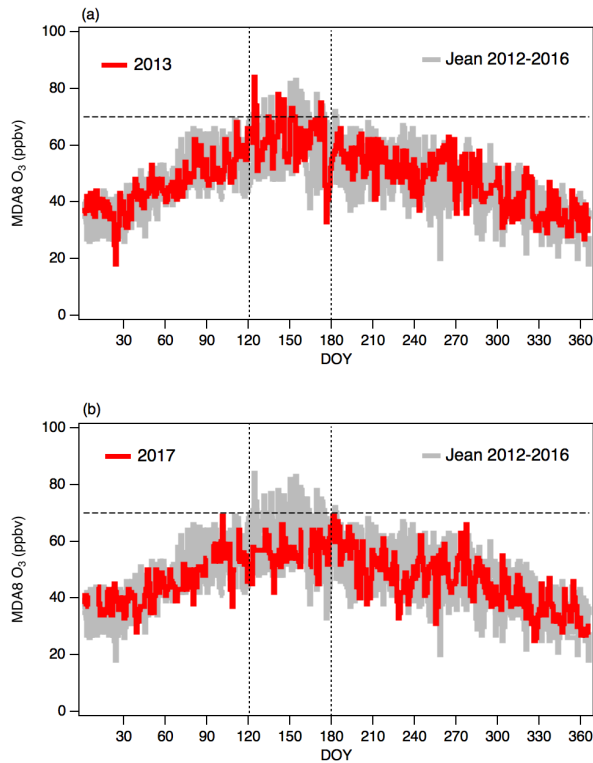
33  
34 These differences are reflected in the MDA8 O<sub>3</sub> measurements from Jean which are shown in  
35 **Figure 11-4**. The MDA8 O<sub>3</sub> measured during May and June of 2017 (57.6±5.7 ppbv) was  
36 generally lower and with fewer short-lived excursions than in the previous 5 years including  
37 2013 (62.2±9 ppbv).

38



1  
2 **Figure 11-3.** NCEP North American Reanalysis (NARR) 300 hPa geopotential anomalies during  
3 (a) LVOS, and (b) FAST-LVOS field campaigns. Plots provided by the NOAA/ESRL Physical  
4 Sciences Division (PSD).

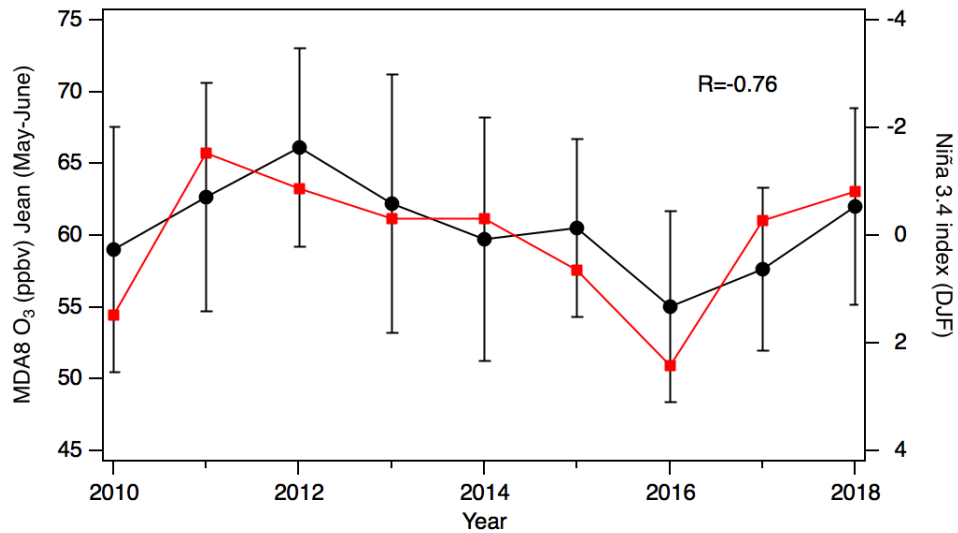
5  
6  
7



8  
9  
10 **Figure 11-4.** MDA8 O<sub>3</sub> measured by the Clark County DAQ monitor at Jean for the years (a)  
11 2013 and (b) 2017. The measurements from 2012-2016 shown in Figure 2-2 are plotted in gray.  
12 The horizontal dashed line marks the 70 ppbv NAAQS. May and June lie between the two  
13 vertical dotted lines.

1  
2  
3  
4  
5  
6  
7  
8

**Figure 11-5** shows that these differences are part of a larger interannual variability (IAV) with the ENSO influence noted above. The correlation with the Niña 3.4 anomaly index [Rayner *et al.*, 2003] is robust and the IAV significant, with the mean May-June MDA8 O<sub>3</sub> ranging by more than 10 ppbv from 55.0±6.6 ppbv in 2016 to 66.2±6.9 ppbv in 2012. Note that the 2012 mean value lies within 4 ppbv of the 2015 NAAQS.



9  
10  
11  
12  
13  
14  
15

**Figure 11-5.** Mean May-June MDA8 O<sub>3</sub> measured at Jean plotted with the Niña 3.4 index ([https://www.esrl.noaa.gov/psd/gcos\\_wgsp/Timeseries/Nino34/](https://www.esrl.noaa.gov/psd/gcos_wgsp/Timeseries/Nino34/)).

## References

- Albers, J. R., J. Perlwitz, A. H. Butler, T. Birner, G. N. Kiladis, Z. D. Lawrence, G. L. Manney, A. O. Langford, and J. Dias (2018), Mechanisms Governing Interannual Variability of Stratosphere-to-Troposphere Ozone Transport, *J. Geophys. Res.-Atmos.*, *123*(1), 234-260, doi:10.1002/2017jd026890.
- Alvarez, R. J., II, et al. (2011), Development and Application of a Compact, Tunable, Solid-State Airborne Ozone Lidar System for Boundary Layer Profiling, *J. Atmos. Ocean Tech.*, *28*(10), 1258-1272, doi:10.1175/Jtech-D-10-05044.1.
- Avnery, S., D. L. Mauzerall, J. F. Liu, and L. W. Horowitz (2011a), Global crop yield reductions due to surface ozone exposure: 1. Year 2000 crop production losses and economic damage, *Atmos. Environ.*, *45*(13), 2284-2296, doi:10.1016/j.atmosenv.2010.11.045.
- Avnery, S., D. L. Mauzerall, J. F. Liu, and L. W. Horowitz (2011b), Global crop yield reductions due to surface ozone exposure: 2. Year 2030 potential crop production losses and economic damage under two scenarios of O-3 pollution, *Atmos. Environ.*, *45*(13), 2297-2309, doi:10.1016/j.atmosenv.2011.01.002.
- Bonin, T. A., A. Choukulkar, W. A. Brewer, S. P. Sandberg, A. M. Weickmann, Y. L. Pichugina, R. M. Banta, S. P. Oncley, and D. E. Wolfe (2017), Evaluation of turbulence measurement techniques from a single Doppler lidar, *Atmos Meas Tech*, *10*(8), 3021-3039, doi:10.5194/amt-10-3021-2017.
- Faloon, I. C., et al. (2019), The California Baseline Ozone Transport Study (CABOTS), *Bull. Am. Meteorol. Soc.*, submitted.
- Gaudel, A., et al. (2018), Tropospheric Ozone Assessment Report: Present-day distribution and trends of tropospheric ozone relevant to climate and global atmospheric chemistry model evaluation, *Elementa-Sci Anthropol*, *6*, doi:ARTN 39 10.1525/elementa.291.
- Grund, C. J., R. M. Banta, J. L. George, J. N. Howell, M. J. Post, R. A. Richter, and A. Weickmann (2000), High-resolution Doppler lidar for boundary layer and cloud research, *J. Atmos. Oceanic Technol.*, *18*, 376-393.
- Jaffe, D. A., O. R. Cooper, A. M. Fiore, B. H. Henderson, G. S. Tonneson, A. G. Russell, D. K. Henze, A. O. Langford, M. Lin, and T. Moore (2018), Scientific assessment of background ozone over the U.S.: Implications for air quality management., *Elem Sci Anth.*, *6*(1), doi:<http://doi.org/10.1525/elementa.309>.
- James, P., A. Stohl, C. Forster, S. Eckhardt, P. Seibert, and A. Frank (2003), A 15-year climatology of stratosphere-troposphere exchange with a Lagrangian particle dispersion model: 2. Mean climate and seasonal variability *J. Geophys. Res.*, *108*, doi:10.1029/2002JD002639.
- Johnson, B. J., S. J. Oltmans, H. Vomel, H. G. J. Smit, T. Deshler, and C. Kroger (2002), Electrochemical concentration cell (ECC) ozonesonde pump efficiency measurements and tests on the sensitivity to ozone of buffered and unbuffered ECC sensor cathode solutions, *J. Geophys. Res.*, *107*(D19), doi:10.1029/2001jd000557.
- Langford, A. O. (1999), Stratosphere-troposphere exchange at the subtropical jet: contribution to the tropospheric ozone budget at midlatitudes, *Geophys. Res. Lett.*, *26*(16), 2449-2452.
- Langford, A. O., et al. (2018), Coordinated profiling of stratospheric intrusions and transported pollution by the Tropospheric Ozone Lidar Network (TOLNet) and NASA Alpha Jet

1 Atmospheric eXperiment (AJAX): Observations and comparison to HYSPLIT, RAQMS, and  
2 FLEXPART, *Atmos. Environ.*, 174, 1-14,  
3 doi:<https://doi.org/10.1016/j.atmosenv.2017.11.031>.

4 Langford, A. O., et al. (2019), Intercomparison of lidar, aircraft, and surface ozone  
5 measurements in the San Joaquin Valley during the California Baseline Ozone Transport  
6 Study (CABOTS), *Atmos. Meas. Tech.*, 12(3), 1889-1904, doi:10.5194/amt-12-1889-2019.

7 Langford, A. O., et al. (2017), Entrainment of stratospheric air and Asian pollution by the  
8 convective boundary layer in the southwestern U.S, *J. Geophys. Res.*, 122(2), 1312-1337,  
9 doi:10.1002/2016JD025987.

10 Langford, A. O., J. Brioude, O. R. Cooper, C. J. Senff, R. J. Alvarez, R. M. Hardesty, B. J. Johnson,  
11 and S. J. Oltmans (2012), Stratospheric influence on surface ozone in the Los Angeles area  
12 during late spring and early summer of 2010, *J. Geophys. Res.*, 117, D00V06,  
13 doi:10.1029/2011JD016766.

14 Langford, A. O., T. J. O'Leary, C. D. Masters, K. C. Aikin, and M. H. Proffitt (1998), Modulation of  
15 middle and upper tropospheric ozone at northern midlatitudes by the El Nino Southern  
16 Oscillation, *Geophys. Res. Lett.*, 25(14), 2667-2670.

17 Langford, A. O., R. B. Pierce, and P. J. Schultz (2015a), Stratospheric intrusions, the Santa Ana  
18 winds, and wildland fires in Southern California, *Geophys. Res. Lett.*, 42(14), 6091-6097,  
19 doi:10.1002/2015gl064964.

20 Langford, A. O., M. H. Proffitt, T. E. VanZandt, and J.-F. Lamarque (1996), Modulation of  
21 tropospheric ozone by a propagating gravity wave, *J. Geophys. Res.*, 101(D21), 26605-  
22 26613.

23 Langford, A. O., C. J. Senff, R. J. Alvarez, R. M. Banta, and R. M. Hardesty (2010), Long-range  
24 transport of ozone from the Los Angeles Basin: A case study, *Geophys. Res. Lett.*, 37,  
25 L06807, doi:10.1029/2010gl042507.

26 Langford, A. O., C. J. Senff, R. J. Alvarez, R. M. Banta, R. M. Hardesty, D. D. Parrish, and T. B.  
27 Ryerson (2011), Comparison between the TOPAZ Airborne Ozone Lidar and In Situ  
28 Measurements during TexAQ5 2006, *J. Atmos. Ocean. Tech.*, 28(10), 1243-1257,  
29 doi:10.1175/Jtech-D-10-05043.1.

30 Langford, A. O., et al. (2015b), An overview of the 2013 Las Vegas Ozone Study (LVOS): Impact  
31 of stratospheric intrusions and long-range transport on surface air quality, *Atmos. Environ.*,  
32 109, 305-322, doi:10.1016/J.Atmosenv.2014.08.040.

33 Leblanc, T., et al. (2018), Validation of the TOLNet lidars during SCOOP (Southern California  
34 Ozone Observation Project), *EPJ Web Conf. (France)*, 176, 05019 (05014 pp.)-05019 (05014  
35 pp.), doi:10.1051/epjconf/201817605019.

36 Lin, M. Y., A. M. Fiore, O. R. Cooper, L. W. Horowitz, A. O. Langford, H. Levy, B. J. Johnson, V.  
37 Naik, S. J. Oltmans, and C. J. Senff (2012a), Springtime high surface ozone events over the  
38 western United States: Quantifying the role of stratospheric intrusions, *J. Geophys. Res.*,  
39 117, D00v22, doi:10.1029/2012jd018151.

40 Lin, M. Y., et al. (2012b), Transport of Asian ozone pollution into surface air over the western  
41 United States in spring, *J. Geophys. Res.*, 117, D00v07, doi:10.1029/2011JD016961.

42 Lin, M. Y., A. M. Fiore, L. W. Horowitz, A. O. Langford, S. J. Oltmans, D. Tarasick, and H. E. Rieder  
43 (2015), Climate variability modulates western US ozone air quality in spring via deep  
44 stratospheric intrusions, *Nat. Comm.*, 6, doi:10.1038/Ncomms8105.

1 Malicet, J., D. Daumont, J. Charbonnier, C. Parisse, A. Chakir, and J. Brion (1995), Ozone UV  
2 Spectroscopy .2. Absorption Cross-Sections and Temperature-Dependence, *J. Atmos.*  
3 *Chem.*, 21(3), 263-273, doi:10.1007/Bf00696758.

4 Proffitt, M. H., and A. O. Langford (1997), Ground-based differential absorption lidar system for  
5 day or night measurements of ozone throughout the free troposphere, *Appl Optics*, 36(12),  
6 2568-2585.

7 Rayner, N. A., D. E. Parker, E. B. Horton, C. K. Folland, L. V. Alexander, D. P. Rowell, E. C. Kent,  
8 and A. Kaplan (2003), Global analyses of sea surface temperature, sea ice, and night marine  
9 air temperature since the late nineteenth century, *J. Geophys. Res.-Atmos.*, 108(D14),  
10 doi:Artn 4407  
11 10.1029/2002jd002670.

12 Seidel, D. J., Y. H. Zhang, A. Beljaars, J. C. Golaz, A. R. Jacobson, and B. Medeiros (2012),  
13 Climatology of the planetary boundary layer over the continental United States and  
14 Europe, *J. Geophys. Res.*, 117, D17106, doi:10.1029/2012jd018143.

15 Senff, C. J., R. J. Alvarez, R. M. Hardesty, R. M. Banta, and A. O. Langford (2010), Airborne lidar  
16 measurements of ozone flux downwind of Houston and Dallas, *J. Geophys. Res.*, 115,  
17 D20307, doi:10.1029/2009jd013689.

18 Skerlak, B., M. Sprenger, and H. Wernli (2014), A global climatology of stratosphere-  
19 troposphere exchange using the ERA-Interim data set from 1979 to 2011, *Atmos. Chem.*  
20 *Phys.*, 14(2), 913-937, doi:10.5194/Acp-14-913-2014.

21 Sprenger, M., and H. Wernli (2003), A northern hemisphere climatology of cross-tropopause  
22 exchange for the ERA15 time period (1979-1993), *J. Geophys. Res.*, 108,  
23 doi:10.1029/2002JD002636.

24 Stewart, J. Q., C. D. Whiteman, W. J. Steenburgh, and X. D. Bian (2002), A climatological study of  
25 thermally driven wind systems of the US Intermountain West, *Bull. Am. Meteorol. Soc.*,  
26 83(5), 699-708, doi:10.1175/1520-0477(2002)083<0699:AcsoTd>2.3.Co;2.

27 Trousdell, J. F., S. A. Conley, A. Post, and I. C. Faloon (2016), Observing entrainment mixing,  
28 photochemical ozone production, and regional methane emissions by aircraft using a  
29 simple mixed-layer framework, *Atmos. Chem. Phys.*, 16(24), 15433-15450,  
30 doi:10.5194/acp-16-15433-2016.

31 Tucker, S. C., W. A. Brewer, R. M. Banta, C. J. Senff, S. P. Sandberg, D. C. Law, A. Weickmann,  
32 and R. M. Hardesty (2009), Doppler lidar estimation of mixing height using turbulence,  
33 shear, and aerosol profiles, *J. Atmos. Oceanic Technol.*, 26, 673-688.

34 U.S. Environmental Protection Agency (2014), Policy Assessment for the Review of the Ozone  
35 National Ambient Air Quality Standards, *Rep. EPA-452/R-14-006*, Research Triangle Park,  
36 North Carolina.

37 U.S. Environmental Protection Agency (2015), National Ambient Air Quality Standards for  
38 Ozone: Final Rule, in *EPA-HQ-OAR-2008-0699; FRL-9933-18- OAR*, edited by U. S.  
39 Environmental Protection Agency, Federal Register.

40 Völger, P., J. Bösenberg, and I. Shult (1996), Scattering properties of selected model aerosols  
41 calculated at UV-wavelengths: Implications for DIAL measurements of tropospheric ozone.,  
42 *Contributions to Atmospheric Physics*, 69, 177-187.

1 Wang, L. H., et al. (2017), Quantifying TOLNet ozone lidar accuracy during the 2014 DISCOVER-  
2 AQ and FRAPPE campaigns, *Atmos Meas Tech*, 10(10), 3865-3876, doi:10.5194/amt-10-  
3 3865-2017.

4 Wernli, H., and M. Bourqui (2002), A Lagrangian "1-year climatology" of (deep) cross-  
5 tropopause exchange in the extratropical Northern Hemisphere, *J. Geophys. Res.*, 107(D1-  
6 D2), doi:10.1029/2001JD000812.

7 Wild, R. J., W. P. Dube, K. C. Aikin, S. J. Eilerman, J. A. Neuman, J. Peischl, T. B. Ryerson, and S. S.  
8 Brown (2017), On-road measurements of vehicle NO<sub>2</sub>/NO<sub>x</sub> emission ratios in Denver,  
9 Colorado, USA, *Atmospheric Environment*, 148, 182-189,  
10 doi:10.1016/j.atmosenv.2016.10.039.

11 Zhang, L., et al. (2019), Characterizing Sources of High Surface Ozone Events in the  
12 Southwestern U.S. with Intensive Field Measurements and Two Global Models, *Atmos.*  
13 *Chem. Phys. Disc.*, *submitted*.

14  
15

## 1 **Appendix A: Model Descriptions**

### 2 ***NOAA NESDIS RAQMS model***

3 The NOAA/NESDIS RAQMS (Realtime Air Quality Modeling System) model is a unified  
4 (stratosphere-troposphere) online global chemical and aerosol assimilation/forecasting system  
5 developed specifically to support airborne field missions [*Pierce et al., 2003; Pierce et al., 2007*].  
6 The meteorological forecasts are conducted using the University of Wisconsin Hybrid Model  
7 [*Schaack et al., 2004*], and the chemical forecasts are initialized daily at 12 UT with real-time  
8 assimilation of Ozone Monitoring Instrument (OMI) cloud-cleared total column ozone and  
9 Microwave Limb Sounder (MLS) ozone profiles from the NASA *Aura* satellite, and MODIS  
10 aerosol optical depth from the NASA *Terra* and *Aqua* satellites. RAQMS has been run routinely  
11 in a forecast mode since 2010 with 2° x 2° resolution analyses and forecasts prior to 2012, and  
12 1° x 1° analyses since 2012. The model predicts global O<sub>3</sub>, CO, SO<sub>4</sub>, and black organic carbon  
13 distributions at 6-hour intervals for the next 4 days. The real-time analyses are archived online  
14 (<http://raqms-ops.ssec.wisc.edu>).  
15

### 16 ***NOAA ESRL RAP-Chem model***

17 The NOAA ESRL Global Systems Division (GSD) RAP-Chem forecast system  
18 (<https://rapidrefresh.noaa.gov/RAPchem/Welcome.cgi>) uses the Weather Research and  
19 Forecasting model coupled to Chemistry (WRF-Chem) model [*Grell et al., 2005; Pagowski et al.,*  
20 *2010*] driven by meteorology from the NCEP's GFS analysis at 00 UTC and 6-hourly forecasts  
21 thereafter. This 13-km resolution North American model uses the Regional Atmospheric  
22 Chemistry Mechanism (RACM) [*Goliff et al., 2013*] and aerosol scheme by *Ahmadov et*  
23 *al.* [*Ahmadov et al., 2012*]. It incorporates MEGAN biogenic emissions [*Guenther et al., 2006*],  
24 and the U.S EPA NEI-11 (CONUS) version-1 anthropogenic emission inventories with oil/gas  
25 sector emissions updated to version-2. Biomass burning emissions are derived from MODIS and  
26 GOES-West satellite observations.

27 The model includes surface deposition, photolysis, and convective and turbulent chemical  
28 transport, and wet removal of aerosols by resolved and convective precipitation with advective  
29 chemical transport performed simultaneously with the meteorology. The lateral boundary  
30 conditions for chemistry are obtained from the RAQM model [*Pierce et al., 2003*]. Operational  
31 forecasts are run at 00 UTC at 3-h forecast intervals for up to 48 hours, and plots of the CO and  
32 O<sub>3</sub> distributions on the 500, 700, and 850 hPa and surface levels were archived for the entire  
33 CABOTS period by M. Pagowski of the NOAA ESRL Global Systems Division and the Cooperative  
34 Institute for Research in Environmental Sciences (CIRES) at the University of Colorado.  
35

### 36 ***FLEXPART particle dispersion model***

37  
38 FLEXPART (FLEXible PARTicle) [*Stohl et al., 2005*] is a passive tracer model (no chemistry) that  
39 calculates the evolving distribution of a multitude of “particles” released from a specified  
40 source region and transported forward in time for up to 20 days. FLEXPART calculations played

1 a key role in earlier TOPAZ studies of long-range transport and stratosphere-to-troposphere  
2 transport (STT) in the western U.S. including LVOS [Langford et al., 2012; Langford et al., 2015].  
3 For FAST-LVOS, evolving particle distributions representing stratospheric ozone (STO3), Asian  
4 pollution (ASCO) and biomass burning (BBCO) were calculated with 0.25° resolution over an  
5 output domain extending from 130 to 70°W and from 20 to 50°N. The particles were  
6 transported by winds from the European Centre for Medium-Range Weather Forecasts  
7 (ECMWF) operational (0.5° x 0.5°) model forecasts and by sub grid motions including  
8 convection and turbulence based on the parameterization schemes of Emanuel and Zivkovic-  
9 Rothman [Emanuel and Zivkovic-Rothman, 1999] and Hanna [Hanna, 1982] respectively. The  
10 tracer distributions were calculated at the surface (1 km above ground level) and on the  
11 700hPa, 500hPa, 400hPa levels at 3-h intervals from May 15 to June 30, 2017.

12  
13 The stratospheric O<sub>3</sub> tracer was represented by particles released into the stratosphere (>2  
14 potential vorticity units or PVU) and converted to O<sub>3</sub> mixing ratios using a linear relationship  
15 between O<sub>3</sub> and potential vorticity (60 ppbv/PVU) at the particle origin. The Asian CO tracer is  
16 based on the amount of CO released into the boundary layer from anthropogenic sources in  
17 East Asia using the EDGAR 3.2 fast track inventory [Olivier et al., 2005]. Biomass burning CO  
18 emissions from North American sources were calculated using the ECMWF Copernicus  
19 Atmosphere Monitoring System (CAMS) near-real time biomass burning emission estimates  
20 based on the Global Fire Assimilation System (GFAS), which converts Fire Radiative Power (FRP)  
21 observations from MODIS satellites into smoke constituents [Di Giuseppe et al., 2016]. Since CO  
22 is chemically inert over the timescale of the FLEXPART calculations, these two tracers show the  
23 relative importance and temporal evolution of these potential O<sub>3</sub> sources, but cannot be  
24 quantitatively compared to the stratospheric O<sub>3</sub> flux since FLEXPART does not include  
25 chemistry. The FLEXPART calculations used here were generously provided by S. Evan and J.  
26 Brioude of the Laboratoire de l'Atmosphere et des Cyclones (LACy), UMR 8105, CNRS,  
27 Université de La Réunion, Météo-France, Saint-Denis, La Reunion, France.

## 28 29 **References**

- 30  
31 Ahmadov, R., et al. (2012), A volatility basis set model for summertime secondary organic  
32 aerosols over the eastern United States in 2006, *J. Geophys. Res.-Atmos.*, 117, doi:Artn  
33 D0630110.1029/2011jd016831.
- 34 Di Giuseppe, F., S. Remy, P. Florian, and W. Fredrik (2016), Improving GFAS and CAMS biomass  
35 burning estimations by means of the Global ECMWF Fire Forecast system (GEFF), edited,  
36 ECMWF.
- 37 Emanuel, K. A., and M. Zivkovic-Rothman (1999), Development and evaluation of a convective  
38 scheme for use in climate models, *J. Atmos. Sci.*, 56, 1766-1782.
- 39 Goliff, W. S., W. R. Stockwell, and C. V. Lawson (2013), The regional atmospheric chemistry  
40 mechanism, version 2, *Atmospheric Environment*, 68, 174-185,  
41 doi:10.1016/j.atmosenv.2012.11.038.
- 42 Grell, G. A., S. E. Peckham, R. Schmitz, S. A. McKeen, G. J. Frost, W. C. Skamarock, and B. Eder  
43 (2005), Fully coupled 'online' chemistry in the WRF model, *Atmospheric Environment*, 39,  
44 6957-6976.

1 Guenther, A., T. Karl, P. Harley, C. Wiedinmyer, P. I. Palmer, and C. Geron (2006), Estimates of  
2 global terrestrial isoprene emissions using MEGAN (Model of Emissions of Gases and  
3 Aerosols from Nature), *Atmospheric Chemistry & Physics*, 6, 29.

4 Hanna, S. R. (1982), Applications in air pollution modeling, in *Atmospheric Turbulence*  
5 *and Air Pollution Modelling*, edited by F. T. M. Nieuwstadt and H. van Dop, D. Reidel Publishing  
6 Company, Dordrecht, Holland.

7 Langford, A. O., J. Brioude, O. R. Cooper, C. J. Senff, R. J. Alvarez, R. M. Hardesty, B. J. Johnson,  
8 and S. J. Oltmans (2012), Stratospheric influence on surface ozone in the Los Angeles area  
9 during late spring and early summer of 2010, *J. Geophys. Res.*, 117, D00V06,  
10 doi:10.1029/2011JD016766.

11 Langford, A. O., et al. (2015), An overview of the 2013 Las Vegas Ozone Study (LVOS): Impact of  
12 stratospheric intrusions and long-range transport on surface air quality, *Atmos. Environ.*,  
13 109, 305-322, doi:10.1016/J.Atmosenv.2014.08.040.

14 Olivier, J. G. J., J. A. Van Aardenne, F. Dentener, L. Ganzeveld, and J. A. H. W. Peters (2005),  
15 Recent trends in global greenhouse gas emissions: regional trends and spatial distribution  
16 of key sources, in *Non-CO<sub>2</sub> Greenhouse Gases (NCGG-4)* edited by A. v. Amstel, pp. 325-  
17 330, Millpress, Rotterdam.

18 Pagowski, M., G. A. Grell, S. A. McKeen, S. E. Peckham, and D. Devenyi (2010), Three-  
19 dimensional variational data assimilation of ozone and fine particulate matter  
20 observations: some results using the Weather Research and Forecasting - Chemistry model  
21 and Grid-point Statistical Interpolation, *Quarterly Journal of the Royal Meteorological*  
22 *Society*, 136(653), 2013-2024, doi:10.1002/qj.700.

23 Pierce, R. B., et al. (2003), Regional Air Quality Modeling System (RAQMS) predictions of the  
24 tropospheric ozone budget over east Asia, *J. Geophys. Res.*, 108(D21), 8825,  
25 doi:10.1029/2002jd003176.

26 Pierce, R. B., et al. (2007), Chemical data assimilation estimates of continental US ozone and  
27 nitrogen budgets during the Intercontinental Chemical Transport Experiment-North  
28 America, *J. Geophys. Res.*, 112(D12), doi:10.1029/2006jd007722.

29 Schaack, T. K., T. H. Zapotocny, A. J. Lenzen, and D. R. Johnson (2004), Global climate simulation  
30 with the university of Wisconsin global hybrid isentropic coordinate model, *J. Climate*,  
31 17(15), 2998-3016, doi:10.1175/1520-0442(2004)017<2998:Gcswtu>2.0.Co;2.

32 Stohl, A., C. Forster, A. Frank, P. Seibert, and G. Wotawa (2005), Technical note: The Lagrangian  
33 particle dispersion model FLEXPART version 6.2, *Atmos. Chem. Phys.*, 5, 2461-2474.

34  
35

1 **Appendix B: FAST-LVOS Daily Summaries**

2

3 Wednesday, May 17

4 TOPAZ arrived at NLVA around 13:00 PDT, the system was set up, the laser was realigned, and  
5 data were taken from 17:37 - 20:57 PDT. Rather cool temperatures and strong winds out of the  
6 NW. High ozone (80 - 120 ppbv) was observed above 4.5 km AGL. Boundary layer and surface  
7 ozone peaked around 19:00 PDT at around 70 ppbv.

8 Thursday, May 18

9 TOPAZ data were taken from 09:37 - 21:13 PDT. The data gap from about 11:00 - 14:00 PDT was  
10 due to an extensive laser system realignment. Cool temperatures throughout the day, low  
11 clouds and strong winds from a NE/NW direction in the afternoon and early evening. Due to the  
12 clouds and strong winds, surface and boundary layer ozone dropped to below 40 ppbv in the  
13 afternoon. High ozone (80 - 120 ppbv) aloft descended during the day to about 2 km AGL, but  
14 did not reach the surface.

15 Friday, May 19

16 TOPAZ data were taken from 10:39 - 18:23 PDT. Still below normal temperatures, light winds.  
17 The high-ozone layer (75 - 95 ppbv, 4 - 6 km AGL) aloft persisted and thinned over the course of  
18 the day. Surface and BL ozone did not vary much during the day and stayed below 60 ppbv.

19

20 Saturday, May 20

21 TOPAZ data were taken from 10:25 - 18:09 PDT. Seasonal temperatures with a high around 33  
22 C, light winds. The high-ozone layer that had been observed the previous three days thinned  
23 further and contained less ozone (~ 80 ppbv). It lowered to about 2.5 km AGL by 14:00 PDT and  
24 then most likely moved away from the Las Vegas area. The mixed layer was not deep enough to  
25 entrain this ozone layer. Surface and BL ozone peaked in the low 60s ppbv in the afternoon

26

27 Sunday, May 21

28 TOPAZ data were taken from 11:08 - 19:08 PDT. Warm temperatures with a high around 38 C,  
29 light winds, and a period of Cu clouds in the late afternoon. Fairly uniform surface and BL ozone  
30 throughout the day with a maximum of 70 ppbv around 17:00 PDT. Enhanced ozone around 6  
31 km AGL.

32

33 Monday, May 22

34 TOPAZ data were taken from 09:14 - 19:14 PDT. Warm temperatures with a high around 38 C,  
35 light winds. Surface and BL ozone peaked in the low 60s ppbv in the early evening. A moderate  
36 ozone layer containing enhanced aerosols was observed between 2 and 4 km AGL until midday.  
37 Enhanced ozone was measured again around 6 km AGL.

38 Tuesday, May 23

39 TOPAZ data were taken from 08:04 - 22:04 PDT. Hot temperatures with a high around 40 C,  
40 light winds. Locally produced ozone built up in the afternoon reaching a maximum

1 concentration of about 80 ppbv at the surface and throughout the 2-km deep BL. The Clark  
2 County DAQ site Walter Johnson recorded a MDA8 ozone value of 71 ppbv, which exceeded the  
3 NAAQS. A high-ozone layer (80 - 90 ppbv) was observed above 6 km AGL.

4 Wednesday, May 24

5 TOPAZ data were taken from 07:45 - 03:53 PDT the next day. Hot temperatures with a high  
6 around 39 C, light winds until midday, followed by a sharp increase in wind speeds to about 15  
7 m/s. An ozone layer aloft (70 - 80 ppbv, 500 m - 4 km AGL) was entrained into the growing BL  
8 around 11:00 PDT, resulting in a sharp increase in surface ozone to just above 70 ppbv.  
9 However, this increase was short-lived as the high winds in the afternoon diluted ozone  
10 concentrations. Surface and BL ozone stayed in the mid 60s ppbv throughout most of the day. A  
11 secondary ozone maximum of approx. 70 ppbv was observed around midnight. High ozone  
12 concentrations up to about 100 ppbv were measured above 6.5 km AGL.

13

14 Thursday, May 25

15 TOPAZ data were taken from 08:03 - 17:55 PDT. Warm temperatures with a high around 36 C,  
16 light winds from the early morning hours until midday, followed by an increase in wind speeds  
17 to about 20 m/s. Moderate ozone in the residual layer aloft was entrained into the growing BL  
18 around 10:30 PDT, resulting in an increase in surface ozone to about 65 ppbv. The very strong  
19 winds in the afternoon and evening diluted ozone concentrations, causing surface ozone to stay  
20 in the 50s ppbv during the remainder of the day. A high-ozone layer (70 - 85 ppbv) was  
21 observed above 4 km AGL after 11:00 PDT.

22

23 Friday, May 26

24 TOPAZ data were taken from 09:23 - 18:51 PDT. The TOPAZ laser needed to be realigned, hence  
25 the data gap between 11:00 and 14:40 PDT. Seasonal temps (33 C max). Winds from the SW.  
26 Breezy overnight and in the early evening. Surface ozone stayed elevated (40-55 ppb)  
27 overnight, increased to about 65 ppb around midday, and then stayed level at about 60 ppb  
28 into the night. In the afternoon, ozone was well mixed up to 3 km AGL. High ozone (80-90 ppb)  
29 was observed above 6 km AGL.

30

31 Saturday, May 27

32 TOPAZ data were taken from 07:40 - 18:20 PDT. High pressure was moving in from the west  
33 with a shortwave trough to the northeast. Seasonal temps (34 C), light winds, a few Cu clouds  
34 over the nearby mountains. MicroDop lidar observed intermittent turbulence at night up to  
35 about 3 km AGL. The convective daytime BL rose to about 2.5 km AGL in the afternoon. Surface  
36 ozone stayed elevated (35-55 ppb) overnight and increased to about 60 ppb in the afternoon.  
37 TOPAZ observed an ozone layer aloft ( $\approx$  65 ppb) between 2.5 and 3.5 km AGL. That layer  
38 thinned during the day and was most likely entrained into the BL in the early afternoon. There  
39 was high ozone ( $\approx$ 80 ppb) above 4.5 km AGL associated with the shortwave trough.

40

41 Sunday, May 28

42 After TOPAZ maintenance in the morning, data were taken from 12:27 - 18:51 PDT. High  
43 pressure in control, hot (36°C max), light to moderate winds, isolated Cu clouds over the nearby

1 mountains. The MicroDop lidar observed intermittent turbulence at night. The convective  
2 daytime BL rose to about 2.5 km AGL in the afternoon. Surface ozone stayed somewhat  
3 elevated (25-45 ppb) overnight and increased to the low 60s ppb in the afternoon. TOPAZ  
4 observed high ozone above 4.5 km AGL (75 - 90 ppb).

5  
6 Monday, May 29

7 TOPAZ data were taken from 10:40 - 22:08 PDT. Hot (39 C max), light winds, isolated Cu clouds  
8 over the nearby mountains. Cirrus shield associated with the West Coast trough was moving in  
9 from the SW. The BL rose to just over 4 km AGL in the afternoon, as evidenced by the MicroDop  
10 lidar and the afternoon sounding at McCarren Airport. The deep BL entrained the bottom part  
11 of the high ozone layer (80-90 ppb), that had been observed by TOPAZ between 4 and 7 km AGL  
12 for several days in a row. The air in this layer was very dry, so the high ozone likely originated in  
13 the UTLS. The entrained ozone mixed down to surface resulting in a several-ppb jump in ozone  
14 concentration.

15  
16 Tuesday, May 30

17 TOPAZ data were taken from 11:28 - 19:20 PDT. Laser maintenance in the morning and around  
18 midday. TOPAZ performance was not optimal during the late AM data segment. Hot (38 C max),  
19 light winds early, increasing in the afternoon. Thick Cirrus shield associated with the West Coast  
20 trough. The BL rose to about 4 km AGL in the afternoon, just to the bottom of the high ozone  
21 layer (80-90 ppb). Contrary to the day before, the high ozone aloft was not entrained into the  
22 BL. Cirrus clouds at 7.5 km AGL caused artifacts in the ozone and aerosol retrievals.

23  
24 Wednesday, May 31

25 TOPAZ data were recorded from 7:34 PDT through the night until 7:02 PDT on June 1 (data  
26 collection was continued the next day without interruption). Slight cooldown compared to the  
27 day before (35 C max), light winds early, increasing to 15 m/s in the afternoon and becoming  
28 light again after sunset. Mid- and high-level clouds associated with the West Coast trough,  
29 clearing out in the early morning hours the next day. Between 11 and 12 PDT, a sudden  
30 increase in ozone by about 10 ppb at the surface and throughout the BL (up to 1.5 km AGL) was  
31 observed. This bump up in ozone was likely associated with the advection of air in southerly  
32 flow aloft that was influenced by fires burning in western Mexico. This was corroborated by the  
33 in-situ observations at Angel Peak (enhanced NO<sub>x</sub>, NO<sub>y</sub>, CO, CO<sub>2</sub>, and CH<sub>4</sub>, but no increase in  
34 O<sub>3</sub>) and back trajectory calculations. The BL rose to about 3.5 km AGL in the late afternoon.  
35 TOPAZ observed a persistent ozone layer (75 - 85 ppb) above 4 km AGL. Clouds above 6 km AGL  
36 caused artifacts in the ozone and aerosol retrievals at times.

37  
38 Thursday, June 1

39 TOPAZ data were recorded from 7:14 - 20:42 PDT. Seasonal temperatures (34°C max) after  
40 trough passage, light winds early, increasing to about 15 m/s around midday, and becoming  
41 light again after sunset. Isolated Cu clouds over the nearby mountain ranges, otherwise clear.  
42 Ozone increased to the mid 60s ppb after the growing BL had entrained the residual layer. In  
43 the late morning, the BL grew rapidly from 700 to 2700 m AGL and clean air above 1.5 km AGL  
44 was entrained into the BL, which likely caused the ≈10 ppbv drop in ozone concentrations. The

1 strong southerly winds kept the area well ventilated and surface ozone stayed in the low to mid  
2 50s ppb. The BL rose to about 3.5 km AGL in the late afternoon and entrained part of the  
3 persistent ozone layer that had been observed near that altitude for several days. This was  
4 likely the cause for the slight increase in ozone around 1700 PDT. A high-ozone layer ( $\approx$  100  
5 ppb) associated with a stratospheric intrusion on the back side of the departing trough was  
6 observed above 5 km AGL, well above the top of the BL.

7  
8 Friday, June 2

9 TOPAZ data were recorded from 7:02 - 23:10 PDT. First day of a long warming trend (36.5°C  
10 max) with high pressure building from the west. Light winds throughout the day. Isolated Cu  
11 clouds over the nearby mountain ranges, otherwise clear. The mixed layer was suppressed by a  
12 strong 1.2 m deep inversion during the morning, but eventually reached about 3 km around  
13 1500 PDT. The growing ML entrained the RL around noon, and entrained the lowest (3-3.5 km  
14 agl) of two elevated ozone layers from yesterday's intrusion around 1500 PDT. The aerosol  
15 measurements suggest that some of the higher layer may also have been mixed with Asian  
16 pollution or fire plumes. A pronounced tongue of ozone subsided after the ML collapsed and  
17 nearly reached the surface in the late evening. Surface ozone hovered around 70 ppbv at NLVA  
18 throughout the afternoon and reached a maximum of nearly 80 ppbv at Angel Peak around  
19 1900 PDT. The Walter Johnson monitor reached an hourly maximum of 74 ppbv and an MDA8  
20 of 68 ppbv.

21  
22 Saturday, June 3

23 TOPAZ data were recorded from 9:47 - 19:55 PDT. Very hot with an official max of 102 F at the  
24 NLVA NWS station (42C or 107 F at TOPAZ). Very light southeasterly winds throughout the day  
25 with broken cirrus and persistent contrails aloft. Mixing was initially suppressed by another  
26 surface inversion, but surface ozone rose rapidly when the RL was entrained between 1200 and  
27 1300 PDT. The monitor in TOPAZ peaked around 80 ppbv at this time, and the hourly mean  
28 surface concentration at the Walter Johnson (WJ) monitor hit 78 ppbv. The MDA8 at WJ  
29 reached 70.5 ppbv and thus did not quite exceed the standard. The winds at AP remained  
30 southerly throughout the day and the mobile van did not see the high ozone measured over the  
31 LVV. The ML at NLVA eventually reached 4 to 5 km deep in the afternoon, first entraining  
32 cleaner air from between 2 and 4 km agl, and then a thin high ozone (and aerosol) layer of  
33 possible Asian origin present around 4.5 km agl, and finally very clean air from above 5 km agl  
34 in the late afternoon.

35  
36 Sunday, June 4

37 TOPAZ data were recorded from 9:38 - 22:18 PDT. Very hot again with an official max of 102°F  
38 at the NLVA NWS station. Clear skies with a few scattered Cu over the mountains. Very light  
39 northwesterly winds in the early morning that shifted abruptly to strong (15 m/s mean)  
40 southwesterly winds associated with a trough moving into the PNW after 1030 PDT. Surface  
41 ozone at the NLVA rose quickly to about 65 ppbv before the wind shift, then fell to less than 50  
42 ppbv, after which it slowly ramped back up to 65 ppbv. The strong wind kept a constant dust  
43 layer in motion near the surface, and contributed to very deep mixing to more than 4 km. The  
44 ozone concentrations were 50-60 ppbv up to about 4 km agl in the morning, with less than 40

1 ppbv between 4.5 and 5.5 km agl. A high ozone layer corresponding to a dry air streamer in the  
2 GOES WV imagery became prominent around 4 km asl at 1400 PDT, and was slowly nibbled  
3 from below by the deep mixed layer. A second layer with more than 100 ppbv of ozone (and  
4 more aerosol) descended and merged with the first layer around 1900 PDT. Both the surface  
5 winds and ozone subsided briefly between 1900 and 2000 PDT, but then shifted to the west  
6 and increased again. The turbulent mixing aloft continued until after 2100 PDT.

7  
8 Monday, June 5

9 TOPAZ data were recorded from 9:46 - 18:10 PDT. Hot once again with a max of 101°F at the  
10 NLVA (VGT) NWS station. Clear skies with a few scattered Cu over the mountains. Strong  
11 southwesterly winds persisted throughout the night (there was an apparent sensor malfunction  
12 around 0300 PDT) before calming between 0800 and 1200 PDT. The winds prevented surface  
13 deposition and in situ ozone remained relatively high except for a period of local titration  
14 around 0600 PDT. TOPAZ showed the high ozone associated with the streamers observed  
15 yesterday to still be present. Some of this ozone was mixed down to the surface when the ML  
16 rapidly grew around 1100 PDT, causing a short-lived increase in the surface concentrations to  
17 more than 70 ppbv. High O3/Low CO UT/LS air also descended to Angel Peak around 0300 PDT  
18 and later in the morning. The MLH was limited to 3.2 km by the stable cap of the streamer, and  
19 the deep SW flow (from the surface to the stratosphere) advected relatively clean air (50-55  
20 ppbv) to Las Vegas beneath the streamer. This air offset any ozone increase caused by  
21 entrainment of the overlying streamer, and the in-situ concentrations at NLVA dropped to 55  
22 ppbv when the 10-15 m/s SW winds resumed at noon, and remained below 65 ppbv for the rest  
23 of the day.

24  
25 Tuesday, June 6

26 TOPAZ data were recorded from 9:49 - 20:21 PDT. Another hot day with a max of 103°F at the  
27 nearby NLVA (VGT) NWS station. Clear skies in the morning followed by widely dispersed  
28 contrail cirrus. The surface winds calmed during the night and ozone decreased to a locally  
29 titrated minimum between 5 and 10 ppbv between 0600 and 0700 PDT. The southwesterly  
30 winds gradually increased during the late morning with a mean speed of 12 m/s during the  
31 afternoon. TOPAZ showed the Pacific streamer to still be above Las Vegas between 3.5 and 4  
32 km. The streamer was lifted up and disrupted by the mixed layer, which reached a height of  
33 about 3.5 km during the afternoon, but recovered most of its ozone density as the ML subsided  
34 in the early evening. A substantial amount of ozone was entrained into the ML, but not enough  
35 to raise the surface concentrations above 70 ppbv.

36  
37 Wednesday, June 7

38 TOPAZ data were recorded from 9:52 - 22:24 PDT. Another hot day with a max of 101°F at the  
39 nearby (500 m) NLVA (VGT) NWS station. Hazy with widely dispersed contrail cirrus all day. The  
40 winds were from the S and SE for most of the day before rotating to the SSW around 1500 PDT.  
41 Winds between 5 and 10 m/s prevented the accumulation of locally produced ozone. A layer of  
42 high ozone was present just above 2 km when the measurements commenced in the morning,  
43 with the bottom of the layer rising to 3.5 km agl by the late afternoon. The concentrations at 3  
44 km agl exceeded 100 ppbv from 1400 to 1600 PDT, when some of the ozone was entrained by

1 the mixed layer, causing the surface concentrations to rapidly increase from 65 to 75 ppbv. The  
2 TOPAZ in situ concentrations remained above 70 ppbv until about 2000 PDT, causing the MDA8  
3 to reach about 68 ppbv. The MDA8 at 5 of the CCDAQ monitors reached 65 ppbv, and the  
4 monitor at Death Valley NP, 150 km WNW of Joe Neal and 120 km W of AP, reached 70 ppbv.  
5 High ozone was also measured at Angel Peak. The measurements there indicate that the  
6 composition of the elevated layer was complex. There was no visible smoke, but the aerosol  
7 backscatter was somewhat enhanced. The O<sub>3</sub> at Angel Peak was sometimes correlated with  
8 NO<sub>y</sub> and CO, but not at other times. It was usually correlated with CH<sub>4</sub>, however. Stratospheric  
9 and (AZ?) fire contributions are suspected.

10  
11 Thursday, June 8

12 TOPAZ data were recorded from 9:57 - 22:45 PDT. Slightly cooler today with a max of 99°F at  
13 the NLVA(VGT) NWS station. There were thick high clouds and winds ahead of the advancing  
14 trough. Surface ozone remained above 60 ppbv from 0900 to 2100 PDT. Surface ozone  
15 concentrations at AP exceeded 70 ppbv for much of the day with different degrees of  
16 correlation with CO and other tracers. The surface winds were from the S to SSW at 10-15 m/s  
17 throughout this period (the CCDAQ wind profiler showed similar winds to at least 3 km agl).  
18 This implies that most of the ozone was advected into the LVV, but photochemical production  
19 and accumulation was also depressed in the SoCAB. TOPAZ once again showed a high (80-90  
20 ppbv) ozone layer between 3 and 4 km agl with relatively high concentrations (65-75 ppbv)  
21 between this layer and the surface. The microDop showed the ML reached about 2500 m agl.  
22 Rapids periods of deep mixing around 1200 and 1900 PDT increased the surface concentrations  
23 by 5 to 10 ppbv. Similar increases were mirrored by the Apex CCDAQ monitor and several other  
24 CCDAQ monitors peaked during the evening episode. The MDA8 at most of the CCDAQ  
25 monitors reached at least 60 ppbv. As was the case yesterday, a combination of aged UT/LS air  
26 and other sources is suspected

27  
28 Friday, June 9

29 TOPAZ data were recorded from 9:50 - 18:54 PDT. Cooler today with a max of 95°F at the NLVA  
30 (VGT) NWS station. Mostly clear with widely dispersed contrails. Strong SW to SSW winds  
31 greater than 20 m/s with gusts exceeding 25 m/s swept away locally produced O<sub>3</sub> and created a  
32 wind-driven dust cloud over the Strip. The surface O<sub>3</sub> concentrations were about 40 ppbv in the  
33 morning, and the remnants of the Pacific streamer were present when TOPAZ measurements  
34 commenced at 10 PDT. The first lidar measurements showed more than 100 ppbv of O<sub>3</sub>  
35 between 2.5 and 3 km agl, but the streamer was highly fragmented with much lower  
36 concentrations during most of the day. A modest amount of entrainment and mixing occurred  
37 after 1300 PDT, but the surface concentrations remained below 55 ppbv, and only one of the  
38 CCDAQ monitors (Mesquite) reached 60 ppbv for the MDA8. As noted before, a combination of  
39 aged UT/LS air and transported biomass burning or pollution sources is suspected. Despite the  
40 location of the streamer near the elevation of Angel Peak, only traces of UT/LS air were  
41 detected there.

42  
43 Saturday, June 10

44 TOPAZ data were recorded from 08:32 to 21:36 PDT. Cooldown prior to the arrival of the deep

1 trough continued with a max temperature of 32 C. After a clear morning, a thick Cirrus cloud  
2 deck moved in from the SW around midday and cleared out of the area after sunset. Strong SW  
3 to SSW winds from 15 to 20 m/s with higher gusts swept away locally produced O3. The Pacific  
4 streamer, with ozone concentrations exceeding 100 ppb at times, reappeared at 10 PDT and  
5 persisted into the evening. Compared to the previous days, the streamer descended to lower  
6 altitudes (1.5 - 3 km AGL) but stayed mostly above the mixed layer with only minimal  
7 entrainment in the late afternoon and evening, which caused a slight increase in surface ozone  
8 concentrations. The high-ozone streamer was also sampled by the ozonesondes launched at  
9 Joe Neal at 9 and 12 PDT, the Mooney aircraft, and the mobile van at Angel Peak. The air above  
10 the streamer up to about 5 km AGL was very clean with ozone concentrations around 30 ppb  
11 and very little aerosol. The Cirrus clouds above 7 km AGL caused a few artifacts in the TOPAZ  
12 ozone and aerosol data between 16 and 20 PDT.

13

14 Sunday, June 11

15 TOPAZ data were recorded from 8:03 PDT through the night until 7:39 PDT on June 12 (data  
16 collection was continued the next day without interruption). Cooldown prior to the arrival of  
17 the deep trough continued with a max temperature around 30 C. Clear throughout the day.  
18 Strong S to SW winds from 15 to 25 m/s with higher gusts swept away any locally produced O3.  
19 Several layers of high ozone aloft were observed, including a tongue of very high ozone (peak  
20 values around 280 ppb near 5.5 km AGL) associated with a strong stratospheric intrusion as the  
21 trough axis passed over Las Vegas in the early morning hours on June 12. The high ozone did  
22 not get transported down to the surface, except in the afternoon on June 11 when entrainment  
23 by the mixed layer pushed surface ozone up to about 70 ppb.

24

25 Monday, June 12

26 TOPAZ data were recorded from 7:44 PDT through the night until 6:32 PDT on June 13 (data  
27 collection was continued the next day without interruption). Cool temperatures (max. of 29°C)  
28 and clear conditions. Decreasing winds in the morning and then light winds veering from SW to  
29 NW during the remainder of the day in the wake of the departing trough. Very high ozone was  
30 observed above 5 km AGL (max. ozone values near 280 ppb in the morning with several ozone  
31 filaments descending to about 3 km AGL. The ML was not deep enough to entrain any of this  
32 ozone. Surface ozone stayed below 50 ppb in the cool post-frontal conditions.

33

34 Tuesday, June 13

35 TOPAZ data were recorded from 6:44 - 21:00 PDT. These measurements were a continuation of  
36 the long-time series that started at 0800 PDT on June 11. Warming temperatures (max. of 34  
37 C), clear conditions, and light to moderate winds from the NW. Highly structured ozone aloft  
38 with multiple thin layers associated with yesterday's intrusion. High ozone descended to below  
39 3 km agl around midday, but the the mixed layer only reached about 2200 m agl and was too  
40 shallow to entrain much of it. The surface concentrations reached about 65 ppbv during the  
41 afternoon with similar concentrations at the CC monitors.

42

43 Wednesday, June 14

44 TOPAZ data were recorded from 10:46 - 21:02 PDT. Warm temperatures (max. of 39°C), clear

1 conditions, and light winds that followed the diurnal flow pattern. The mixed layer only reached  
2 about 1800 m agl. It entrained a thin ozone layer aloft containing moderate ozone  
3 concentrations ( $\approx 75$  ppb) in the early afternoon and then slowly declined in depth through the  
4 afternoon. The warm temperatures, light winds, and the shallow boundary layer caused a  
5 buildup of ozone that reached 83 ppb at the surface in the late afternoon. MDA8 ozone  
6 reached 74 ppb.

7 Thursday, June 15

8 TOPAZ data were recorded from 09:19 - 19:51 PDT. Hot (max. of  $41^{\circ}\text{C}$ ), clear conditions, except  
9 some high clouds to the north in the evening. Light winds that followed the diurnal flow pattern  
10 thru mid-afternoon, then a wind shift to the S and then W with wind speeds increasing to  $\approx 8$   
11 m/s. The mixed layer was very shallow until midday and then grew quite rapidly to a depth of  
12 2800 m agl. Surface and boundary layer ozone increased to almost 80 ppb around 14:00 PDT,  
13 dropped down to around 60 ppb in the middle of the afternoon, and then increased again at  
14 16:30 to around 70 ppb, before dropping below 60 ppb at sunset.

15 Friday, June 16

16 TOPAZ data were recorded from 09:05 - 20:33 PDT. Very hot (max. of  $43^{\circ}\text{C}$ ), clear conditions,  
17 and light winds that followed the diurnal flow pattern. The mixed layer gradually grew to 3300  
18 m agl. It entrained a thin ozone layer aloft containing moderate ozone concentrations ( $\approx 70$  ppb)  
19 in the early afternoon. The hot temperatures and light winds caused a buildup of ozone that  
20 reached 87 ppb at the surface in the afternoon. MDA8 ozone reached 76 ppb.

21 Saturday, June 17

22 TOPAZ data were recorded from 08:56 - 18:48 PDT. Very hot (max. of  $44^{\circ}\text{C}$ ). Clear conditions,  
23 except for a few Cirrus clouds to the north in the afternoon. Generally light winds that followed  
24 the diurnal flow pattern. Wind speeds increased to 5 - 10 m/s in the afternoon and early  
25 evening. The mixed layer stayed shallow through 1200 PDT and then grew to about 3000 m agl  
26 by 1500 PDT. Surface ozone quickly increased to 95 ppb by midday. The growing mixed layer  
27 entrained cleaner air from aloft, which caused surface ozone to drop in a series of steps down  
28 to the mid 60s ppb by 1600 PDT. Despite this afternoon decrease, MDA8 ozone at three  
29 monitoring sites in the Las Vegas Valley exceeded the 70 ppbv standard.

30 Sunday, June 18

31 TOPAZ data were recorded from 09:31 - 19:07 PDT. Extremely hot (max. of  $46^{\circ}\text{C}$  at the lidar  
32 site). Shallow Cumulus over the nearby mountain ranges in the afternoon. Light winds that  
33 followed the diurnal flow pattern. Overnight, clean marine air had been advected into southern  
34 Nevada, which decreased ozone concentrations to below 40 ppb in the lower troposphere.  
35 TOPAZ observed a layer with moderate aerosol concentrations and 45-50 ppb ozone between 3  
36 and 5 km AGL. Local production caused a late increase of surface ozone, which peaked at 53  
37 ppb around 1800 PDT.

38

39 Monday, June 19

40 TOPAZ data were recorded from 09:23 - 18:43 PDT. Extremely hot (max. of  $47^{\circ}\text{C}$  at the lidar

1 site). Generally light winds that followed the diurnal flow pattern. Cumulus clouds and isolated  
2 t-storms over the nearby mountain ranges. A few clouds drifted over the Las Vegas Valley in the  
3 late afternoon. The clean marine air from the previous day with lower tropospheric ozone  
4 concentrations of less than 40 ppb was still in place. TOPAZ observed a layer with moderate to  
5 high aerosol concentrations and 55-60 ppb ozone above 4 km AGL. This layer descended to 2.5  
6 km AGL by late afternoon and was partially entrained into the boundary layer. Back trajectory  
7 calculations suggest that this layer may be associated with fires in Arizona. Surface ozone  
8 peaked at 55 ppb around 1730 PDT.  
9

10 Tuesday, June 20

11 TOPAZ data were recorded from 09:54 - 22:02 PDT. Extremely hot again (max. of 48°C at the  
12 lidar site) with the all-time Las Vegas record of 117 F tied at McCarran Intl Airport. Scattered  
13 fair weather cumulus clouds formed over the nearby mountain ranges with a few drifting over  
14 the Las Vegas Valley in the late afternoon. Very light NW winds in the early morning that  
15 rotated CCW to the east between 0900 and 1500 PDT. Surface ozone at NLVA increased rapidly  
16 during this time and reaching 84 ppb around 1300 PDT; the 1 h mean at Walter Johnson peaked  
17 at 78 ppbv between 1300 and 1400 PDT. The mixed layer grew explosively to more than 5 km  
18 deep around 1500 PDT and the surface winds abruptly increased to nearly 15 m/s, rotating first  
19 to the NW and then to the SW. This caused the surface ozone concentrations to drop to about  
20 65 ppbv where they remained with very little variation into the early evening. The SW winds  
21 blew the ozone towards Apex, which measured the hourly concentrations of 75 to 76 ppbv  
22 during the late afternoon. The initial TOPAZ measurements showed the high aerosol/ozone  
23 layer attributed to the AZ and MEX fires and seen the day before near 3.5 km asl, but with  
24 much high aerosol loadings and 70-80 ppb of ozone. This layer was apparently entrained as the  
25 ML deepened after 1400 PDT, but the resulting dilution, mixing, and venting decreased and  
26 homogenized the concentrations to an average value of around 64 ppbv. The 00 UT (17 PDT)  
27 VEF sounding put the top of the ML at more than 6 km asl (about 5.5 km agl), in good  
28 agreement with the afternoon TOPAZ ozone and aerosol measurements. The ML did not begin  
29 subsiding until after 2200 PDT.  
30

31 Wednesday, June 21

32 TOPAZ data were recorded from 09:20 - 19:20 PDT. Another extremely hot day (max. of 45°C at  
33 the lidar site) and 113 F at the NLVA NWS tower. Very clear with only a few FWC over the  
34 mountains. The elevated smoke layer from AZ and Mexico was visible to the eye and prominent  
35 in the TOPAZ aerosol backscatter between 3 and 5 km agl. There was very little ozone  
36 enhancement in the smoke layer, however, and modest entrainment of the smoke by the  
37 mixed layer, which reached a depth of 'only' about 4 km. The ML subsided around 1700 PDT.  
38 The winds were weak and NW in the early morning, but rotated to the S and increased to 10-15  
39 m/s around 1000 PDT. Surface ozone also increased to about 65 ppbv, but then decreased to  
40 55-60 ppbv as the winds rotated to the SW. TOPAZ measured similar concentrations up to  
41 about 5 km agl. There was no sign of smoke from the Holcomb Fire near San Bernardino.  
42

43 Thursday, June 22

44 TOPAZ data were recorded from 09:10 - 20:06 PDT. Another extremely hot day (max. of 45°C at

1 the lidar site) and 113 F at the NLVA NWS tower. Very clear with only a very few clouds over the  
2 mountains. The winds were light during most of the day, shifting from northwesterly  
3 downslope flow to very weak southerly flow around 0900 PDT. The elevated smoke layer seen  
4 the previous two days was mostly gone, with only two thin and weak aerosol layers (but no  
5 ozone) remaining near 4 and 5 km agl. A thin, but much more concentrated aerosol layer was  
6 present at the surface in the morning. Ozone began to increase early in the lowest 1 km, rising  
7 from about 50 to more than 80 ppbv between 0900 and 1100 PDT. Another layer of enhanced  
8 ozone and aerosol was present between 2.5 and 3 km agl and intensified around 1100 PDT.  
9 Surface O<sub>3</sub>, CO, and CH<sub>4</sub> began increasing at AP around the same time, and HYSPLIT back  
10 trajectories suggest that this layer originated from the Holcomb Fire near Big Bear Lake  
11 although there was no obvious smoke associated with the fire plume. This layer was entrained  
12 by the growing mixed layer between 1300 and 1400 PDT, contributing to the high surface  
13 ozone. The surface and ML column O<sub>3</sub> decreased around 1500 PDT as the growing ML  
14 entrained lower O<sub>3</sub> air from above 3 km agl. A brief shift in the surface winds to the north  
15 caused a short-lived drop in the O<sub>3</sub> and aerosol concentrations below 1 km around 1600 PDT,  
16 but the concentrations recovered and the ML grew to more than 4 km agl. Ozone fell to about  
17 60 ppbv throughout the column after the winds shifted to the west and increased to more than  
18 10 m/s around 1800 PDT. The MDA<sub>8</sub> was greater than 75 ppbv at the TOPAZ truck, and reached  
19 values of 77,73,73, and 70 at the Joe Neal, Palo Verde, Walter Johnson, and Apex monitoring  
20 sites, respectively.

21  
22 Friday, June 23

23 TOPAZ data were recorded from 09:29 - 20:57 PDT. Another extremely hot day (max. of 45°C at  
24 the lidar site) and 112 F at the NLVA NWS tower. Very clear with a few scattered FWC in the  
25 late afternoon. Calm for most of the day with very light (5 m/s) NW winds before 0900 and W  
26 after 1800 PDT. There was no evidence of elevated aerosol or ozone layers from either the aged  
27 AZ and Mexican Fires, or from the Holcomb Fire aloft, and the in situ ozone concentrations  
28 remained below 65 ppbv at Angel Peak. Surface ozone at NLVA was about 40 ppbv at 0900 PDT,  
29 but increased monotonically to a peak of more than 100 ppbv around 1600 PDT. TOPAZ found  
30 similar concentrations throughout the mixed layer, which remained less than 1500 m deep until  
31 after 1400 PDT. The ML then developed a series of short-lived 4 km deep plumes that persisted  
32 until nearly 1900 PDT, and modulated the aerosol and ozone concentrations above the surface.  
33 The ML abruptly collapsed around 1900 PDT, leading to a rapid drop in ozone from the surface  
34 to 2 km agl as the surface winds shifted to the west and increased to 5 m/s. The MDA<sub>8</sub>  
35 calculated from the 1-min running average ozone was greater than 80 ppbv at the TOPAZ truck,  
36 and the MDA<sub>8</sub> reached values of 77,76,78, and 75 at the Joe Neal, Palo Verde, Walter Johnson,  
37 and JD Smith monitoring sites, respectively. Note: The strange ozone and aerosol profiles  
38 around 1300 PDT are spurious.

39  
40 Saturday, June 24

41 TOPAZ data were recorded from 09:45 - 20:13 PDT. Another extremely hot day (max. of 45°C at  
42 the lidar site) and 111 F at the NLVA NWS tower. Mostly clear with scattered high clouds and  
43 some cumulus development to the SW and over the mountains. Calm or very light winds all  
44 day. The elevated aerosol and ozone layer from the AZ and Mexican fires was present once

1 again between 4 and 6 km asl, but was only weakly entrained by the relatively shallow mixed  
2 layer. Ozone production was modest with peak concentrations of 65 ppbv, despite very similar  
3 conditions as yesterday when surface ozone reached 100 ppbv. This Friday-Saturday  
4 combination could be a good candidate for a modeling study.

5  
6 Sunday, June 25

7 TOPAZ data were recorded from 09:36 - 18:56 PDT. Another extremely hot day (max. of 45°C at  
8 the lidar site) and 111 F at the NLVA NWS tower. Scattered high clouds in the morning, followed  
9 by mostly clear skies in the afternoon. Calm or very light winds all day. Very similar to yesterday  
10 with modest ozone production and peak concentrations of about 70 ppbv. The mixed layer  
11 grew to more than 4 km around 1500 PDT, which helped to dilute the ozone concentrations.  
12 This Friday-Saturday-Sunday combination will be a good candidate for a modeling study.

13  
14 Monday, June 26

15 TOPAZ data were recorded from 09:49 - 17:49 PDT. Slightly cooler today (max. of 42°C at the  
16 lidar site) and 108 F at the NLVA NWS tower. Clear skies all day, but a blowing dust cloud to the  
17 south driven by the 10-15 m/s (in the afternoon) SW winds associated with the approaching  
18 trough. Some entrainment of ozone from above 4 km by the mixed layer, but little  
19 accumulation near the surface where the peak mixing ratios remained less than 60 ppbv.

20  
21 Tuesday, June 27

22 TOPAZ data were recorded from 09:17 - 20:13 PDT. Normal temperatures today (max. of 42°C  
23 at the lidar site) and 106 F at the NLVA NWS tower. Clear skies all day, with some suspended  
24 dust in the lowest 500 m during the morning. A thin aerosol layer (with no ozone enhancement)  
25 of possible fire origin was also present around 2 km agl in the morning. The normal morning  
26 NW winds were light, but the afternoon SW winds increased to about 10 m/s. A layer of high  
27 ozone with very low aerosol of probable UT/LS origin was present above 4.5 km agl for much of  
28 the day, but disappeared around 1600 PDT with no obvious entrainment by the ML, which only  
29 reached to about 3.6 km agl. Surface ozone peaked at about 65 ppbv around noon, but  
30 decreased as the ML expanded and the surface winds increased.

31  
32 Wednesday, June 28

33 TOPAZ data were recorded from 09:19 - 22:47 PDT. Normal temperatures today (max. of 42°C  
34 at the lidar site) and 106 F at the NLVA NWS tower. Severe clear skies all day, with haze/smoke  
35 below 2 km that was transported from the SJV during the night. The winds were generally light,  
36 but followed the usual pattern of morning northwesterly winds, weak mid-day southwesterly  
37 winds, and stronger (10 m/s) evening westerlies. The nocturnal low-level transport from the SJV  
38 also led to relatively high ozone at Jean and several other CC sites during the night. A residual  
39 layer containing this transported ozone was entrained by 1000 PDT, increasing the surface  
40 concentrations at NLVA to about 65 ppbv. A narrow layer of predominantly UT/LS origin with  
41 high (100-120 ppbv) ozone, and some aerosol consistent with mixing of pollution or fire plumes  
42 from Asia, descended from 4 km asl at 0920 PDT to 3 km asl at 1400 PDT, when it was entrained  
43 by the ML, which grew to about 3.6 km agl. This helped increase the surface concentrations at  
44 NLVA to a peak of about 80 ppbv. Peak hourly concentrations in excess of 70 ppbv were

1 measured at 8 of the CC regulatory monitors, with the 2015 NAAQS of 70 ppbv exceeded at Joe  
2 Neal (74 ppbv) and Apex (71 ppbv).

3  
4 Thursday, June 29

5 TOPAZ data were recorded from 09:21 - 20:41 PDT. High-normal temperatures today (max. of  
6 42°C at the lidar site) and 106 F at the NLVA NWS tower. Clear skies all day. The winds followed  
7 the usual pattern of morning northwesterly winds, and weak mid-day southwesterly winds, but  
8 with 10-15 m/s ESE winds in the late afternoon and evening. Thick haze/smoke near the surface  
9 in the morning. HYSPLIT suggests this haze may have come from fires in northwestern Nevada  
10 or Northern California. Possible smoke from Arizona or the Brian Head fire in Utah after ESE  
11 winds of 10-15 m/s kicked up at 1800 PDT. The elevated UT/LS layer advected from the Pacific  
12 Ocean was still present above 4 km asl, but was thicker and more diffuse with 80-90 ppbv of  
13 ozone. A probable Asian pollution layer with lower ozone, but higher aerosol lay just beneath it.  
14 This lower layer was mostly entrained and the upper layer partially entrained by the mixed  
15 layer, which grew to about 3.2 km. The surface concentrations at NLVA peaked at 75-80 ppbv,  
16 and the nearby Joe Neal monitor recorded peak hourly concentrations of 77 and MDA8 of 70  
17 ppbv.

18  
19 Friday, June 30

20 TOPAZ data were recorded from 09:07 - 20:31 PDT. The final day of FAST-LVOS measurements.  
21 High-normal temperatures again today (max. of 42°C at the lidar site) and 106 F at the NLVA  
22 NWS tower. Clear skies all day. The winds followed the usual pattern of morning northwesterly  
23 winds, and weak mid-day southwesterly winds, but were very light all day, allowing ozone to  
24 accumulate near the surface. Thick haze/smoke near the surface in the morning once again. As  
25 before, HYSPLIT suggests this haze may have come from fires in northwestern Nevada or  
26 Northern California. The elevated UT/LS layer advected from the Pacific Ocean was still present  
27 above 5 km asl in the morning, but was thicker and more diffuse with 80-90 ppbv of ozone.  
28 Another UT/LS layer with higher concentrations lay above it and a diffuse Asian pollution layer  
29 with lower ozone, but higher aerosol still lay beneath it. This lower layer was mostly entrained  
30 by the ML, which grew to about 3 km. The surface concentrations at NLVA peaked at 90 ppbv,  
31 and the CCDAQ monitors at Joe Neal, Walter Johnson, and Palo Verde recorded MDA8  
32 concentrations in excess of 70 ppbv.

## 1 **Appendix C: Angel Peak Summary Plots**

2  
3 This first section of this Appendix shows time series and scatter plots of the O<sub>3</sub>, CO, CH<sub>4</sub>, H<sub>2</sub>O,  
4 NO<sub>y</sub>, N<sub>2</sub>O, wind speed and direction measurements from the mobile laboratory on Angel Peak  
5 on or before high O<sub>3</sub> days in Clark County. The second section shows weekly summary plots.  
6

7 The complete mobile laboratory data set is available at:

8 [https://esrl.noaa.gov/csd/groups/csd7/measurements/csd\\_mobilelab/MobileLabLVOS/DataDo](https://esrl.noaa.gov/csd/groups/csd7/measurements/csd_mobilelab/MobileLabLVOS/DataDownload/)  
9 [wnload/](https://esrl.noaa.gov/csd/groups/csd7/measurements/csd_mobilelab/MobileLabLVOS/DataDownload/)

### 15 **1. Angel Peak measurements on high ozone days**

16  
17 **Table 7-1** shows the 2015 NAAQS of 70 ppbv was equaled or exceeded by one or more of the  
18 Clark County regulatory monitors on 10 of the 45 FAST-LVOS measurement days: May 23, June  
19 3, June 14, June 16-17, June 22-23, and June 28-30. The 2B O<sub>3</sub> measurements from the TOPAZ  
20 truck at the NLVA also exceeded the NAAQS on all 10 of these days, and the CRDS  
21 measurements from the NOAA/ESRL mobile laboratory on Angel Peak exceeded the NAAQS on  
22 June 14, 16, 29, and 30. The correlation among the AP measurements during these high O<sub>3</sub>  
23 episodes provides some insight into the origin of the high O<sub>3</sub>.  
24

25 The first figure in each section shows the MDA8 ozone distribution on the high O<sub>3</sub> day(s). The  
26 monitors are colorized using the U.S. EPA AQI scale. The NOAA monitors at Angel Peak and the  
27 NLVA are represented by triangles.  
28

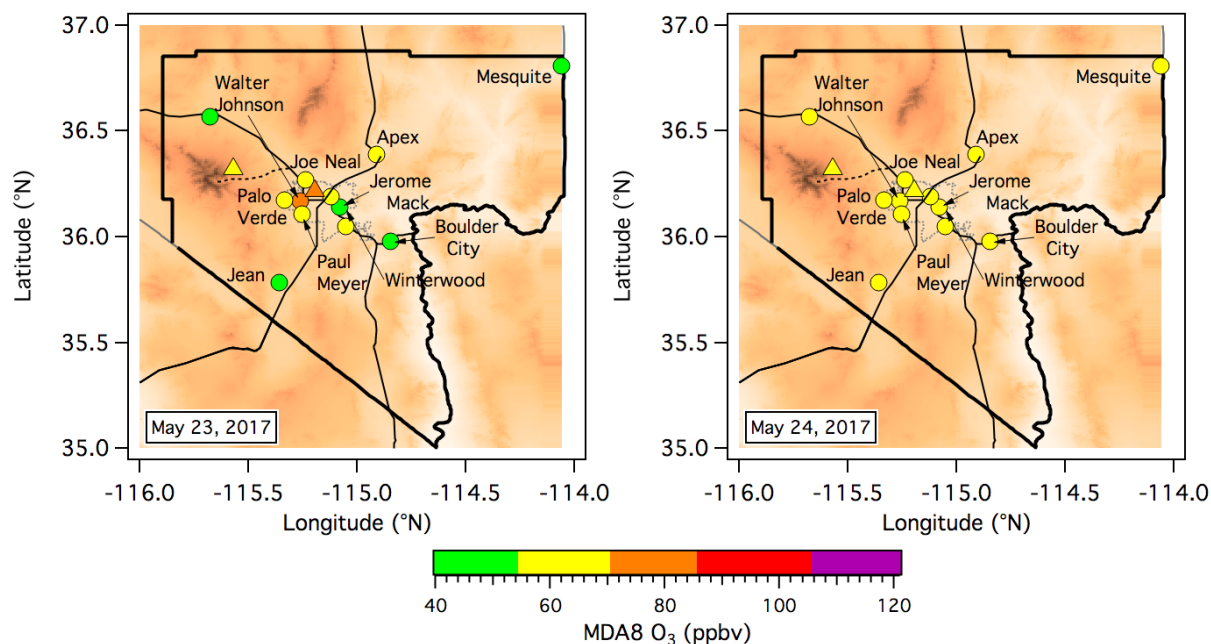
29 The second set of figures shows a 2 or 3-day time series plot(s) of the mobile laboratory in-situ  
30 measurements of (a) O<sub>3</sub> and CO, (b) CO<sub>2</sub> and CH<sub>4</sub>, (c) NO<sub>y</sub> and N<sub>2</sub>O, (d) T and RH, and (e) wind  
31 speed and direction from Angel Peak. The horizontal dashed and dotted lines in the O<sub>3</sub> plots  
32 correspond to 60 and 70 ppbv, respectively. The O<sub>3</sub> measurements made between 1200 and  
33 2300 PDT are highlighted by filled circles.  
34

35 The third set of figures shows scatter plots of the Angel Peak (a) zonal and meridional winds, (b)  
36 O<sub>3</sub>-CO, (c) O<sub>3</sub>-CH<sub>4</sub>, (d) O<sub>3</sub>-N<sub>2</sub>O, (e) O<sub>3</sub>-NO<sub>2</sub>, and (f) O<sub>3</sub>-NO<sub>y</sub>. The O<sub>3</sub>-CO<sub>2</sub> relationship is  
37 complicated by the drawdown of CO<sub>2</sub> by local vegetation and are not shown. The gray points  
38 show all of the FAST-LVOS measurements, and the points colorized by the H<sub>2</sub>O concentrations  
39 correspond to the 1200-2300 PDT measurements highlighted in the O<sub>3</sub> time series plots.

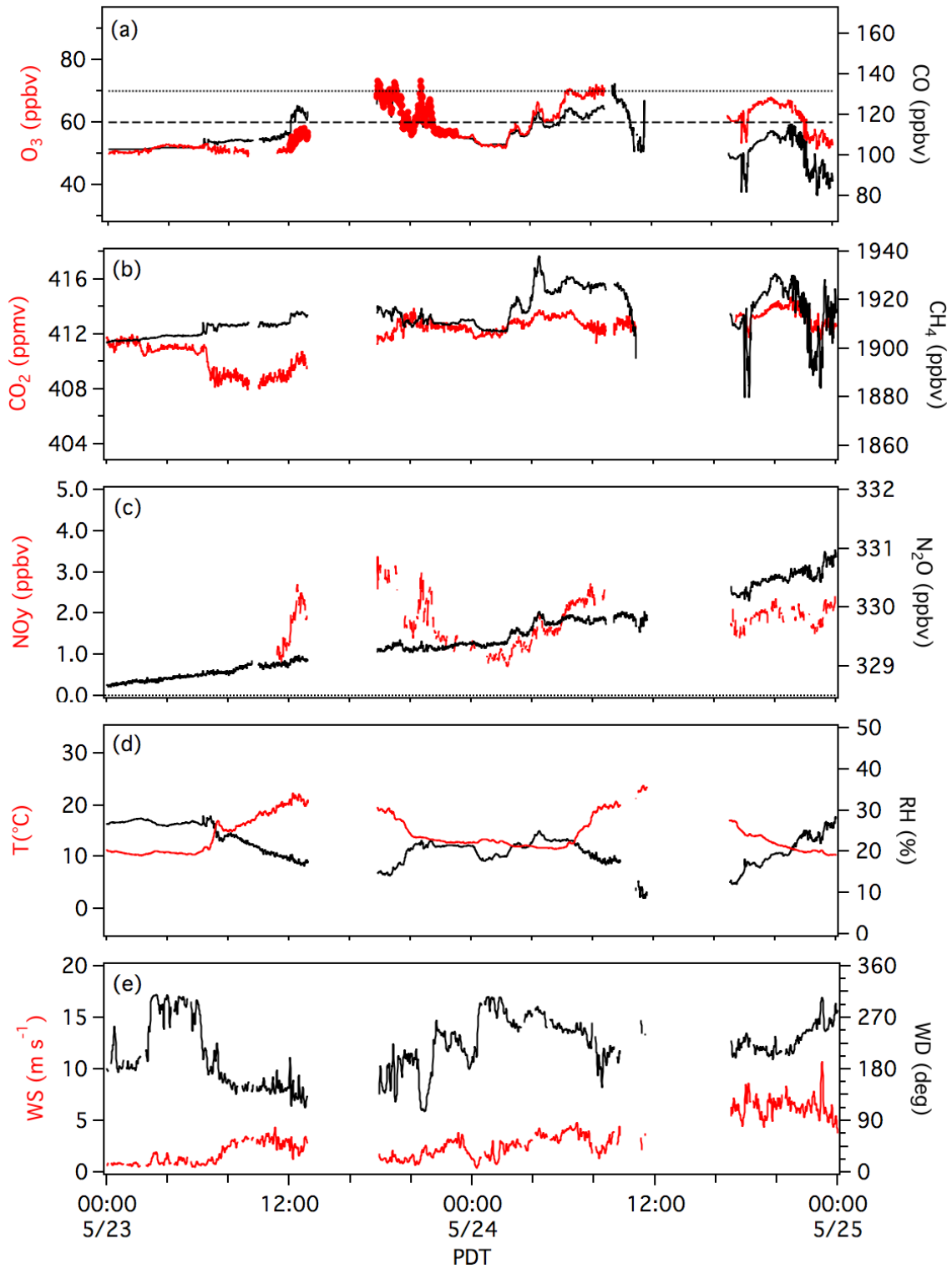
1  
2 **May 23-24**  
3

4 The first ozone NAAQS exceedance in Clark County during 2017 occurred on May 23 when the  
5 Walter Johnson monitor (C71) recorded an MDA8 concentration of 71 ppbv. MDA8 O<sub>3</sub> of 65  
6 ppbv or more was also measured at 3 other nearby monitors: Joe Neal, Palo Verde, and Paul  
7 Meyer. The TOPAZ monitor at the NLVA recorded an MDA8 of 72 ppbv. **Figure C-1** shows that  
8 the high O<sub>3</sub> on the 23<sup>rd</sup> was confined to the northwest Las Vegas area. Ozone was moderate  
9 (60-65 ppbv) at all of the LVV monitors on the 24<sup>th</sup>.

10  
11 The NOAA mobile laboratory spent the early afternoon driving between Angel Peak and the  
12 LVV, but measured an 8-h average of 64 ppbv after it returned to Angel Peak around 1745 PDT  
13 (**Figure C-2**). The TOPAZ measurements showed a layer of high O<sub>3</sub> above 5 km asl on both days,  
14 but this O<sub>3</sub> remained well above the elevation (2.7 km asl) of Angel Peak. The mobile lab  
15 measurements show that the high O<sub>3</sub> measured there on the 23<sup>rd</sup> was transported up to the  
16 summit from the LVV by moist southeasterly upslope flow and strongly correlated with CO, CH<sub>4</sub>,  
17 and NO<sub>y</sub> (**Figure C-3**).  
18  
19  
20

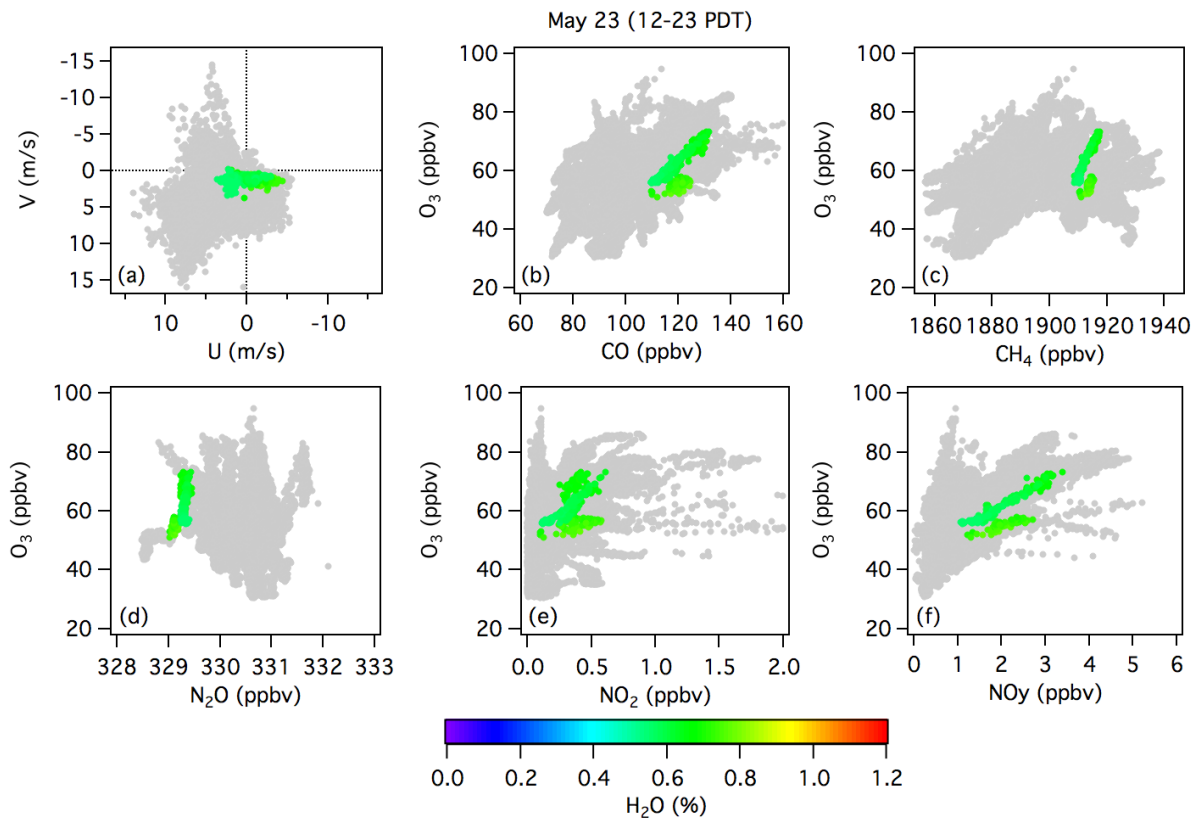


21  
22  
23 **Figure C-1.** Topographic maps of Clark County showing the May 23-24 MDA8 O<sub>3</sub> distributions.  
24  
25



1  
 2 **Figure C-2.** Time series of the Angel Peak mobile laboratory measurements on May 23-24.  
 3

1  
2



3  
4  
5  
6  
7  
8

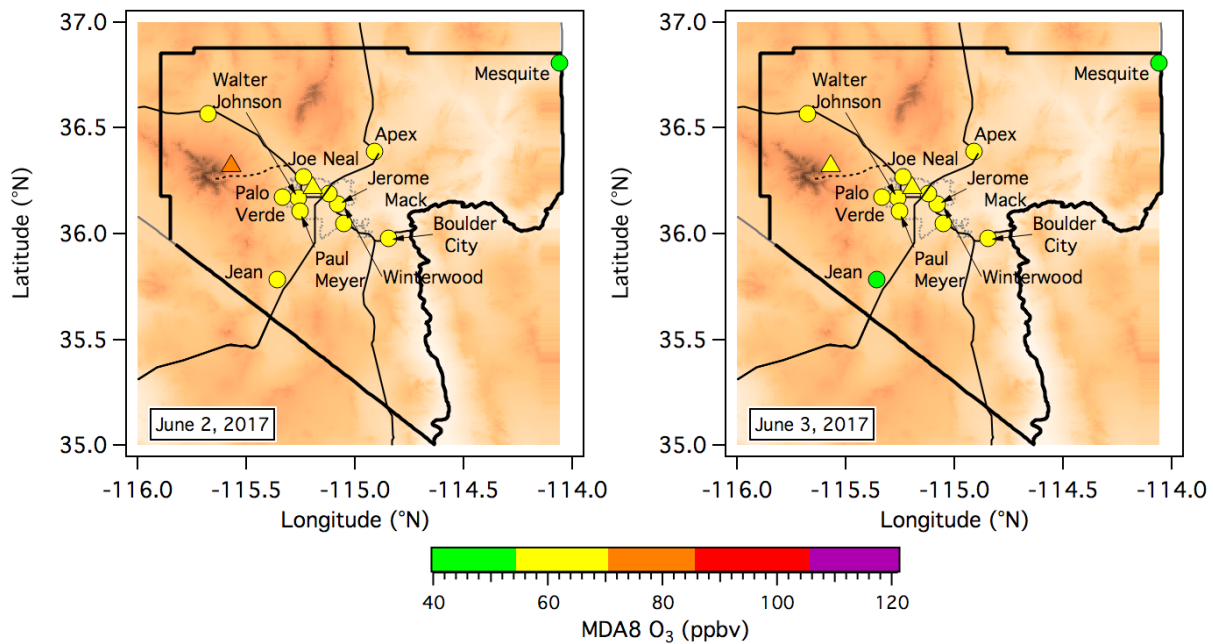
**Figure C-3.** Scatter plots showing the relationships between O<sub>3</sub> and the other parameters measured by the mobile laboratory on May 23.

1 **June 2-3**

2  
3 Moderate to high O<sub>3</sub> was measured by most of the CCDAQ monitors on June 2-3 with MDA8 O<sub>3</sub>  
4 concentrations in excess of 65 ppbv recorded by 3 monitors on June 2, and by 5 monitors on  
5 June 3 (**Figure C-4**). The highest O<sub>3</sub> was measured by the Joe Neal and Walter Johnson  
6 monitors, which reported 69 and 70 ppbv, respectively, on June 3. The NOAA monitors at the  
7 NLVA and AP recorded 67 and 71 ppbv, respectively, on June 2, and 70 and 60 ppbv on June 3.  
8

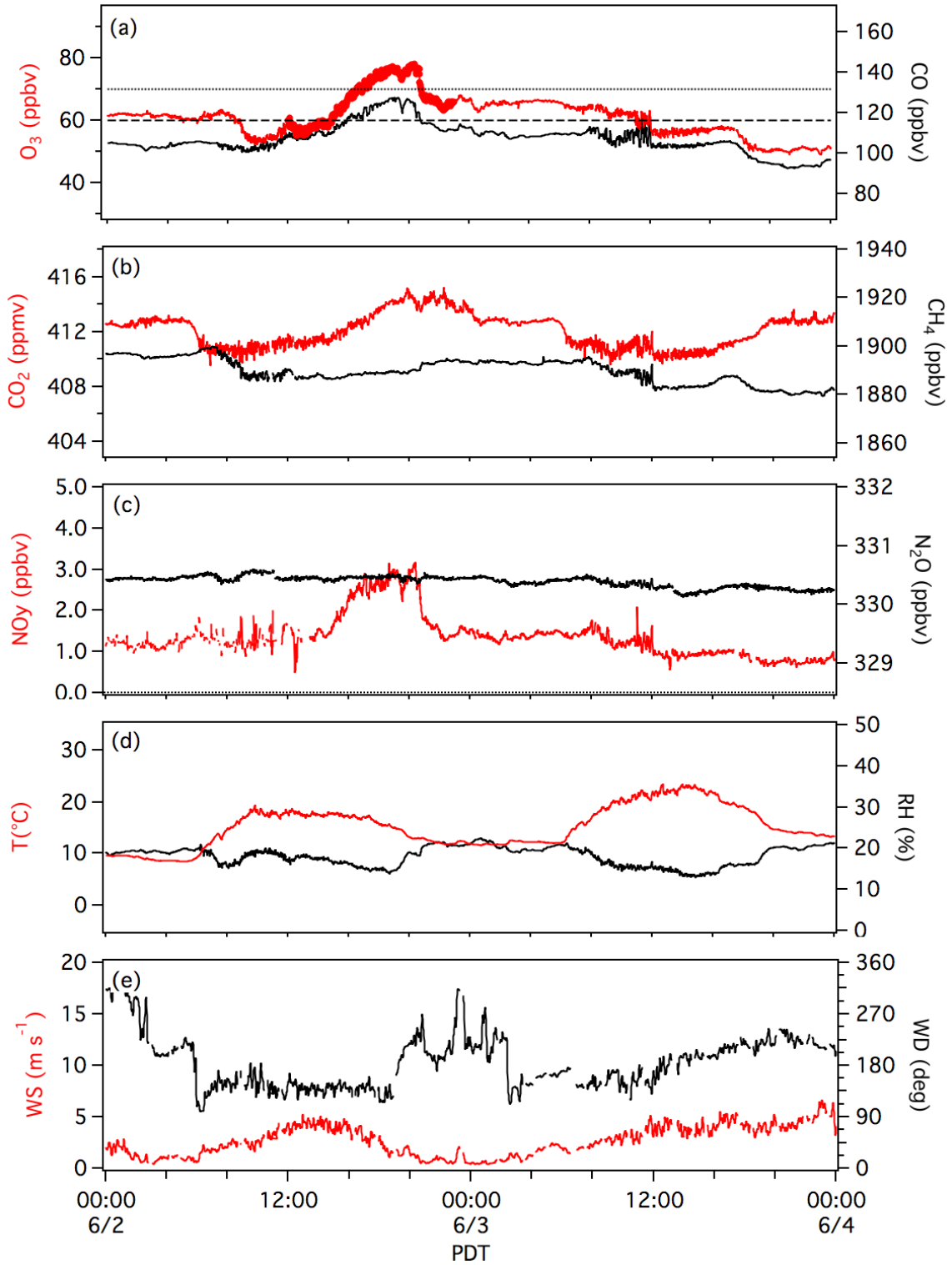
9 **Figure C-7a** shows that the high O<sub>3</sub> on June 2 was measured during the afternoon when  
10 relatively moist air was transported to AP from the LVV by southeasterly upslope winds. The  
11 high O<sub>3</sub> was positively correlated with CO and NO<sub>y</sub>, but not with CH<sub>4</sub> or N<sub>2</sub>O. This suggests that  
12 pollution from the LVV was the primary source of the high O<sub>3</sub> at Angel Peak on June 2.  
13

14 The MDA8 O<sub>3</sub> at AP was much lower (60 ppbv) on June 3, and the time series plots show that  
15 the O<sub>3</sub> concentrations at AP dropped from a high of 64 at 0700 PDT to 53 ppbv at 1900 PDT as  
16 the winds rotated from S to SSW. Ozone remained correlated with CO, however, suggesting  
17 that these measurements reflected regional photochemistry.  
18  
19



20 **Figure C-4.** Topographic maps of Clark County showing the June 2-3 MDA8 O<sub>3</sub> distributions.  
21  
22  
23

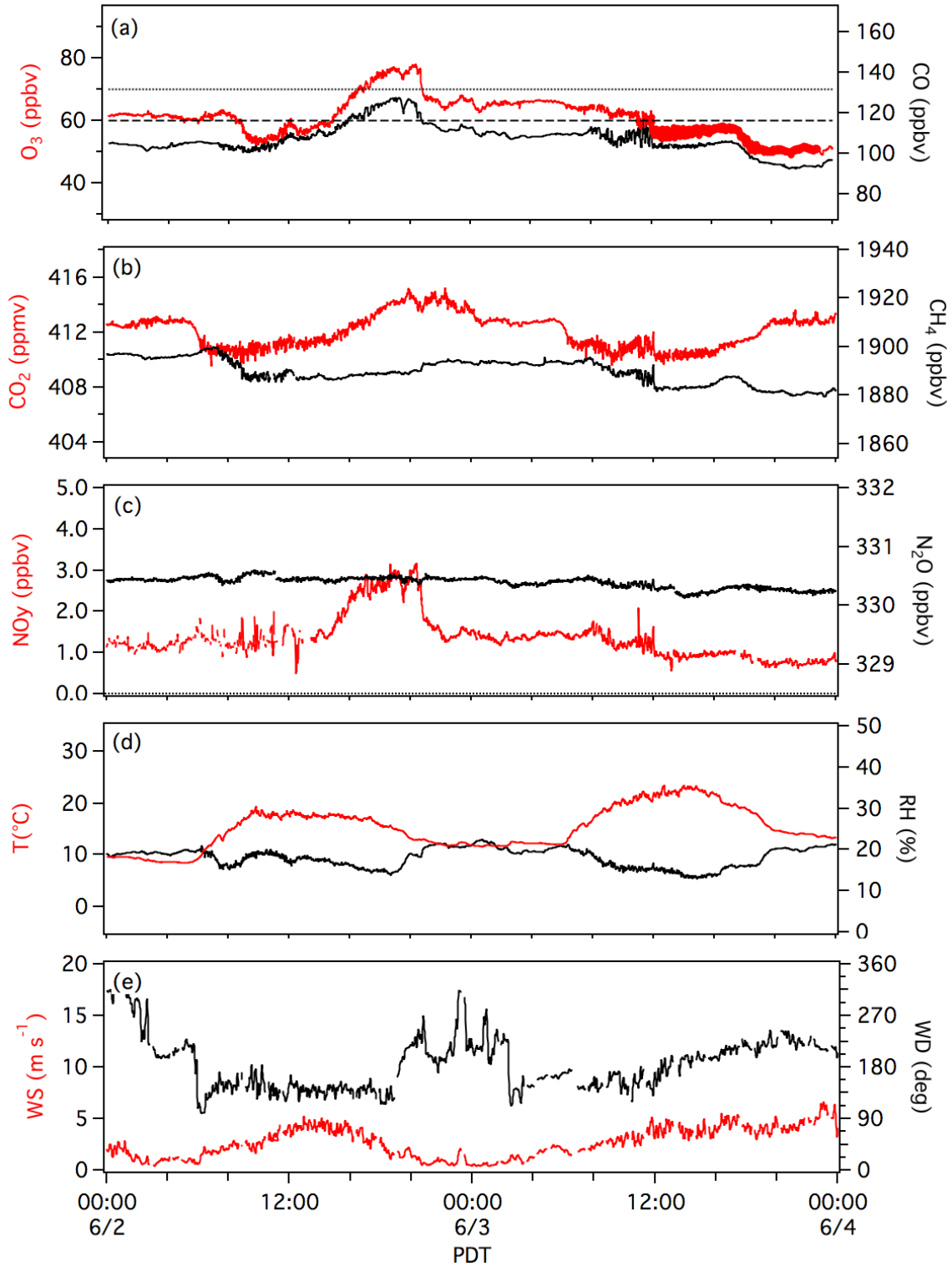
1  
2



3  
4  
5

**Figure C-5.** Time series of the Angel Peak mobile laboratory measurements on June 2.

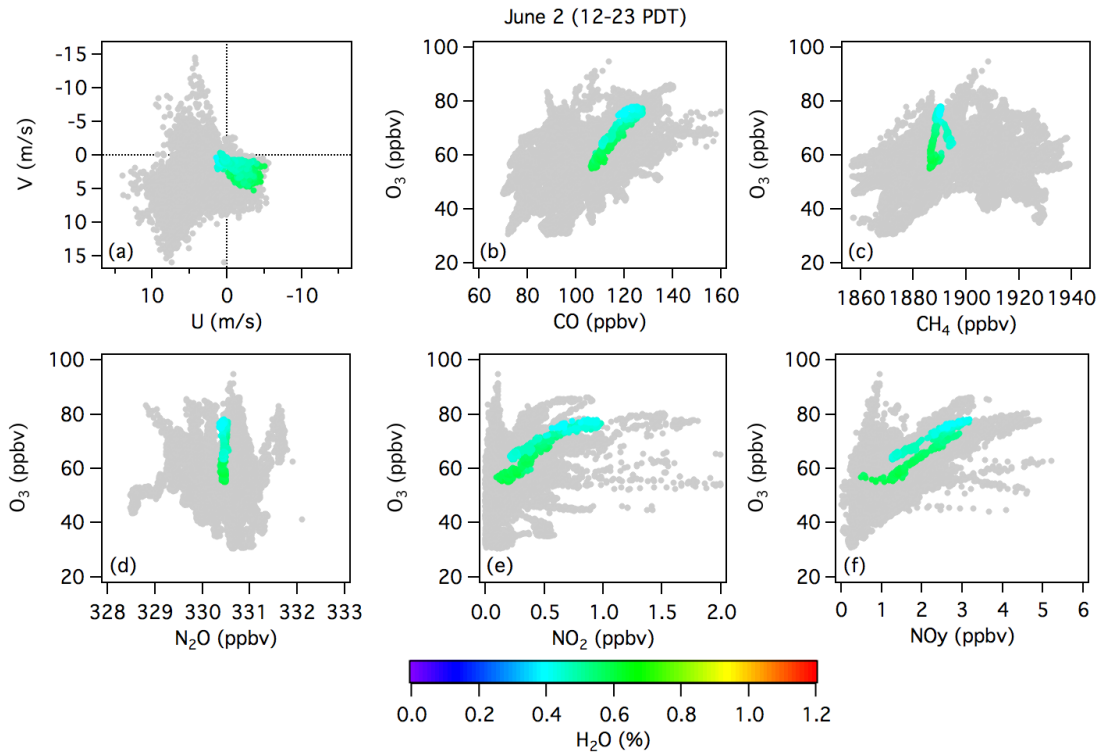
1  
2



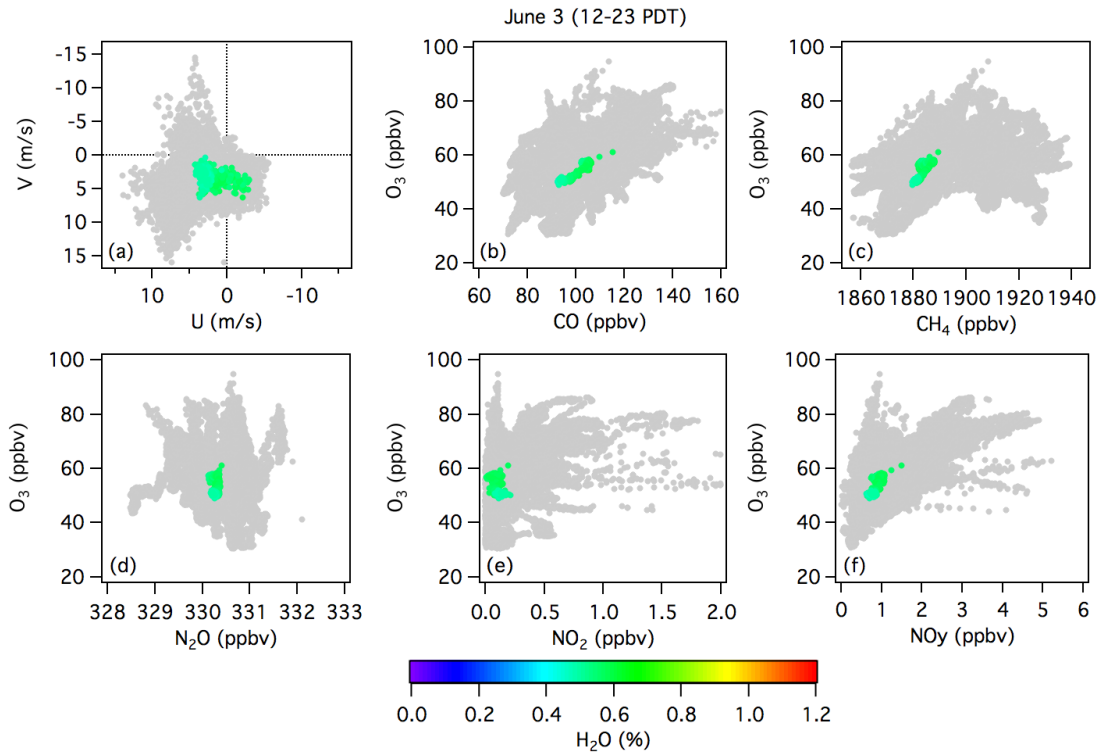
3  
4  
5

Figure C-6. Time series of the Angel Peak mobile laboratory measurements on June 3.

1



2



3

4

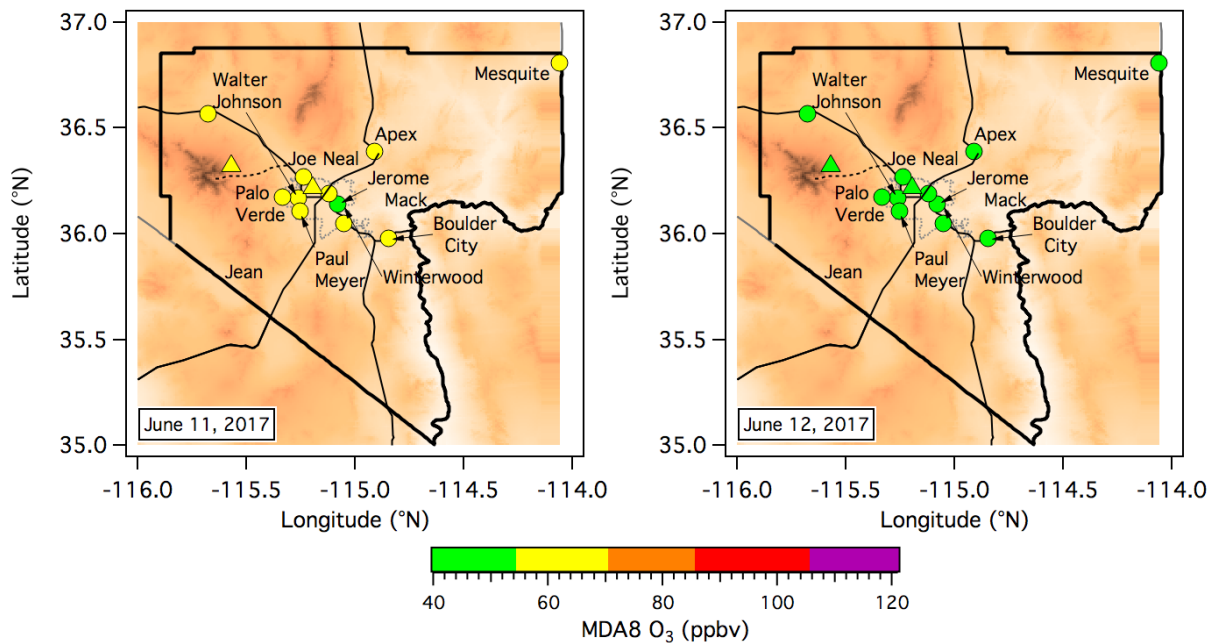
5 **Figure C-7.** Scatter plots showing the relationships between  $O_3$  and the other parameters

6 measured by the mobile laboratory on June 2 and 3.

1  
2 **June 11-12**  
3

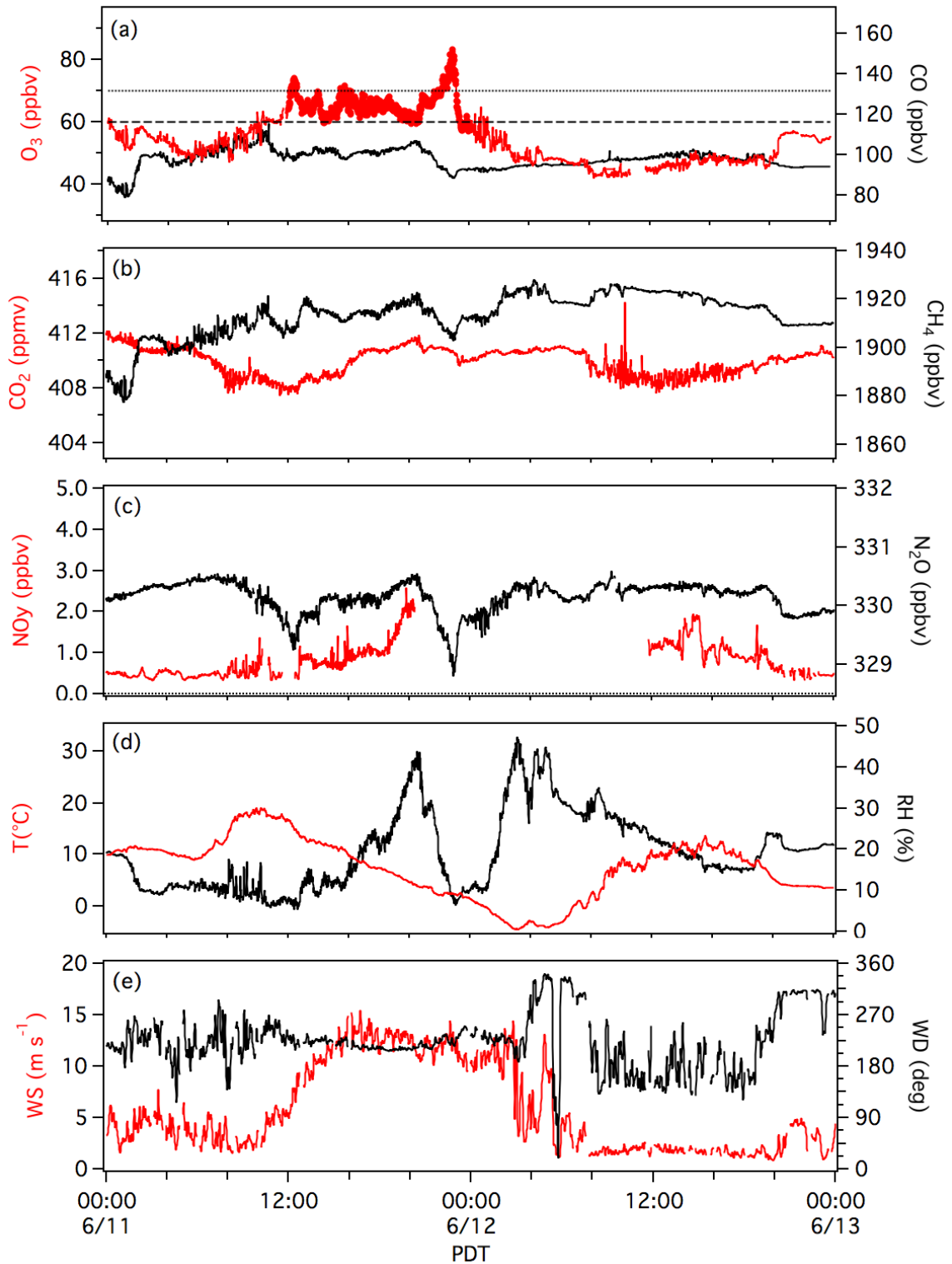
4 The cold front associated with the deep upper level low that passed through the SWUS on June  
5 10-12 brought cool temperatures to Clark County and the temperature on Angel Peak fell below  
6 freezing on the night of June 11-12. Ozone also decreased across the LVV as O<sub>3</sub>-poor mid-  
7 tropospheric air was advected inland from the Pacific Ocean. This wholesale replacement of the  
8 continental airmass more than offset the impact of the O<sub>3</sub>-rich air transported downward from  
9 the lower stratosphere by the tropopause fold. This stratospheric intrusion descended to the  
10 summit of Angel Peak on June 11, but **Figure C-8** shows that O<sub>3</sub> remained moderate in Clark  
11 County. The CRDS instrument on Angel Peak recorded an MDA8 O<sub>3</sub> concentration of 66 ppbv,  
12 but the highest regulatory MDA8 O<sub>3</sub> values recorded in the LVV were 60 ppbv at Apex and 63  
13 ppbv at Indian Springs. The concentrations at all of the Clark County monitors fell to much  
14 lower levels (40-50 ppbv) on June 12 as the intrusion moved south and east into Arizona and  
15 was followed by the clean Pacific air.

16  
17 **Figures C-9** through 11 show that the 1-min O<sub>3</sub> peaks of 74 ppbv at 1221 PDT and 82 ppbv at  
18 2300 PDT followed the strong southwesterly winds of the approaching trough and were  
19 accompanied by very dry air with low NO<sub>y</sub>. This O<sub>3</sub> was also anticorrelated with CO, CH<sub>4</sub>, and  
20 N<sub>2</sub>O; hallmarks of stratospheric intrusions. The two O<sub>3</sub> peaks were separated by moister mid-  
21 tropospheric Pacific air that was also anticorrelated with the surface air markers. Clean middle  
22 and upper tropospheric Pacific air followed behind the intrusion on June 11-12 as the synoptic  
23 flow rotated to the northwest behind the receding trough.



25  
26  
27  
28 **Figure C-8.** Topographic maps of Clark County showing the June 11-12 MDA8 O<sub>3</sub> distributions.

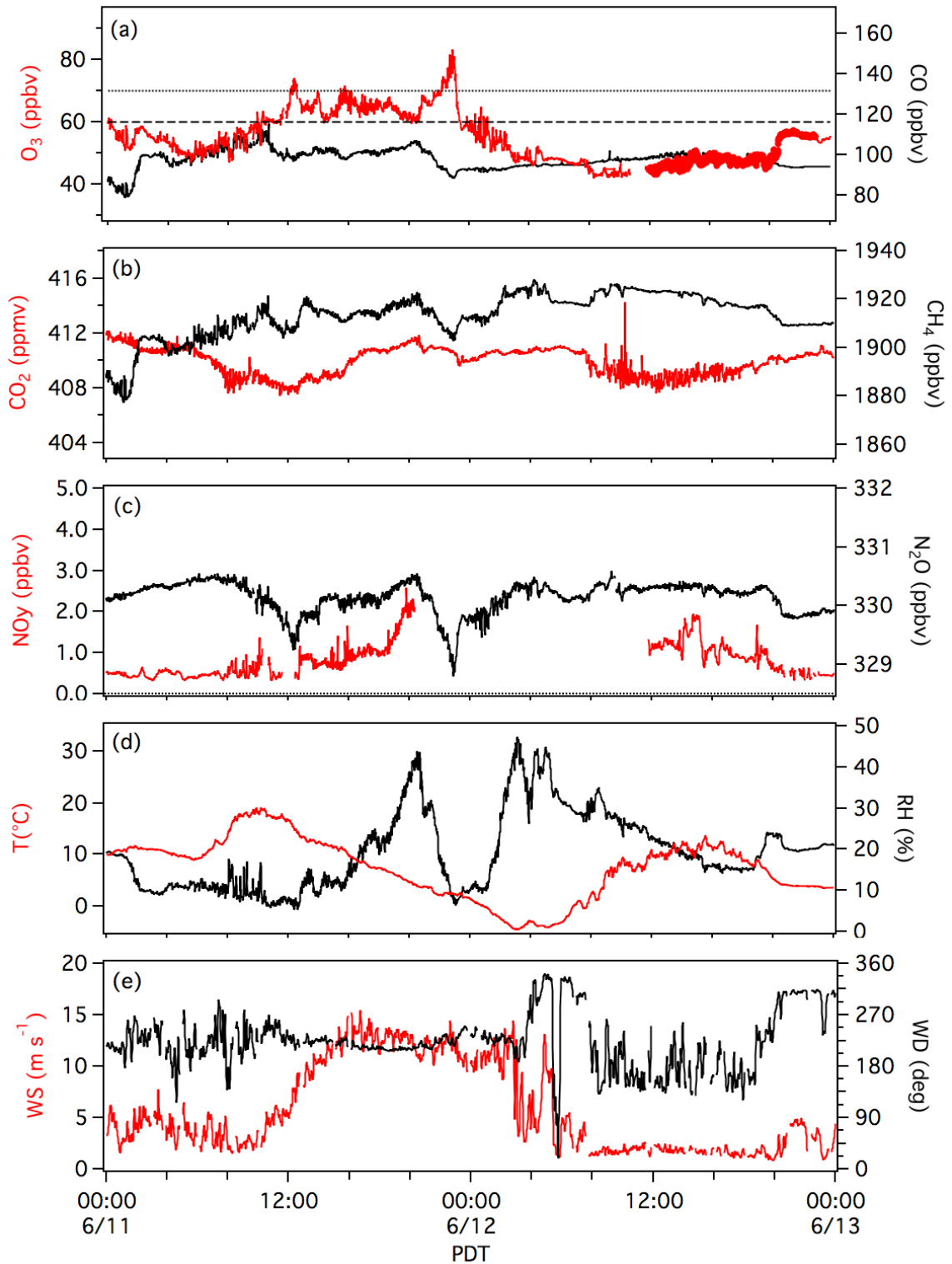
1  
2



3  
4  
5

Figure C-9. Time series of the Angel Peak mobile laboratory measurements on June 11.

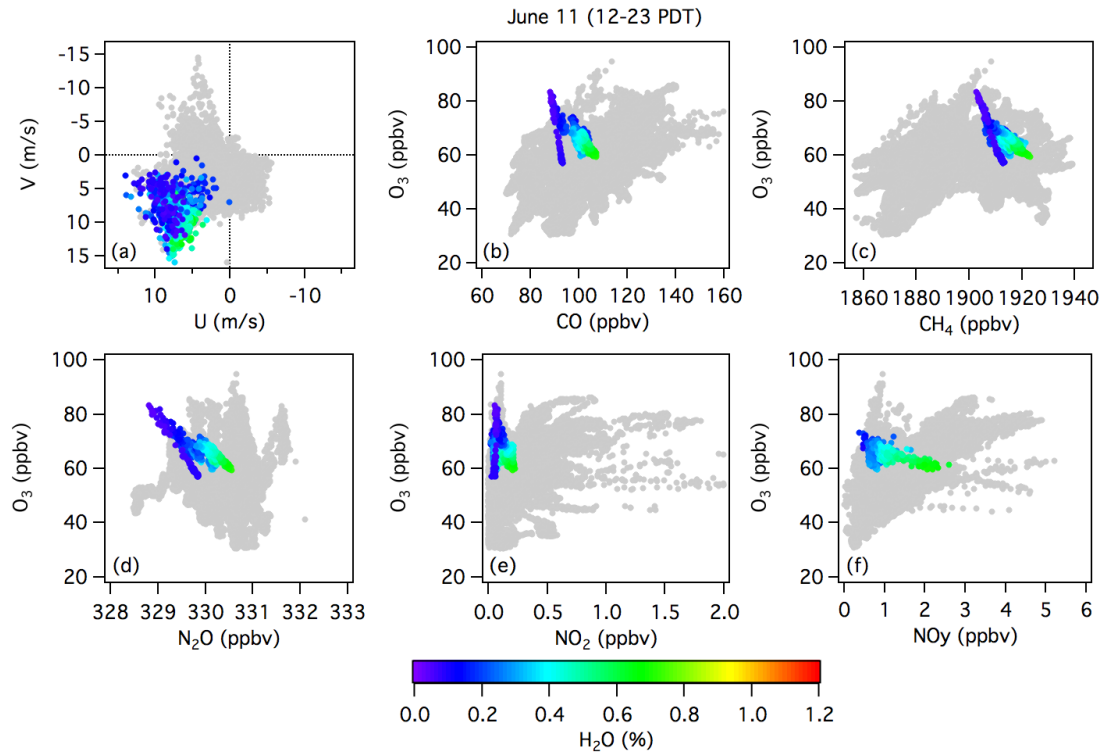
1  
2



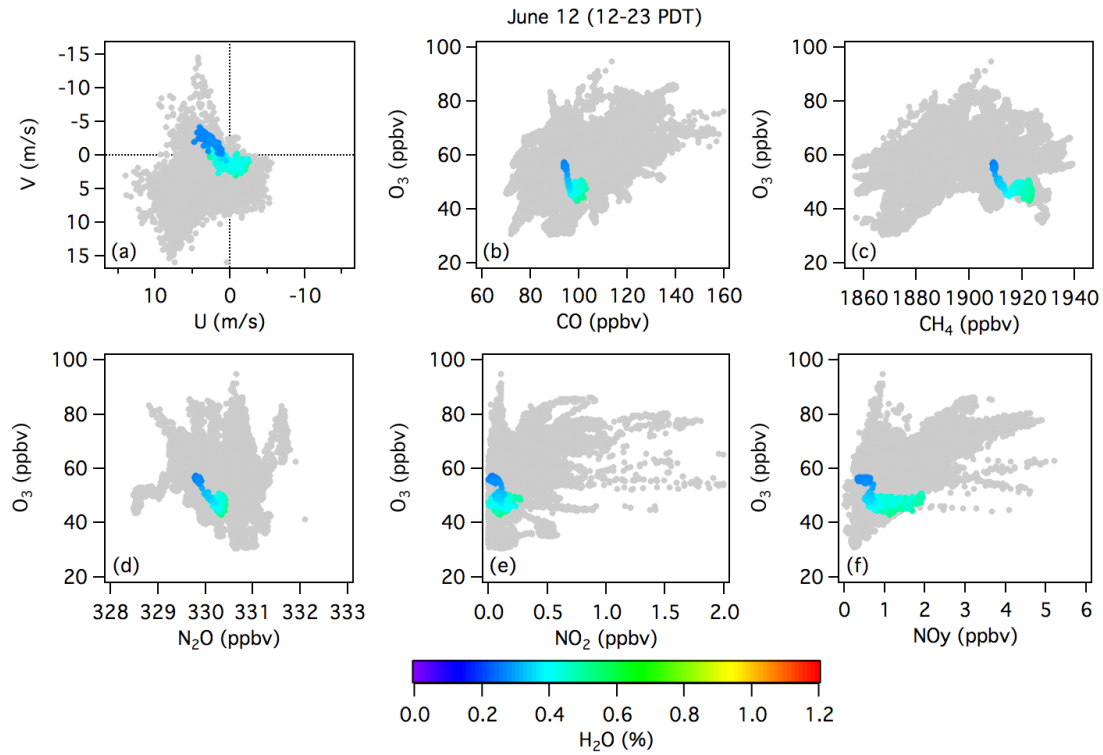
3  
4  
5

Figure C-10. Time series of the Angel Peak mobile laboratory measurements on June 12.

1



2



3

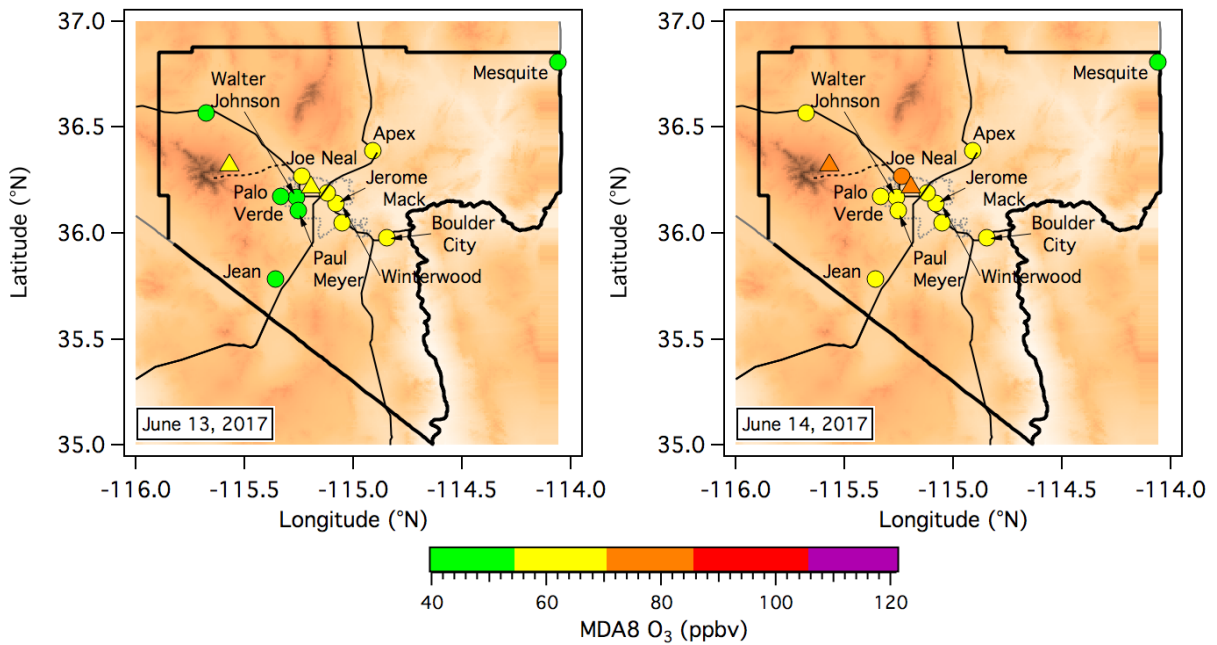
4

5 **Figure C-11.** Scatter plots showing the relationships between O<sub>3</sub> and the other parameters

6 measured by the mobile laboratory on June 11 and 12.

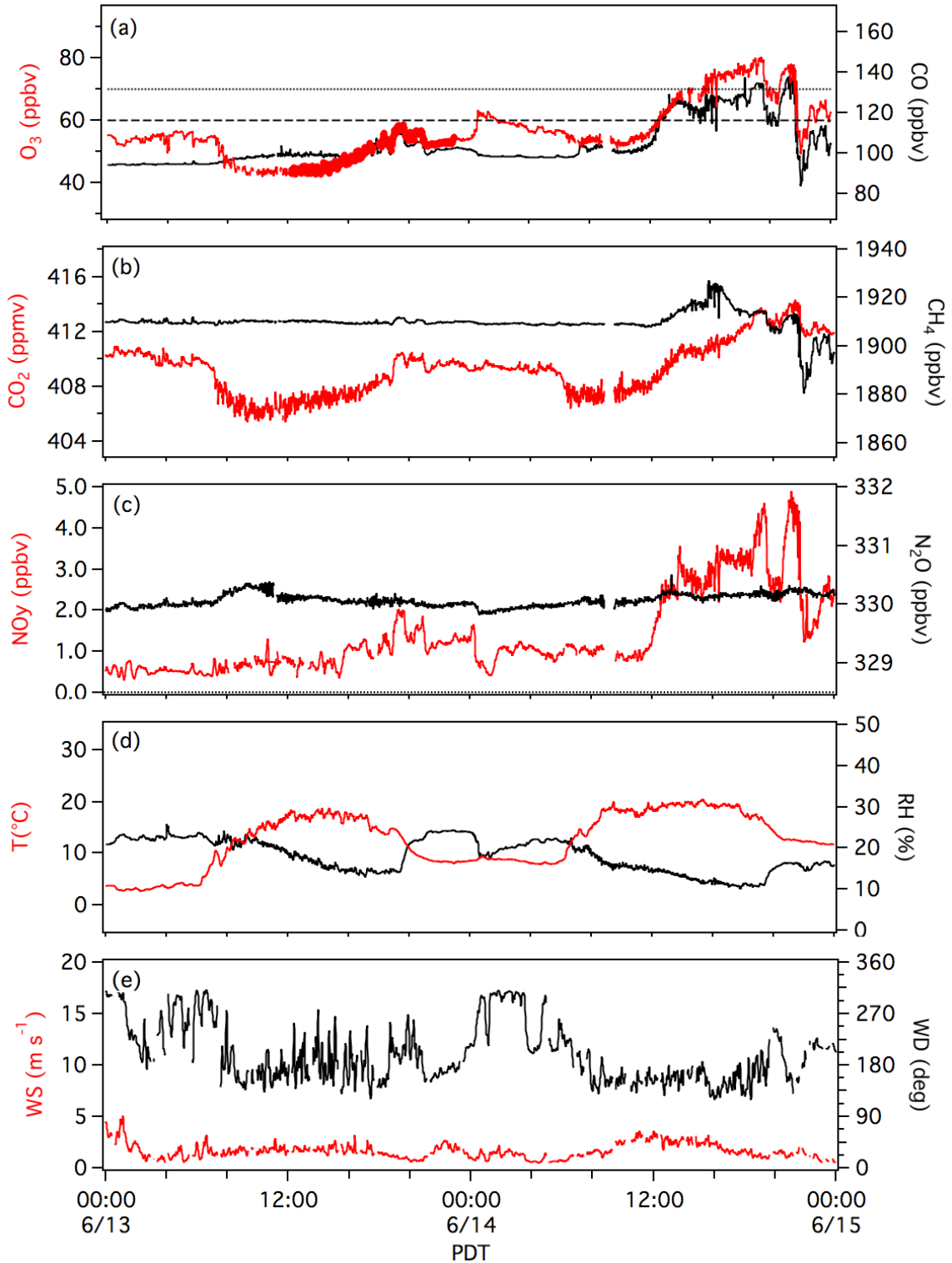
1  
2 **June 13-14**  
3

4 Surface O<sub>3</sub> slowly increased across the LVV on June 13 as warmer temperatures followed the  
5 passage of the upper level low and cold front and promoted local photochemical production.  
6 **Figure C-12** shows that MDA8 O<sub>3</sub> remained good-to-moderate on June 13, but increased  
7 significantly on June 14 when the NAAQS was exceeded by the Joe Neal monitor with 73 ppbv,  
8 and equaled by the Walter Johnson monitor with 70 ppbv. The NLVA monitor recorded an  
9 MDA8 of 74 ppbv and the CRDS instrument on AP 71 ppbv. The correlations between O<sub>3</sub> and  
10 CO, CH<sub>4</sub>, and NO<sub>y</sub> became stronger as moister polluted air was transported from the valley to  
11 AP by the afternoon upslope. The AP measurements show no evidence of undiluted lower  
12 stratospheric air.  
13



14  
15 **Figure C-12.** Topographic maps of Clark County showing the June 13-14 MDA8 O<sub>3</sub> distributions.  
16  
17  
18  
19  
20  
21  
22  
23  
24  
25  
26  
27  
28

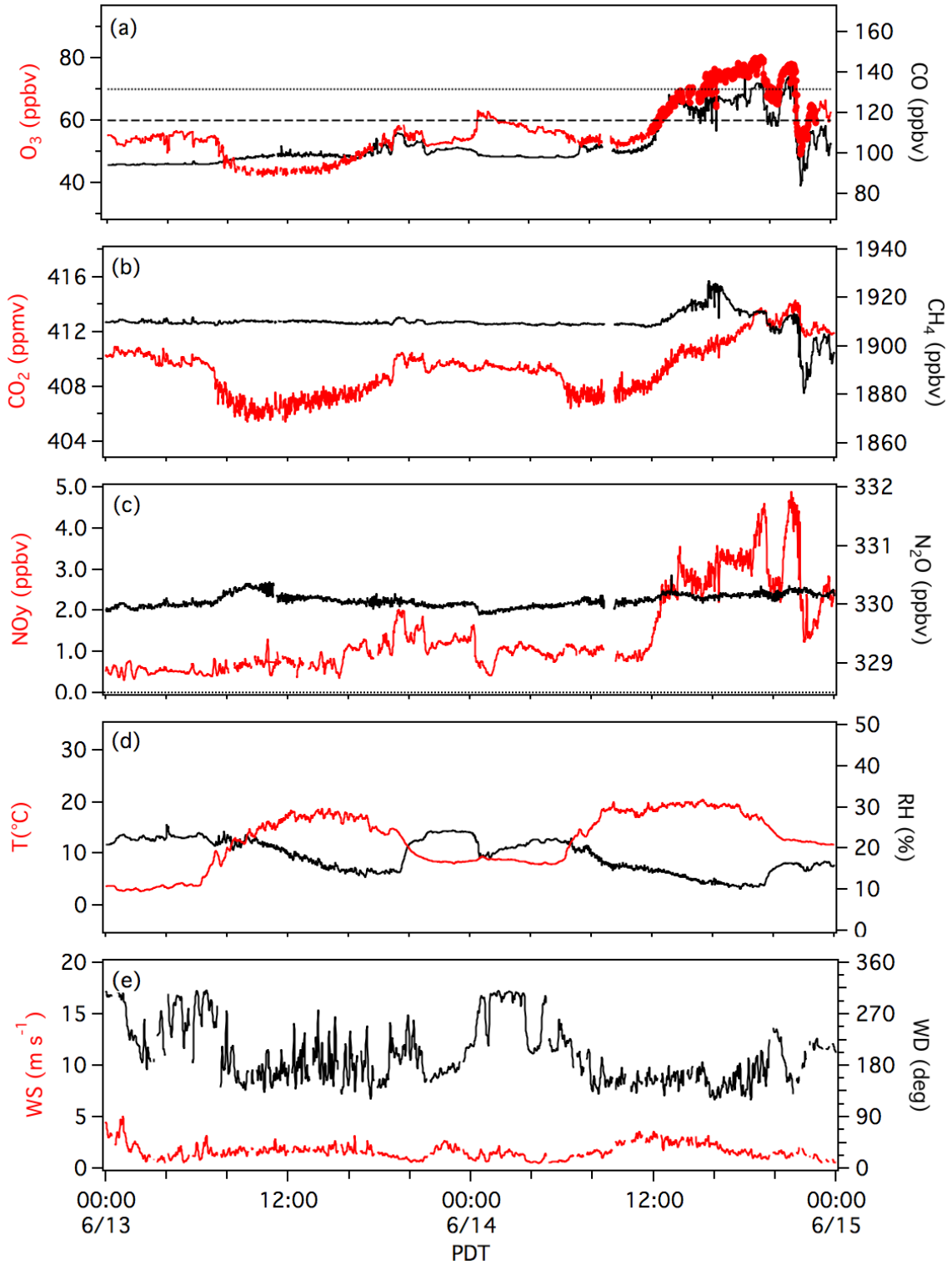
1  
2



3  
4  
5

Figure C-13. Time series of the Angel Peak mobile laboratory measurements on June 13.

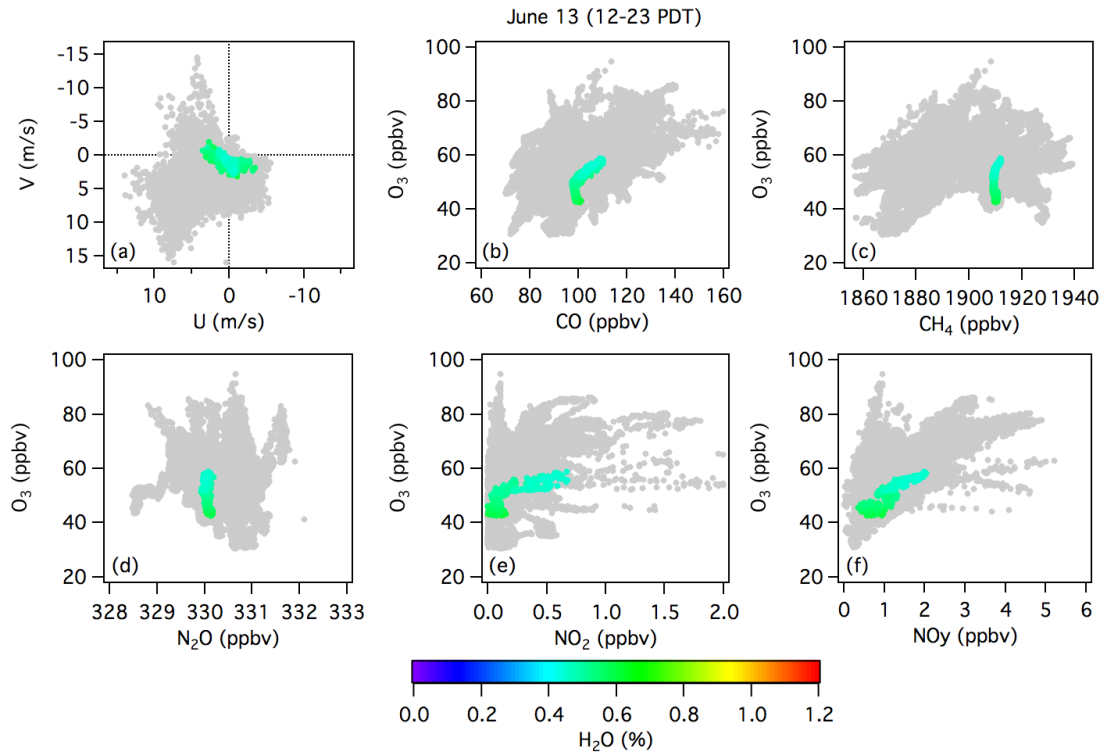
1  
2



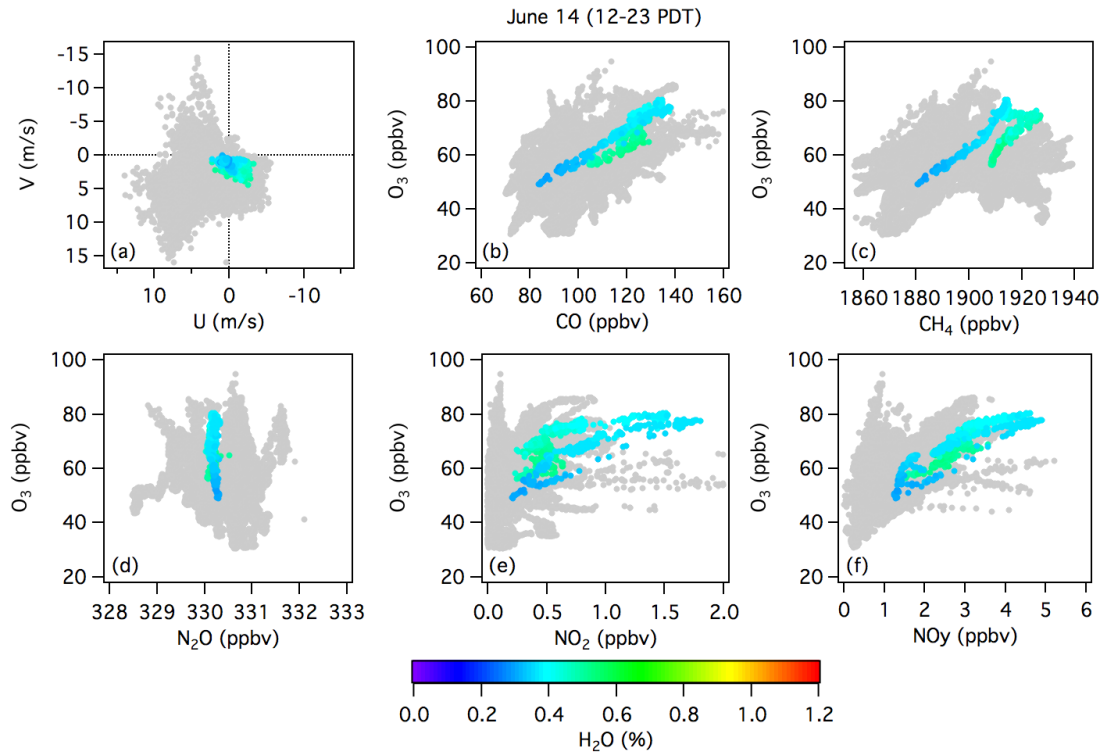
3  
4

Figure C-14. Time series of the Angel Peak mobile laboratory measurements on June 14.

1



2



3

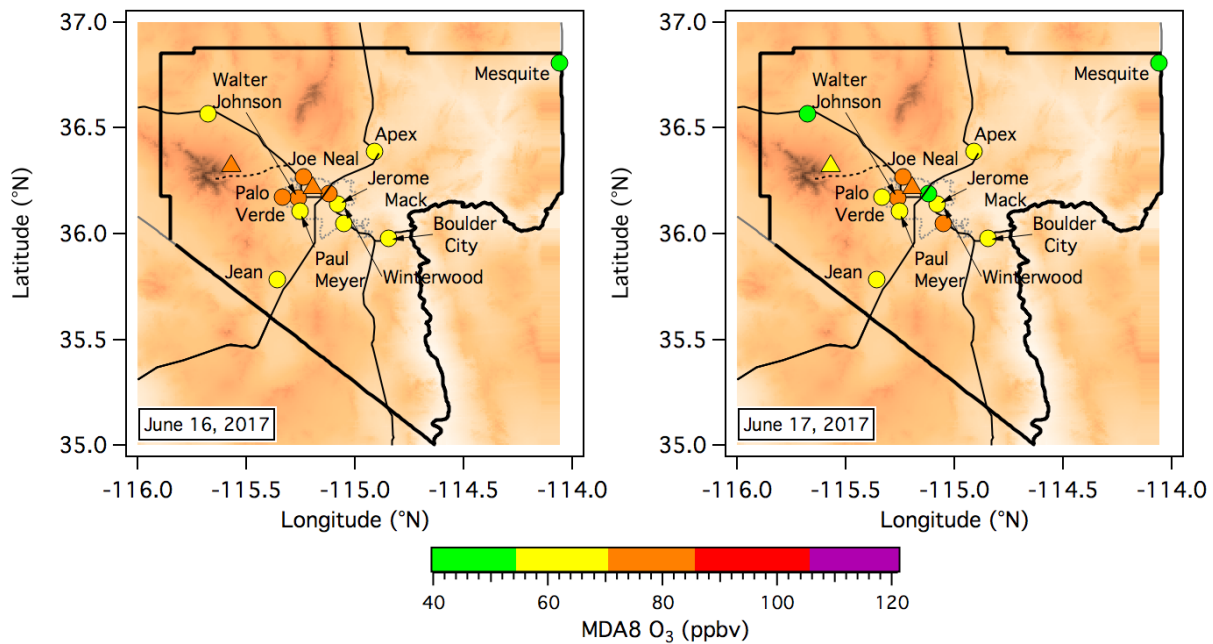
4 **Figure C-15.** Scatter plots showing the relationships between  $O_3$  and the other parameters

5 measured by the mobile laboratory on June 13 and 14.

6

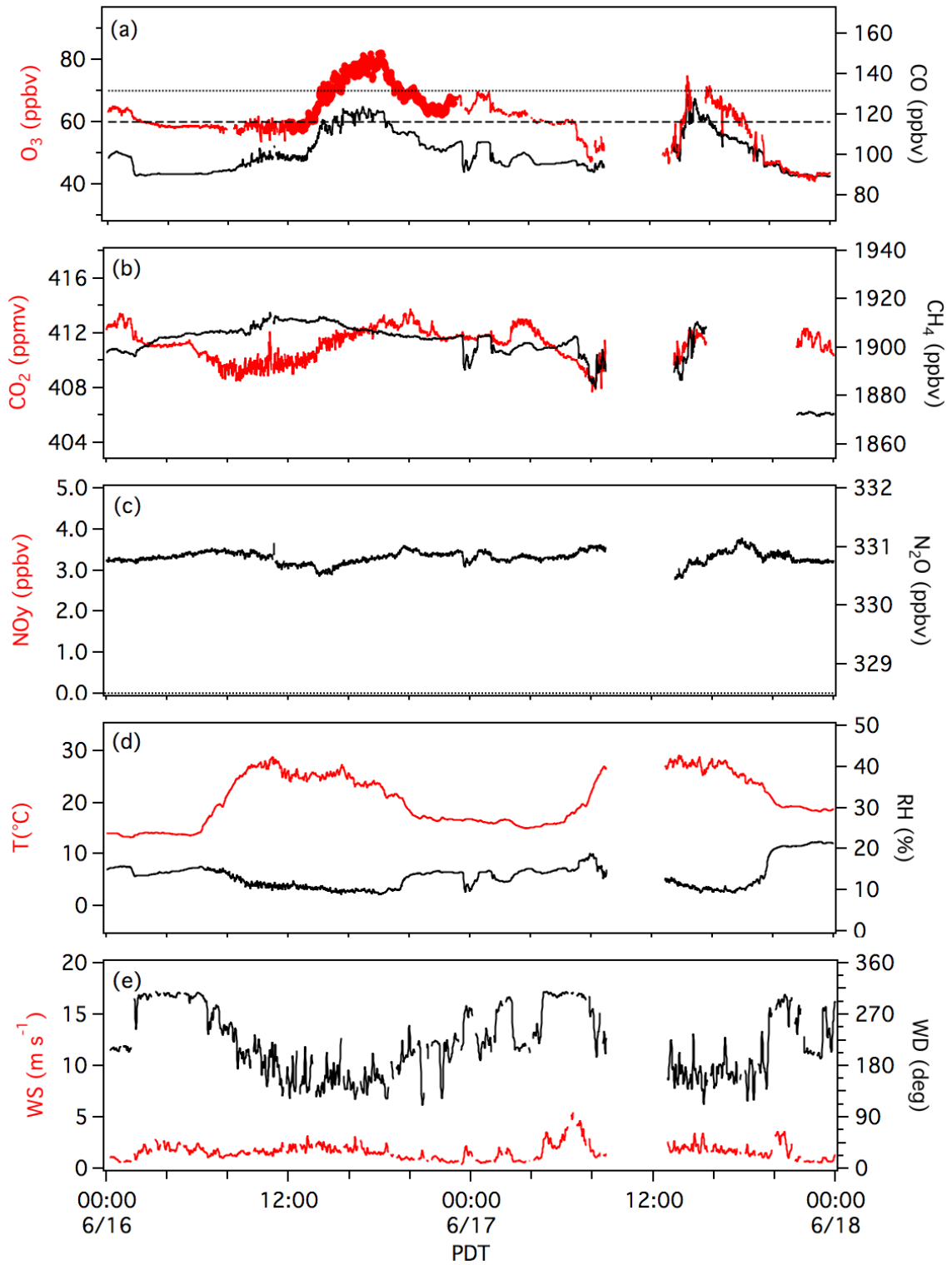
1  
2 **June 16-17**  
3

4 High ozone was present all across the LVV on both June 16-17 with MDA8 concentrations of 63  
5 ppbv or more at all of the CCDAQ monitors except Mesquite, and exceedances at 3 of the  
6 monitors on the 16<sup>th</sup> and 4 on the 17<sup>th</sup>. The Joe Neal monitor measured the highest MDA8 O<sub>3</sub>  
7 with 74 ppbv on June 16 and 72 ppbv on June 17. The NLVA monitor measured 76 and 73 ppbv,  
8 respectively, on these two days, and the CRDS instrument on Angel Peak measured 74 and 61  
9 ppbv. The AP time series and scatter plots show that O<sub>3</sub> was positively correlated with CO on  
10 both days, and the highest concentrations occurred during periods of upslope flow from the  
11 valley. Ozone was uncorrelated with N<sub>2</sub>O on both days, suggesting that there were no fire  
12 influences. Ozone was also uncorrelated with CH<sub>4</sub> on the 16<sup>th</sup>, but positively correlated on the  
13 17<sup>th</sup>. Unfortunately, there were no NO<sub>y</sub> measurements at AP during this period, but the  
14 available measurements suggest that the high O<sub>3</sub> in both the LVV and AP was associated with  
15 regional pollution with no fire, long-range transport, or stratospheric influences.  
16  
17  
18  
19



20  
21 **Figure C-16.** Topographic maps of Clark County showing the June 13-14 MDA8 O<sub>3</sub> distributions.  
22  
23  
24  
25  
26

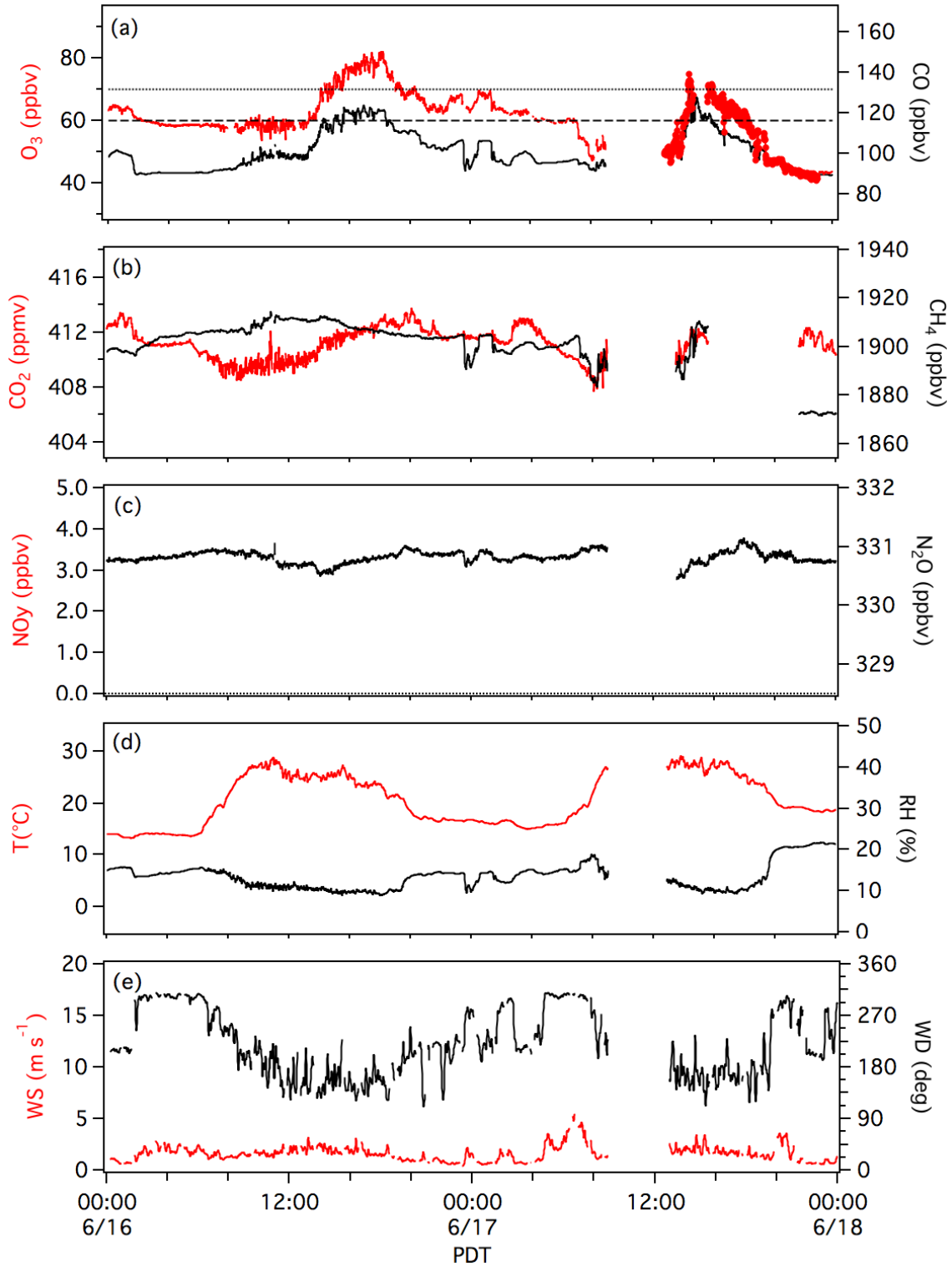
1  
2



3  
4  
5

Figure C-17. Time series of the Angel Peak mobile laboratory measurements on June 16.

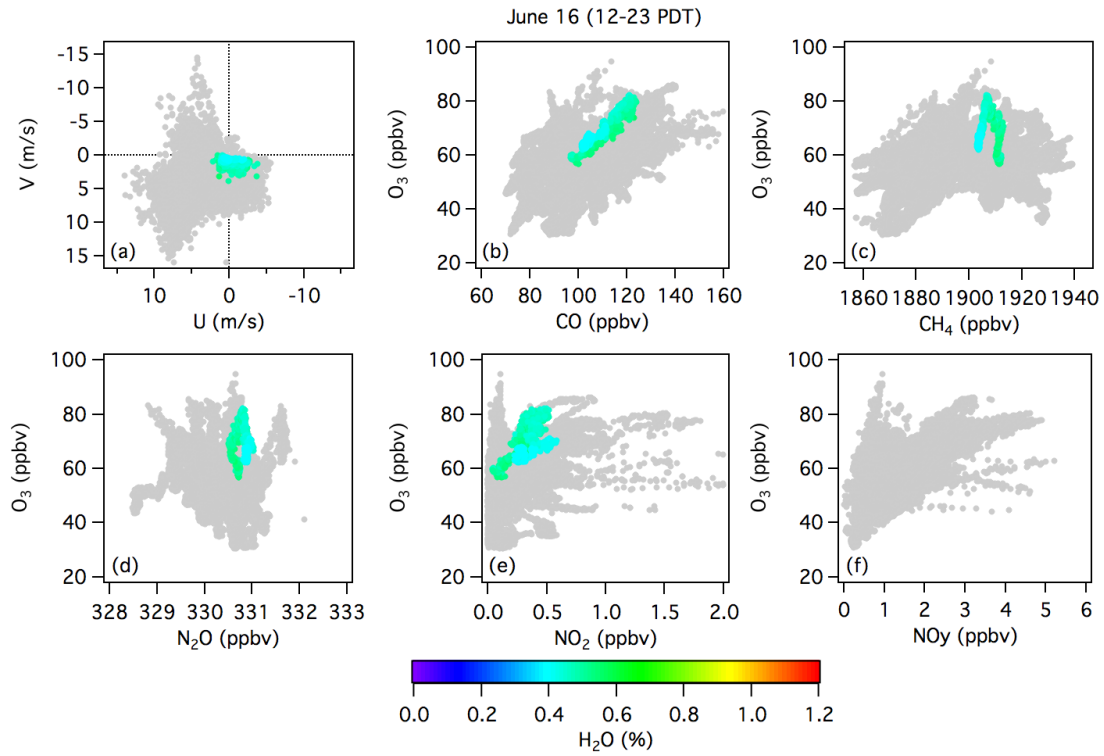
1  
2



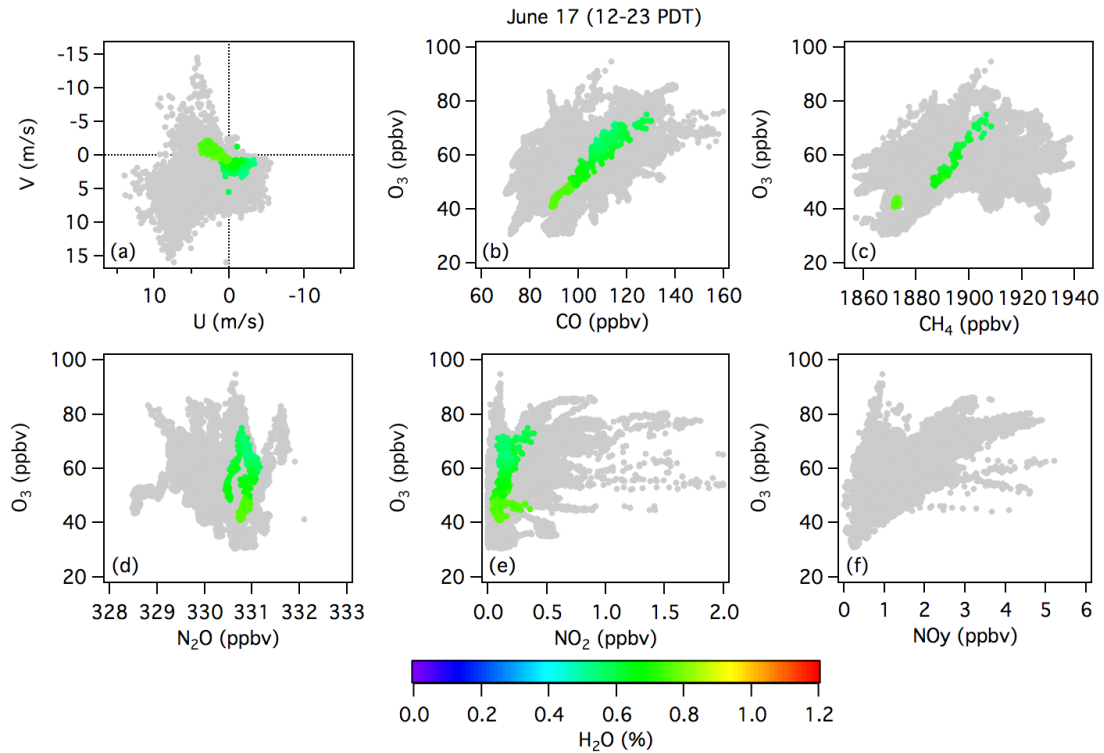
3  
4  
5

Figure C-18. Time series of the Angel Peak mobile laboratory measurements on June 17.

1



2



3

4

5 **Figure C-19.** Scatter plots showing the relationships between  $O_3$  and the other parameters

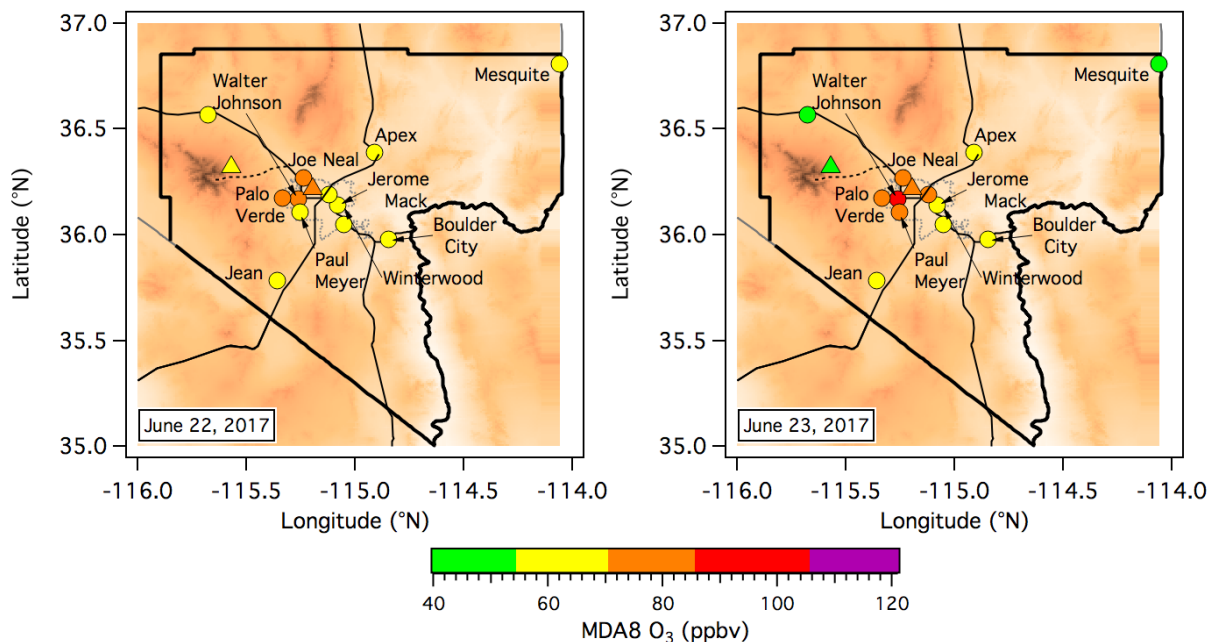
6 measured by the mobile laboratory on June 16 and 17.

1  
2 **June 22-23**  
3

4 The hottest temperatures of the FAST-LVOS campaign were measured on June 22 when the all-  
5 time Las Vegas record of 117°F was tied at McCarran International Airport. The highest O<sub>3</sub> of  
6 the campaign was also measured on June 22-23, with peak MDA8 concentrations of 77 ppbv at  
7 Joe Neal on both June 22 and 23. The Walter Johnson monitor reported 87 ppbv on June 23,  
8 but this number was based on only 6 hours of measurements and the actual value should be  
9 somewhat lower. The NLVA monitor measured 76 and 83 ppbv on June 22 and 23, respectively,  
10 but the CRDS instrument on Angel Peak measured only 63 and 58 ppbv.

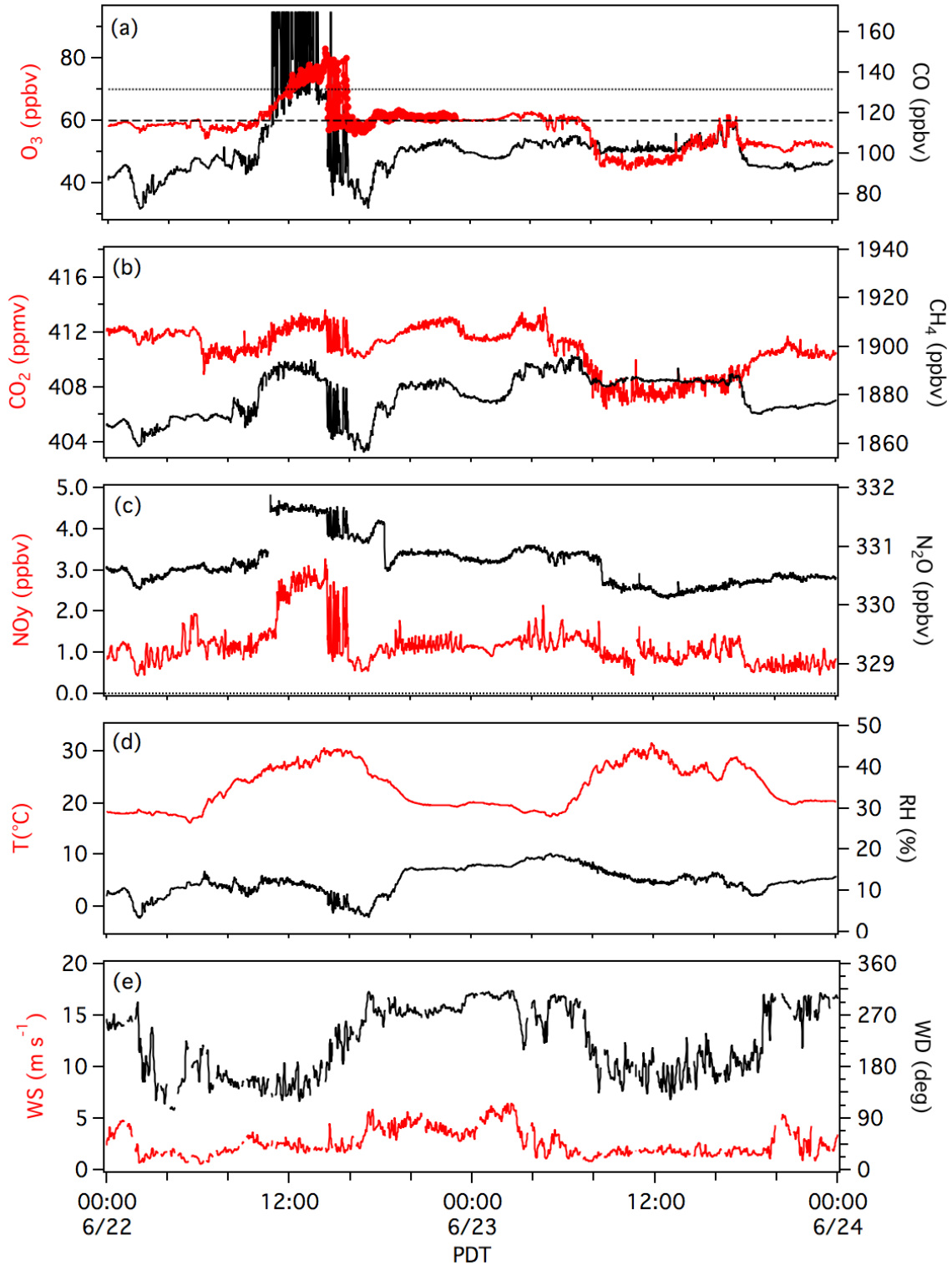
11  
12 The instruments in the mobile laboratory sampled a distinctive plume with very high CO (≈450  
13 ppbv) and elevated O<sub>3</sub> (≈80 ppbv) and around midday on June 22 (**Figure C-21**). This plume,  
14 which has been attributed to the Holcomb Fire near Big Bear, CA, was also enhanced in CO<sub>2</sub>,  
15 CH<sub>4</sub>, NO<sub>y</sub>, and N<sub>2</sub>O, and disappeared when the winds shifted from southerly to northwesterly in  
16 the afternoon, bringing much drier clean air to the summit (blue points in **Figure C-23**, top).

17  
18 Ozone remained relatively low at AP on June 23, with the highest concentrations of ≈60 ppbv  
19 appearing around 1700 PDT in the moister air transported to the summit by the afternoon  
20 upslope flow. Ozone decreased again when the winds shifted from southeasterly to  
21 northwesterly in the early evening.



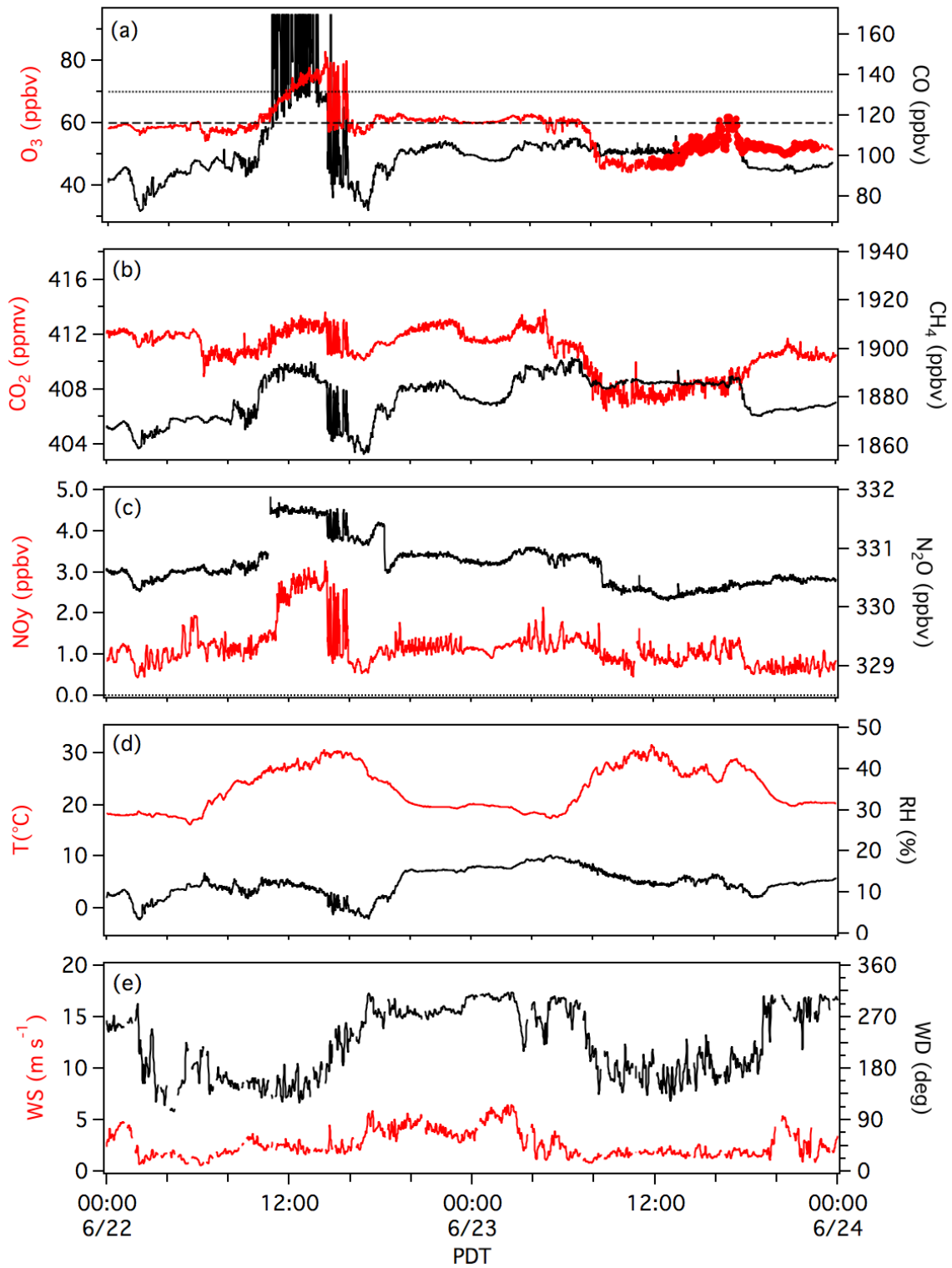
24 **Figure C-20.** Topographic maps of Clark County showing the June 13-14 MDA8 O<sub>3</sub> distributions.  
25  
26  
27  
28

1  
2



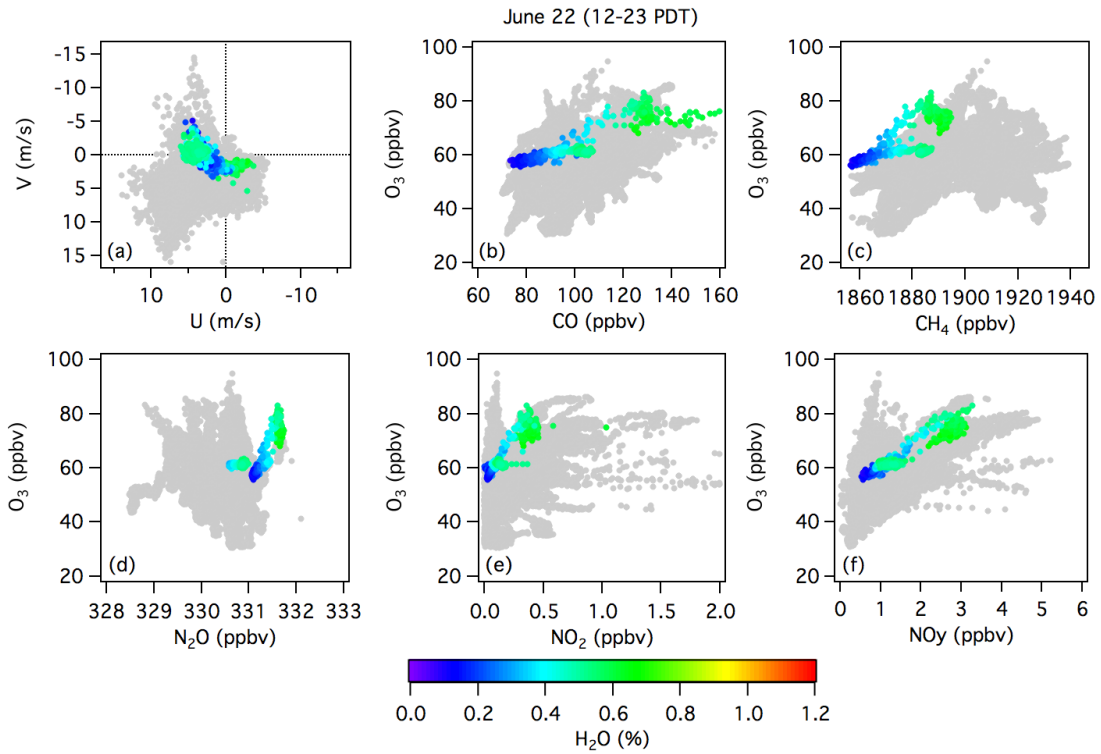
3  
4  
5

Figure C-21. Time series of the Angel Peak mobile laboratory measurements on June 22.

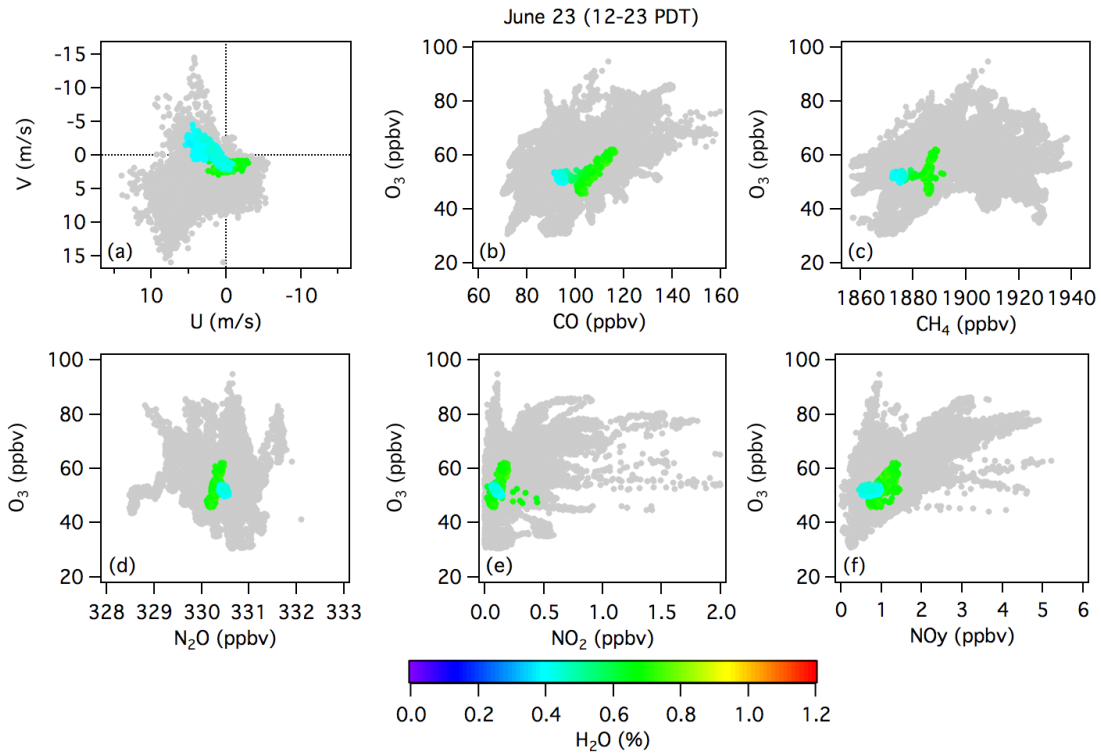
2  
3  
4

**Figure C-22.** Time series of the Angel Peak mobile laboratory measurements on June 23.

1



2



3

4 **Figure C-23.** Scatter plots showing the relationships between  $O_3$  and the other parameters  
5 measured by the mobile laboratory on June 22 and 23.

6

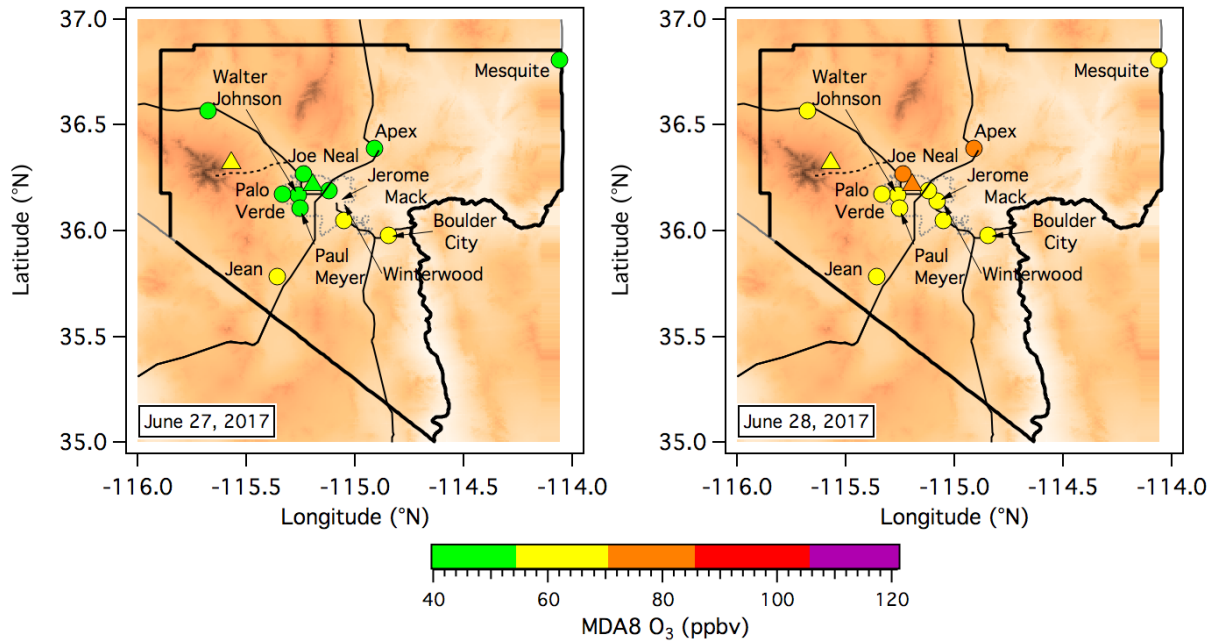
1  
2 **June 28-30**  
3

4 The last three days of FAST-LVOS were also very hot with high O<sub>3</sub> measured throughout Clark  
5 County (**Figure C-24**). Ozone was good to moderate on June 27, but MDA8 mixing ratios of 59  
6 ppbv or more were recorded by all of the CCDAQ monitors, including the outlying Mesquite and  
7 Jean CAMS, on June 28-30 days. The NAAQS was exceeded at Joe Neal on all 3 days, with MDA8  
8 concentrations of 74,70, and 75 ppbv, respectively. The NOAA measurements at the NLVA were  
9 very similar with 74,71, and 76 ppbv. The NOAA CRDS instrument on AP also measured high O<sub>3</sub>  
10 with 68, 71, and 74 ppbv, respectively.

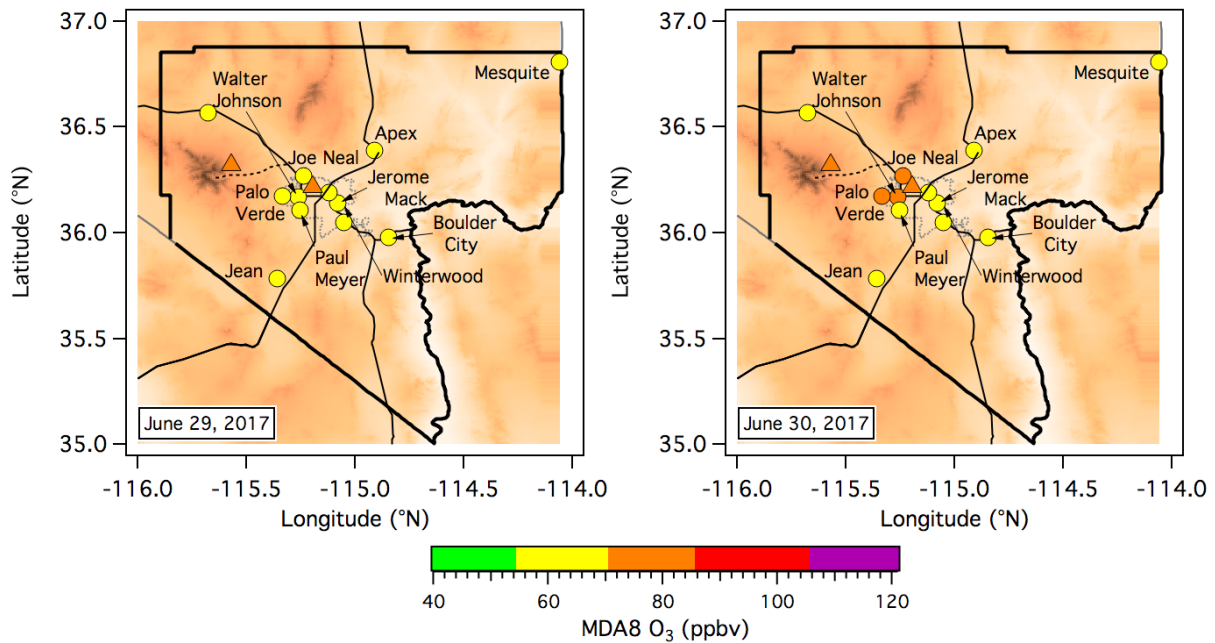
11  
12 The TOPAZ measurements from June 28 (**Figure 9-42**) showed the entrainment of a suspected  
13 fire plume by the convective mixed layer above the LVV near midday, but this plume remained  
14 well above the summit of Angel peak and was not detected in the mobile laboratory in-situ  
15 measurements. The highest O<sub>3</sub> appeared several hours later in a short-lived (50 min) spike of  
16 dry air advected over the summit when the winds shifted from SSE to NW around 1830 PDT  
17 (**Figure C-25**). The scatter plots show that the O<sub>3</sub> in this spike was positively correlated with  
18 both CO and CH<sub>4</sub>, but with a very steep slope. The low H<sub>2</sub>O content suggests that the spike was  
19 caused by a filament of Asian pollution that had descended from the upper troposphere.

20  
21 These measurements stand in contrast to the high O<sub>3</sub> concentrations detected on June 29 and  
22 30 that were positively correlated with both CO and NO<sub>y</sub>, and uncorrelated with CH<sub>4</sub>. This O<sub>3</sub>  
23 was embedded in moister air brought to AP by the afternoon upslope flow and is attributed to  
24 regional pollution.  
25

1  
2



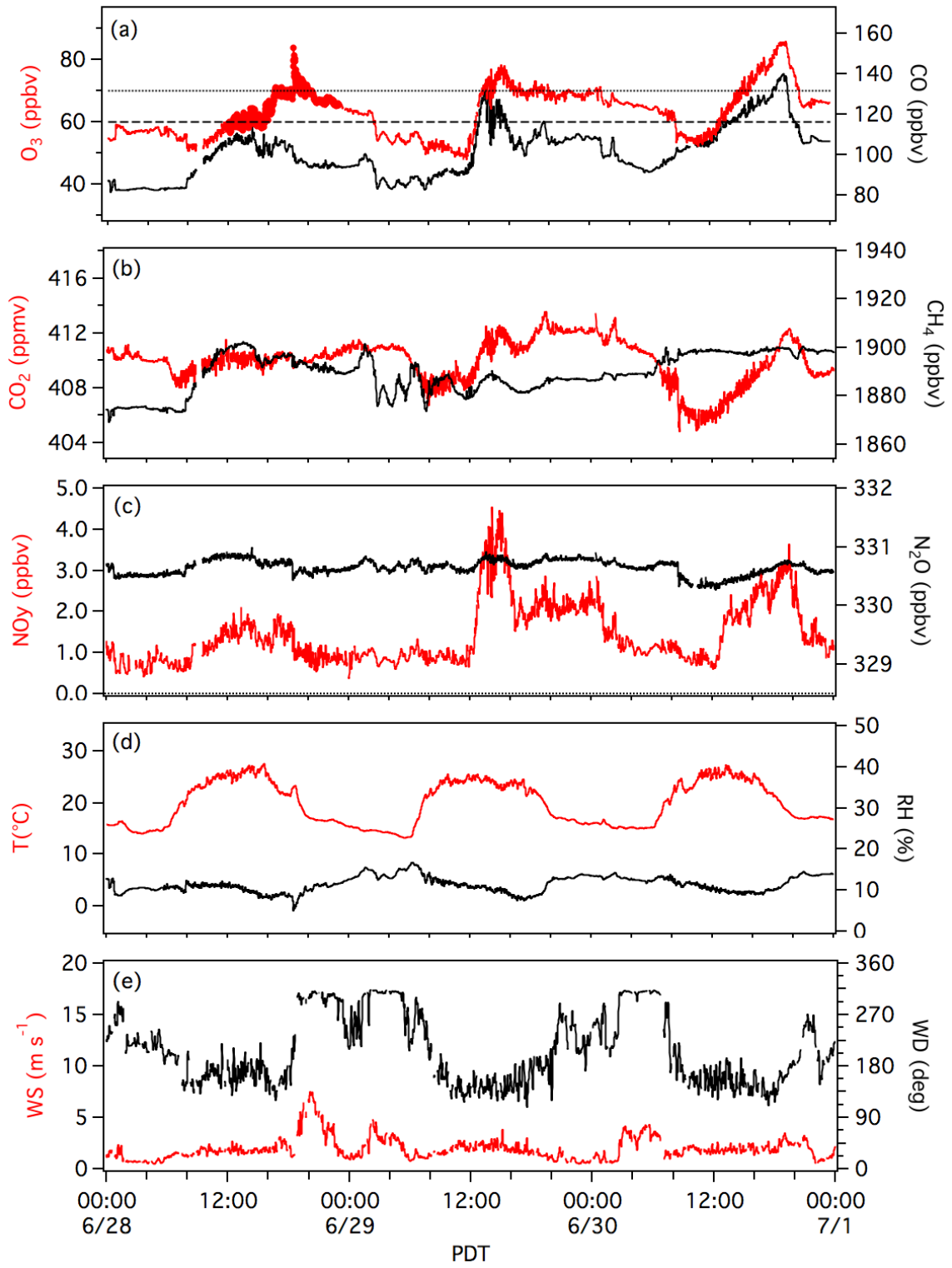
3  
4  
5



6  
7  
8  
9  
10  
11

**Figure C-24.** Topographic maps of Clark County showing the June 27-30 MDA8 O<sub>3</sub> distributions.

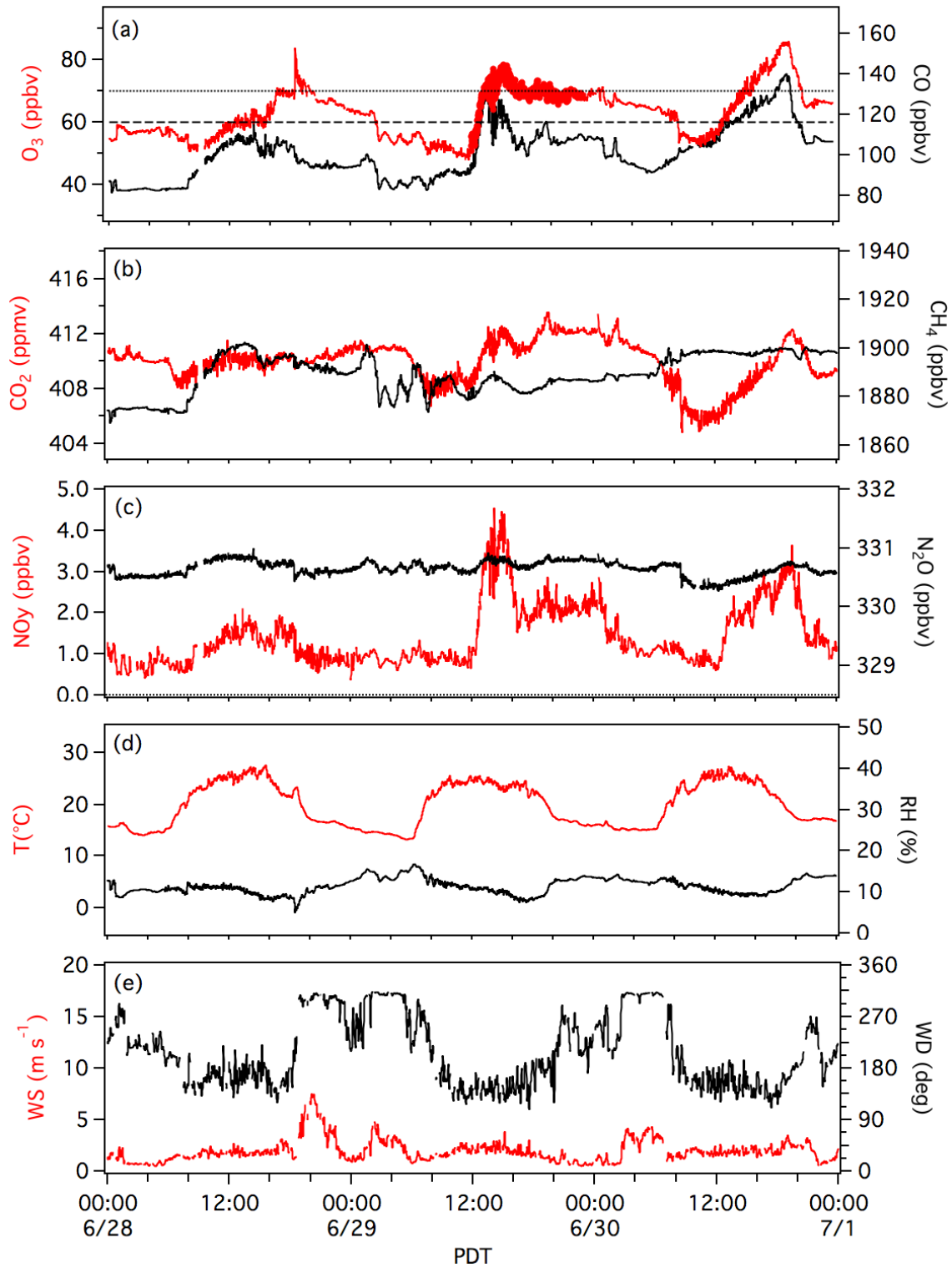
1  
2



3  
4  
5

Figure C-25. Time series of the Angel Peak mobile laboratory measurements on June 28.

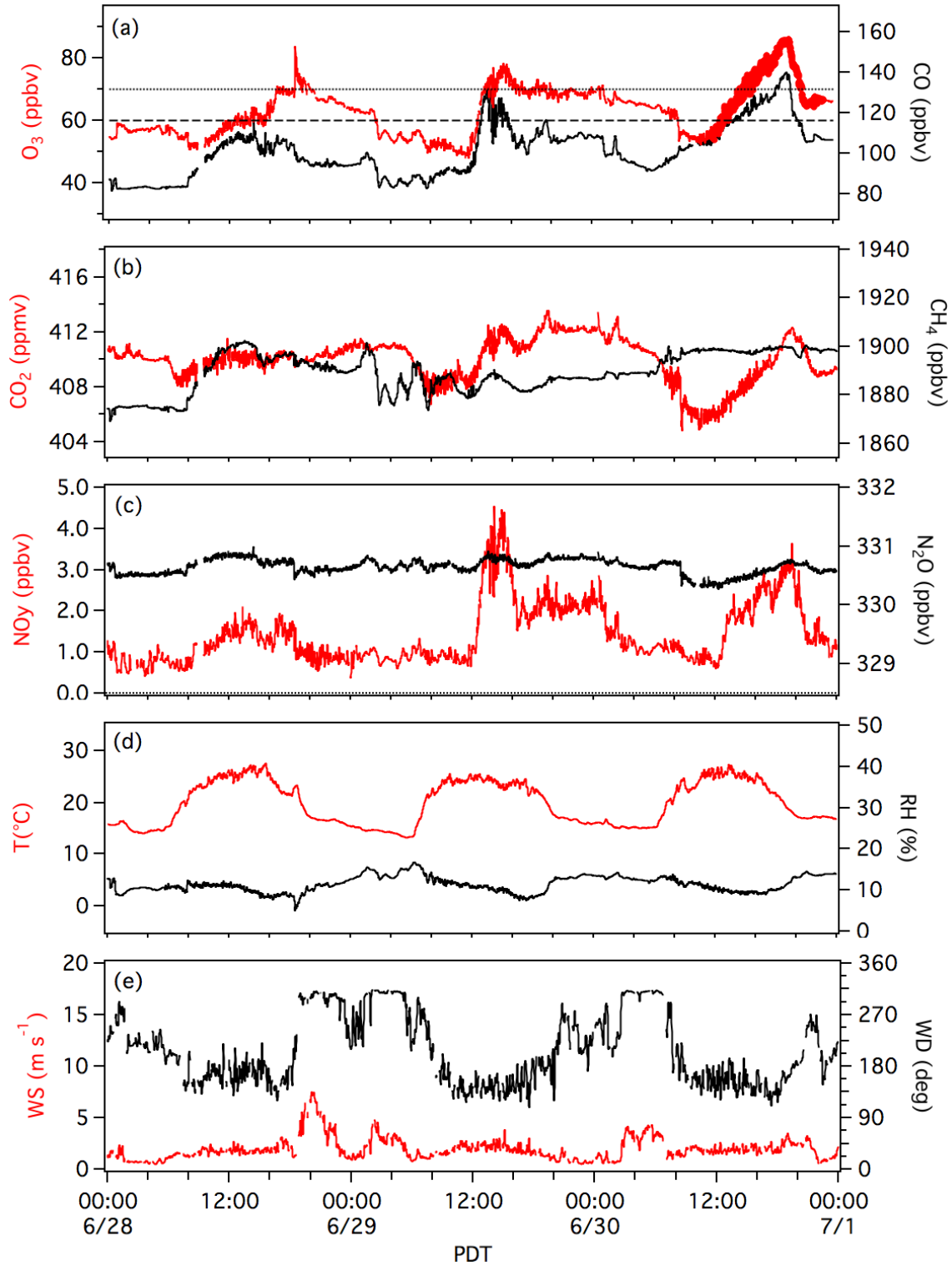
1  
2



3  
4  
5

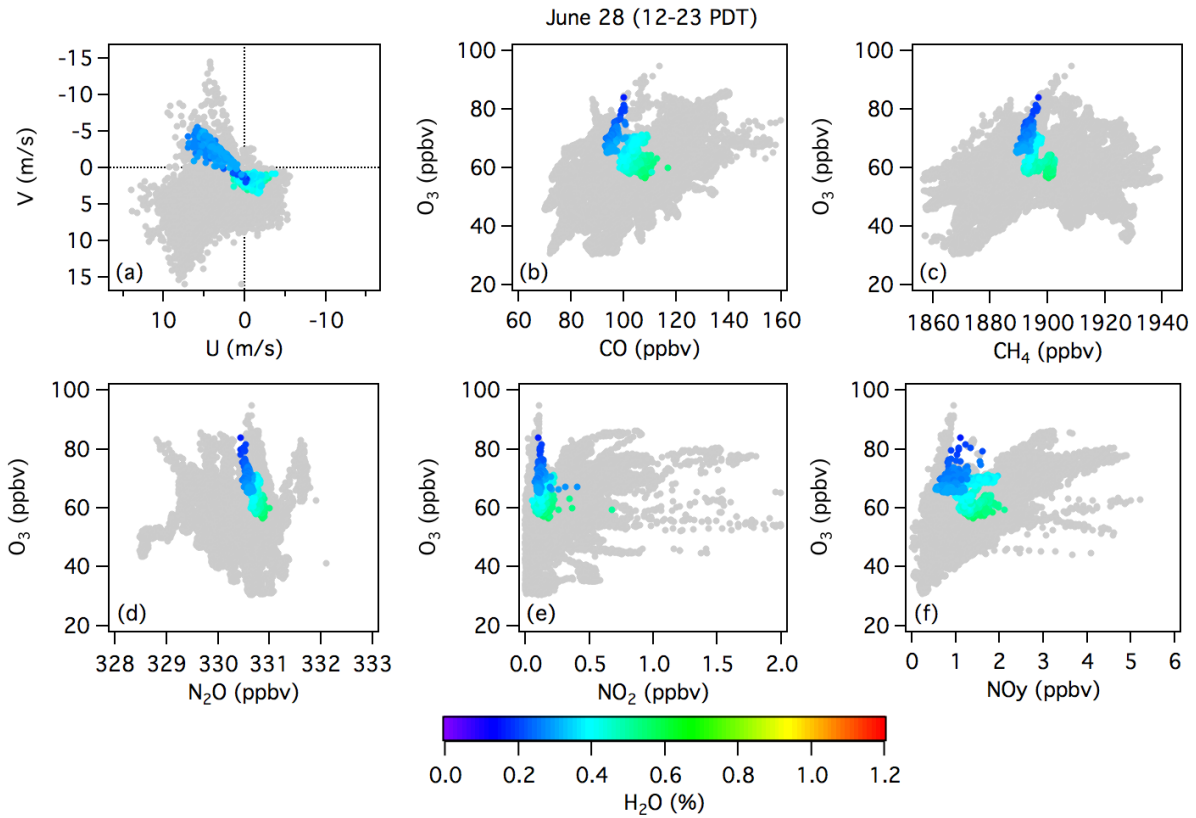
Figure C-26. Time series of the Angel Peak mobile laboratory measurements on June 29.

1  
2

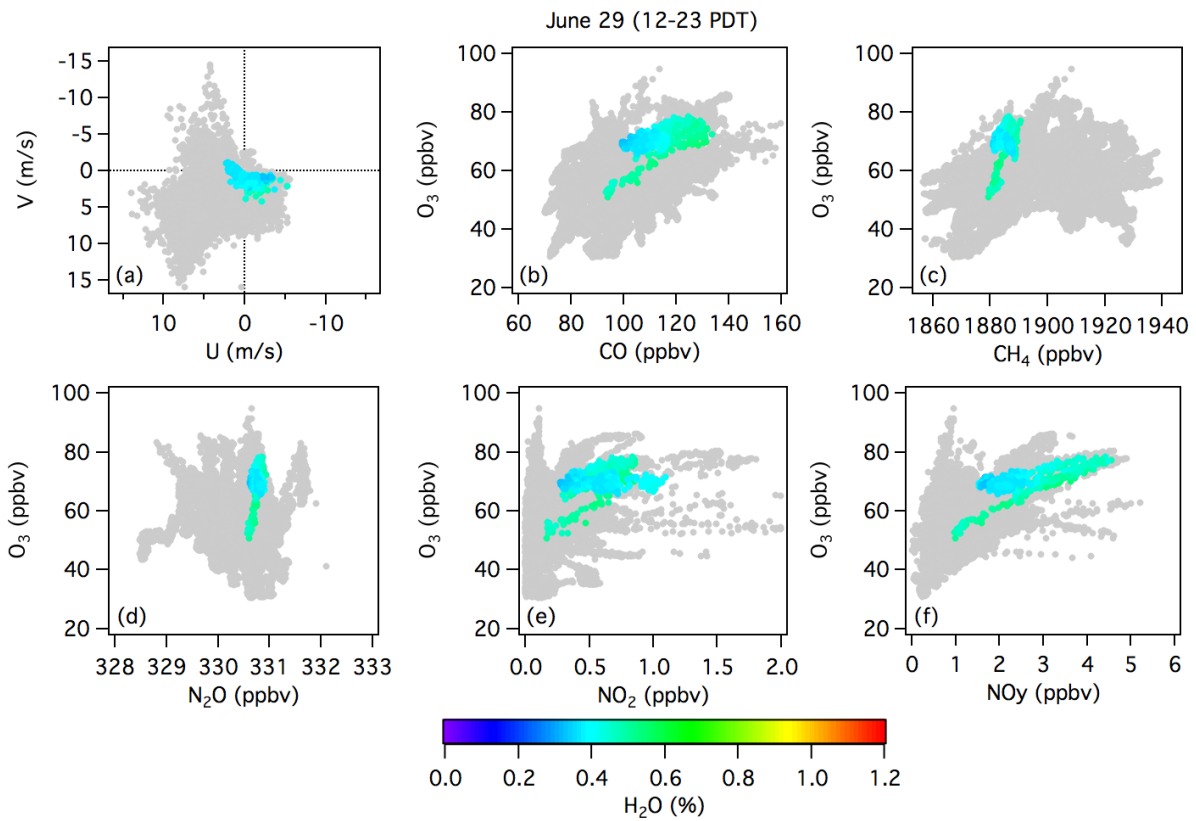


3  
4  
5

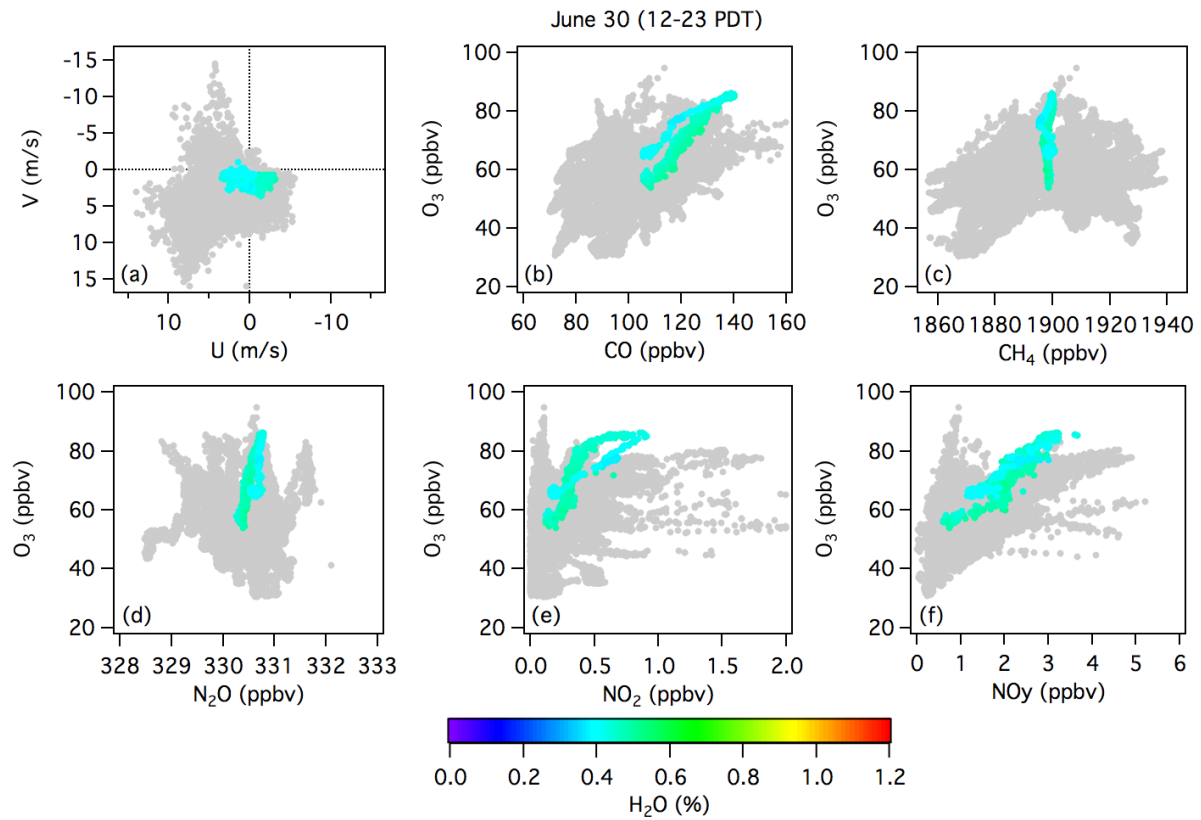
Figure C-27. Time series of the Angel Peak mobile laboratory measurements on June 30.



1



2  
3

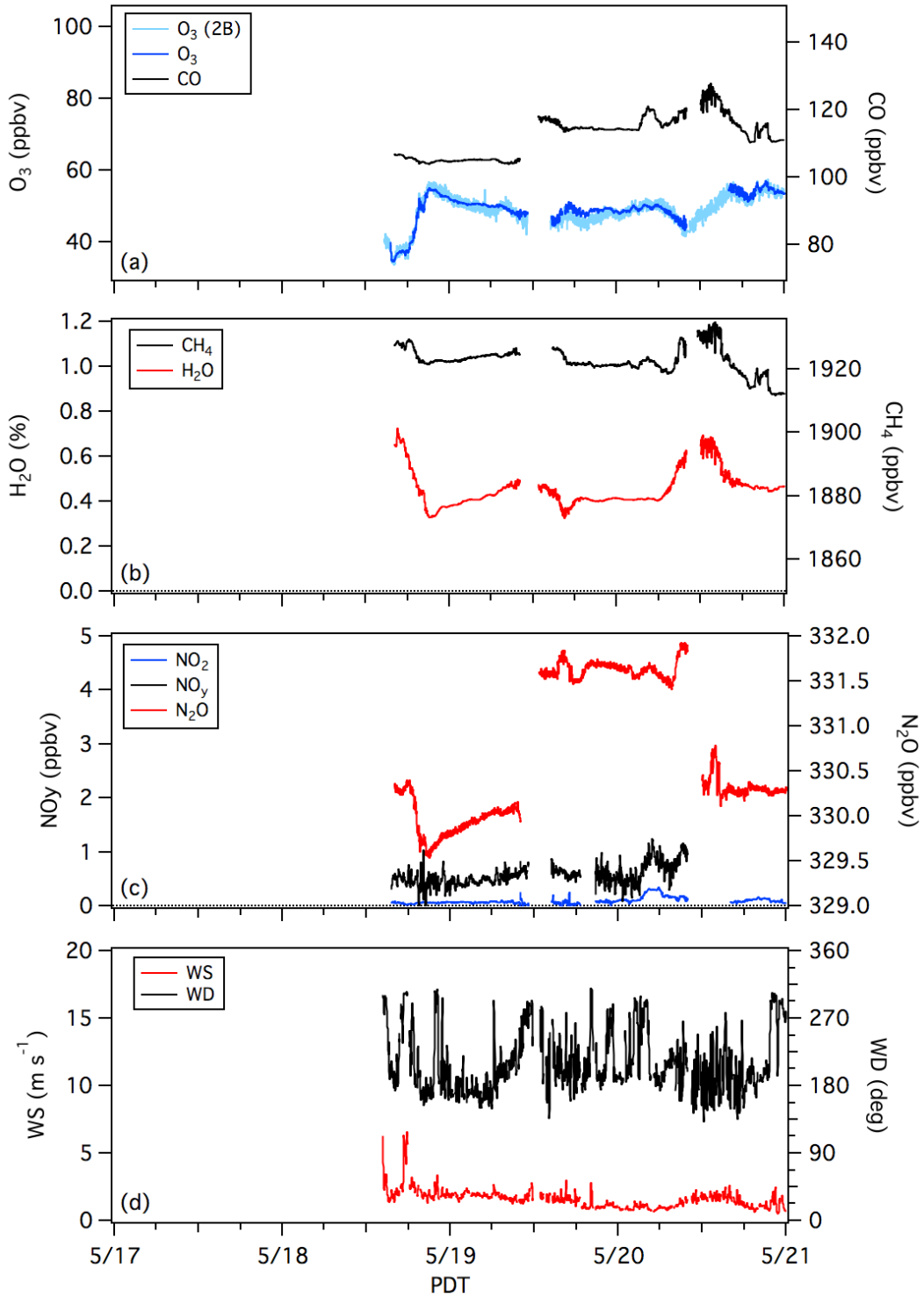


1  
 2 **Figure C-28.** Scatter plots showing the relationships between O<sub>3</sub> and the other parameters  
 3 measured by the mobile laboratory on June 28, 29, and 30.  
 4

1 **2. Angel Peak weekly summary plots**

2  
3  
4  
5

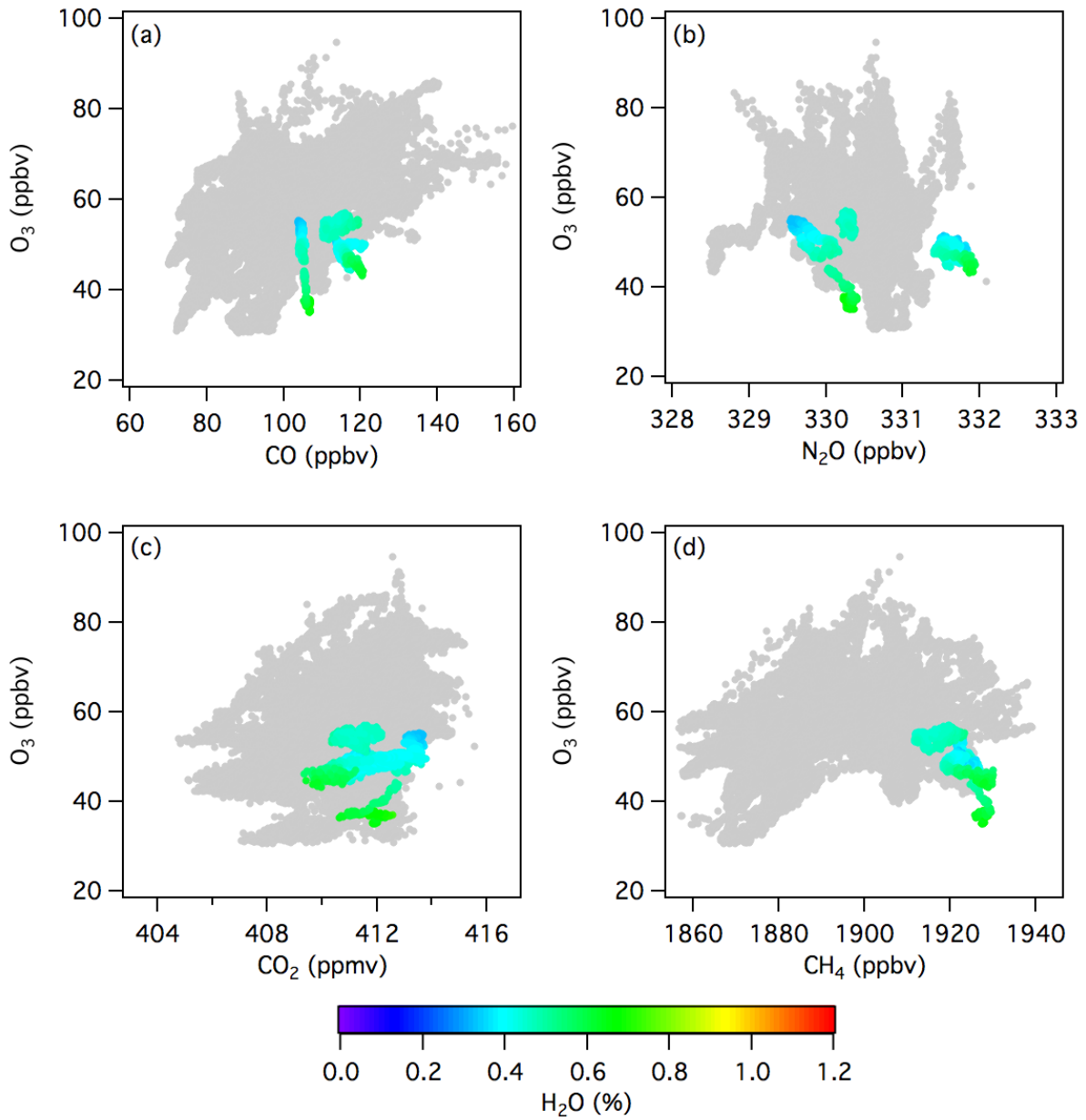
**Week 1**



6

1  
2  
3  
4  
5  
6  
7

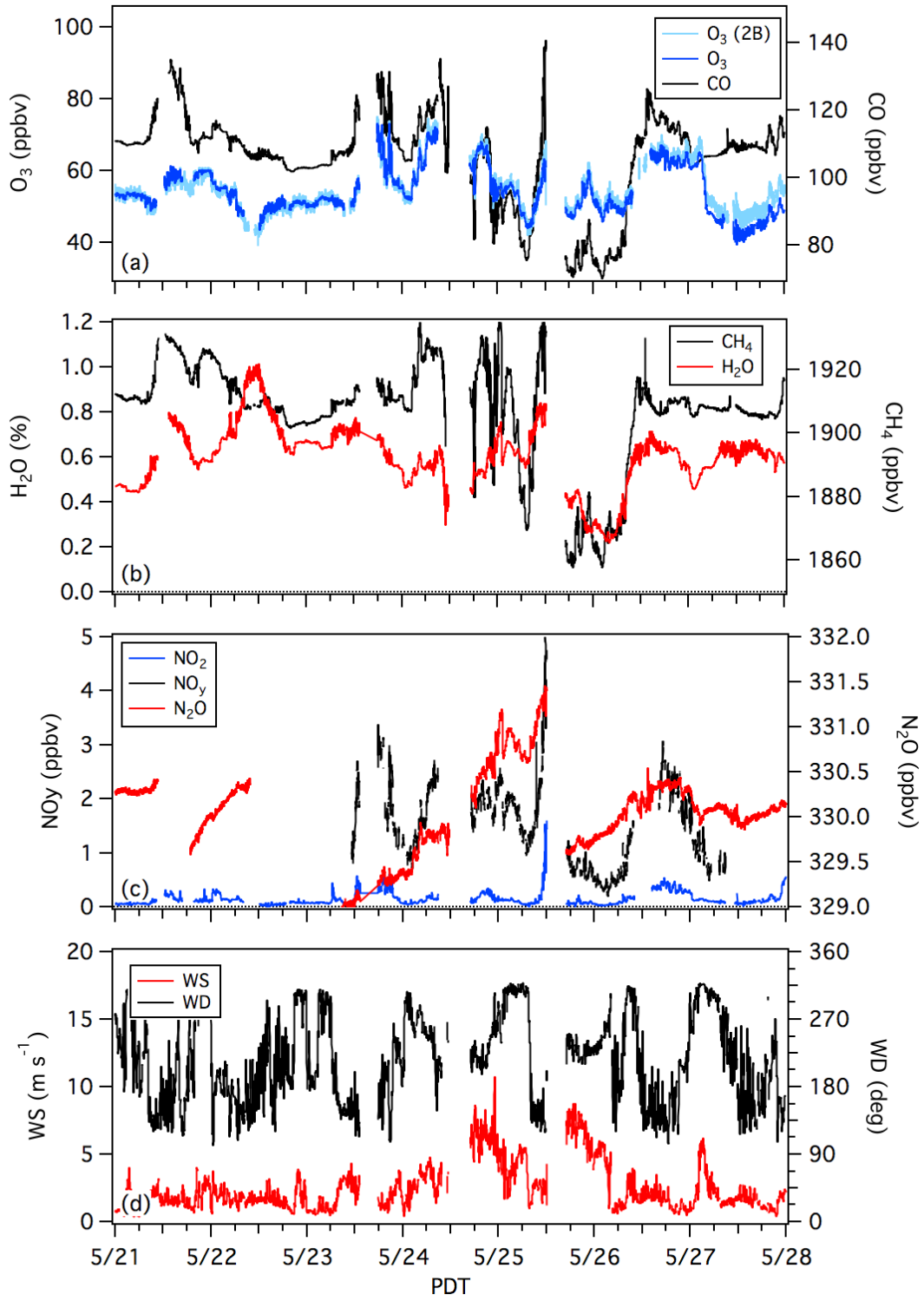
**Week 1**



8  
9  
10

1  
2  
3

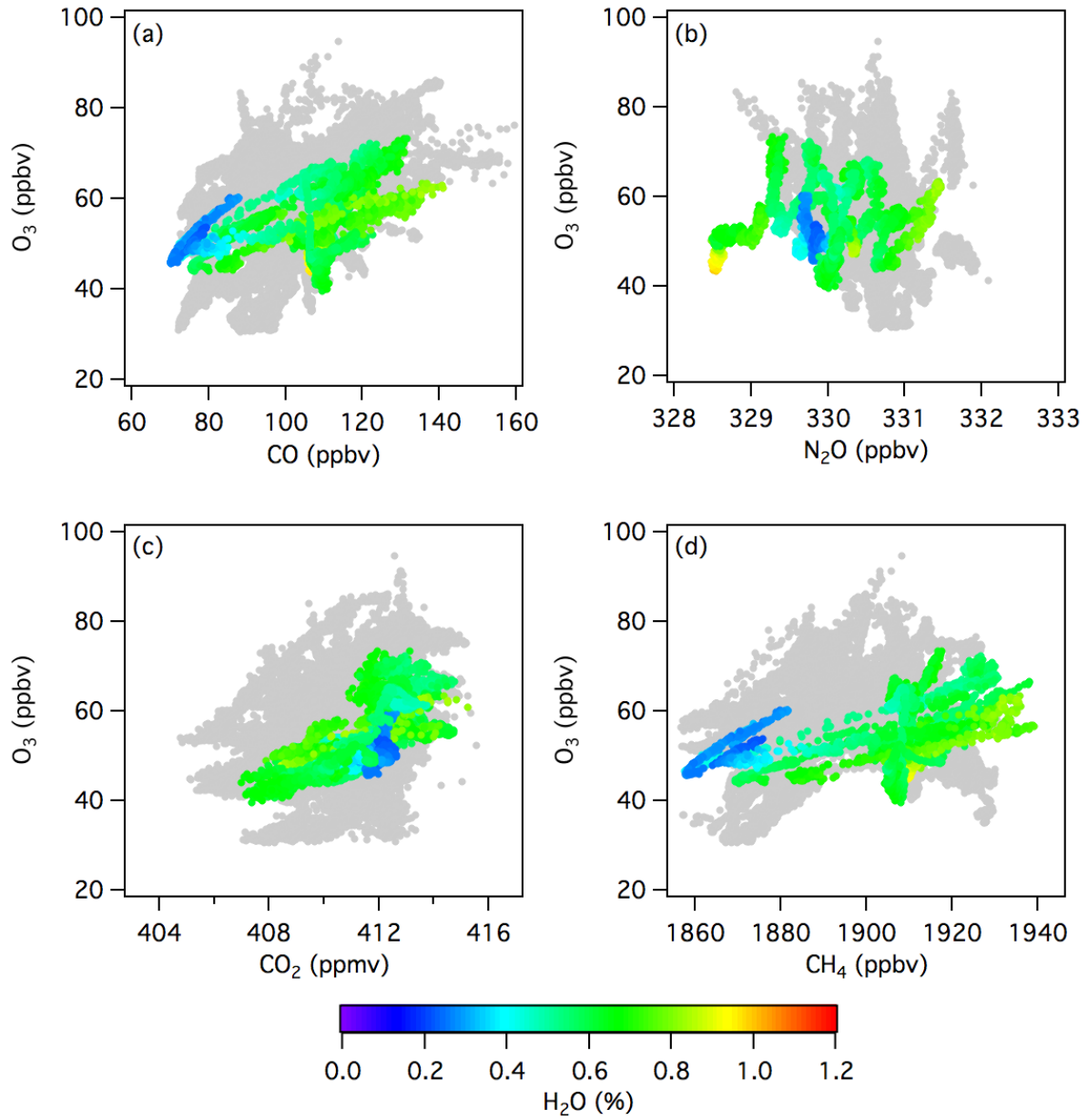
### Week 2



4  
5

1  
2  
3  
4  
5  
6

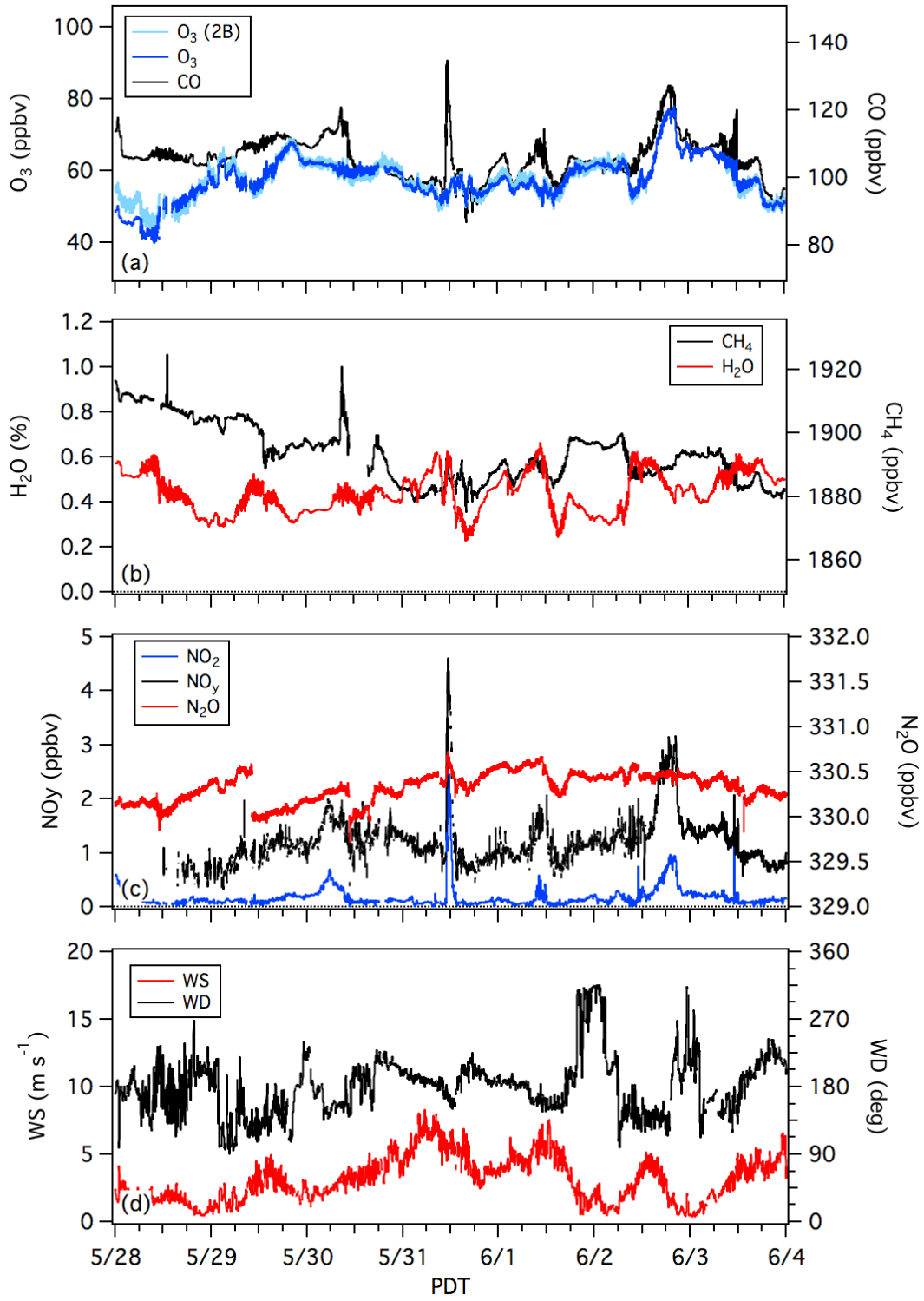
Week 2



7  
8  
9

1  
2  
3

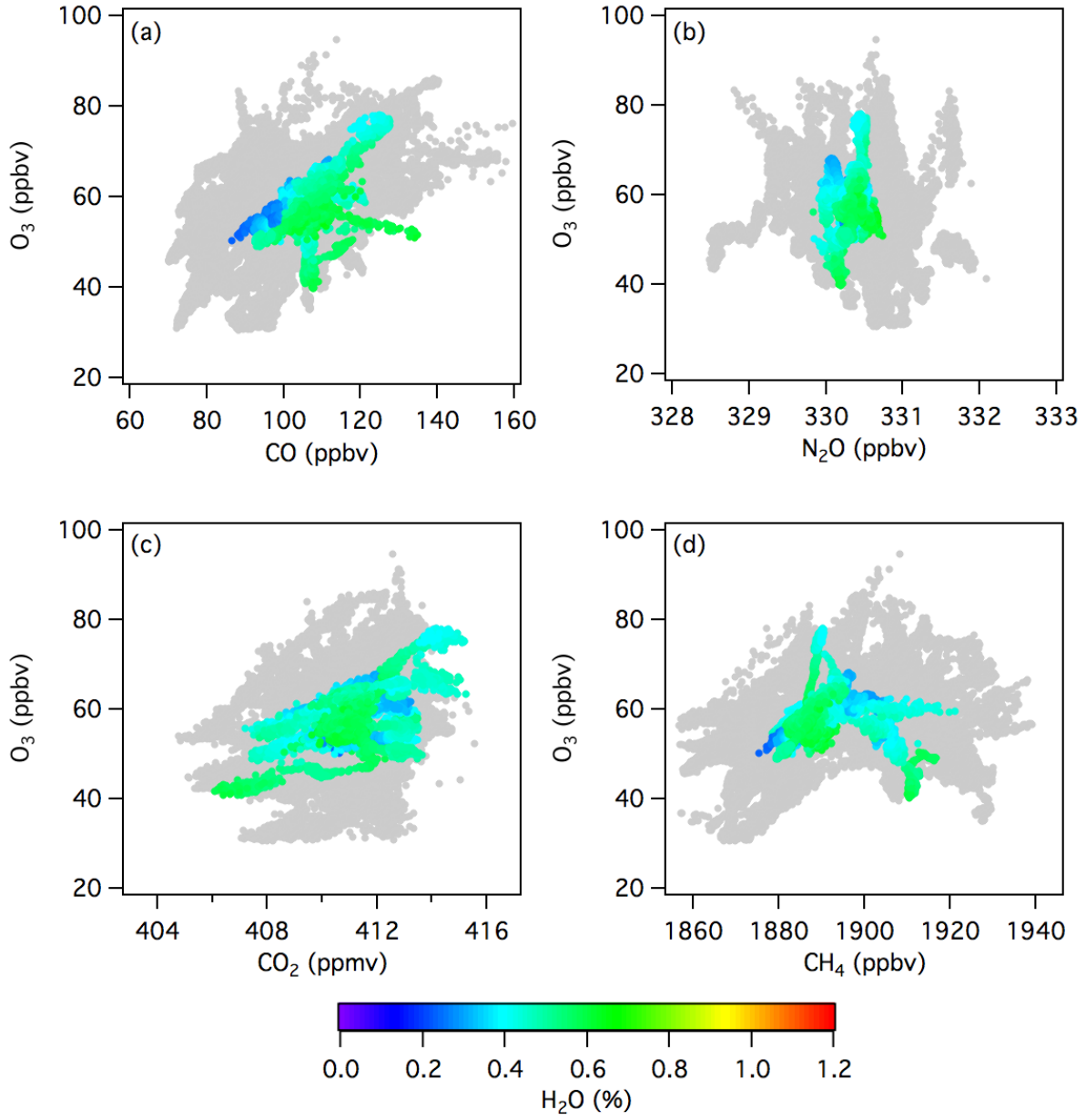
### Week 3



4  
5

1  
2  
3  
4  
5  
6

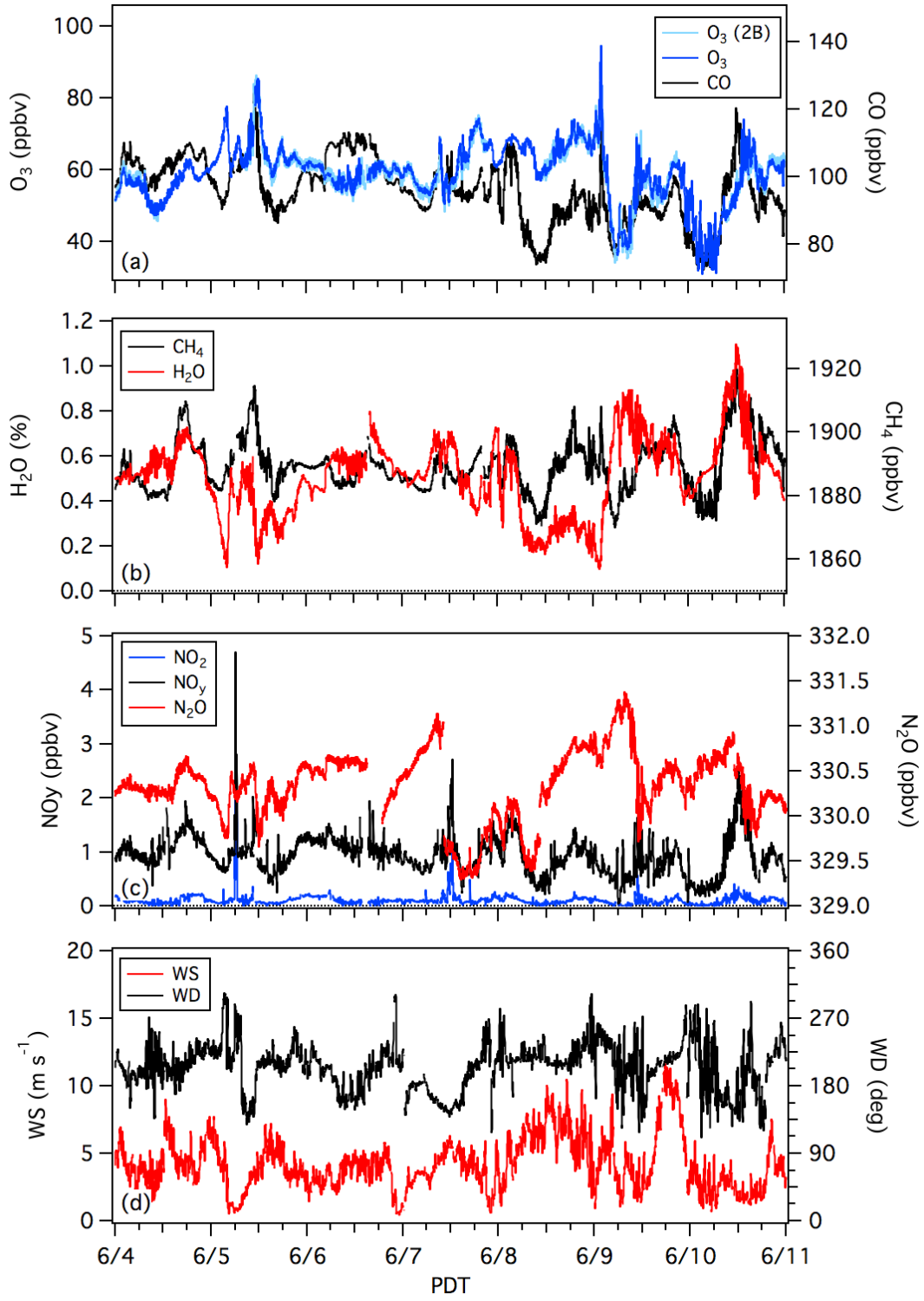
Week 3



7  
8  
9  
10  
11  
12

1  
2

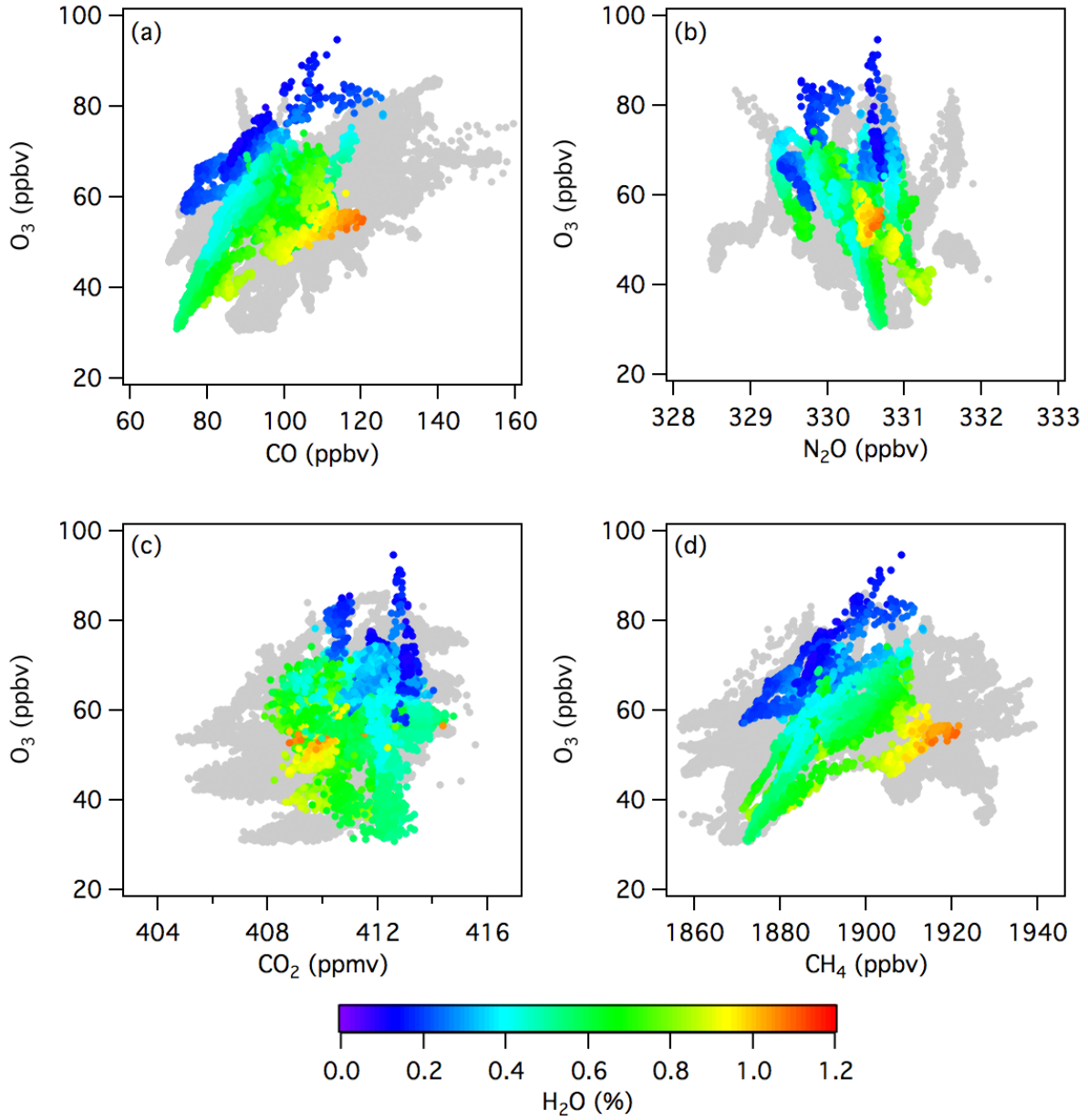
### Week 4



3  
4  
5

1  
2  
3  
4  
5  
6

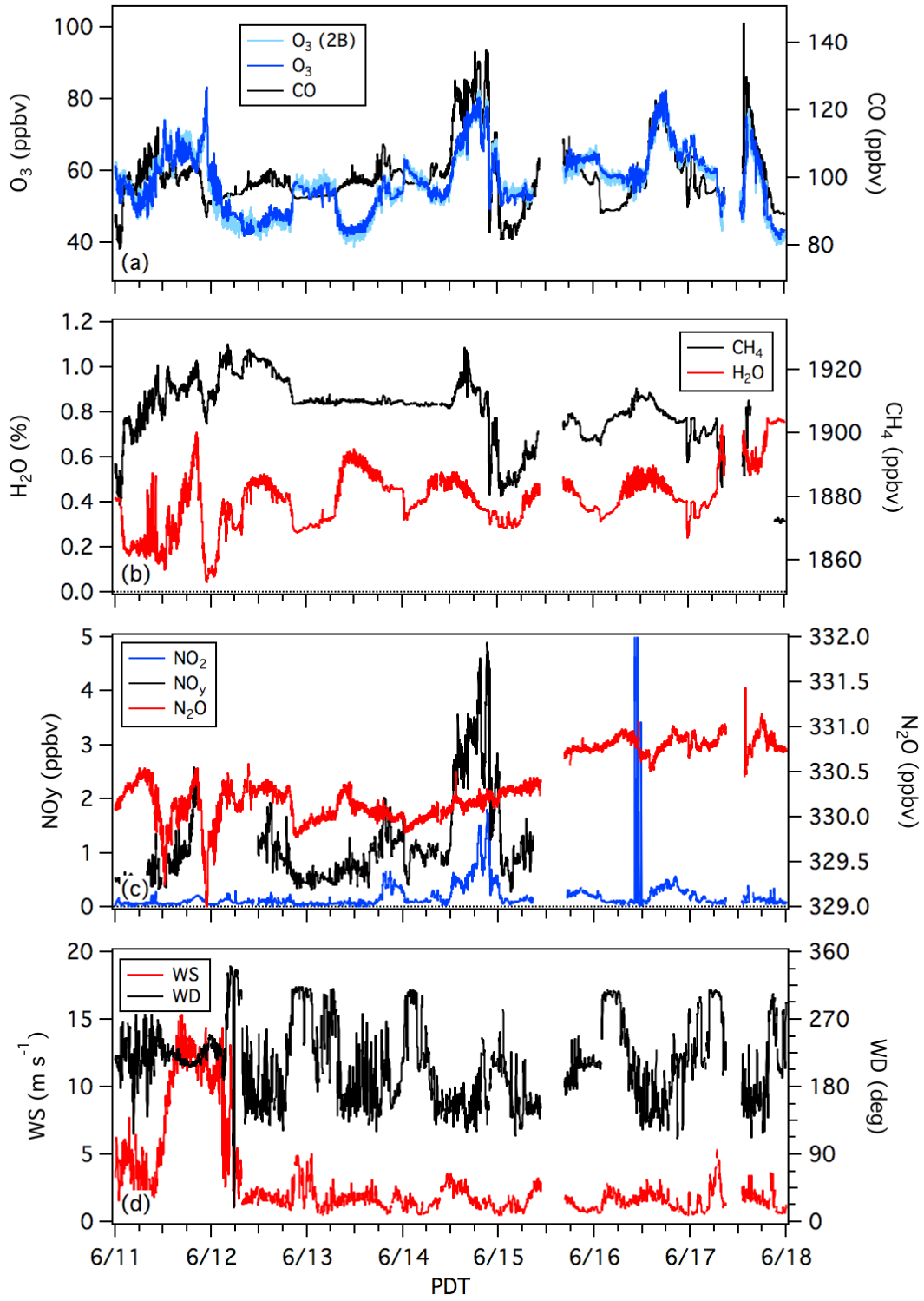
Week 4



7  
8  
9  
10  
11  
12

1  
2  
3

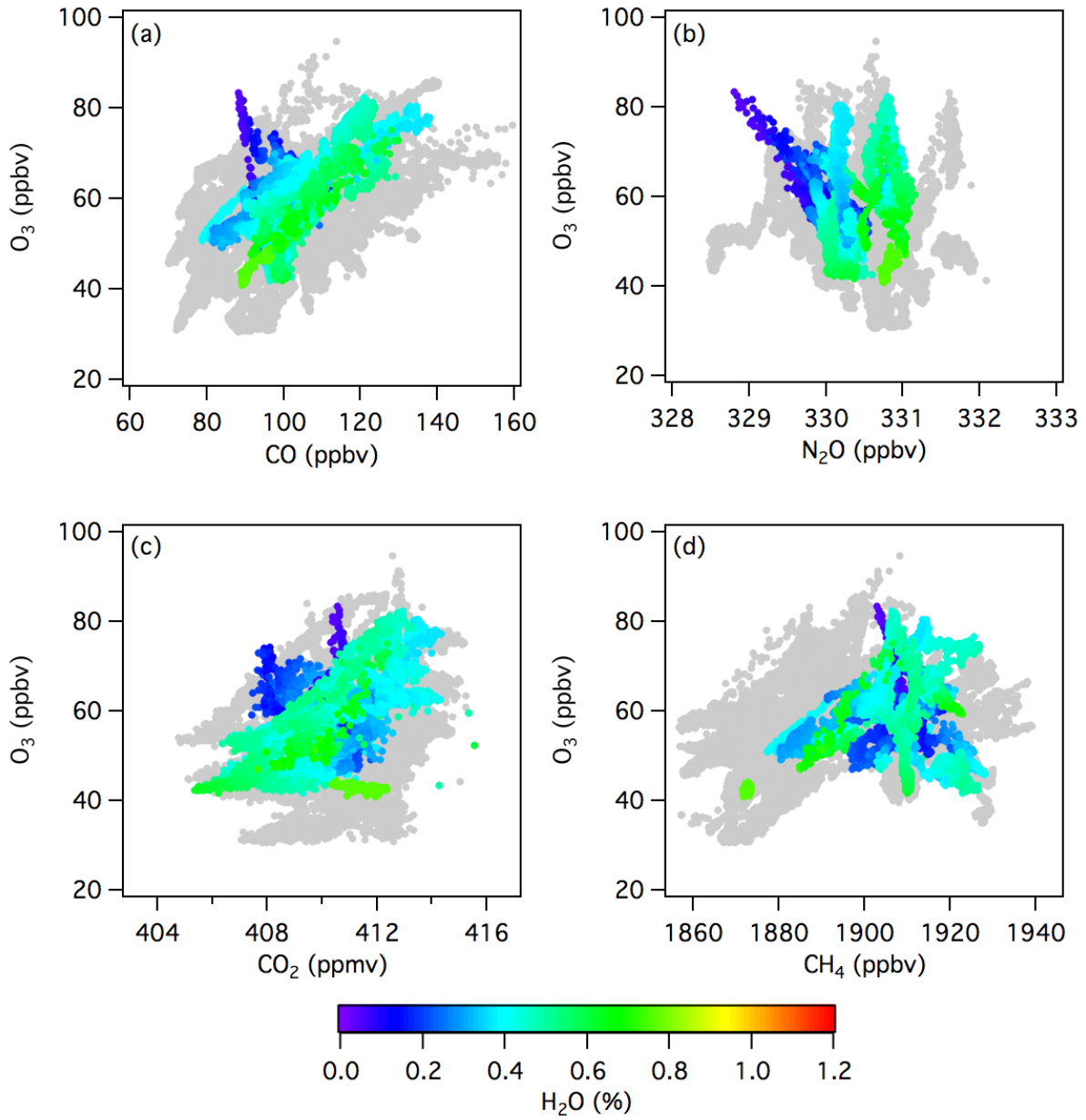
### Week 5



4  
5

1  
2  
3  
4  
5  
6

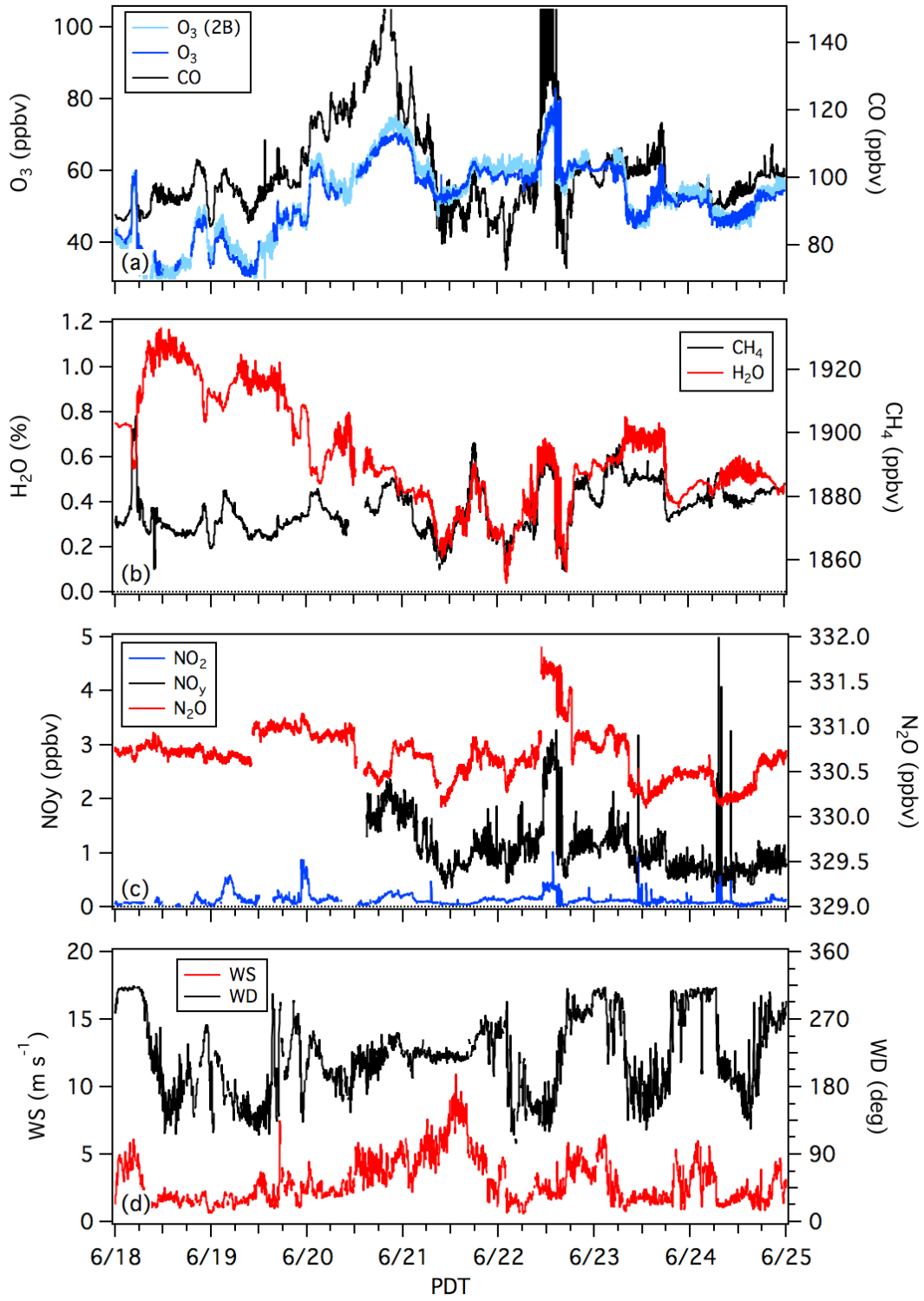
Week 5



7  
8  
9  
10  
11  
12

1  
2  
3

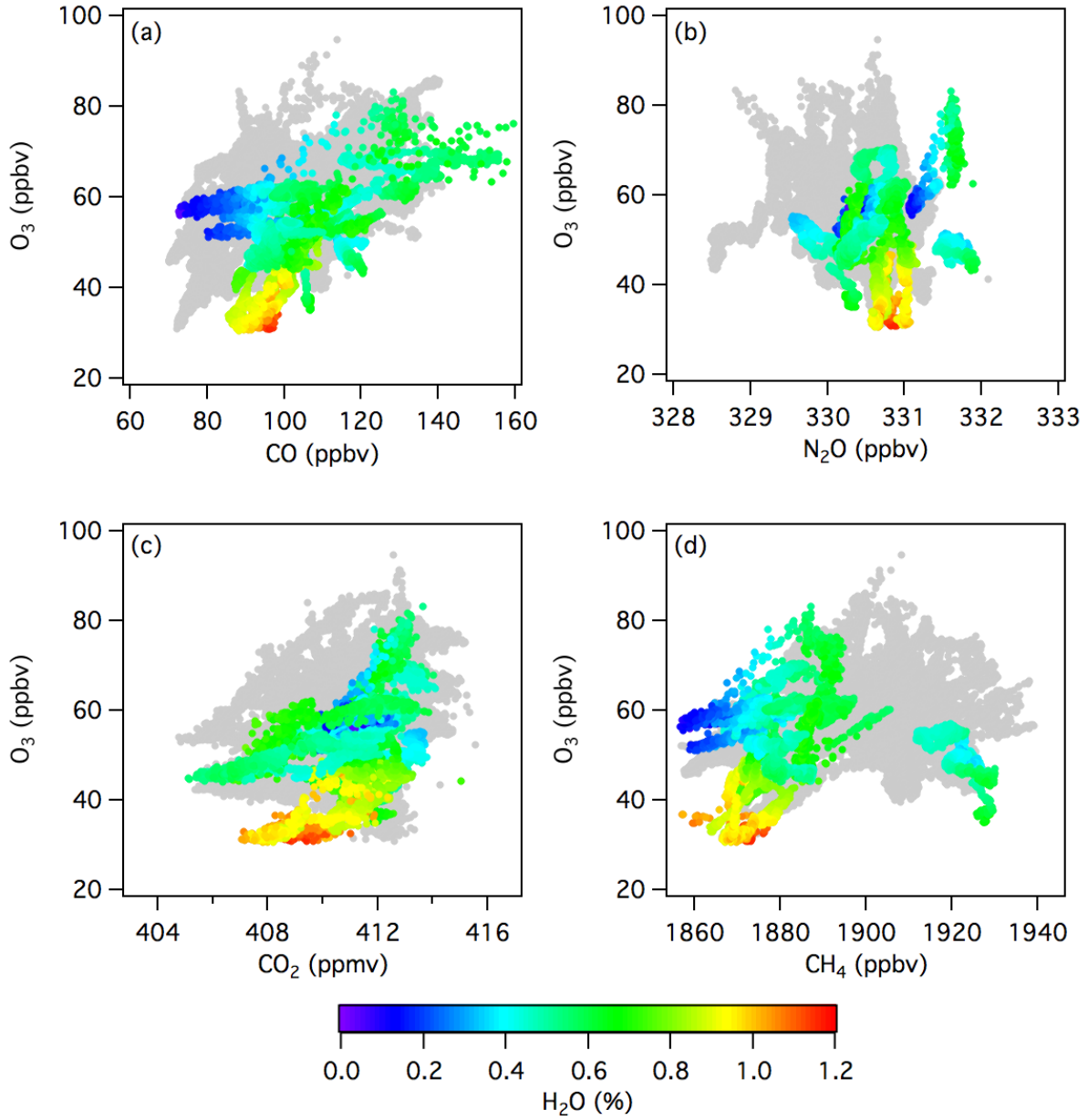
### Week 6



4  
5

1  
2  
3  
4  
5  
6

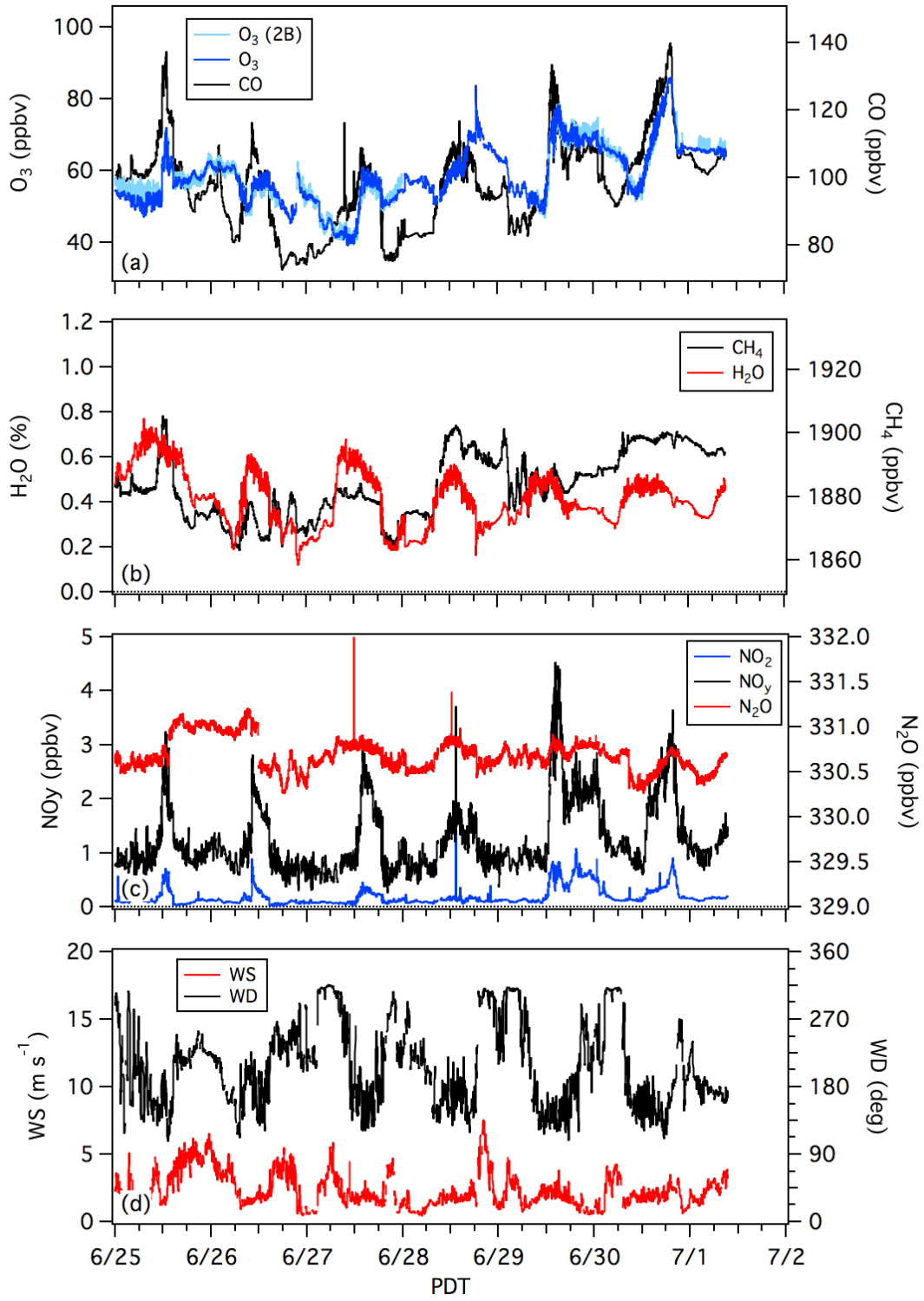
Week 6



7  
8  
9  
10  
11  
12

1  
2  
3

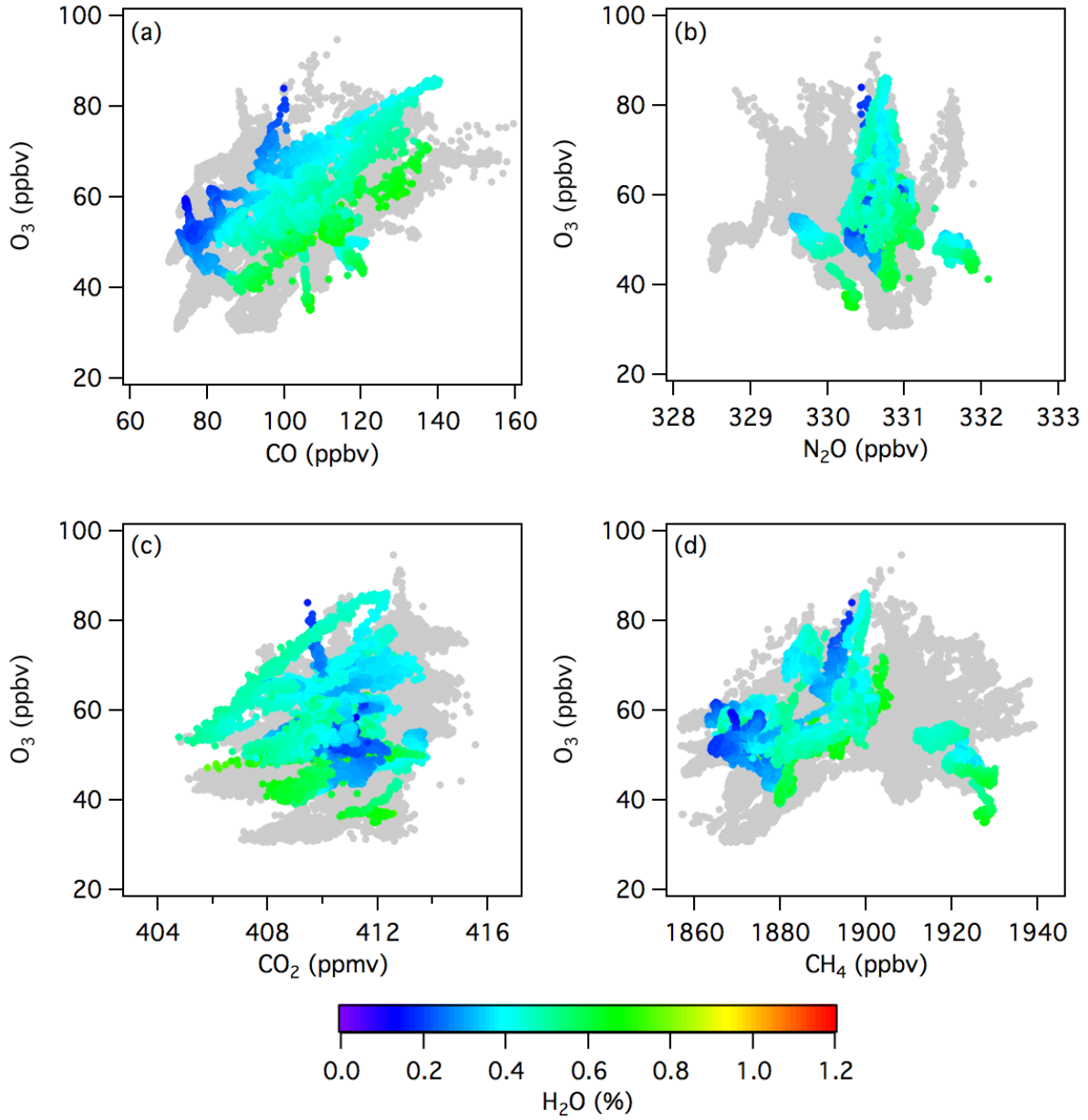
### Week 7



4  
5

1  
2  
3  
4  
5  
6

Week 7



7  
8  
9  
10

1 **Appendix D: NOAA/ESRL/GMD Ozonesonde Profiles**

2

3 This Appendix contains profile plots showing the O<sub>3</sub>, RH, and potential temperature profiles  
4 from the ozonesonde ascents during the FAST-LVOS IOPs. The horizontal dashed lines show the  
5 top of boundary layer inferred from the measurements.

6

7 The complete data are available at:

8 <https://www.esrl.noaa.gov/csd/groups/csd3/measurements/fastlvos/ozonesondes/>

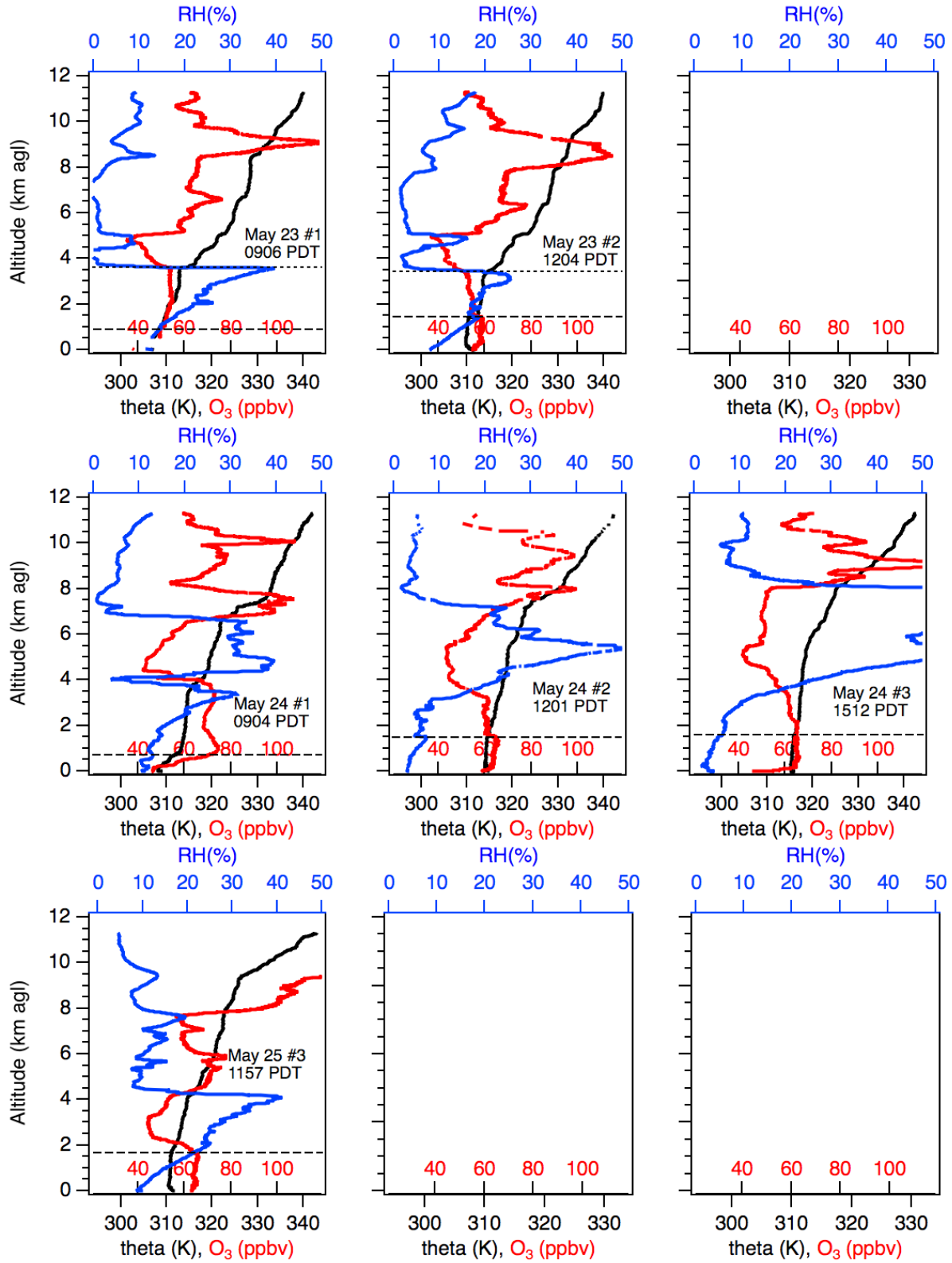
9

10

11

1  
2

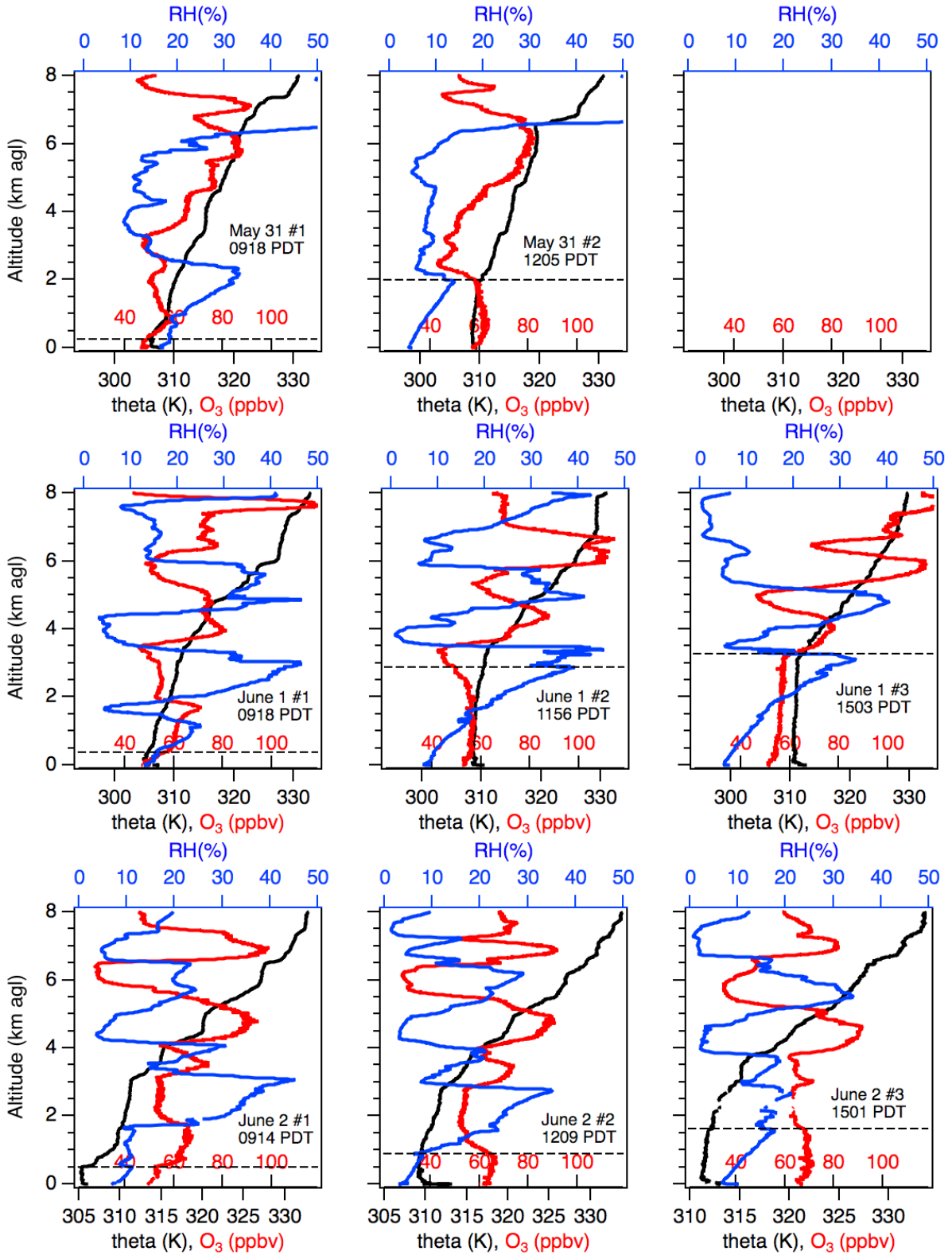
### IOP 1



3  
4

1  
2

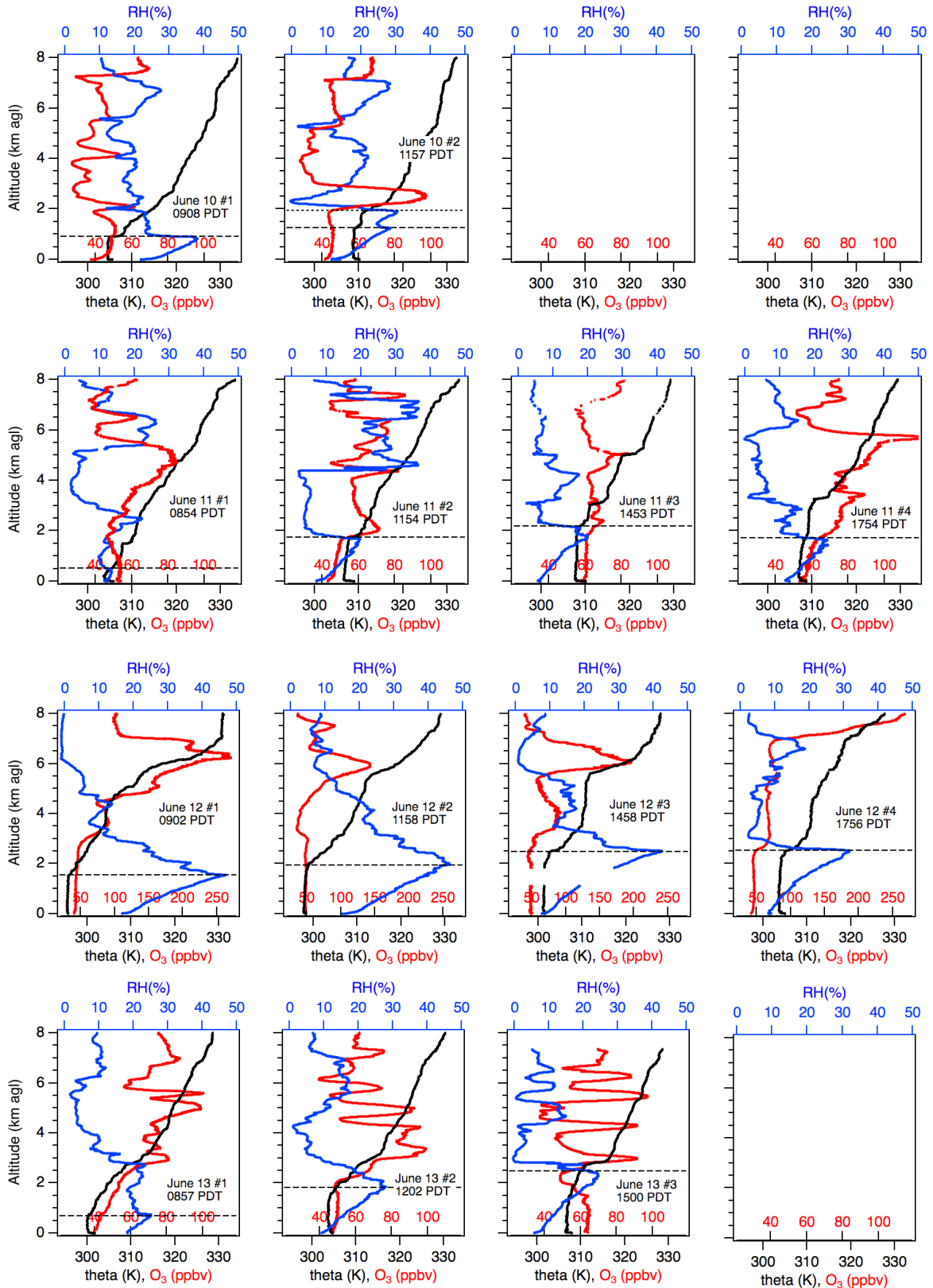
### IOP2



3

1  
2

### IOP3

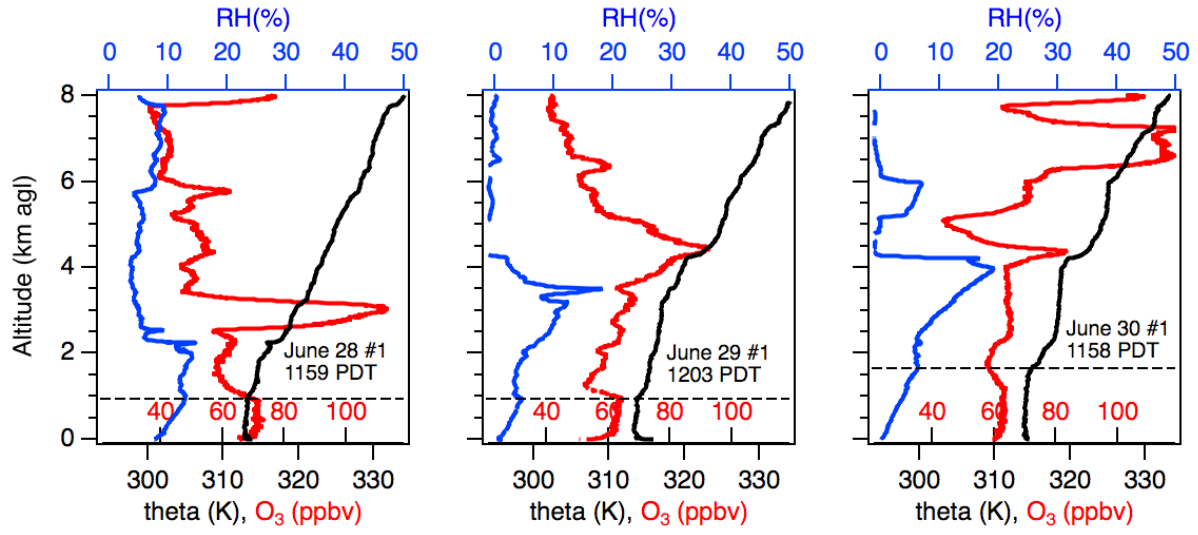


3

4

1  
2

### IOP4



3  
4  
5  
6  
7  
8

1 **Appendix E: Scientific Aviation Airborne Measurements**

2

3 This Appendix contains flight track maps and profile plots showing the Scientific Aviation O<sub>3</sub>  
4 measurements during the FAST-LVOS IOPs. The daily maps shown first also display the MDA8  
5 ozone measured by the regulatory monitors; both these and the flight tracks are colorized using  
6 the TOLNet color scale. The altitude-latitude (northern Clark County only) and altitude-  
7 longitude plots shown next are also colorized by ozone using this scale. The final set of plots for  
8 each IOP shows the relative humidity, ozone, and methane profiles measured on the late  
9 morning ascents from and afternoon descents into the NLVA.

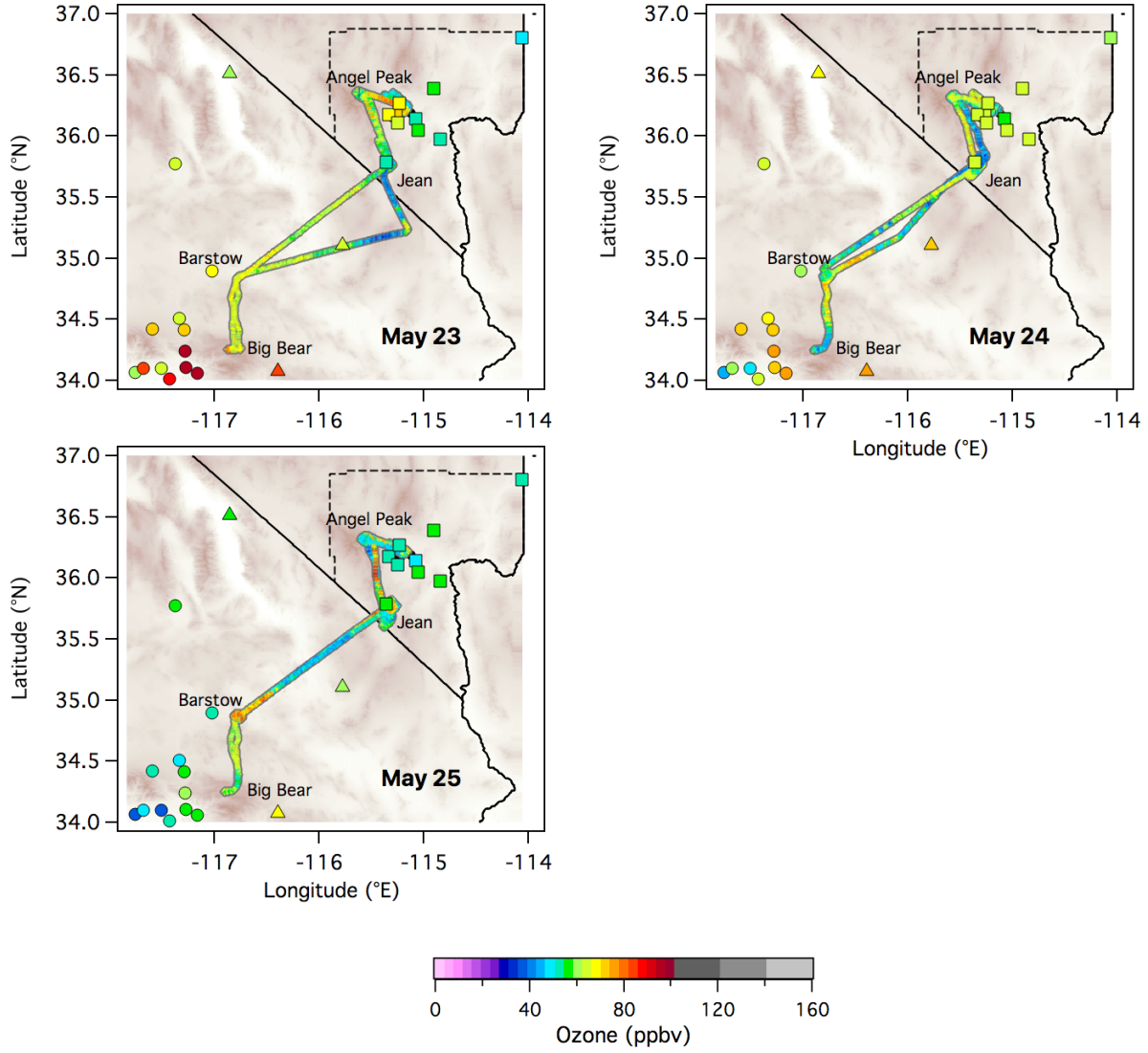
10

11 The complete data files are available on request from [andrew.o.langford@noaa.gov](mailto:andrew.o.langford@noaa.gov).

12

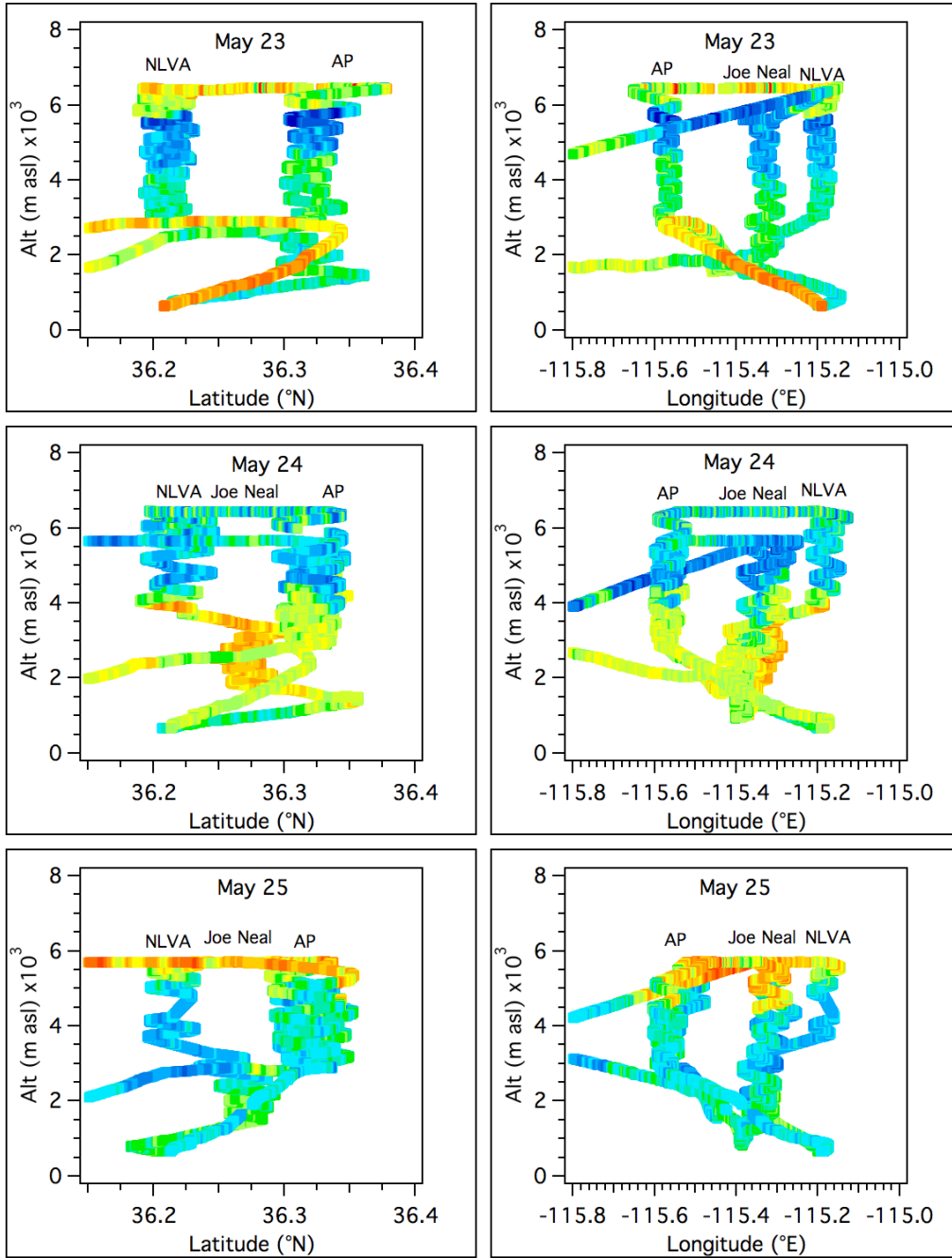
1  
2  
3  
4  
5

### IOP 1



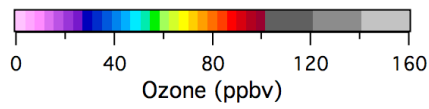
6  
7  
8

1  
2

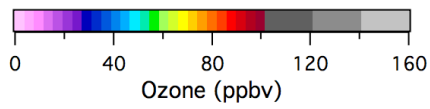
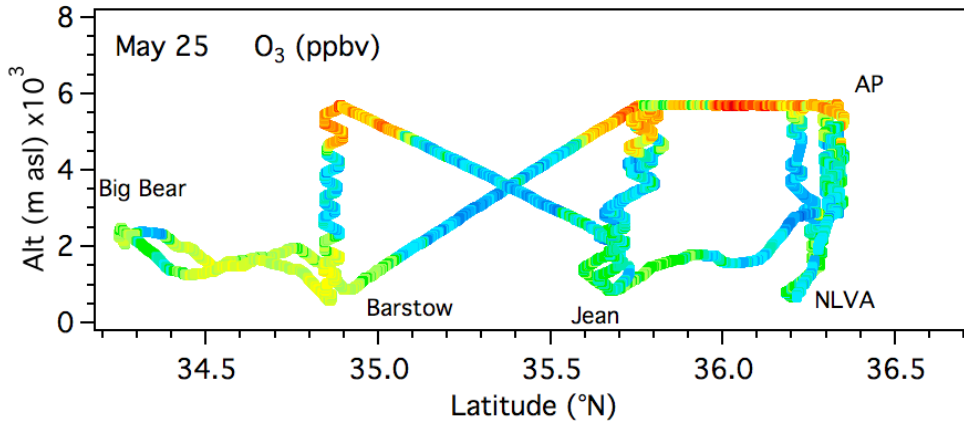
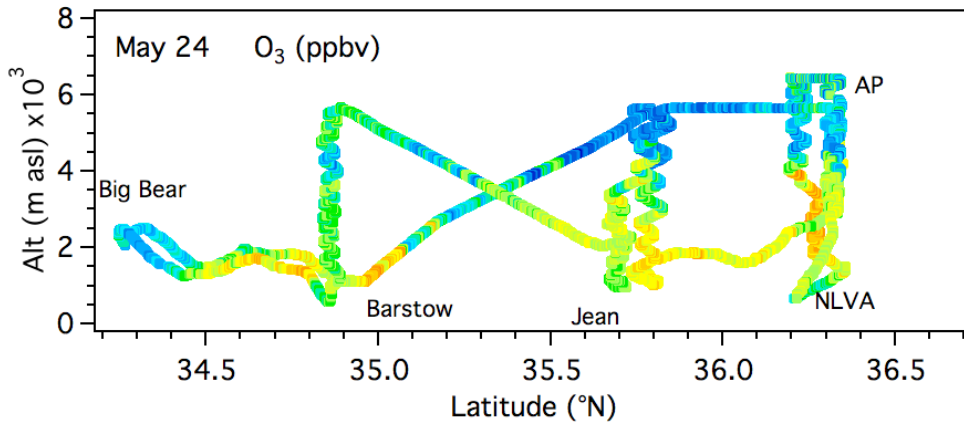
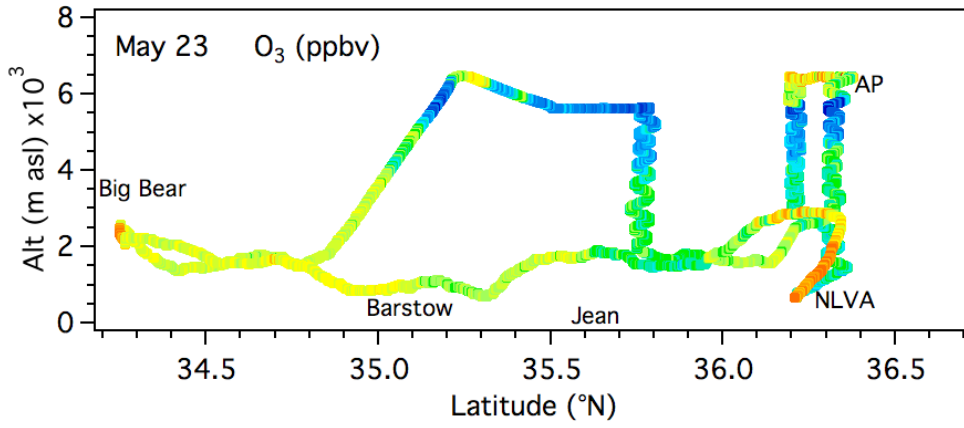


3  
4

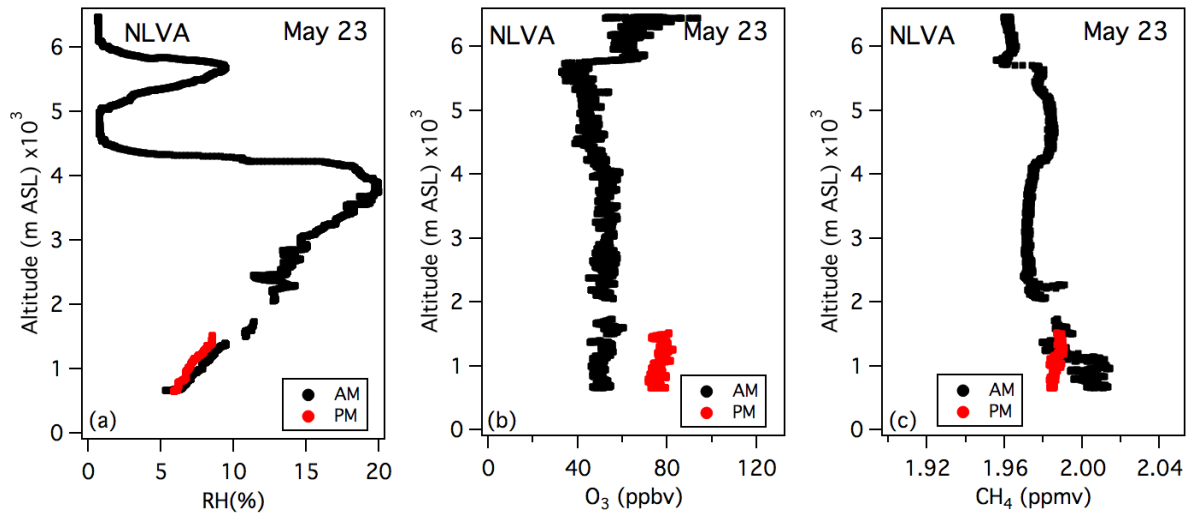
5  
6  
7  
8



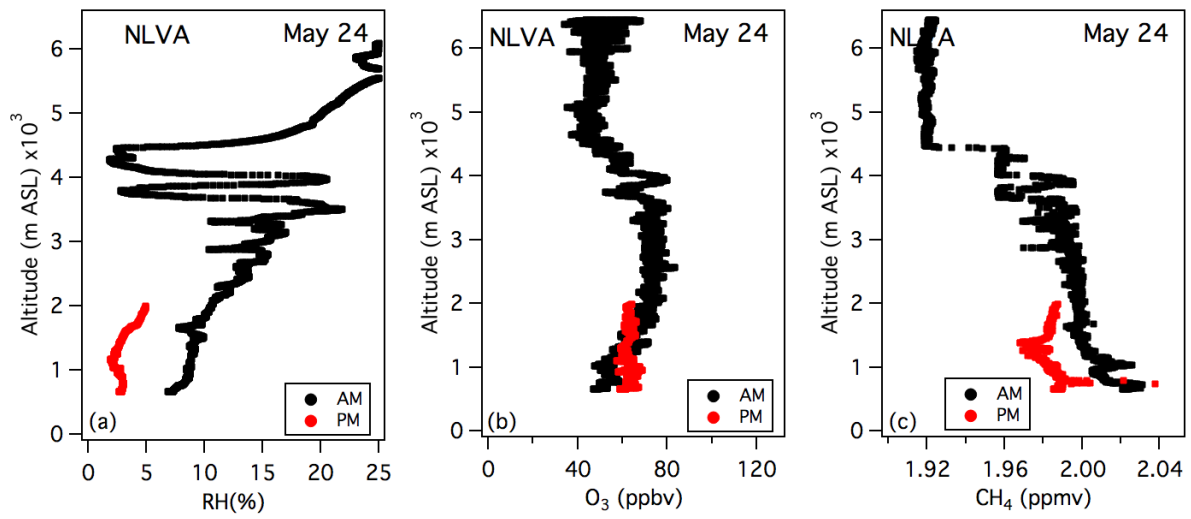
1  
2



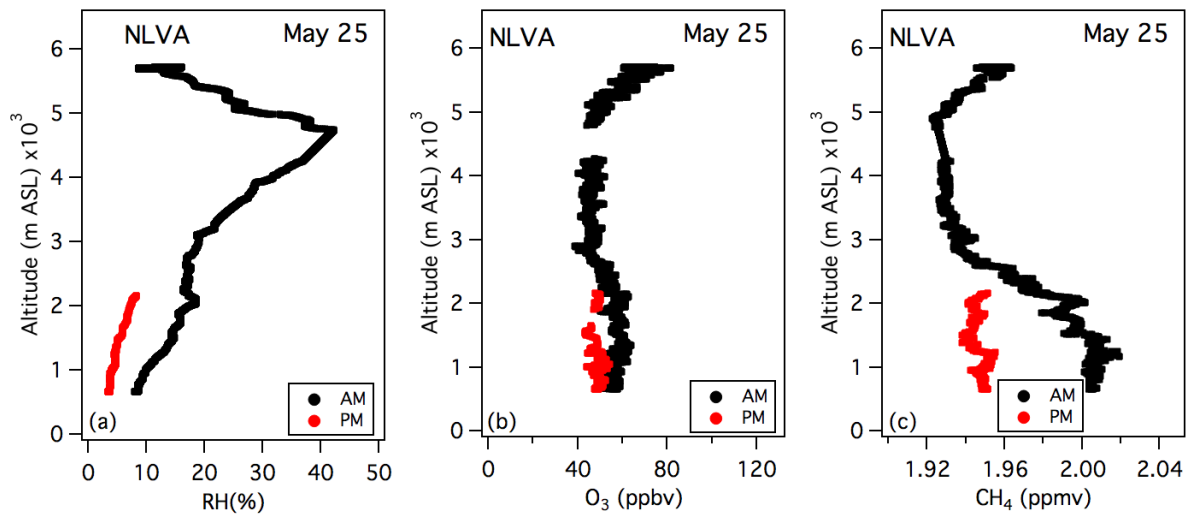
3  
4  
5



1



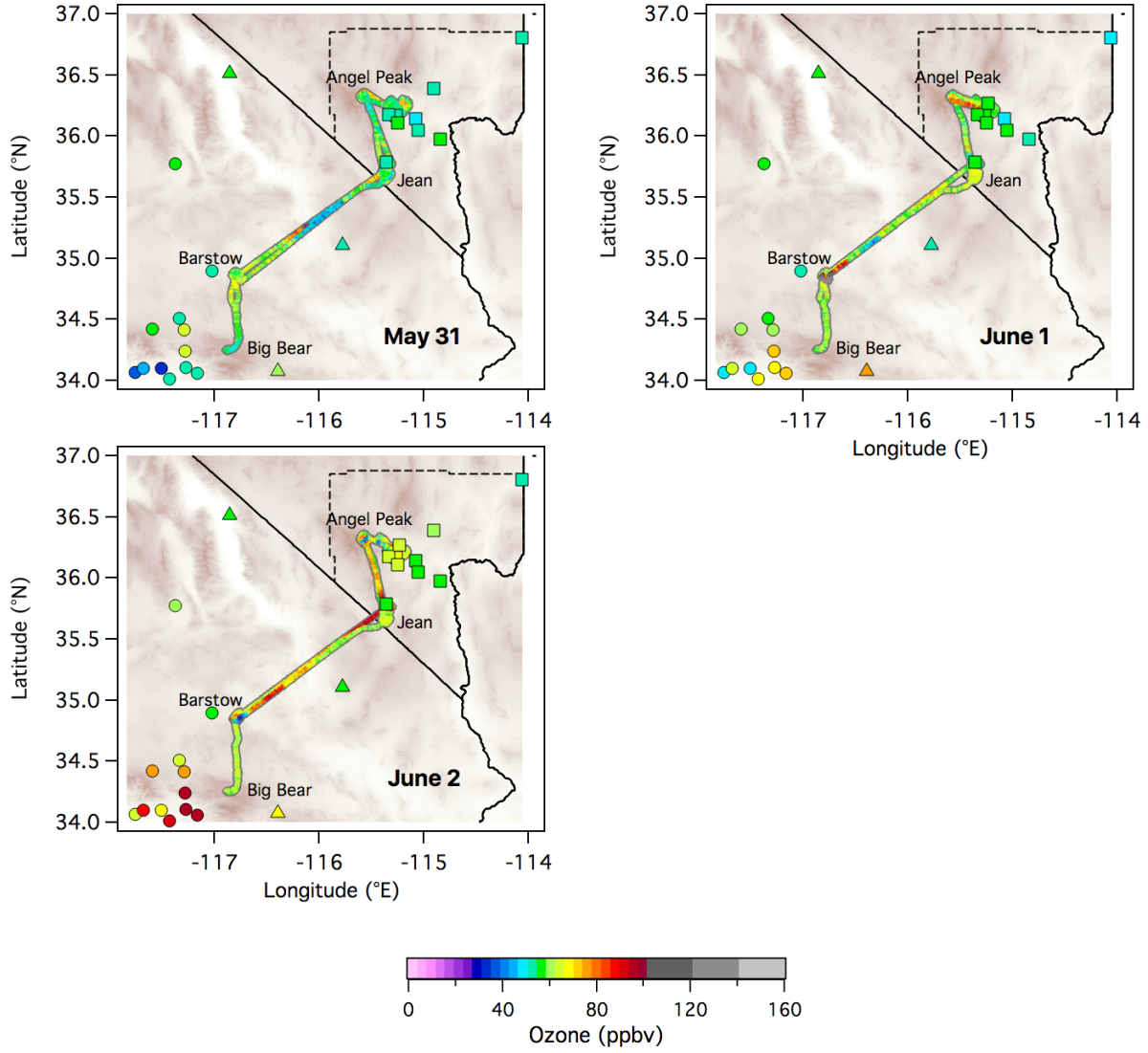
2



3

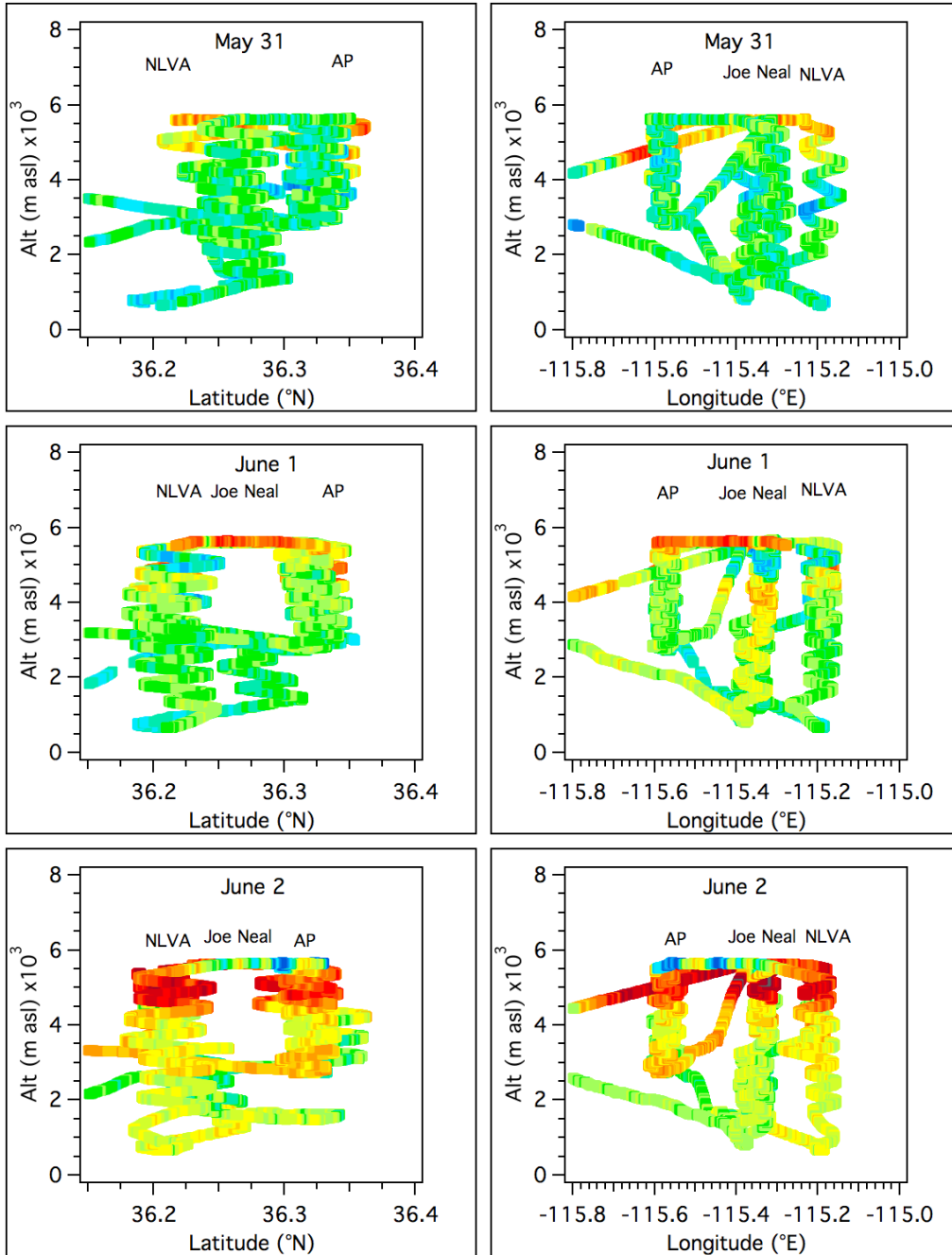
1  
2  
3  
4  
5

### IOP2



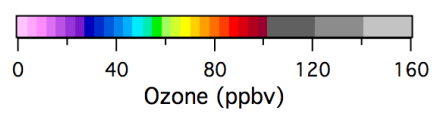
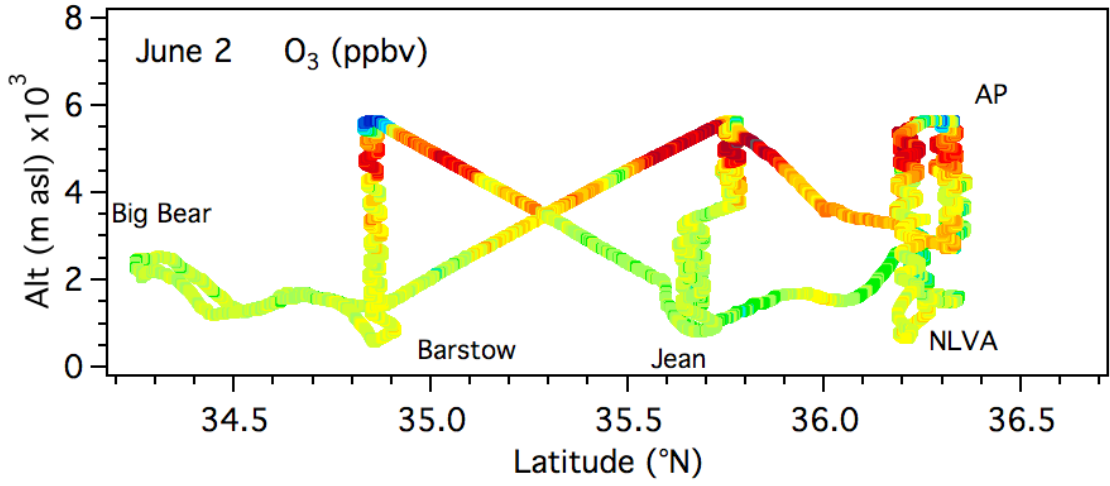
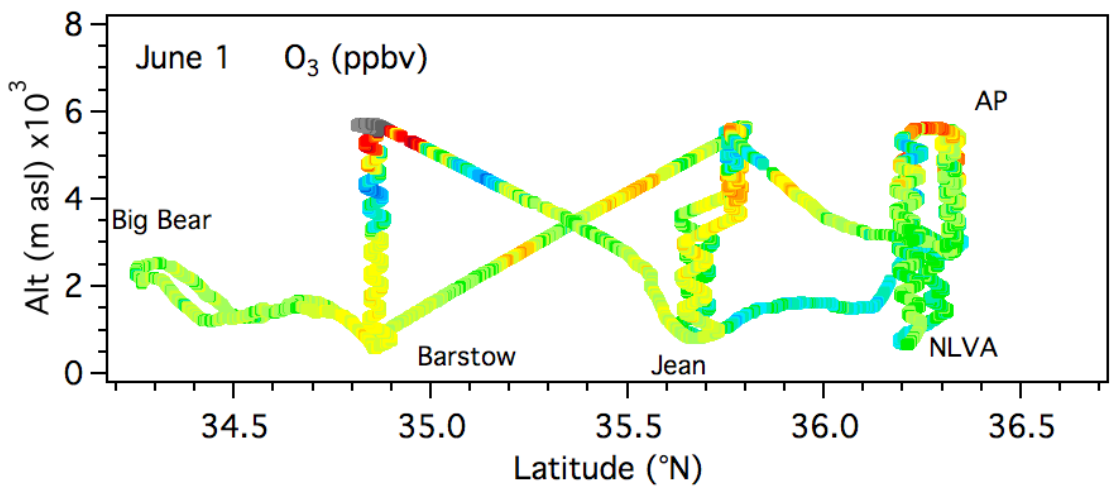
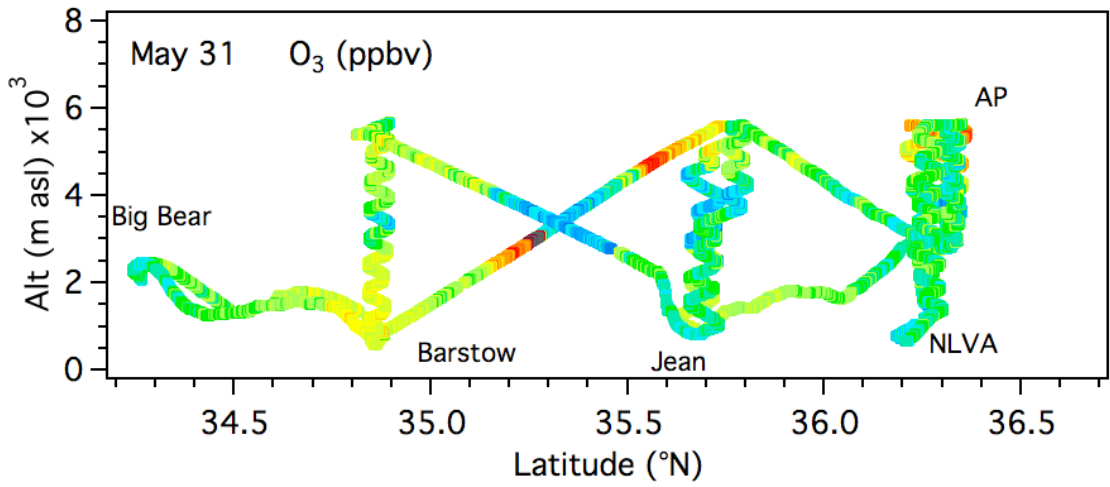
6  
7

8  
9  
10  
11  
12  
13  
14  
15  
16  
17  
18

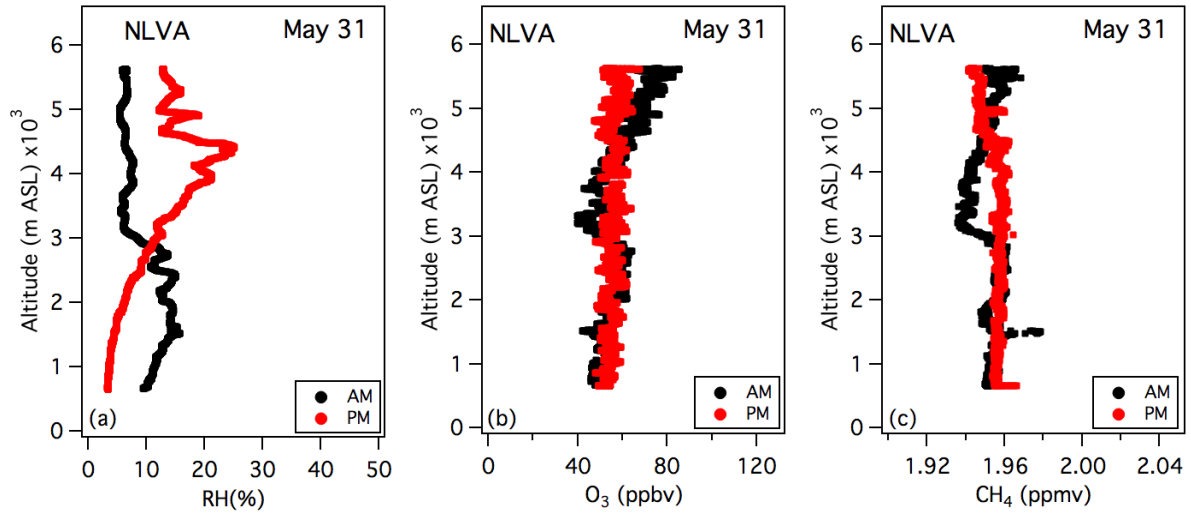


1  
2

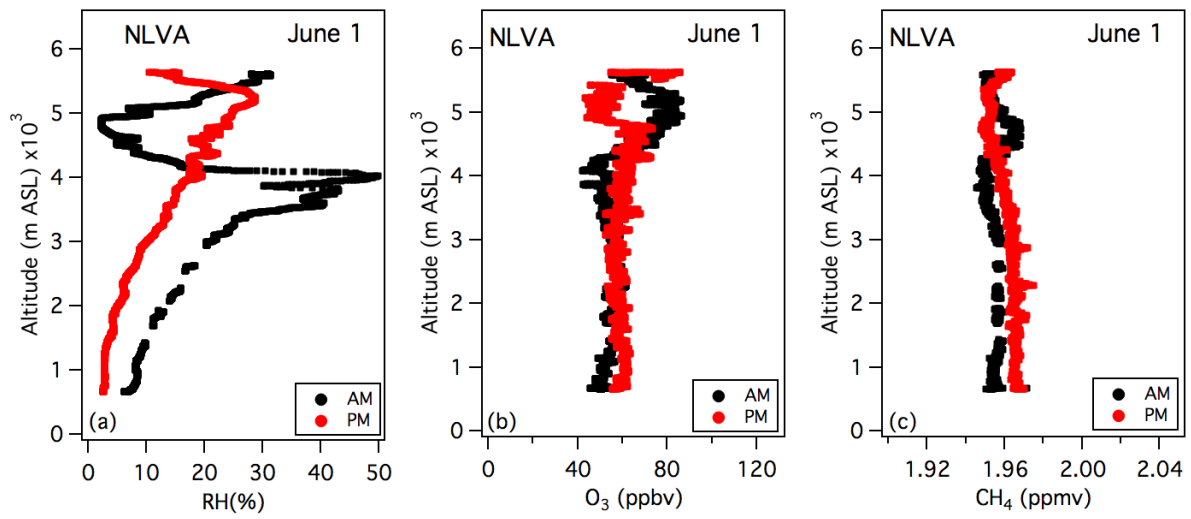
3  
4  
5  
6  
7



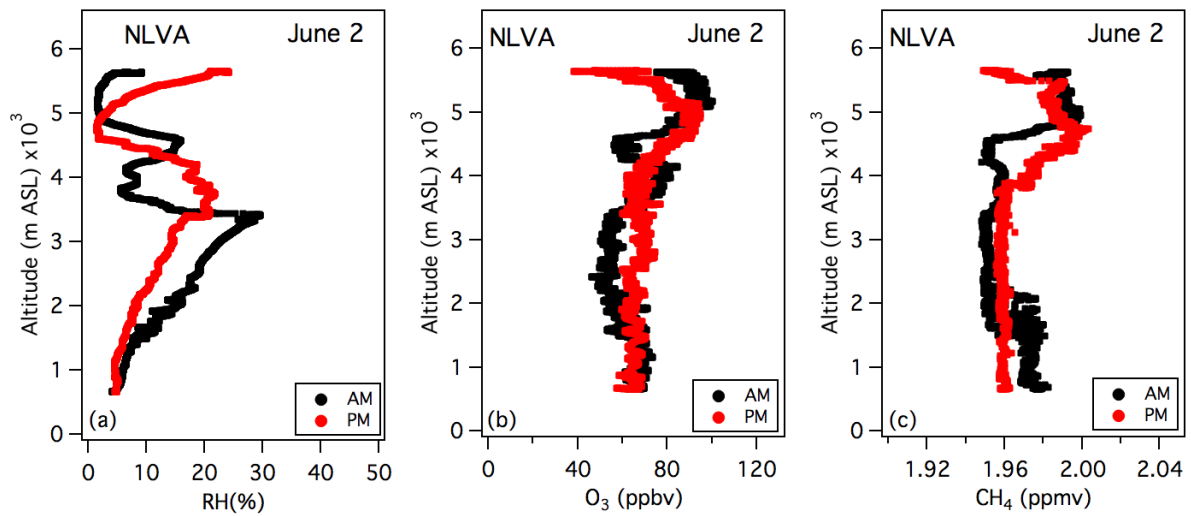
1  
2  
3



1



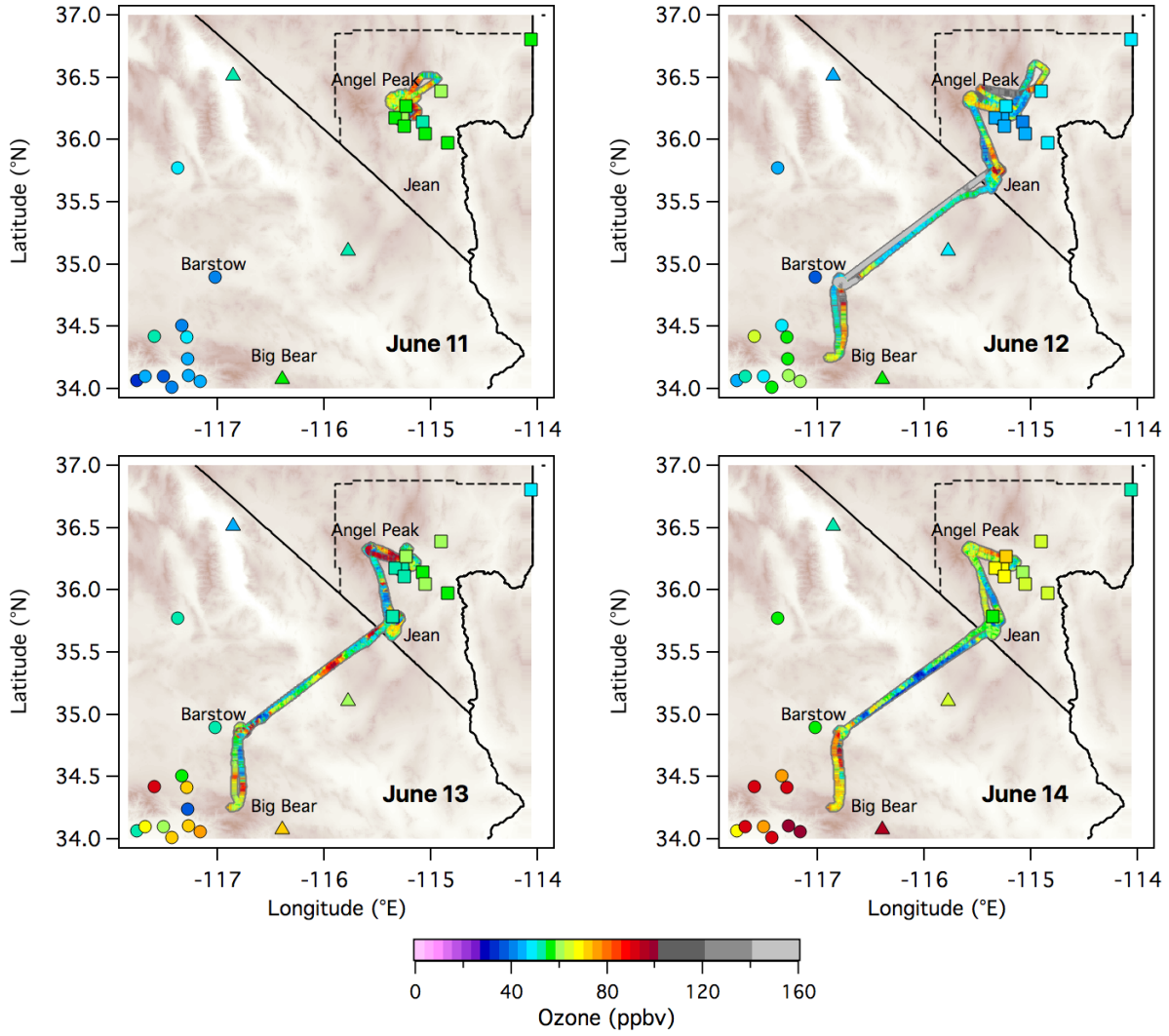
2



3

1  
2  
3  
4

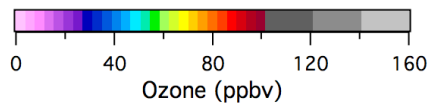
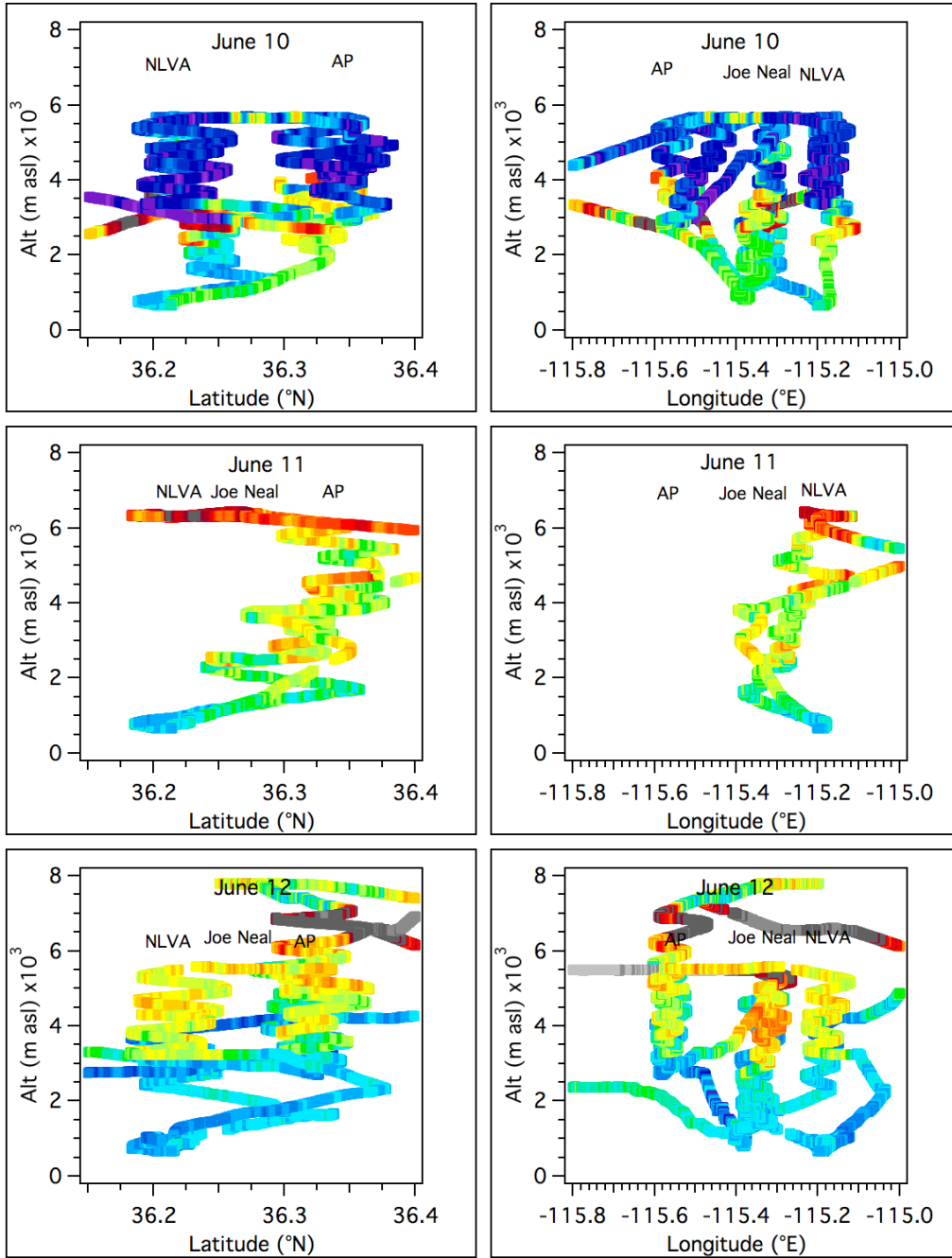
### IOP3



5

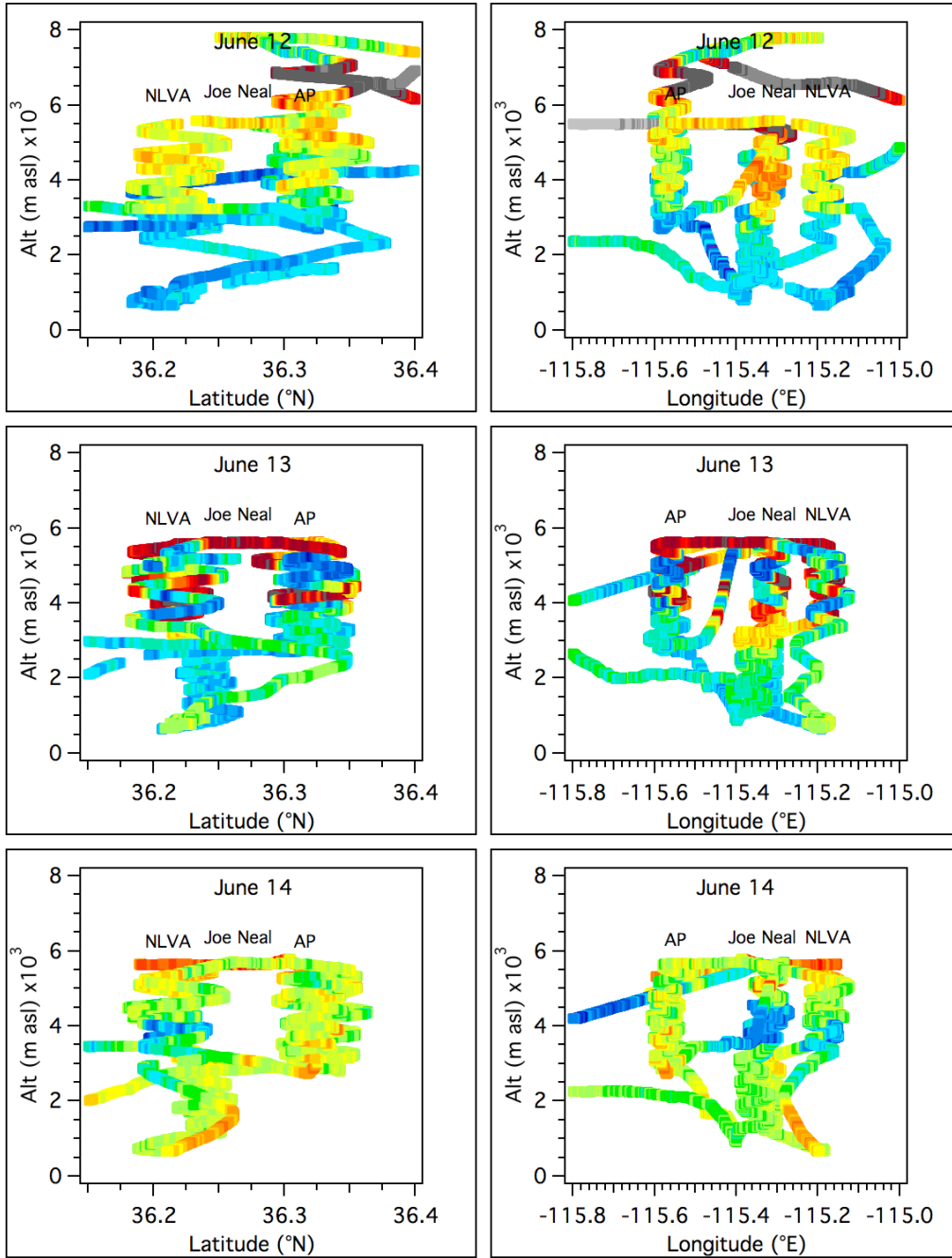
6  
7  
8  
9  
10  
11  
12  
13  
14  
15  
16  
17  
18

1  
2



3  
4  
5  
6  
7  
8

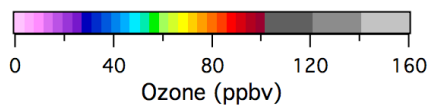
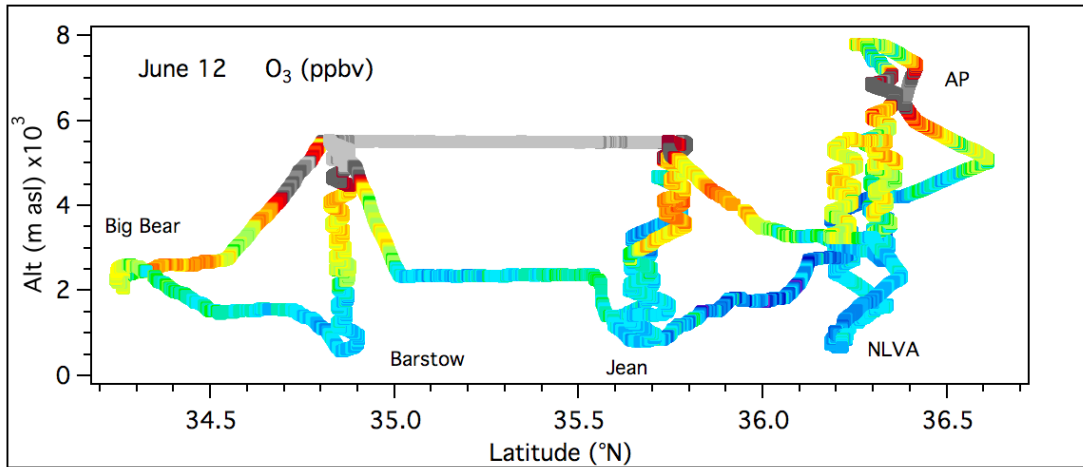
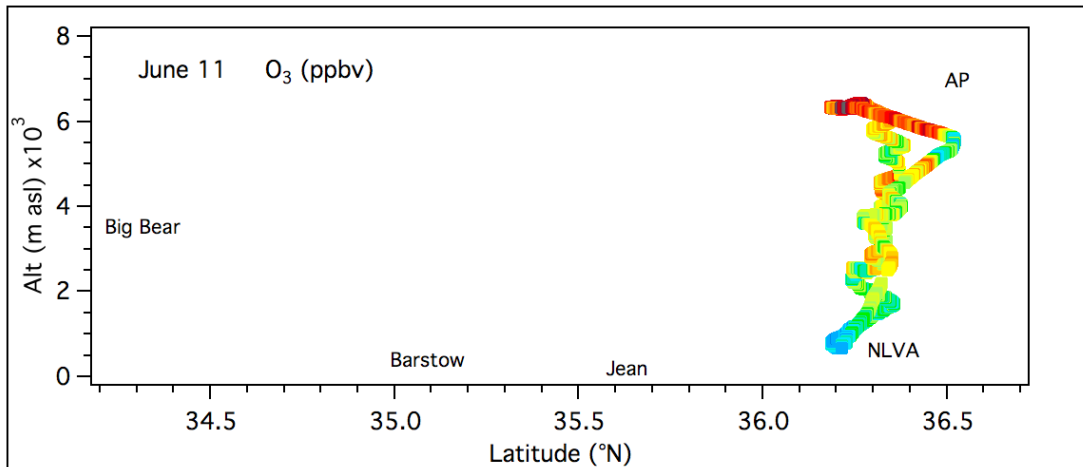
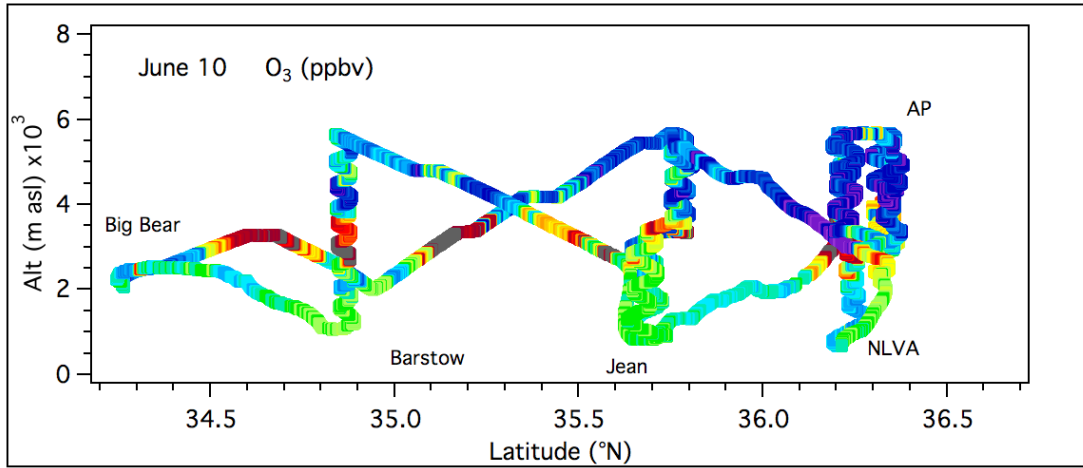
1  
2



3  
4

5  
6

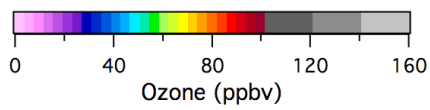
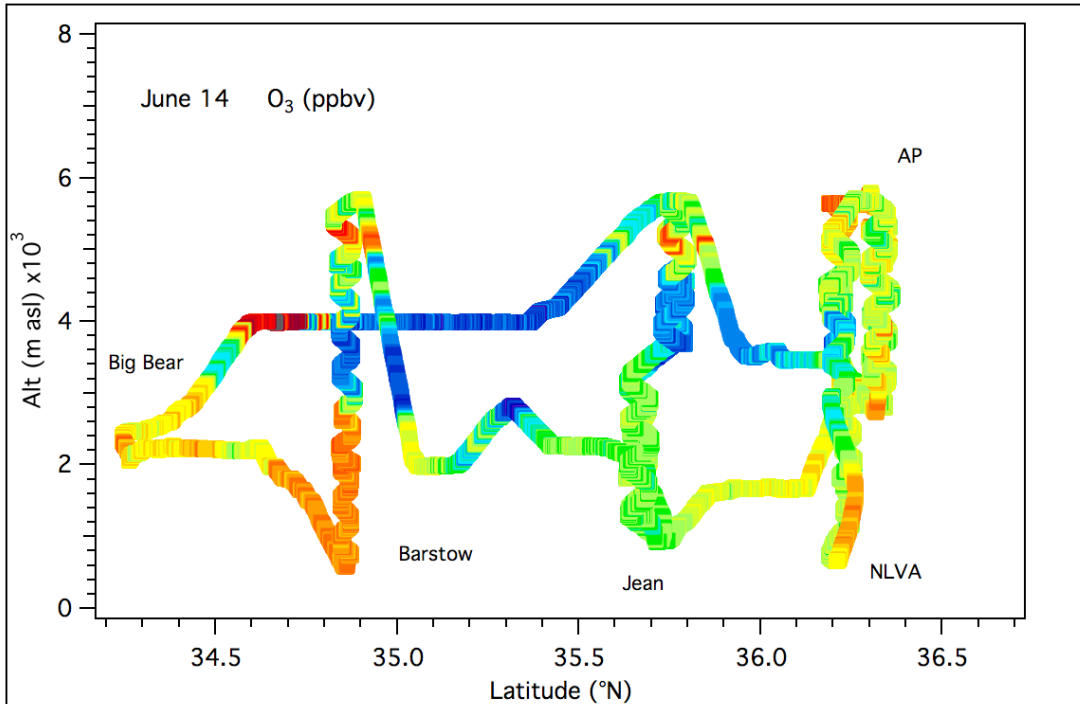
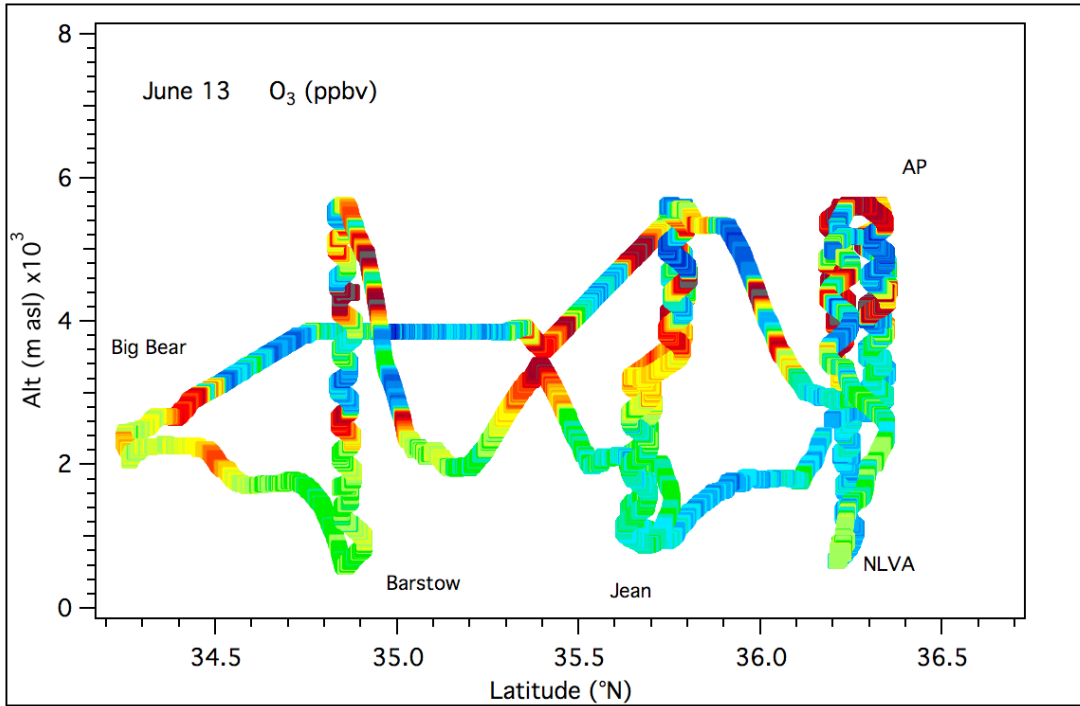
1  
2



3  
4

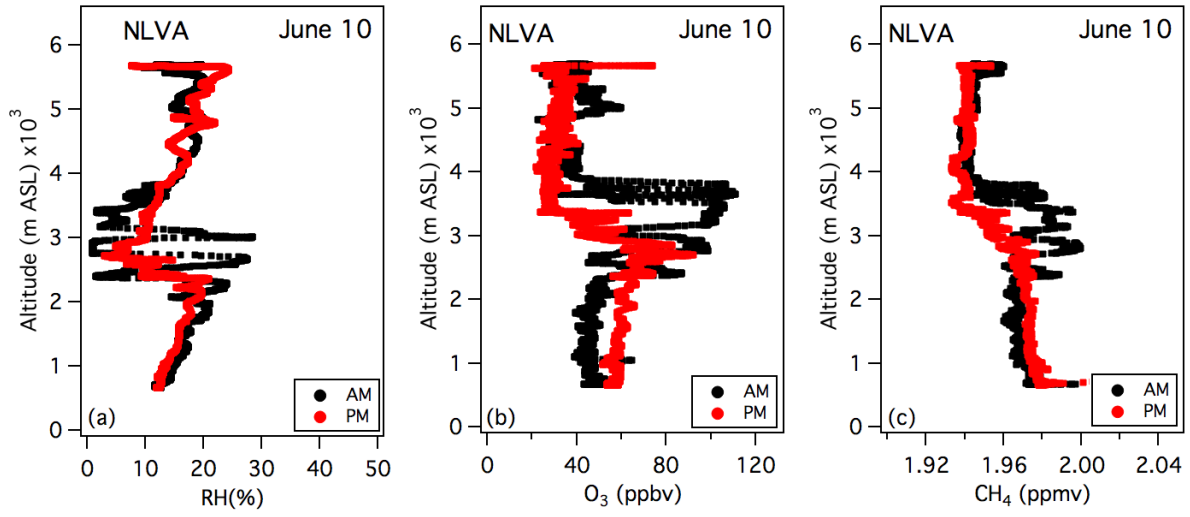
5  
6

1  
2

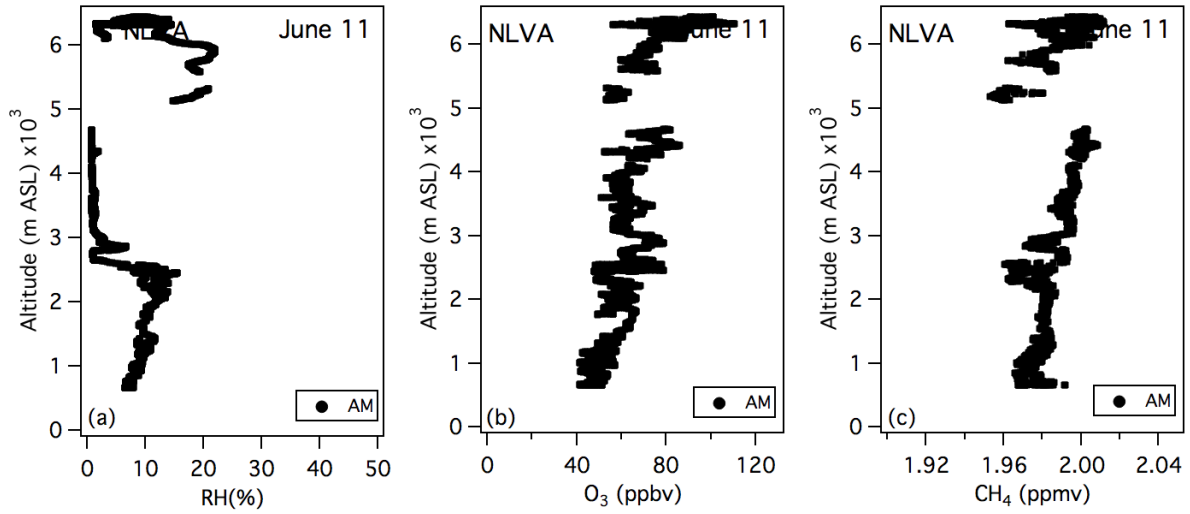


3  
4  
5

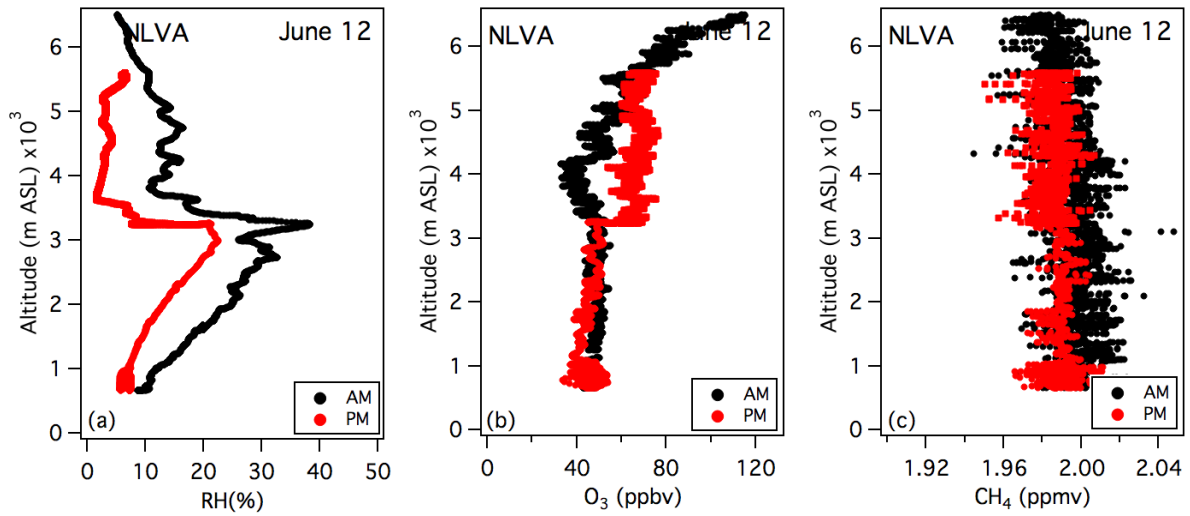
1  
2



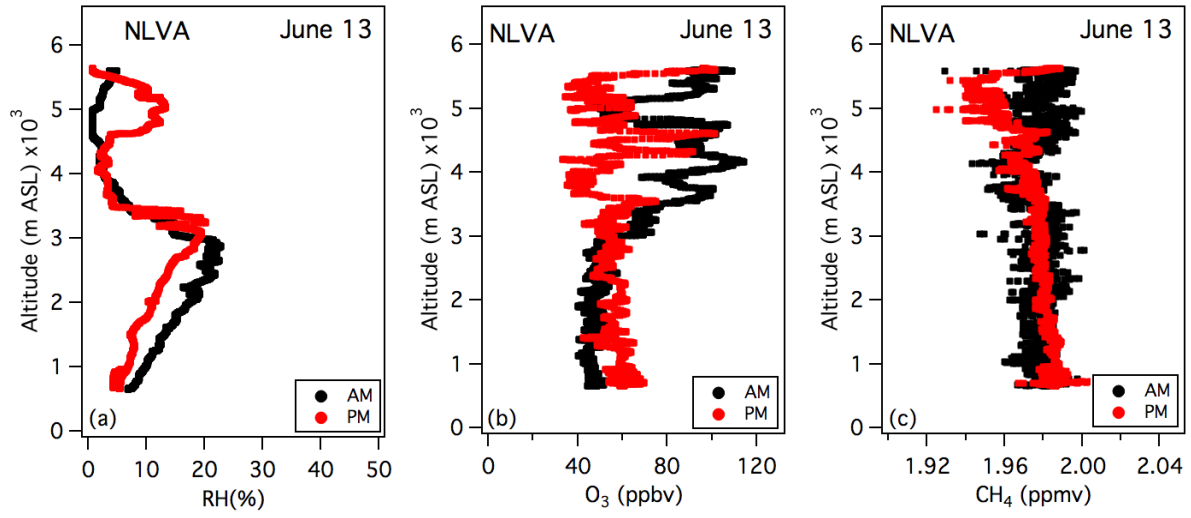
3



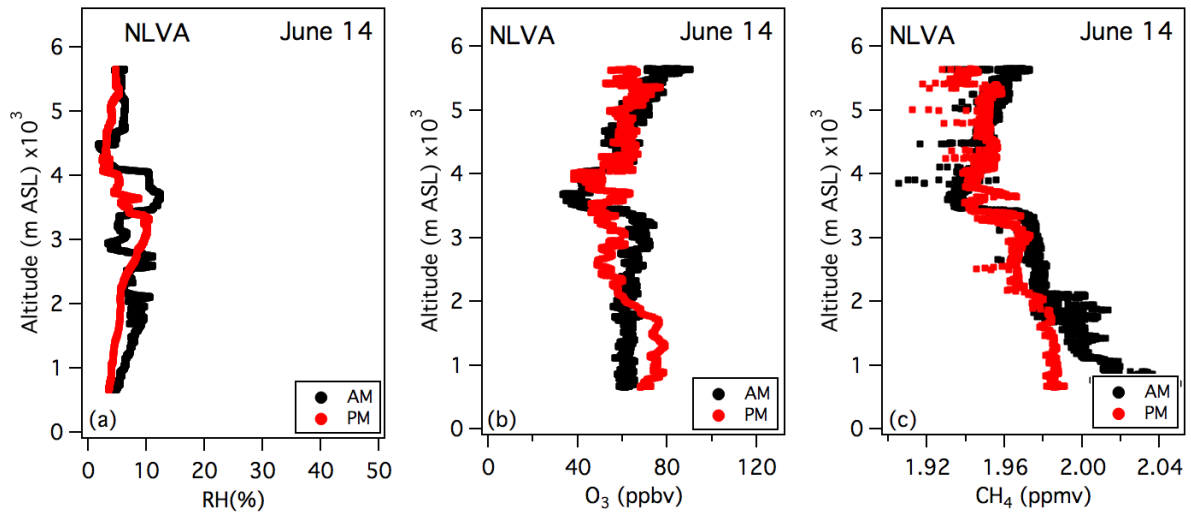
4



5



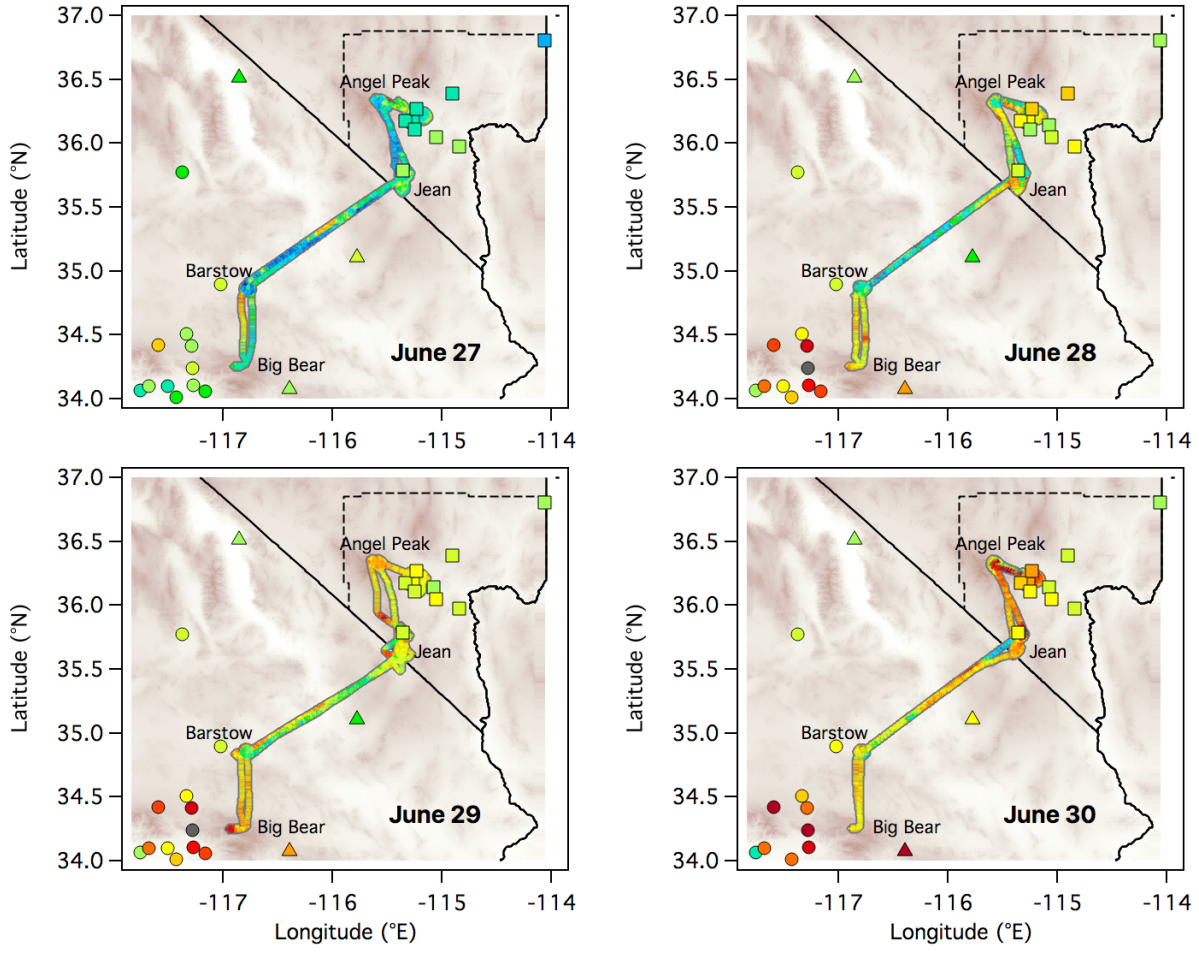
1



2

1  
2  
3  
4

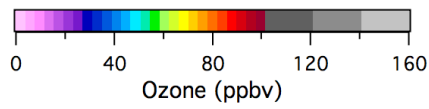
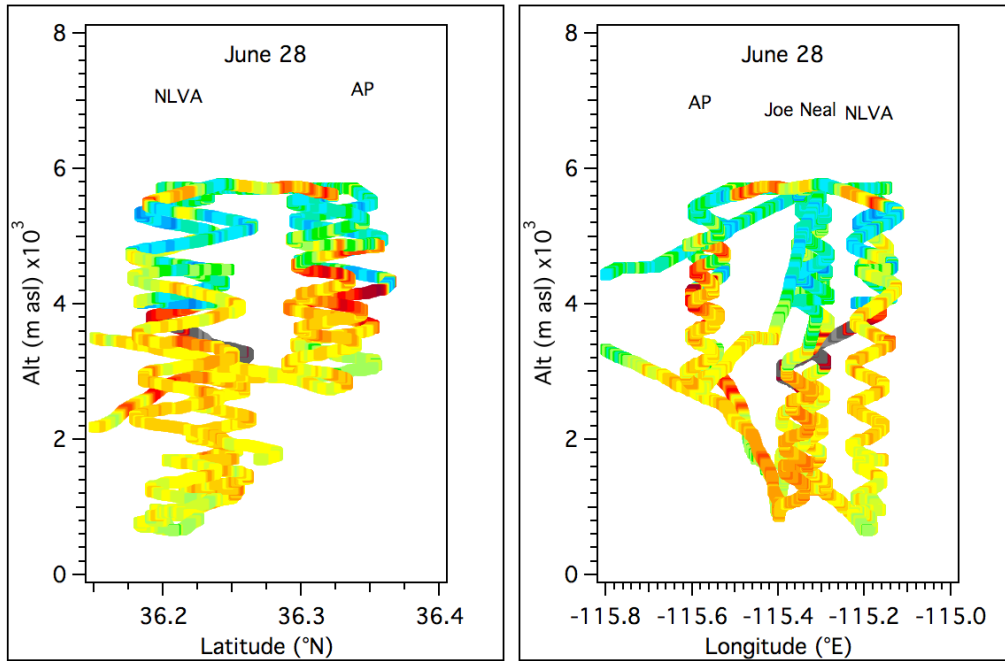
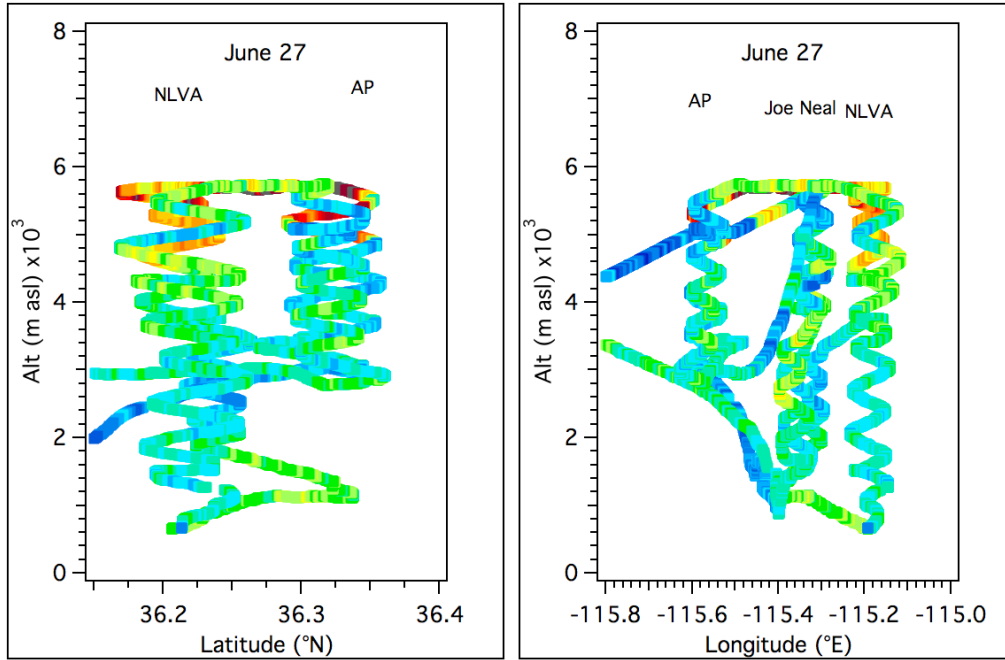
### IOP4



5  
6

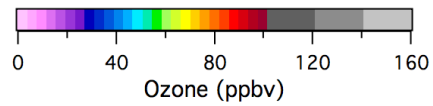
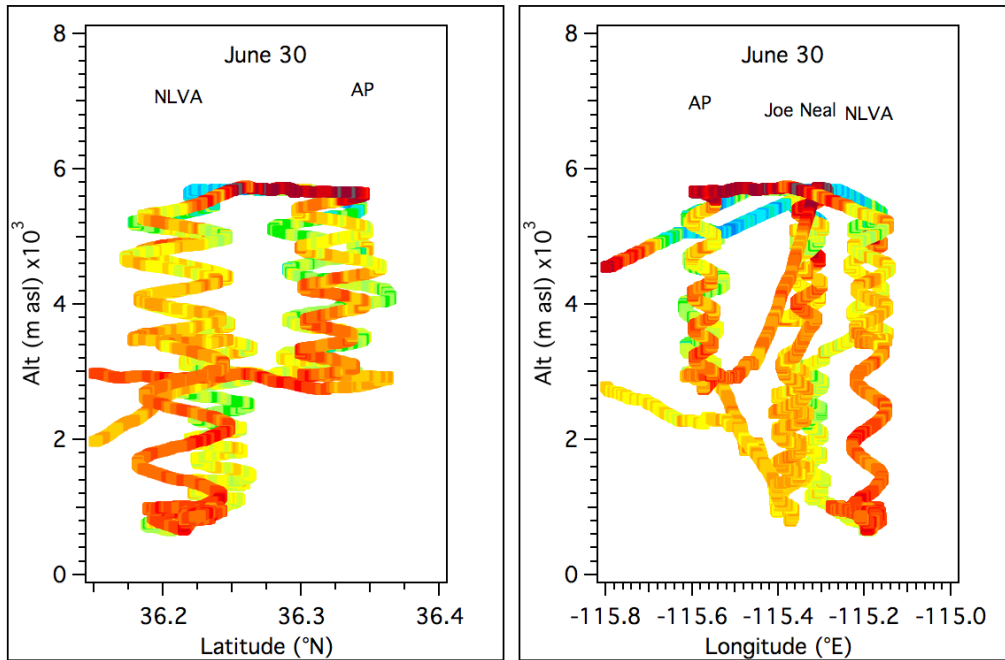
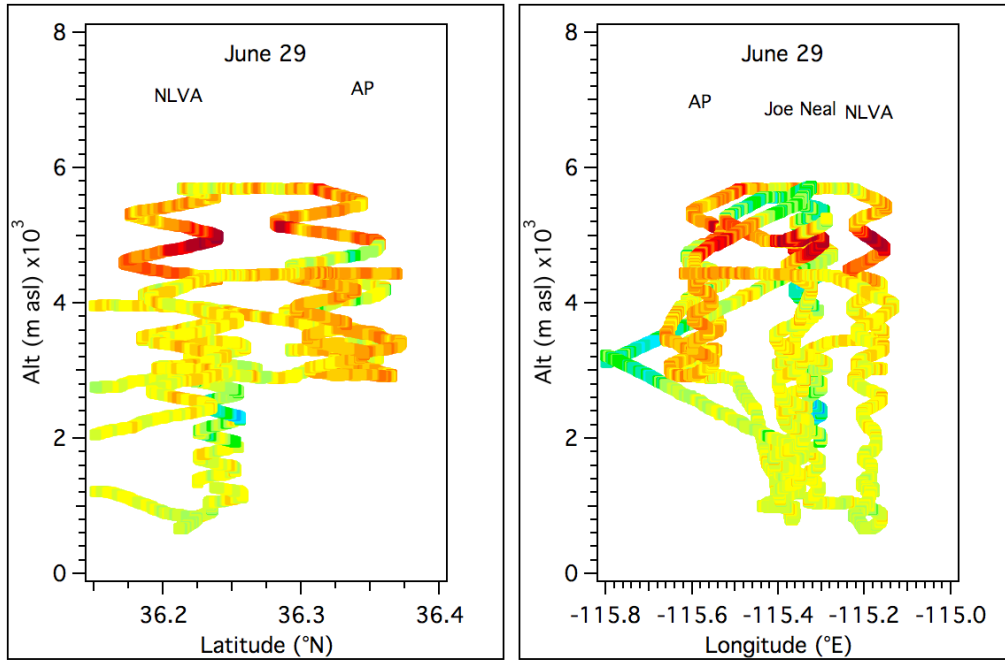
7  
8  
9  
10  
11  
12  
13  
14  
15  
16  
17  
18

1  
2



3  
4  
5  
6  
7  
8

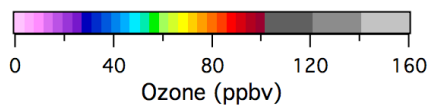
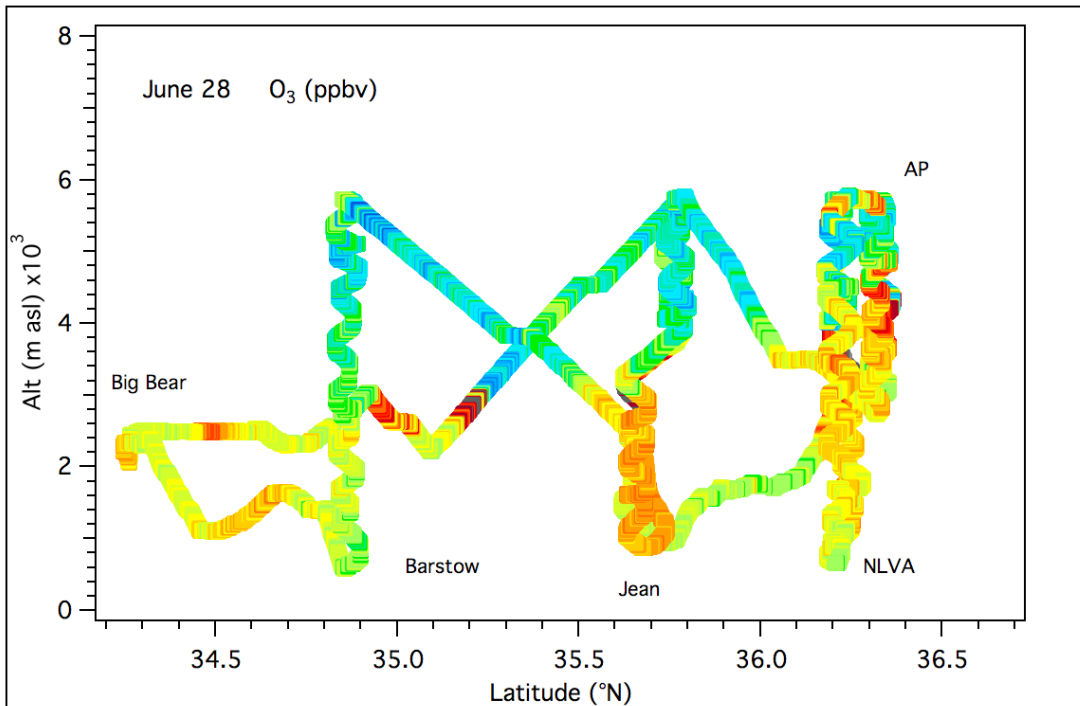
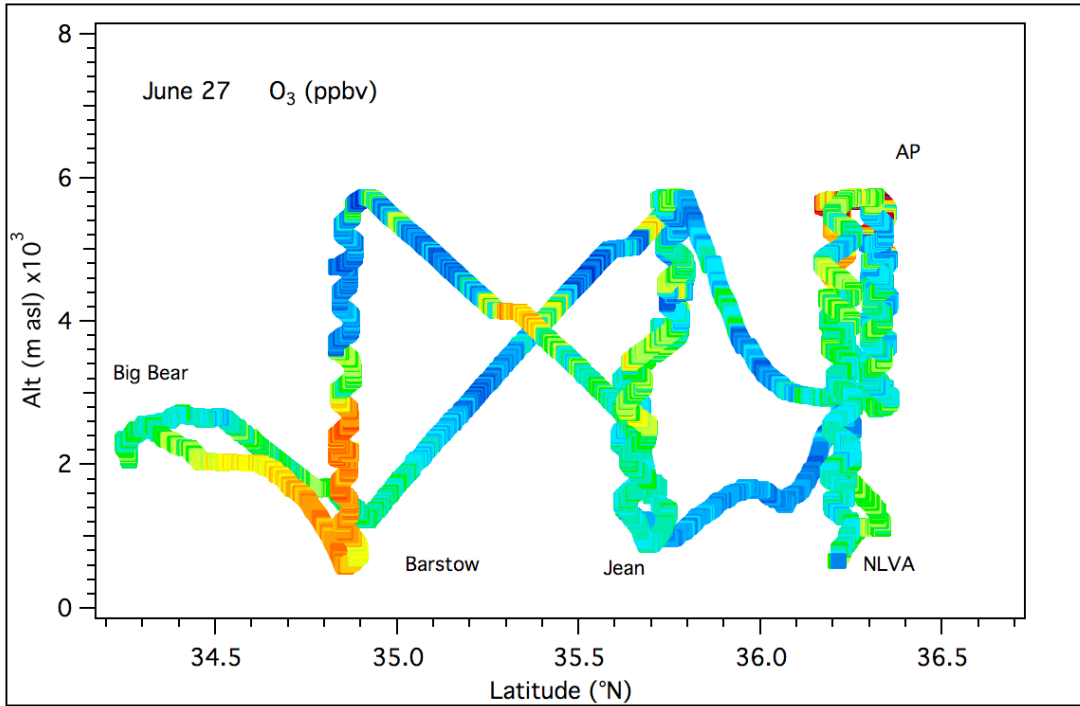
1



2  
3

4  
5

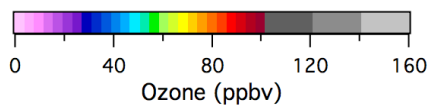
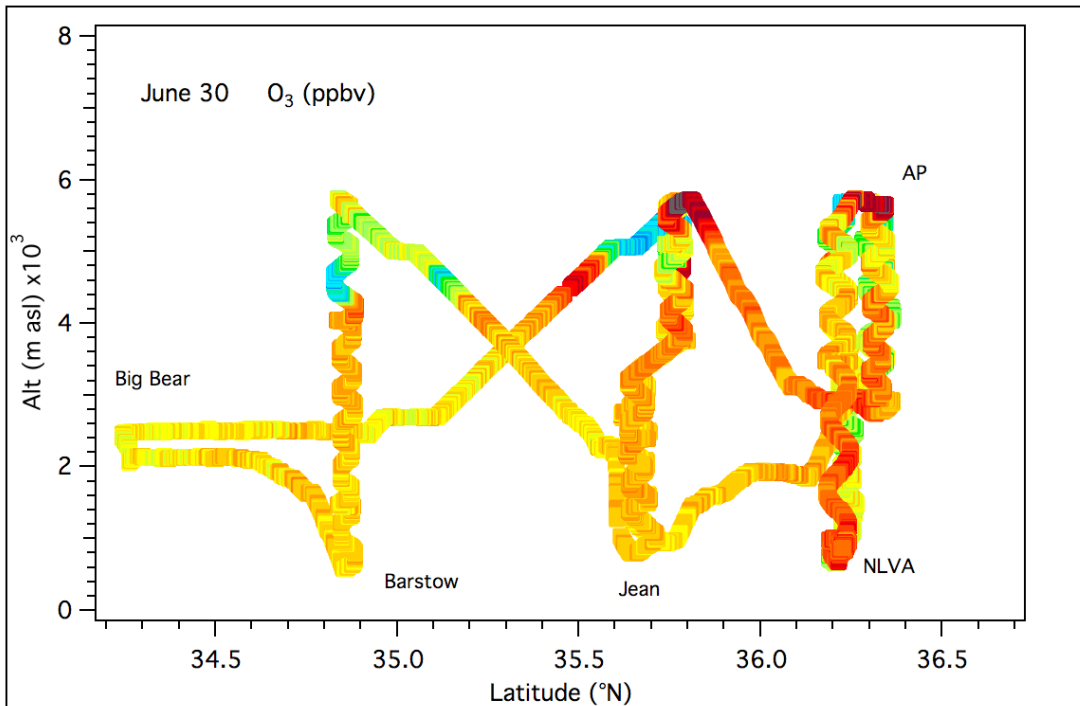
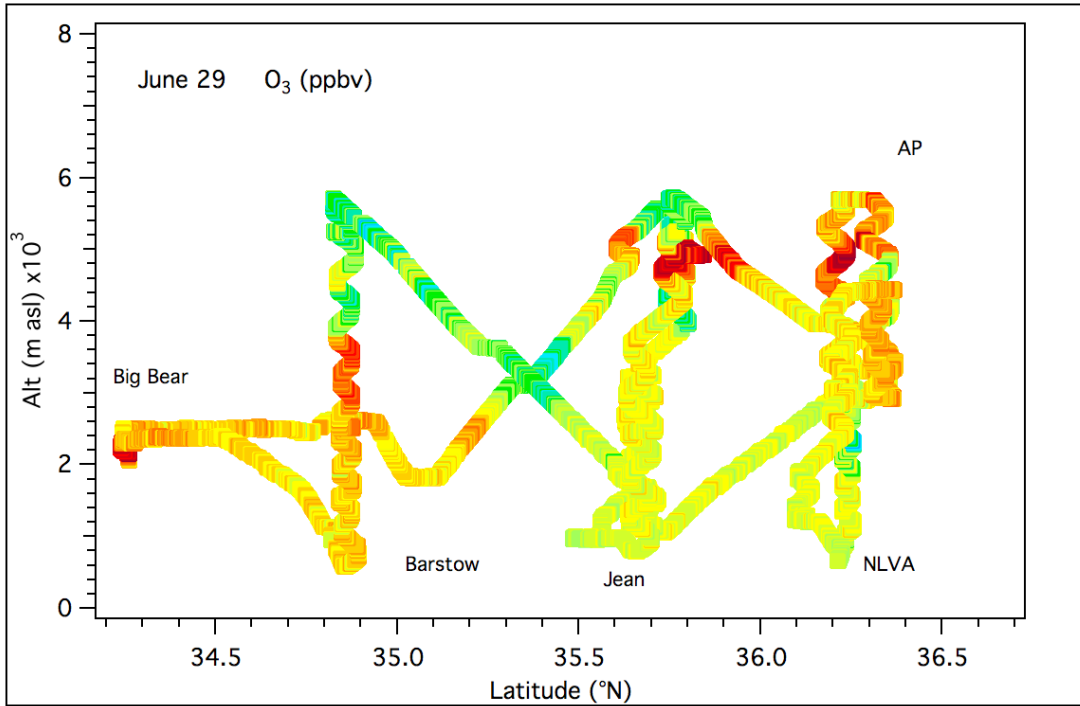
1  
2



3  
4

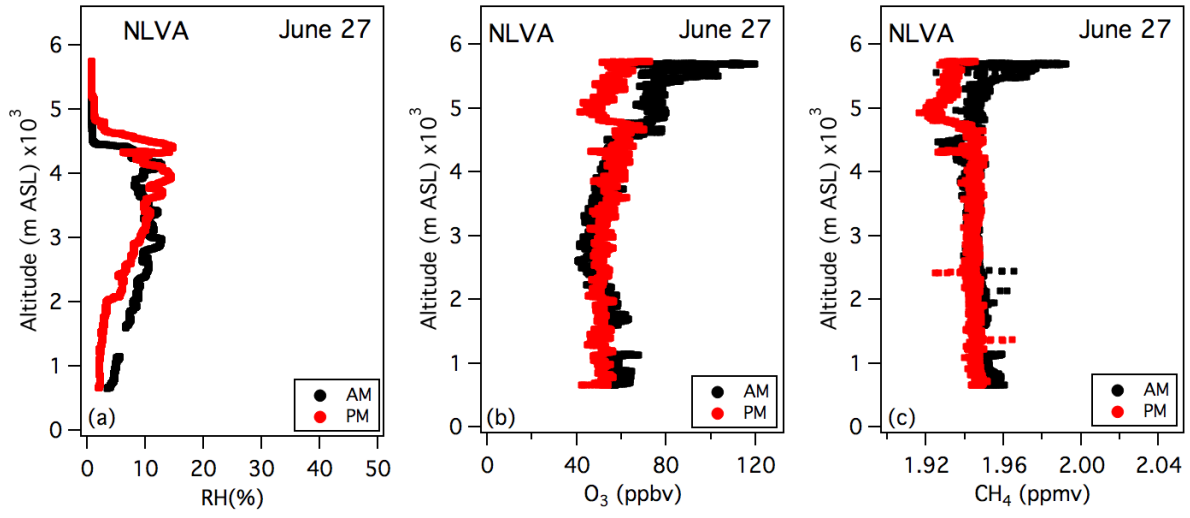
5  
6

1  
2

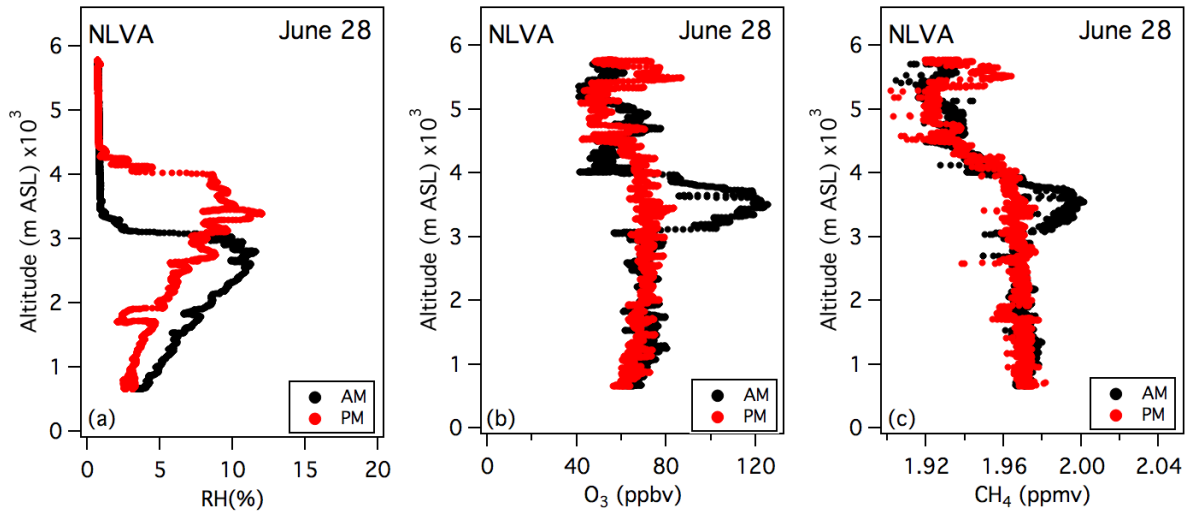


3  
4  
5

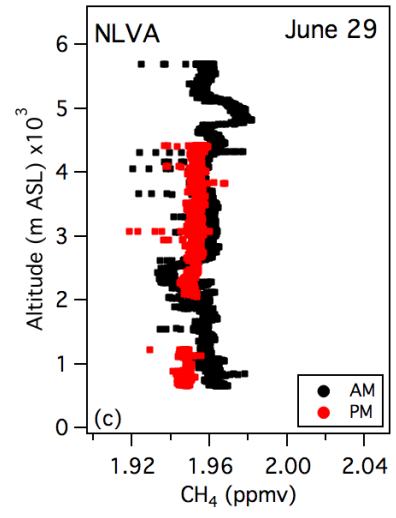
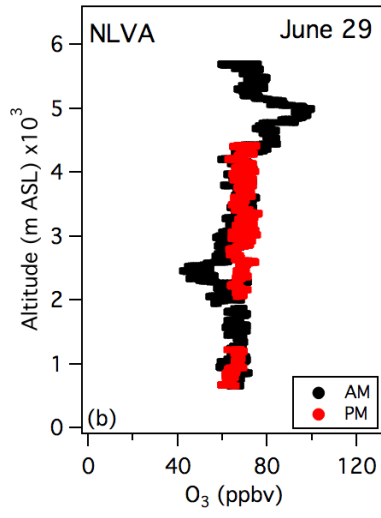
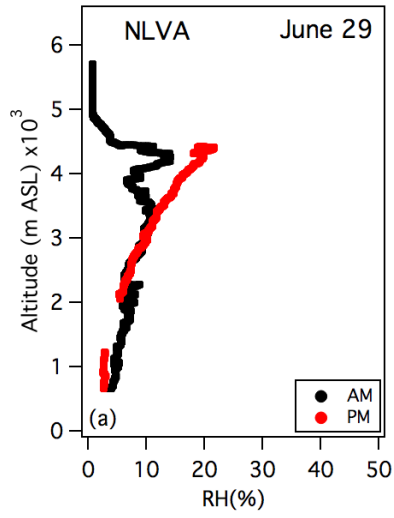
1



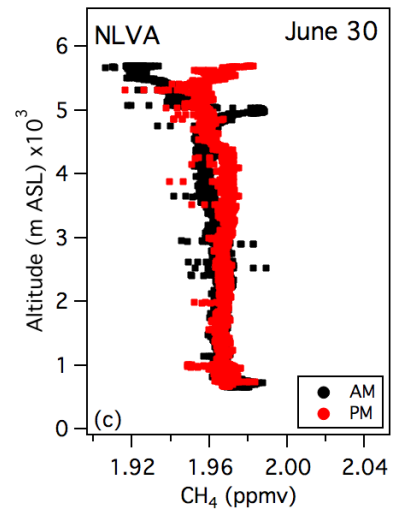
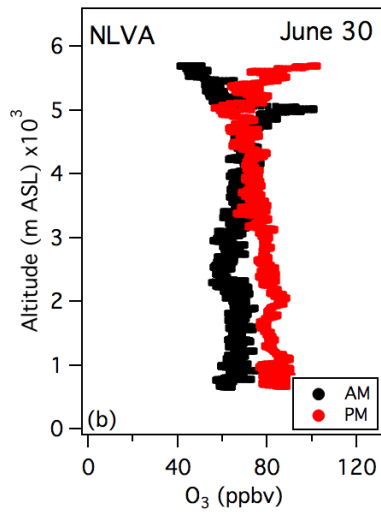
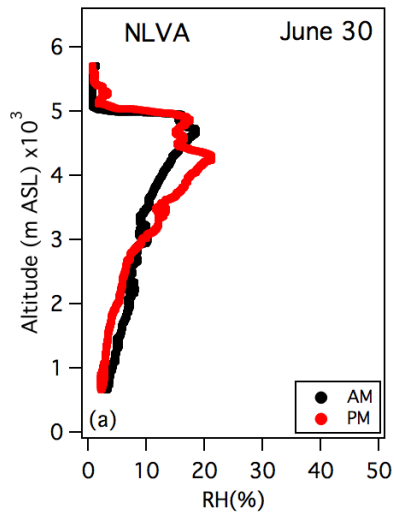
2



3



1



2

3

4

5